

1 **A new phylogenetic analysis of Phytosauria (Archosauria: Pseudosuchia) with the**
2 **application of continuous and geometric morphometric character coding**

3 Andrew S. Jones¹, Richard J. Butler¹

4 ¹ School of Geography, Earth and Environmental Sciences, University of Birmingham, Edgbaston,
5 Birmingham, B15 2TT, UK

6

7 Corresponding author:

8 Andrew Jones¹

9

10 Email address: andrew.jones.sp@gmail.com

11 Abstract

12

13 Phytosauria is a clade of large, carnivorous, semi-aquatic archosauromorphs which reached its peak
14 diversity and an almost global distribution in the Late Triassic (c. 230-201 Mya). Previous phylogenetic
15 analyses of Phytosauria have either focused primarily on the relationships of specific subclades, or were
16 limited in taxonomic scope, and no taxonomically comprehensive dataset is currently available. We here
17 present the most taxonomically comprehensive cladistic dataset of phytosaurs to date, based on extensive
18 first-hand study, identification of novel characters and synthesis of previous matrices. This results in an
19 almost two-fold increase in phylogenetic information scored per taxon over previous analyses. Alongside
20 a traditional discrete character matrix, three variant matrices were analysed in which selected characters
21 were coded using continuous and landmarking methods, to more rigorously explore phytosaur
22 relationships. Based on these four data matrices, four tree topologies were recovered. Relationships
23 among non-leptosuchomorph phytosaurs are largely consistent between these four topologies, whereas
24 those of more derived taxa are more variable. *Rutiodon carolinensis* consistently forms a sister
25 relationship with *Angistorhinus*. In three topologies *Nicrosaurus* nests deeply within a group of
26 traditionally non-Mystriosuchini taxa, leading us to redefine Mystriosuchini by excluding *Nicrosaurus* as
27 an internal specifier. Two distinct patterns of relationships within Mystriosuchini are present in the four
28 topologies, distinguished largely by the variable position of *Mystriosuchus*. In two topologies
29 *Mystriosuchus* forms the most basal clade in Mystriosuchini, whilst in the others it occupies a highly
30 derived position within the *Machaeroprotopus* clade. '*Redondasaurus*' is consistently recovered as
31 monophyletic; however, it also nests within the *Machaeroprotopus* clade. The greatest impact on tree
32 topology was associated with the incorporation of continuous data into our matrices, with landmark
33 characters exerting a relatively modest influence. All topologies correlated significantly with stratigraphic

34 range estimates. Topological variability in our results highlights clades in which further investigation may
35 better elucidate phytosaur relationships.

36 Introduction

37

38 Phytosaurs were a group of large-bodied archosauromorph reptiles that achieved an almost global
39 distribution during the Late Triassic (c. 230–201 Mya; Stocker & Butler, 2013). In overall morphology,
40 they are highly convergent with modern crocodilians, and this observation, in combination with the
41 common recovery of their fossils from fluvial and lacustrine depositional environments, indicates that
42 phytosaurs may have occupied a semi-aquatic niche, with their dentition suggestive of piscivory and
43 carnivory (Stocker & Butler, 2013).

44 By far the most intensively investigated aspect of Phytosauria is their systematics. The
45 phylogenetic position of phytosaurs within Archosauromorpha remains debated, having been recovered by
46 recent analyses as either the sister group to Archosauria (Nesbitt, 2011), or as the earliest diverging clade
47 within the crocodilian stem-group Pseudosuchia (Ezcurra, 2016). Regardless of their exact phylogenetic
48 position, time-calibration of phylogenies indicates that phytosaurs originated in the Early Triassic, soon
49 after the Permo-Triassic mass extinction, although only one confirmed phytosaur specimen is known prior
50 to the Late Triassic (Stocker *et al.*, 2017). Their abundance, rich fossil record and cosmopolitan
51 distribution indicate that phytosaurs were an important component of Late Triassic ecosystems; as a
52 result, aspects of phytosaur palaeobiology such as ontogeny (Irmis, 2007) and neurosensory adaptations
53 (Holloway, Claeson & O'keefe, 2013; Lautenschlager & Butler, 2016), as well as biogeography (~~e.g.e.g.~~
54 Buffetaut, 1993; Brusatte *et al.*, 2012; Stocker & Butler, 2013), have received considerable interest.
55 Furthermore, phytosaurs have featured heavily in biostratigraphical hypotheses for the Late Triassic
56 terrestrial record (Long & Ballew, 1985; Parrish & Carpenter, 1986; Lucas & Hunt, 1993; Lucas, 1998,
57 2010; ~~Martz & Parker, 2017~~). An important factor for these analyses and others is a robust understanding
58 of evolutionary relationships within Phytosauria. Phytosaur taxonomy has long been problematic and

Commented [WGP1]: Lucas 2010 is just a self-plagiarized version of Lucas 1998 with some additional text. You should only cite one.

Commented [WGP2]: Most recent for North America

59 convoluted, complicating attempts to understand phytosaur evolutionary history (Hungerbühler, 2002;
60 Stocker & Butler, 2013). However, with the advent and continued improvement of cladistic techniques, a
61 more cohesive picture has begun to form.

62 Most previous phylogenetic analyses of the ingroup relationships of Phytosauria have primarily
63 been focused on elucidating the relationships of individual or specific sets of taxa (Table 1). To achieve
64 this, many analyses have been restricted in their taxonomic scope. These analyses have greatly enhanced
65 current knowledge of many areas in phytosaur systematics; however, there is currently no taxonomically
66 comprehensive cladistic dataset which can be used to investigate relationships across all known phytosaur
67 species and clades. The development of such a dataset is an essential prerequisite for carrying out broader
68 evolutionary analyses. To address this gap, this paper has three primary aims:

69 1) To present the most taxonomically comprehensive phylogeny of Phytosauria to date, including
70 nearly all currently recognized species;

71 2) To use this phylogeny to investigate the phylogenetic relationships of a number of species and
72 higher-level taxa that have previously been recognized as problematic;

73 3) To assess the utility of continuous and geometric morphometric character coding techniques, as
74 tools that can potentially expand the information available to assess phytosaur interrelationships.

75

76 **Previous work**

77 **Previous cladistic analyses.** The first cladistic analysis of the ingroup relationships of Phytosauria was
78 performed by Ballew (1989). Her analysis included 11 operational taxonomic units (OTUs) and 64
79 characters with the aim of establishing character polarity and revising the diagnoses and species
80 assignments of the genera *Rutiodon* and '*Pseudopalatus*'. The analysis generated a tree topology which, in
81 its general structure, has changed relatively little in subsequent analyses. '*Paleorhinus*' and *Angistorhinus*

were recovered at the base of Phytosauria, and a polytomy of taxa which Ballew synonymized into *Rutiodon* was recovered as the sister taxon to a clade consisting of *Nicrosaurus*, '*Pseudopalatus*' and *Mystriosuchus* (Fig. 1A).

Ballew's phylogeny (Fig. 1A) was used as a basis for Long & Murry (1995) to present a comprehensive taxonomic review of Phytosauria, including the erection of three new genera ('*Arganarhinus*', *Smilosuchus*, '*Arribasuchus*') and the identification of numerous new anatomical characters with potential taxonomic or phylogenetic significance. No numerical phylogenetic analysis or phylogenetic tree was presented, but based on the identification of novel characters a taxonomy was constructed, differing from the phylogeny of Ballew (1989) most importantly in the separation of the taxa included in *Rutiodon* by Ballew into *Leptosuchus* Case, 1922 and the new genus *Smilosuchus*, and in the basal position of *Mystriosuchus* as the sister taxon to '*Paleorhinus*' (previously suggested by Gregory [1962] and Hunt & Lucas [1989]).

Hungerbühler (1998) increased taxonomic sampling, including 22 species-level OTUs, and presented a largely novel matrix of 49 characters, of which 12 were based on or reused from previous studies (Ballew, 1989; Long & Murry, 1995). The aims were twofold: to test the concept of a monophyletic '*Paleorhinus*' (Ballew, 1989; Hunt & Lucas, 1991; Long & Murry, 1995), and to more thoroughly assess the phylogenetic position of *Mystriosuchus*. '*Paleorhinus*' was found to be paraphyletic, with the species previously assigned to the genus recovered as a grade of iteratively more derived taxa at the base of Phytosauria. In agreement with Ballew (1989; Fig. 1A), *Mystriosuchus* was found in a more derived position than '*Paleorhinus*', but nested as the sister taxon to '*Pseudopalatus*' rather than within this genus (Fig. 1B).

A heavily revised version of Hungerbühler's (1998) matrix was used by Hungerbühler (2002) to further investigate the relationships of *Mystriosuchus* and assess the phylogenetic position of the newly

described species *Mystriosuchus westphali*. Sampling was reduced to only 11 taxa and 47 characters (of which 16 were taken directly from the previous study), to focus the analysis on the clade formed of *Nicrosaurus*, *Mystriosuchus* and ‘*Pseudopalatus*’, named ‘Pseudopalatinae’ by Long & Murry (1995). *Mystriosuchus* was again recovered as the sister taxon to ‘*Pseudopalatus*’; additionally, the genus ‘*Redondasaurus*’ was found to be monophyletic and outside of ‘*Pseudopalatus*’, contra Hungerbühler, Chatterjee & Cunningham (2003), but closer to the latter taxon than to *Mystriosuchus*. *Nicrosaurus* was recovered as the sister-taxon of the *Mystriosuchus* + (‘*Redondasaurus*’ + ‘*Pseudopalatus*’) clade (Fig. 1C).

The matrix of Hungerbühler (2002) was subsequently used to test the phylogenetic position of ‘*Pseudopalatus*’ *jablonskiae* by Parker & Irmis (2006). This taxon was the only addition to the matrix and was found to occupy the most basal position in the genus ‘*Pseudopalatus*’, with no other changes in tree topology (Fig. 2A).

In order to better resolve the relationships of the stratigraphically important genus *Leptosuchus* (Camp, 1930; Hunt & Lucas, 1991; Lucas, 1998) and other associated taxa (including those that were synonymized into *Rutiodon* by Ballew 1989), Stocker (2010) produced a largely novel matrix, incorporating three characters from the matrix of Sereno (1991), and 18 either directly taken or modified from Hungerbühler (2002). The full matrix consisted of 43 characters scored for 24 OTUs and found *Leptosuchus* to be polyphyletic, with ‘*Leptosuchus*’ *adamanensis* forming a monophyletic group with *Smilosuchus gregorii* and ‘*Machaeroprotopus*’ *lithodendrorum* (Fig. 2B). As a result, ‘*Leptosuchus*’ *adamanensis* and ‘*Machaeroprotopus*’ *lithodendrorum* were reassigned to the genus *Smilosuchus*. *Rutiodon* was not found to be synonymous with *Angistorhinus*, *Brachysuchus* or *Leptosuchus*, contra Ballew (1989), Long & Murry (1995) and Hungerbühler & Sues (2001). The new genus and species

127 *Pravusuchus hortus* was recovered as the sister taxon to ‘Pseudopalatinae’, and ‘*Paleorhinus*’ *scurriensis*
128 Langston, 1949 was found to occupy the most basal position within Phytosauria (Fig. 2B).

129 Following this, Stocker (2012, 2013) presented two further studies in which she first described the
130 new taxon *Protome batalaria* and then redescribed ‘*Paleorhinus*’ *scurriensis*, assigning the latter to the
131 new genus *Wannia*. Phylogenetic aspects of both studies were based entirely on the dataset of Stocker
132 (2010) with no changes or additions to the dataset. In the latter study, Stocker (2013) provided further
133 discussion questioning the existence of a monophyletic ‘*Paleorhinus*’, supporting the findings of
134 Hungerbühler (1998; Fig. 1B).

135 Although not a phylogenetic study, an important taxonomic alteration was made by Parker,
136 Hungerbühler & Martz (2012). The genus name *Machaeroprosope* was previously considered invalid
137 because the sole specimen of its presumed type species (*Machaeroprosope validus*, UW 3807) has been
138 lost (Gregory, 1962); however, Parker, Hungerbühler & Martz (2012) established that the holotype
139 specimen of the species *Machaeroprosope buceros* actually takes priority. The species
140 *Machaeroprosope buceros* was initially assigned to the genus ‘*Belodon*’, but subsequently made the type
141 species of the genus *Metarhinus* (Jaekel, 1910); however, when this genus was found to be preoccupied, a
142 replacement genus, *Machaeroprosope*, was erected by Mehl (1915). Inexplicably, the species
143 *Machaeroprosope validus* was long used as the genotype of *Machaeroprosope* despite
144 *Machaeroprosope buceros* having priority. As the holotype specimen of *Machaeroprosope buceros* is
145 readily available to study, the genus *Machaeroprosope* was considered valid by Parker, Hungerbühler &
146 Martz (2012), with the type species being *Machaeroprosope buceros*. Furthermore, *Machaeroprosope*
147 *buceros* has been recovered frequently as the sister taxon to ‘*Pseudopalatus*’ *pristinus*, the type species of
148 ‘*Pseudopalatus*’, and has taxonomic priority over that species. As a result, all of the species previously
149 assigned to ‘*Pseudopalatus*’ were reassigned to *Machaeroprosope* by Parker, Hungerbühler & Martz

150 (2012). The clade ‘Pseudopalatinae’ was, however, retained, as its usage lies outside of the remit of the
151 ICZN, although it has subsequently been replaced by Mystriosuchini (see below, but see Martz & Parker,
152 2017).

153 The monophyly of the newly diagnosed *Machaeroprosoopus* with respect to ‘*Redondasaurus*’ was
154 tested by Hungerbühler *et al.* (2013); the two species of ‘*Redondasaurus*’ were previously found to nest
155 paraphyletically within *Machaeroprosoopus* (Hungerbühler, Chatterjee & Cunningham, 2003). The
156 primary purpose of the analysis was, however, to test the phylogenetic position of the newly described
157 species *Machaeroprosoopus lottorum*. Taxonomic sampling was restricted to 12 OTUs, focussing entirely
158 on the group ‘Pseudopalatinae’, and 41 characters of which 21 were to some extent based on characters
159 from previous studies (Hungerbühler, 1998; 2002; Stocker, 2010). ‘*Redondasaurus*’ was found to be
160 paraphyletic and nest within *Machaeroprosoopus* (Fig. 2C), contra Hungerbühler (2002; Fig. 1C) and
161 Parker & Irmis (2006; Fig. 2A). *Machaeroprosoopus lottorum* was also found to nest within
162 *Machaeroprosoopus*, bridging the gap between the more derived species and specimens previously referred
163 to ‘*Redondasaurus*’ and the specimens traditionally belonging to *Machaeroprosoopus*.

164 Finally, two further studies were carried out based on the matrix of Stocker (2010, 2012, 2013),
165 both with the aim of redescribing basal phytosaur taxa previously assigned to ‘*Paleorhinus*’ and
166 elucidating the relationships of basal phytosaurs. Butler *et al.* (2014) redescribed the taxa ‘*Paleorhinus*’
167 *angustifrons* (Kuhn, 1936) (formerly ‘*Francosuchus*’) and *Ebrachosuchus neukami* Kuhn, 1936, and
168 established a robust set of synapomorphies (which were incorporated into the phylogenetic data matrix) to
169 diagnose a revised, restricted definition of ‘*Paleorhinus*’ that included the species ‘*Paleorhinus*’ *bransonii*
170 and ‘*Paleorhinus*’ *angustifrons* (Fig. 3A).

171 Kammerer *et al.* (2015) produced a redescription of *Parasuchus hislopi* Lydekker, 1885 and found
172 it to be the sister taxon to ‘*Paleorhinus*’ *angustifrons*, supported by two unambiguous synapomorphies.

Commented [WGP3]: Because clade names are not regulated by the ICZN it was unnecessary to replace Pseudopalatinae with Mystriosuchini. Unfortunately, however, there are no rules governing clade names so even priority does apply to retain Pseudopalatinae. However, see the argument for retaining this name in Martz & Parker, 2017.

173 Given the designation by the ICZN of a neotype for *Parasuchus* (Chatterjee, 2001; ICZN, 2003), this
174 genus takes priority over ‘*Paleorhinus*’ as the senior synonym. As a result, all species in the monophyletic
175 ‘*Paleorhinus*’ group were reassigned to the genus *Parasuchus* (Fig. 3B). Kammerer *et al.* (2015) also
176 presented an update to phytosaur family-level and subfamily groups, including the following groups, from
177 most inclusive to most exclusive: Parasuchidae Lydekker, 1885, Mystriosuchinae von Huene, 1915
178 (formerly Phytosauridae Jaeger, 1828), Leptosuchomorpha Stocker, 2010, and Mystriosuchini von Huene,
179 1915 (formerly ‘Pseudopalatinae’ Long & Murry, 1995). For consistency, the nomenclature used by
180 Kammerer *et al.* (2015) is used henceforth throughout this study, with some minor modification to
181 phylogenetic definitions (Table 2; see below).

Commented [WGP4]: Defined phylogenetically by Parker & Irmis 2006 based on Hungerbühler 2002.

Commented [WGP5]: The Kammerer et al nomenclature was unnecessary and has not been widely used yet. Consistency would use Pseudopalatinae, which has been stable and understood since 1995!

183 ~~Weaknesses-Limitations~~ of previous work. There are a number of problems with previous phylogenetic
184 analyses, including (i) lack of comprehensive taxonomic sampling and geographic biases; (ii) limited first-
185 hand examination of key specimens; (iii) inclusion of parsimony uninformative characters; (iv) poorly
186 defined characters; (v) outgroup choice. Examples of all these problems are given below.

Commented [WGP6]: The goal of these previous studies was not an exhaustive phylogenetic study of the phytosaurs so I don't think 'weaknesses' is the right word here.

187 Limited geographic sampling is one of the predominant biases in phylogenetic analyses of
188 phytosaurs. Previous data sets have often focused on either predominantly North American or
189 predominantly European taxa (only a small number of named phytosaur taxa are known from outside
190 these regions, from Morocco and India); this is particularly noticeable in the studies of Stocker (2010,
191 2012, 2013) (Fig. 2B). Of the 20 OTUs included by Stocker (2010), only *Mystriosuchus westphali* is from
192 Europe. The exclusion of another key European genus, *Nicrosaurus*, could be problematic for the
193 resulting inferred phylogenetic position of *Pravusuchus*, because *Nicrosaurus* has been recovered by other
194 analyses as the most basal member of ‘Mystriosuchini/‘Pseudopalatinae’ (Hungerbühler, 2002; Parker &
195 Irmis, 2006) (Fig. 1C, Fig. 2A). Stocker’s (2010) placement of *Pravusuchus* as the immediate sister-taxon

Commented [WGP7]: This exemplifies how the new nomenclature causes confusion.

196 to **Mystriosuchini/“Pseudopalatinae”** implies a potential close relationship between *Pravusuchus* and
197 *Nicrosaurus*; however, this remains untested and has the potential to affect the relationships of other
198 closely related species.

Commented [WGP8]: Ditto.

199 Hungerbühler (1998) scored only four of 22 OTUs based on first-hand study, with the rest scored
200 based upon published figures and descriptions. Hungerbühler (1998) noted that caution should be used
201 when interpreting such data as ‘descriptions of even well-preserved specimens of “well-known” taxa may
202 contain significant misinterpretations’. A consequence of this, not explicitly mentioned by Hungerbühler
203 (1998), relates to character sampling; the majority of Hungerbühler’s characters were novel and were
204 therefore created with first-hand reference to only four taxa. This raises questions regarding the
205 applicability of these characters to the remaining 18 OTUs and the validity of the character states. The
206 matrix of Hungerbühler (2002), which was scored entirely from first-hand study, retained only 16
207 characters identified in the previous analysis with the states of many having been altered.

208 The analysis of Ballew (1989) also suffered from issues around choice and definition of
209 characters. As noted by Hungerbühler (1998), of the 64 characters used 39 were autapomorphies of the
210 OTUs and are therefore parsimony uninformative, and five more were characters that describe a clade that
211 is not present in the tree. As a result, the number of phylogenetically informative characters included in
212 this dataset was only 20.

213 Long & Murry (1995) presented numerous new characters to support various clades identified in
214 their taxonomic review. However, many were criticized for being either plesiomorphic for Phytosauria,
215 susceptible to taphonomic bias, or generally vague (Hungerbühler, 1998). This is especially true of their
216 expansion of the definition of ‘*Paleorhinus*’ given by Hunt & Lucas (1991), which included such
217 characters as ‘external nares anterior to antorbital fenestra,...orbits directed dorsally or

218 dorsolaterally,...lateral temporal fenestra large', all of which are likely to represent plesiomorphies for
219 Phytosauria.

220 Finally, the analysis of Hungerbühler (1998) used *Proterochampsia barrionuevoi* as a second
221 outgroup (Fig. 1B); *Proterochampsia* was chosen due to shared cranial similarities with phytosaurs, and
222 historically had been suggested to be the basalmost phytosaur (Walker, 1968). However, its position was
223 subsequently re-evaluated as a derived proterochampsid archosauriform, outside of Archosauria (Romer,
224 1972; Benton and Clark, 1988; Sereno and Arcucci, 1990; Sereno, 1991; Parrish, 1993; Juul, 1994). This
225 re-evaluation was noted by Hungerbühler (1998); however, the derived morphology of *Proterochampsia*
226 represents homoplastic, rather than plesiomorphic, character states, raising potential problems as an
227 outgroup choice.

228

229 **Current consensus.** Following the revision conducted by Kammerer *et al.* (2015), phytosaurs are
230 currently considered to fall into five successively less inclusive groups: Phytosauria, Parasuchidae,
231 Mystriosuchinae, Leptosuchomorpha and Mystriosuchini (Table 2).

232 Phytosauria Jaeger, 1828, is a stem-based clade which encompasses all phytosaurs. Previously the
233 membership of the groups Phytosauria and Parasuchidae overlapped completely (Kammerer *et al.*, 2015);
234 however, since the re-evaluation of *Diandongosuchus* (Stocker *et al.*, 2017) this taxon has been included
235 within Phytosauria, but excluded from Parasuchidae. However, this placement remains untested in any
236 analysis of ingroup phylogeny to date.

237 Parasuchidae Lydekker, 1885 (Chatterjee, 1978; Kammerer *et al.*, 2015) contains the basal genera
238 *Parasuchus*, *Ebrachosuchus* and *Wannia*, plus all phytosaurs belonging to Mystriosuchinae,
239 Leptosuchomorpha and Mystriosuchini. Following the work of Stocker (2013), *Wannia* has consistently
240 been recovered as the most basal phytosaur within Parasuchidae (Fig. 2B), being distinct from the more

241 derived *Parasuchus* clade defined by Butler *et al.* (2014) and Kammerer *et al.* (2015). The latter two
242 studies also recovered *Ebrachosuchus* in a more derived position than *Parasuchus* (Fig. 3A,B).

243 Mystriosuchinae von Huene, 1915 excludes basal phytosaurs, being defined as ‘the last common
244 ancestor of *Mystriosuchus planirostris* (Meyer, 1863) and *Angistorhinus grandis* Mehl, 1913 and all of its
245 descendants’ (Kammerer *et al.*, 2015), and is largely equivalent to Phytosauridae of previous analyses. In
246 addition to Leptosuchomorpha and Mystriosuchini, this group may also contain taxa previously
247 synonymized with ‘*Paleorhinus*’, such as ‘*Paleorhinus*’ *sawini*, and other genera, including *Rutiodon*,
248 *Angistorhinus*, *Brachysuchus*, and *Protome*. The relationships between *Angistorhinus*, *Brachysuchus* and
249 ‘*Paleorhinus*’ *sawini* are unresolved, but all of these taxa have been recovered as more derived than
250 *Parasuchus* and basal to *Rutiodon* and *Protome*, with the latter two taxa being placed in a polytomy
251 together with Leptosuchomorpha (Fig. 2B, Fig. 3A,B).

252 Leptosuchomorpha Stocker, 2010, was previously defined as ‘the most recent common ancestor of
253 *Leptosuchus studeri* and *Machaeroprotopus pristinus* and all descendants thereof’. We introduce a slight
254 modification to this definition here (Table 2) in response to our phylogenetic results, and include
255 ‘*Smilosuchus*’ *lithodendrorum* as an additional internal specifier to ensure that minor topological
256 rearrangements between taxa that have consistently been considered as leptosuchomorphs do not
257 jeopardize the stability of the clade. Therefore, in addition to members of Mystriosuchini,
258 Leptosuchomorpha contains all species of *Leptosuchus* and *Smilosuchus*, as well as probably the taxa
259 ‘*Phytosaurus*’ *doughty* and *Pravusuchus hortus*. *Leptosuchus* has been supported as monophyletic by
260 recent analyses, though its possible relationship with ‘*Phytosaurus*’ *doughty* is unresolved. *Smilosuchus*
261 has also been supported as monophyletic, and recovered as the sister taxon to *Pravusuchus* +
262 Mystriosuchini.

263 Mystriosuchini von Huene, 1915, excludes all but the most derived phytosaurs, and was defined
264 by Kammerer *et al.* (2015) as ‘the last common ancestor of *Mystriosuchus planirostris* (Meyer, 1863),
265 *Nicrosaurus kapffi* (Meyer, 1860) and *Machaeroprotopus buceros* (Cope, 1881) and all of its
266 descendants’. We modify this definition here by excluding *Nicrosaurus kapffi* from the list of internal
267 specifiers and introducing *Machaeroprotopus jablonskiae* as a replacement to maximize the taxonomic
268 stability of Mystriosuchini among the trees recovered here (Table 2; see below). Mystriosuchini is largely
269 synonymous with ‘Pseudopalatinae’ as defined by Long & Murry (1995), with the exception of the
270 inclusion of *Mystriosuchus* and the possible exclusion of *Nicrosaurus*. Although a basal position of
271 *Mystriosuchus* within Phytosauria, such as positioned as the sister taxon to ‘*Paleorhinus*’, has been
272 suggested in multiple studies (Gregory 1962; Hunt & Lucas, 1989; Long & Murry, 1995), this hypothesis
273 has not been supported by quantitative cladistic analyses. A derived position for *Mystriosuchus* within
274 Mystriosuchini has been found in all cladistic analyses thus far (Ballew, 1989; Hungerbühler, 1998; 2002;
275 Parker & Irmis, 2006; Stocker, 2010; 2012; 2013; Hungerbühler *et al.*, 2013; Butler *et al.*, 2014;
276 Kammerer *et al.*, 2015), and therefore seems relatively uncontroversial. The position of *Mystriosuchus*
277 with respect to other taxa in Mystriosuchini is less well resolved, as discussed below. The European genus
278 *Nicrosaurus* has been included within Mystriosuchini (Long & Murry, 1995; Parker & Irmis, 2006;
279 Kammerer *et al.*, 2015); however, the validity of this is also discussed below. The remainder of
280 Mystriosuchini consists of species referred to *Machaeroprotopus* and ‘*Redondasaurus*’, the relationships
281 of which also differ between studies.

282
283 **Current uncertainties.** Although *Rutiodon* has been consistently found close to, but in a more derived
284 position than, *Angistorhinus*, this relationship has been tested in only three relatively independent matrices
285 (Ballew, 1989; Hungerbühler, 1998; Stocker, 2010), of which the two earliest contain a number of

Commented [WGP9]: Essentially Pseudopalatinae Parker and Irmis, 2006.

Commented [WGP10]: Parker & Irmis, 2006.

286 problems, as described above. It has previously been suggested that *Angistorhinus* and *Rutiodon* may be
287 synonymous (Hungerbühler & Sues, 2001), although this has never been explicitly tested or fully
288 published.

289 Aside from the study of Hungerbühler (1998), *Angistorhinus* has only been used as a generic-level
290 OTU, or represented by a single species (Kammerer *et al.*, 2015). Kammerer *et al.* (2015) used
291 *Angistorhinus grandis* to score the genus; however, no further discussion of relationships within the genus
292 was presented. The systematics of the genus *Angistorhinus* are another important area which is currently
293 poorly understood within phytosaurs.

294 *Nicrosaurus* is generally accepted as the most basal member of Mystriosuchini, and was used as a
295 reference taxon in the previous phylogenetic definition of the group (Kammerer *et al.*, 2015; Table 2);
296 however, only the early studies of Ballew (1989) and Hungerbühler (1998) have tested this position.
297 *Nicrosaurus* has been included in two other relatively independent analyses (Hungerbühler, 2002;
298 Hungerbühler *et al.*, 2013); however, neither included taxa from outside of Mystriosuchini, and therefore
299 did not test the position of the genus within global phytosaur phylogeny. Therefore, although the position
300 of *Nicrosaurus* has not been contested, it is also not especially well supported by available data.

301 The position of *Mystriosuchus* within Mystriosuchini remains unclear, having been placed as
302 either sister to the clade of *Machaeroprotopus* + ‘*Redondasaurus*’ (Hungerbühler, 1998; 2002; Parker &
303 Irmis, 2006; Hungerbühler *et al.*, 2013) or nested within *Machaeroprotopus* (Ballew, 1989; Stocker,
304 2010; Butler *et al.*, 2014; Kammerer *et al.*, 2015). As the genus name *Mystriosuchus* Fraas, 1896 has
305 priority over *Machaeroprotopus* Mehl, 1915, this later relationship may have extensive taxonomic
306 implications.

307 In multiple studies ‘*Redondasaurus*’ has been found to nest within *Machaeroprotopus* (Ballew,
308 1989; Hungerbühler, Chatterjee & Cunningham, 2003; Stocker, 2010; Hungerbühler *et al.*, 2013; Butler *et*

Commented [WGP11]: This would be unfortunate as the name differences are useful to tell quickly if someone is discussing North American or European taxa.

309 *al.*, 2014; Kammerer *et al.*, 2015), whereas in others ‘*Redondasaurus*’ is monophyletic to the exclusion of
310 *Machaeroprotopus* (Hungerbühler, 1998; 2002; Parker & Irmis, 2006). In the most recent phylogeny of
311 derived phytosaurs (Hungerbühler *et al.*, 2013), ‘*Redondasaurus*’ was found to nest within
312 *Machaeroprotopus* and the two were tentatively synonymized, but this hypothesis requires further testing.

313

314 **Materials & Methods**

315

316 **Institutional abbreviations**

317 **AMNH**: American Museum of Natural History, New York, USA; **GPIT**: Institut für Geologie und
318 Paläontologie Tübingen, Tübingen, Germany; **KU**: University of Kansas, Lawrence, USA; **MB**: Museum
319 für Naturkunde, Berlin, Germany; **MNHN**: Muséum National d’Histoire Naturelle, Paris, France; **MU**:
320 University of Missouri, Columbia, Missouri, USA; **NHMW**: Naturhistorisches Museum Wien, Vienna,
321 Austria; **NMMNHS**: New Mexico Museum of Natural History and Science, Albuquerque, USA; **OMNH**:
322 Oklahoma Museum of Natural History, Norman, USA; **PEFO**: Petrified Forest National Park, Arizona,
323 USA; **SMNS**: Staatliches Museum für Naturkunde Stuttgart, Stuttgart, Germany; **TMM**: Texas Memorial
324 Museum, Austin, USA; **TTU-P**: Museum of the University of Texas Tech, Lubbock, USA; **UCMP**:
325 University of California Museum of Paleontology, Berkeley, USA; **UMMP**: University of Michigan
326 Museum of Paleontology, Ann Arbor, USA; **USNM**: National Museum of Natural History, Washington
327 D.C., USA; **UW**: University of Wisconsin Geological Museum, Madison, USA; **YPM**: Yale Peabody
328 Museum, New Haven, USA.

329

330 **Material**

331 The analysis presented here uses species as OTUs to facilitate comparison with previous phylogenetic
332 analyses. There has been recent interest in specimen-level phylogenetic analyses in vertebrate
333 palaeontology (~~e.g.e.g.~~, Upchurch, Tomida & Barrett, 2004; Tschopp, Mateus & Benson, 2015), but the
334 validity of this approach and its results remain largely unexplored. We did not use a specimen-level
335 phylogeny here as it would be hampered by the range of intraspecific variation found in most taxa, and
336 would be further compounded by poor preservation in many specimens resulting in high quantities of
337 missing data and widespread polytomies due to unstable terminals.

338 The OTUs included in this analysis consist of 34 species across 18 genera which are fully detailed
339 in Appendix 1. An additional nine specimen level OTUs were also included to test their affinities. We
340 attempted to sample all phytosaur species currently regarded as taxonomically valid or potentially
341 taxonomically valid, with the exception of a number of problematic species that were excluded for reasons
342 discussed below. *Euparkeria capensis* was used to root the analysis as it displays a generalized
343 archosauriform cranial morphology (Sookias, 2016) which has been used in previous studies for character
344 polarization (Hungerbühler, 2002; Parker & Irmis, 2006; Stocker, 2010; 2012; 2013; Butler *et al.*, 2014;
345 Kammerer *et al.*, 2015). *Diandongosuchus fuyuanensis*, a taxon from the Middle Triassic of China
346 initially identified as a basal poposauroid (Li *et al.*, 2012), was recently re-interpreted as the basal-most
347 phytosaur currently known (Stocker *et al.*, 2017) and is therefore included in this analysis to verify its
348 basal position within Phytosauria.

349 Of the 43 OTUs included in this analysis, 39 were scored based on first-hand study of at least one
350 of the referred specimens. Photographs and published descriptions and figures were also used where
351 available. The remaining four terminals (*Leptosuchus studei*, *Diandongosuchus fuyuanensis*, *Euparkeria*
352 *capensis* and *Parasuchus hislopi*) were not studied first hand for the purposes of this study, and were
353 scored from photographs and/or published descriptions and figures.

354

355 **Excluded taxa**

356 Although this analysis was designed to be the most comprehensive cladistic dataset for phytosaurs to date,
357 a small number of taxa were excluded for various reasons.

358 *Angistorhinus gracilis* Mehl, 1915, from the Popo Agie Formation in Wyoming, was only very
359 briefly described in the original paper, and a holotype was not formally designated, despite apparently
360 consisting of a large skull and much of the postcrania of a single phytosaur. When ASJ visited the
361 University of Missouri this material could not be found; however, it may be located in one of many
362 footlockers containing the ‘Mehl collection’ in the basement of the department (James Schiffbauer, pers.
363 comm. to ASJ, 2016). At present this material is considered lost with no images available other than a line
364 drawing of the antorbital region and two photographs of an anterior thoracic vertebra (Mehl, 1915);
365 because the proportion of missing data would likely hinder any analysis more than its inclusion would
366 contribute, we excluded this taxon.

367 *Angistorhinus maximus* Mehl, 1928 is known from the orbital and postorbital portions of a single
368 skull (MU 531) from the top of the Popo Agie Formation in Wyoming. Long & Murry (1995) noted
369 apparent similarities between this species and *Angistorhinus talaini* from Morocco, but also suggested
370 this material may represent a more derived taxon, not referable to *Angistorhinus*. They noted that
371 determining the taxonomic affinities would require detailed study and the type material ‘may be lost’
372 (Long & Murry, 1995:42). This material is also suspected to reside in the ‘Mehl collection’ of the
373 University of Missouri. As this material is considered lost and no images exist aside from the five line
374 drawings in Mehl (1928), it was excluded from analysis.

375 *Angistorhinus alticephalus* Stovall and Wharton, 1936 is represented by an incomplete skull, nine
376 vertebrae, rib fragments and osteoderms (OMNH 733) from the Dockum Group of Texas. This species is

377 differentiated from other *Angistorhinus* species primarily by the more laterally directed orbits, the shape
378 of the squamosal and the straight mediolateral frontal-parietal suture (Stovall and Wharton, 1936). It has
379 been suggested that the direction of the orbits should be used cautiously due to taphonomic distortion
380 (Gregory, 1962; Hungerbühler, 1998) and is ‘severely restricted’ in practical use due to the difficulty in
381 taking measurements and previous scoring subjectivity (Hungerbühler, 1998: 130); therefore, a more
382 detailed taxonomic analysis of this specimen is required to verify its distinctness, which is beyond the
383 scope of this study. Given the incomplete nature of the type material, the range of better *Angistorhinus*
384 material available to study and the taxonomic uncertainty regarding its validity, *A. alticephalus* was
385 excluded from this study.

386 *Angistorhinus aeolamnis* Eaton, 1965 is known from a single skull, lacking approximately its
387 dorsal 50–80 millimetres (KU 11659) from the Dockum Group of Texas. As far as can be seen from its
388 original description, the skull does not preserve any of the features indicative of the genus *Angistorhinus*,
389 such as posterior parietal extensions or the parietal-squamosal bars forming a posterolateral curve when
390 viewed dorsally (Long & Murry, 1995). The loss of the dorsal part of the skull also greatly reduces the
391 number of characters for which this specimen could be scored, making it likely to be problematic in
392 phylogenetic analysis; this combined with its unclear taxonomic affinities leads us to exclude this taxon.

393 *Brachysuchus megalodon* Case, 1929 is a very robust taxon, represented by the largely complete,
394 but dorsoventrally crushed holotype skull (UMMP 10336), a likely associated mandible (UMMP 10336a)
395 and a second, well preserved, also largely complete skull (UMMP 14366), from the Dockum Group of
396 Texas. *B. megalodon* has historically been a difficult taxon to interpret, being synonymized with
397 ‘*Phytosaurus*’ (Gregory, 1962) and *Angistorhinus* (Long and Murry, 1995) before being provisionally
398 resurrected by Stocker (2010) pending a full reanalysis of the taxon. *B. megalodon* is excluded here
399 because the material was unavailable for study due to the redevelopment of the UMMP museum.

400 Although the original description by Case is very detailed and contains many line drawings, it was
401 deemed unfeasible to score such a taxonomically problematic specimen that has been subjected to severe
402 taphonomic distortion from images alone, especially as the less distorted referred specimen has only ever
403 been figured in palatal view (Case & White, 1934).

404 ‘*Machaeroprosopus validus*’ Mehl *et al.*, 1916 was erected on the basis of an incomplete skull
405 (UW 3807) from the Chinle Formation of Arizona ~~or New Mexico~~. This specimen, which has been lost
406 (Westphal, 1979), was long considered to be the holotype specimen for the genus *Machaeroprosopus*
407 (Case, 1920; Camp, 1930; Colbert, 1947; Ballew, 1989; Hungerbühler, 1998). However, the holotype of
408 *Machaeroprosopus buceros* was recently found to take priority (Parker, Hungerbühler & Martz, 2012).
409 Considering the loss of the only specimen and its now decreased taxonomic significance and uncertain
410 taxonomic position this taxon is here excluded.

411 *Mesorhinosuchus fraasi* (Jaekel, 1910) was named based on a single partial skull, reportedly from
412 the Middle Buntsandstein of Saxony-Anhalt, Germany. The supposed type locality is dated as Olenekian
413 in age, making this potentially the stratigraphically oldest phytosaur, and predating even
414 *Diandongosuchus* by approximately 10 million years. The specimen, which was housed at the University
415 of Göttingen, was destroyed in WWII and only one photograph exists in the original description by Jaekel
416 (1910); moreover, its stratigraphic provenance has frequently been questioned (Gregory, 1962; 1969;
417 Hunt and Lucas, 1991). In any case this species is excluded due to the loss of the type specimen.

418 ‘*Paleorhinus magnoculus*’ Dutuit, 1977 is represented by a single, very small (275 mm
419 anteroposterior length) juvenile skull (MNHN ALM 1) from the Argana Formation of Morocco. It was
420 originally described as a unique species of ‘*Paleorhinus*’ due to (among other features) its proportionately
421 enormous orbits and small antorbital fenestrae; however, these putative autapomorphies were later
422 reinterpreted as a reflection of the early ontogenetic stage of the type specimen (Fara and Hungerbühler,

2000) and the species was reclassified as an indeterminate specimen of *Parasuchus*, a view that is shared in this study (but see Kammerer *et al.*, 2015). This taxon is therefore excluded from this study because the inclusion of ontogenetically variable features could affect its phylogenetic placement, as has been extensively reported in dinosaurs (Rozhdestvensky, 1965; Dodson, 1975; Sampson, Ryan & Tanke, 1997; Scanella & Horner, 2010; Tsuihiji *et al.*, 2011).

Promystriosuchus ehlersi (Case, 1922) is known from a poorly preserved partial skull from the Dockum Group in Texas (UMMP 7487). The specimen displays extensive dorso-ventral crushing with many elements not retaining their original associations; as such, it is a difficult specimen to interpret. It has previously been referred to ‘*Paleorhinus*’ (= *Parasuchus*) (Gregory, 1962; Hunt and Lucas, 1991; Long and Murry, 1995), but more recently its taxonomic position has been seen as uncertain (Kammerer *et al.*, 2015). As with *B. megalodon* the sole specimen of this taxon was unavailable for study, and it represents a taxonomically uncertain specimen with challenging morphology and few images available in the literature; for these reasons *Promystriosuchus ehlersi* is not included in this study.

436

437 **Continuous data in cladistics**

The use of continuous characters in cladistics has historically been controversial, with many researchers questioning their validity and appropriateness to cladistic methods (Crisp & Weston, 1987; Pimentel & Riggins, 1987; Cranston & Humphries, 1988; Felsenstein, 1988; Stevens, 1991). The majority of concerns raised have been around the discretization of frequently overlapping taxonomic ranges of continuous measurements into distinct character states using methods often criticized as arbitrary (Poe & Wiens, 2000).

Indeed, techniques such as gap-coding (Mickevich & Johnson, 1976) and segment-coding (Thorpe, 1984; Chappill, 1989) do suffer from elements of arbitrariness: in gap-coding the size of the

446 fundamental gap, and in segment-coding the number of segments, must be specified by the researchers
447 (Rae, 1998). These metrics may be based on various statistical concepts, such as 95% confidence intervals
448 or standard deviations about the mean, and data may be treated on a linear or logarithmic scale; however,
449 as shown by Gift & Stevens (1997) the choice of which metric to use can have a profound effect on the
450 final character states.

451 Despite the general rejection of continuous data by many authors, continuous ranges of
452 overlapping data have remained common in cladistic matrices, scored via character states with arbitrary
453 ‘discrete’ cutoffs, which are generally not explained or justified, ~~e.g.e.g.~~ ‘ratio of femoral length to width:
454 <6 [0], ≥ 6 [1]’, or ‘shape of orbit: circular [0], oval [1]’ (Stevens, 1991; Poe & Wiens, 2000; Wiens,
455 2001). These arbitrary character states have been shown to convey little phylogenetic information
456 compared to identical data ranges coded using gap-weighting (Garcia-Cruz & Sosa, 2006). Despite this,
457 these types of characters are frequently found in modern cladistic datasets, including recent analyses of
458 phytosaur phylogeny (Hungerbühler, 2002; Hungerbühler *et al.*, 2013; Parker & Irmis, 2006; Stocker,
459 2010; 2012; 2013; Butler *et al.*, 2014; Kammerer *et al.*, 2015). This study aims to incorporate continuous
460 morphological data, including that of ‘shape’, characterized in a non-arbitrary manner to increase the
461 quantity of phylogenetically useful information available to studies of phytosaur systematics, with the
462 goal of increasing their accuracy and resolution.

463 As expressed above, the main problem with many continuous coding techniques is the arbitrary
464 splitting of range data into discrete character states. The software package TNT overcomes this problem
465 by employing a similar technique to gap-weighting (Thiele, 1993) and step-matrix gap-weighting (Wiens,
466 2001). Gap-weighting splits the range of species mean values into as many character states as allowed by
467 the software (32 in PAUP*), thus increasing coding resolution and (as the characters are ordered) ensuring
468 large changes must pass through many steps in comparison to small changes, thus increasing their weight.

469 This technique is, however, hampered by the limits imposed by the software. Step-matrix gap-weighting
470 follows a similar initial procedure, but circumvents the limit on character weighting by using the sizes of
471 the gaps between unique character states, rescaled along a range from zero to the maximum steps allowed
472 by the software (1000 in PAUP*), to create step-matrix values to weight character state changes.
473 Although gap-weighting provides a higher resolution of states into which measured variation can be
474 categorized, the categorization method is still fundamentally arbitrary and, due to this, taxon ranges that
475 are significantly different may be grouped together and those that are statistically identical may be split up
476 (Farris, 1990).

477 The techniques developed in TNT (Goloboff, Mattoni & Quinteros, 2006; Goloboff, Farris &
478 Nixon, 2008b), and used in this study, remove arbitrary discretization by analysing the taxon range values
479 as they are, i.e. without being grouped into character states. This is possible through the use of Farris'
480 (1970) down-pass and Goloboff's (1993) up-pass algorithms which are designed to use numerical
481 differences between the states being optimized; therefore, the actual intervals between taxon data ranges,
482 being numerical, are treated in the same way as ordered character states (Goloboff, Mattoni & Quinteros,
483 2006). As mentioned in Goloboff, Mattoni & Quinteros (2006), step-matrix gap-weighting would produce
484 the same outcome as the TNT technique; however, this approach becomes difficult with a large number of
485 taxa and is not capable of handling ranges of variation. As the scale of the step changes, and therefore
486 weights, are directly proportional to the measured data, the magnitude on which the original
487 measurements were made could have a large (and often unwarranted) influence on character weighting.
488 Goloboff, Mattoni & Quinteros (2006) suggested that implied weighting (re-weighting of characters based
489 on their level of homoplasy) can reduce this issue, however, this was found to be only a partial solution
490 and a combination of implied weighting and re-scaling trait measurement values to unity produced far
491 more satisfactory results (Koch, Soto & Ramírez, 2015).

492

493 **Geometric morphometric data**

494 Geometric morphometric (GM) characters are a relatively new development in cladistics (Catalano,
495 Goloboff & Giannini, 2010; Goloboff & Catalano, 2011; Goloboff *et al.*, 2016). In relation to
496 phylogenetics, the use of geometric morphometrics tends to be equated with phenetic studies and the use
497 of techniques such as principal components analysis to reduce overall morphology to a small number of
498 axes of covariation. The method presented by Catalano, Goloboff & Giannini, (2010) avoids this; x, y and
499 z landmark coordinates are used, without transformation, to generate ancestral state reconstructions using
500 a spatial optimization technique which minimizes displacement between individual, or configurations of,
501 landmarks from two descendants. A thorough discussion of the applicability of geometric morphometrics
502 in phylogeny is given by Catalano, Goloboff & Giannini, (2010) in which previous arguments against its
503 use are also addressed. When integrated into a phylogenetic analysis of Vespinae (Perrard, Lopez- Osorio
504 & Carpenter, 2015), landmark characters were generally found to improve tree resolution when combined
505 with a morphological character matrix. Landmark characters still exerted a noticeable effect with the
506 addition of molecular data, though only four of the ten relationships generated by landmark data were
507 supported in the morphological + landmark + molecular data trees (Perrard, Lopez- Osorio & Carpenter,
508 2015). In these trees the landmark data mostly affected poorly supported nodes - allowing greater
509 resolution, though possibly only due to over-resolution due to the analysis techniques. It was also found
510 that the landmark data alone were insufficient to reliably resolve relationships, likely due to homoplasy
511 arising from the functional unit in which the landmark characters were placed (Perrard, Lopez- Osorio &
512 Carpenter, 2015). Although the quantity of information may be increased by using landmark characters,
513 not all information is included, which could lead to important features being excluded.

514

515 **Character coding**

516 The character list (Appendix 2) was constructed by combining those used in previous analyses
517 (Ballew, 1989; Hungerbühler, 2002; Stocker, 2010; Butler *et al.*, 2014; Kammerer *et al.*, 2015) as well as
518 by identifying new characters based on first-hand study of specimens and published literature. In order to
519 compare the effects of different character types on phylogenetic results, all characters (including
520 continuous and GM) were scored and input into one matrix, each character type as a different data block.
521 The resulting matrix contained three blocks of data: discrete scores, continuous ranges and GM
522 coordinates. Many of the continuous and GM characters were based on discrete characters from previous
523 analyses, for which the categorization of character states seemed inappropriate, ~~e.g.e.g.~~ for relative linear
524 measurements of morphological features, or complex morphologies. Therefore, some characters in the
525 discrete data block are discrete versions of continuous or GM characters. Some continuous and GM
526 characters incorporated here were novel; therefore, discrete versions of these were also created in the
527 discrete data block to ensure that where phylogenies were analysed using different data types, any
528 differences in results would not be affected simply by differences in the exact morphological information
529 included. The different combinations of character types were incorporated into different analyses by
530 setting either the continuous, GM, or both character blocks to 'active' or 'inactive' in the phylogenetic
531 software TNT (see below).

532 The number of characters and proportion of missing data in each data block are summarized in
533 Table S1. No characters were excluded based on quantity of missing data in scored taxa as including more
534 characters, even if this increases the proportion of missing data, has been shown to increase accuracy in
535 phylogenetic analysis (Wiens, 1998). This technique increases the possibility of long branch attraction
536 (Swofford *et al.*, 1996), but is less likely in a dataset where missing data is distributed randomly among all
537 taxa (Poe & Wiens, 2000); in our dataset missing data seem more likely to occur in certain taxa and

538 certain characters, therefore the possibility of long branch attraction should be kept in mind when
539 interpreting the results.

540 A consistent discrete matrix was used as a base for each analysis, into which continuous or GM
541 characters were swapped with their discrete counterparts. The discrete data block consisted of 94
542 characters, the continuous 10 characters and the GM five characters. These were combined in four
543 analyses: 1) discrete characters only (D coding treatment) (94 characters, 21 of which are ordered), 2)
544 discrete + continuous characters (DC coding treatment) (94 characters, 21 ordered), 3) discrete + GM
545 (DM coding treatment) (90 characters, as some GM characters encompass variation described by more
546 than one character in the discrete dataset; 19 ordered), 4) discrete + continuous + GM (DCM coding
547 treatment) (90 characters, 19 ordered). A full list of all characters, ordering and the correspondences of
548 continuous and GM to discrete characters is available in Appendix 2. The coding procedures used here for
549 continuous and GM characters are described below, as are the methods of character state distinction for
550 their discretized counterparts.

551 It is important to note here that when incorporating continuous and geometric morphometric
552 character scorings for analysis, the format of the TNT data file requires these characters to be presented
553 first in the file. This differs from how the characters are ordered in our character list (Appendix 2). Our
554 character list presents characters in the order in which they occur for the base discrete matrix; where a
555 character possesses a continuous or GM variant this is flagged next to that character. It should also be
556 noted that characters in a TNT file begin at zero, whereas we shift our characters such that the list begins
557 at one.

558
559 **Continuous characters.** Measurements were taken from all referred specimens with the appropriate
560 morphology preserved, either directly, using digital callipers, or from photographs, using the software

561 ImageJ. Standard error was calculated about the mean score of each species, this was then used to
562 calculate min-max species ranges with statistically meaningful differences (Goloboff, Mattoni &
563 Quinteros, 2006). Min-max species range values were rescaled in each character using the formula: $z_i = x_i$
564 $- \min(x) / \max(x) - \min(x)$ where z_i is the rescaled value, x_i is the original value and $\min/\max(x)$ are
565 respectively the minimum and maximum original values in the range of variation across all taxa for that
566 character. This rescales values onto a 0–1 scale, ensuring that magnitudes of interspecific differences
567 within characters are maintained, whilst between-character weighting is standardized. The rescaled range
568 values (and where only one specimen is known, the single values) were input into the data matrix file and
569 treated as ordered.

570
571 **GM characters.** Many features of phytosaur skulls that are appropriate for shape analysis contain few
572 discrete landmark positions, making traditional landmark analysis difficult, and the resolution of the
573 morphology influencing the results would be poor. For example, only two sutures regularly form
574 connections on the border of the antorbital fenestra that could be landmarked in all phytosaurs, and due to
575 the variable shape of the fenestra there are no consistent ‘corners’ or other morphological features that can
576 be traditionally landmarked on the border, aside from the most anterior and posterior extremities.
577 Conversely, these problems can be resolved by using sliding semi-landmarks to approximate outline
578 shape; this is the technique used here. In techniques such as principal components analysis, semi-
579 landmarks require special treatment, on account of their reduced dimensionality and therefore degrees of
580 freedom (Bookstein, 1996; Zelditch, Swiderski & Sheets, 2012); however, as TNT does not use such
581 analyses and providing the user employs appropriate Procrustes alignment techniques, nothing precludes
582 their use. Semi-landmarks were digitized from photographs using the ‘Draw background curves’ tool in
583 the software tpsDig2 (Rohlf, 2015) to capture a detailed outline of the structure; this was then resampled

584 to contain a consistent number of equally spaced points which were used for alignment. See Fig. S1 for
585 configurations of landmarks in GM characters. Semi-landmarks were subjected to sliding and Procrustes
586 superimposition to minimize distances between configurations using the R package Geomorph (Adams &
587 Otárola-Castillo, 2013). In TNT, landmark configurations were scaled to unity using the command '*lmark*
588 *rescale = *;*'. Whole configurations of landmarks were used for optimization and to calculate support
589 values, rather than a pairwise approach with each individual landmark, as semi-landmarks define curves
590 and not homologous points.

591
592 **Discrete characters.** Characters consisting of continuous measurements such as ratios were discretized
593 into character states using primarily quantitative, but also qualitative approaches; all measurements from
594 all referred specimens were sorted numerically and character state divisions were introduced where gaps
595 occurred in their sequence. Where no substantial gaps occurred character states were introduced at points
596 between substantial transitions in the data. For example: in a hypothetical dataset of four taxa, A–D, each
597 represented by four specimens which all occupy a 0–10 continuous scale for one of their characters, if all
598 or a substantial majority of specimens from taxa A and B sit between zero and five, whereas those of taxa
599 C and D sit between five and ten, the continuous character range would be divided into two character
600 states at number five. This therefore splits the continuous range into discrete states in the absence of gaps.

601 This treatment was designed to mimic the presumably qualitative techniques for dividing
602 continuous data into discrete states used in previous analyses (although the delimitation technique has
603 never been described in any previous phytosaur phylogeny), and represents a similar treatment to the
604 'arbitrary' method of García-Cruz and Sosa (2006). Discrete characters used as counterparts to implicitly
605 ordered continuous characters were also treated as ordered. This means that different topologies resulting

606 from different combinations of character types reflect changes in character coding approach rather than
607 differences in the approach to character ordering.

608

609 **Implied weighting.** Implied weighting (Goloboff, 1993) is a method of character weighting in which the
610 number of step changes a character undergoes in its current tree topology is compared to the minimum
611 possible for that character, as a metric for homoplasy. Each character in a tree topology is then weighted
612 in inverse proportion to its level of homoplasy, with a concavity constant (k) ascribing the severity of
613 weighting. These weighted scores of ‘character fit’ are then summed to provide an estimate of character
614 fit for the whole tree; each tree topology in the analysis undergoes the same procedure, with the ‘best’
615 overall tree(s) having the best character fit score. We primarily use implied weights here for its apparent
616 advantages in the analysis of matrices high in homoplasy (Goloboff *et al.*, 2008a); a problem well-
617 recognized in Phytosauria (Hungerbühler, 1998, 2002). Although implied weighting has been criticized
618 recently (Congreve & Lamsdell, 2016) it does also have advantages when using continuous and GM
619 character scorings. Continuous characters may be measured on different scales, and this difference in
620 scaling is transferred to a character’s step-matrix (arbitrarily increasing the impact of ‘large-scale’
621 characters); accordingly, homoplasy in characters measured on large scales tends to be greater and these
622 characters are thus down-weighted in proportion with this (Goloboff, Mattoni & Quinteros, 2006). In this
623 study we further address issues of scaling by standardizing continuous character ranges into a 0–1 range,
624 as described above. Implied weighting also provides a method for weighting landmark-based characters
625 and can be performed either for each individual landmark within a configuration or for whole
626 configurations using the average homoplasy. The latter method is particularly useful in this study as we
627 use semilandmarks; as such the individual landmarks do not necessarily represent homologous points,

rather it is the overall structure that is important - it is therefore the whole configuration of landmarks that should be treated as a single character for weighting.

Analyses

All analyses were performed in the software TNT version 1.5 (Goloboff & Catalano, 2016), under extended implied weighting with the concavity constant 'k' set to vary for each character depending on the quantity of missing entries (using '*xpiwe* (*)' commands). Implied weighting requires the minimum possible length for each character coding in order to calculate homoplasy; however, this is problematic in landmark data (Goloboff *et al.*, 2016). Therefore, TNT provides an option to find minimum values for each landmark using heuristic searches; this search function was applied before analysing any dataset incorporating GM characters, then the minima were added to the file for use during tree searching. Furthermore, GM characters were each weighted separately according to the average homoplasy of their landmark configuration (using '*xpiwe* [' commands); therefore, weighting was based on entire configurations rather than the sum of component landmarks, which as stated above, may not be individually homologous.

Analysis parameters. Tree searches were performed using the new technology algorithms in TNT: 10,000 random addition sequences, analysed using TBR swapping with 10 iterations of drift and ratchet, followed by a sectorial search and finally three rounds of tree fusing. The search was performed until the minimum tree length was hit five times. The duration of tree searches dramatically increased with the addition of GM characters; therefore, only 200 random addition sequences were used and minimum length was found only once. Furthermore, because landmark data is relatively unstructured the perturbation phases of ratchet and drifting can produce trees that are 'too suboptimal' and therefore

651 greatly increase the search time (Goloboff *et al.*, 2016). We therefore followed the suggestion of Goloboff
652 *et al.* (2016) and increased the drift 'xfactor' to 5, decreased the percentage of swapping to be completed
653 to 90%, decreased the number of substitutions to 45, and for ratchet, lowered the probability of
654 reweighting (both up and down) to 3 and decreased the number of substitutions to 30.

655 Bremer supports were calculated using 10,000 (D and DC) or 1000 (DM and DCM) trees
656 suboptimal by a fit of 10; branch swapping using TBR was performed and absolute supports were
657 calculated based on the results. Robusticity analysis was carried out using symmetric frequencies, with
658 TBR swapping beginning from 10 Wagner trees and 10,000 (D, DC) or 100 (DM, DCM) replicates. As
659 the matrices including GM data were exceptionally computationally heavy and time consuming,
660 parameters were altered such that trees were accepted without consideration of error margin during
661 landmark searches and that swapping distance for branch swapping was reduced (commands respectively:
662 '*lmark errmarg 0*' and '*bbreak : limit 5*').

663
664 **Output processing and comparisons.** Where more than one tree of best character fit resulted from an
665 analysis, a strict consensus was generated. With implied weighting in effect, ties in tree length (resulting
666 in multiple best fitting trees) become very uncommon due to the use of floating-point character-fit
667 calculations. Additionally, continuous data are analysed as actual numerical differences, rather than
668 categorical steps, also reducing the chance of exact ties. To avoid over-resolution due to the acceptance of
669 a single or few trees showing only an extremely small difference in character fit compared to other
670 topologies, an arbitrary Bremer support cut-off value of 0.08 was implemented, below which nodes were
671 judged to be poorly supported and were collapsed. In addition a second cut-off value was used (0.11)
672 which was equal to the average step-length of a single character following weighting. This particular
673 number was used in an attempt to emulate the procedure common in phylogenetics, to collapse nodes with

674 a Bremer support of less than one step. These cut-offs were maintained throughout the four treatments,
675 allowing the effects on tree resolution to be compared.

676 Best character fit trees resulting from each of the four analyses using different combinations of
677 character data types (see above) were compared using several techniques. CI and RI were compared to
678 assess the homoplasy present in the trees resulting from each analysis. Maximum agreement subtrees were
679 constructed for each comparison to compare the number of congruent relationships between the trees; this
680 was supplemented with a strict consensus of the two trees in case lower level congruence was masked in
681 the agreement subtree by higher level polytomies (Goloboff, Mattoni & Quinteros, 2006). Subtree pruning
682 and regrafting (SPR) distances were calculated to find the minimum number of changes under the SPR
683 search algorithm required to convert one tree topology into the other - essentially a numerical description
684 of tree similarity. The rooted Robinson-Foulds (RF) distance, which measures the differential
685 presence/absence of phylogenetic relationships between trees, was also used to measure tree-similarity.

686 The effect of each coding technique was assessed and compared to its alternative counterparts in
687 several ways. Trees were initially compared using mean and summed frequency and Bremer supports
688 across each collapsed tree, alongside the number of nodes retained after collapsing each tree to get a broad
689 view of any major differences. For a more detailed view of the effects of data type on the nodal support
690 each non-collapsed best fit tree was split into five tree-regions; 1) the most basal portion of the tree,
691 including all non-Mystriosuchinae members of Phytosauria; 2) the clade formed by *Rutiodon* and
692 *Angistorhinus*; 3) *Leptosuchus*-grade taxa, here composed of all *Leptosuchus*, *Smilosuchus* and
693 *Nicrosaurus* species, plus PEFO 34852, '*Phytosaurus*' *doughtyi*, *Pravusuchus hortus* and *Coburgosuchus*
694 *goeckeli*; 4) all members of *Machaeroprotopus* and '*Redondasaurus*', plus USNM V 17098, NMMNHS-
695 P 4256, NMMNHS-P 31094 and *Protome batalaria*; 5) the clade composed of named species of
696 *Mystriosuchus* plus NHMW 1986 0024 0001 and MB.R. 2747. The mean frequency and Bremer supports

697 were calculated within each region to investigate the effects of different character coding techniques at a
698 greater resolution.

699 The support for monophyly of groups/taxa of interest was investigated by placing them in
700 alternative positions in a constraint tree, then re-running the analysis whilst imposing those constraints
701 and observing the effect on character fit in the resulting trees.

702 The accuracy of trees, as denoted by the various nodal support metrics and comparisons described
703 above, is a measure of internal consistency; regardless of a tree's accuracy it may still be spurious.

704 Stratigraphic congruence was used here as an independent estimate of tree-validity; four metrics were
705 employed which measure stratigraphic congruence differently. (1) The stratigraphic consistency index
706 (SCI) (Huelsenbeck, 1994) measures the proportion of nodes within which the first appearance datum is
707 of the same age or younger than the sister node; these nodes are considered stratigraphically consistent.
708 (2) The relative completeness index (RCI) (Benton & Storrs, 1994) reports the ratio between the sum of
709 ranges for taxa in the tree and the sum of ghost-range length within the tree. (3) The Manhattan
710 stratigraphic measure (MSM*) (Siddall, 1998; Pol & Norell, 2001) optimizes the difference in age
711 between the first appearances of taxa (Manhattan distance) as a Sankoff character on the proposed tree.
712 The MSM is the ratio between the minimum possible tree length based on taxon ranges (topology
713 determined by the Manhattan distance character), and the tree length when Manhattan distance is
714 optimized to the original topology. The MSM is basically the consistency index of the distance character
715 (Pol & Norell, 2006). Pol & Norell (2001) introduced a correction to prevent reversals in the Manhattan
716 distance character 'states', presenting the updated metric, MSM*. (4) The gap excess ratio (GER) (Wills,
717 1999) finds the proportion of ghost range in a tree, relative to the minimum and maximum possible sum of
718 ghost ranges for the corresponding dataset. It also optimizes age range differences on the tree in the same

719 manner as the MSM*, but is calculated as the retention index for the distance character (Pol & Norell,
720 2006).

721 The 'strap' package (Bell & Lloyd, 2014) for the software R version 3.2.5 (R Core Team, 2016)
722 implements all the above metrics, and was used for all analyses of stratigraphic congruence in this study.
723 The strap package also implements a test of statistical significance for each metric, based on random
724 permutations. In calculating significance values we made use of two additional options offered by strap:
725 the first is to generate random trees by swapping OTUs, whilst maintaining tree shape; the second is to fix
726 the outgroup OTU such that it is not randomized. These additions respectively resolve issues of random
727 trees being more symmetrical than commonly found in fossil groups (Wills, Barrett & Heathcote, 2008),
728 and the deliberate assignment of the outgroup prior to analysis, removing the need for its position to be
729 tested (Bell & Lloyd, 2014). The random trees therefore provide a closer estimate of the original tree
730 topology and a more robust test of significance (Bell & Lloyd, 2014). Primarily the P-values from the
731 significance tests are used here for comparisons of stratigraphic congruence, rather than the raw metrics,
732 as the latter are strongly influenced by tree balance, the arrangement of taxon stratigraphic ranges and tree
733 size (Siddall, 1996; Willis, 1999). The results of randomization tests are free from these influences and
734 should therefore be more directly comparable (Wills, 1999; Benton, Hitchin & Wills, 1999).

735 In this study significance tests were carried out with 1000 random permutations. The strict
736 consensus trees resulting from the four data treatments were analysed, as were the three most recent
737 alternative phylogenetic hypotheses of phytosaur relationships (Parker & Irmis, 2006; Hungerbühler *et al.*,
738 2013; Kammerer *et al.*, 2015). Where a previous analysis included specimen-level OTUs or taxa not
739 present in this study, these terminals were removed; three terminals were removed from the tree of
740 Kammerer *et al.* (2015) and two from Hungerbühler *et al.* (2013). Three alternate hypotheses of topology
741 were presented by Hungerbühler *et al.* (2013), though with the two terminals missing from this analysis

742 removed, two of the trees become synonymous; therefore, only two hypotheses are tested here from
743 Hungerbühler *et al.* (2013).

744

745 **Results**

746

747 A total of eight best fit trees were found across all four coding variants; in each of the D and DC
748 treatments three equally ‘fitting’ trees were found, whereas DM and DCM each returned only one best fit
749 tree. Our results are presented as the strict consensus trees of the best fit trees or single best fit trees
750 resulting from each of the four different variants of character coding (D, DC, DM and DCM) with
751 absolute and relative symmetric resampling frequencies above nodes, and Bremer supports below (Figs.
752 4–7). We also present the strict consensus and maximum agreement subtree of these four trees, to
753 summarize the most consistent relationships across all coding treatments (Fig. 8).

754 The tree lengths resulting from the four coding treatments are summarized in Table 3, as are the
755 consistency and retention indices (CI and RI). Tree lengths are not directly comparable between
756 treatments including or excluding GM coding; this arises because the morphology encoded in some GM
757 characters encompasses more than one discretely coded character. Therefore, analyses incorporating GM
758 data contain fewer characters than the other scoring types and will likely show lower tree lengths as a
759 result.

760 Conversely, providing that continuous characters replace their corresponding discrete characters
761 with one-to-one equivalence (which they do here), their alternative coding method alone should not affect
762 tree length. Continuous characters are here scored as ratios and are transformed to occupy a 0–1 scale; the
763 standard treatment of continuous characters by TNT uses the numerical differences between scores to
764 create the step-matrix. As these values are constantly below 1 it may be expected that the greater

765 proportion of continuous characters in a dataset would result in lower tree length. However, due to our use
766 of implied weighting this should not present a problem, as tree length is the sum of homoplasy-adjusted
767 character weight. Homoplasy is, in the simplest sense, calculated as a proportion of the minimum length
768 of a character in topology X, and the minimum possible length of a character in any topology. Character
769 weight is then calculated from this proportion (homoplasy) and is then summed across all characters to
770 generate tree length. As character weight is based on a character-specific proportion, the actual size of
771 changes in the character step-matrix should not affect the final tree length. Simply put, if equivalent
772 discrete and continuous characters share a consistent proportion of homoplasy, their effect on tree-length
773 under implied weighting will be identical regardless of how they are scored.

774

775 **Comparisons of similarity**

776 Comparisons of trees are presented in Tables 4 and 5, using the number of taxa retained by maximum
777 agreement subtrees, the SPR distance and the RF distance as metrics of similarity. Maximum agreement
778 subtrees essentially produce fully resolved consensus trees by pruning taxa in conflict between the input
779 trees; the number of taxa retained in a maximum agreement subtree can be used as a measure of
780 topological similarity between two or more trees.

781 All four trees were found to be significantly similar to each other. For all pairwise comparisons
782 between different coding treatments the number of taxa retained in the maximum agreement subtrees was
783 statistically much greater than expected by chance. Statistical significance was established using 5,000
784 agreement subtrees constructed with randomized tree topologies. None of these subtrees retained more
785 than 14 OTUs and subtrees retaining the highest number of OTUs (14) comprised only 0.96% of the data.
786 All pairwise comparisons yielded multiple maximum agreement subtrees of the same length showing
787 alternative prunings (Table 4).

788 The two coding treatments that utilized continuous data (DC and DCM: Figs. 5, 7) were
789 consistently found to be the most similar tree topologies using all similarity metrics. The trees generated
790 from discrete and discrete + GM coding treatments (D and DM: Figs. 4, 6) also showed a high degree of
791 similarity to each other. However, there is greatly reduced similarity when the DC/DCM trees are
792 compared with the D/DM trees. Broadly speaking, this suggests there are two partially conflicting
793 phylogenetic hypotheses, one represented by the DC and DCM trees and one by the D and DM trees.
794 However, the agreement subtrees suggest that the amount of overlap between these hypotheses is still
795 greater than would be expected to occur by chance.

796

797 **Consistent relationships**

798 A list of nodal synapomorphies for each tree is presented in Appendix 3. The following relationships were
799 found to be consistent in the trees of all four scoring treatments, and match the topology of the strict
800 consensus tree (Fig. 8).

801 *Diandongosuchus* is recovered as the most basal phytosaur in every tree. Its position outside of all
802 other phytosaurs is supported well by frequency and Bremer supports, and two consistent synapomorphies
803 supporting Parasuchidae (Fig. 8, node B) to the exclusion of *D. fuyuanensis* in every tree [13: 0→1; 22:
804 0→1].

805 *Wannia scurriensis* is consistently found as the most basal member of Parasuchidae, outside the
806 clade that includes *Parasuchus* and *Mystriosuchinae*. The latter clade (Fig. 8, node C) is, however, poorly
807 supported, with only two synapomorphies supporting *Parasuchus* + *Mystriosuchinae* to the exclusion of
808 *Wannia* in all four trees [36: 0→1; 69: 0→1].

809 *Parasuchus* (Fig. 8, node D) is consistently found to include the species *Parasuchus bransoni*,
810 *Parasuchus hislopi*, and *Parasuchus angustifrons*, and is well supported by frequency and Bremer scores,
811 with three synapomorphies common to all trees [23: 0→1; 26: 0→1; 50: 0→1].

812 ‘*Paleorhinus*’ *parvus*, ‘*Paleorhinus*’ *sawini* and *Ebrachosuchus neukami* are closer to
813 *Mystriosuchinae* than to *Parasuchus* in all trees; however, the interrelationships of these species and their
814 exact relationships to *Mystriosuchinae* are variable in the different coding treatments. *Mystriosuchinae*
815 itself (Fig. 8, node G) is supported by three synapomorphies common to all trees [9: 0→1; 14: 1→2; 80:
816 0→1].

817 *Rutiodon carolinensis* and *Angistorhinus* form a clade at the base of *Mystriosuchinae* that is
818 consistently well supported by frequency and Bremer supports (Fig. 8, node H) and is united by two
819 synapomorphies in all trees [22: 2→1; 92: 0→1]. Within this clade, *Rutiodon* is consistently the sister
820 taxon to *Angistorhinus*; the clade composed of *Angistorhinus* and *Angistorhinus*-like specimens, to the
821 exclusion of *Rutiodon carolinensis* (Fig. 8, node I), is supported by two synapomorphies [56: 0→1; 58:
822 0→1]. The relationships of the species and specimen-level OTUs within *Angistorhinus* are consistent in
823 all coding treatments: *A. talanti* is the most basal of the two named species and *A. grandis* is more
824 derived, with the specimen-level OTUs representing either potential additional species within the genus,
825 or morphologically diverse representatives of existing *Angistorhinus* species.

826 *Leptosuchomorpha* (Fig. 8, node M) possesses two synapomorphies common to all tree topologies
827 that separate it from the more basal taxa [16: 1→0; 25: 0→1]. Within *Leptosuchomorpha* the four
828 phylogenies are more variable (Fig. 8, node M). Among the leptosuchomorph OTUs not included in
829 *Mystriosuchini* there is only one clade common to all tree topologies: the clade which unites *Nicrosaurus*
830 *kapffi* and *Nicrosaurus meyeri* with *Coburgosuchus goeckeli*, although the relationships between these

three species are variable in the different coding treatments (Fig. 8, node N). This clade is supported by a single synapomorphy [57: 1→2].

Although there are conflicting relationships, the majority of the leptosuchomorph taxa that have been excluded from Mystriosuchini by previous analyses (e.g., Kammerer *et al.*, 2015) are also consistently excluded from Mystriosuchini as defined in the current analysis (with *Mystriosuchus planirostris*, *Machaeroprotopus jablonskiae* and *Machaeroprotopus buceros* as exemplars of the clade; see Table 2). Non-Mystriosuchini leptosuchomorphs in this analysis include all members of *Smilosuchus*, *Leptosuchus* and *Nicrosaurus* plus ‘*Phytosaurus*’ *doughty*, *Pravusuchus hortus*, *Coburgosuchus goeckeli* and PEFO 34852, as well as *Protome* in some of the coding treatments (see below).

There is only one synapomorphy of Mystriosuchini common to all trees (Fig. 8, node O) [43: 2→0]. Much like the non-Mystriosuchini leptosuchomorphs, interrelationships within Mystriosuchini are generally inconsistent across the different coding treatments; however, as in previous analyses, the clade includes all named species of *Machaeroprotopus*, ‘*Redondasaurus*’ and *Mystriosuchus*, as well as USNM v 17098, NMMNHS P4256, NMMNHS P31094, MB.R. 2747 and NHMW 1986 0024 0001. *Protome batalaria* has been placed close to *Rutiodon* by previous studies (Stocker, 2012; Butler *et al.*, 2014; Kammerer *et al.*, 2015). In this study it is consistently found to be either nested just inside Mystriosuchini (Fig. 4, Fig. 6) or as the sister taxon to this clade (Fig. 5, Fig. 7).

Within Mystriosuchini, *Mystriosuchus* (Fig. 8, node P) is the only consistently supported clade. Within this clade MB. R. 2747 and NHMW 1986 0024 0001 form successive sister taxa to *Mystriosuchus planirostris* and *Mystriosuchus westphali*; it is likely that these two specimen-level OTUs also represent unnamed species of *Mystriosuchus*. *Mystriosuchus* and its internal nodes are statistically well supported. The basal node of the clade and the internal nodes are each supported by single synapomorphies common to all trees (Fig. 8, node P) [85: 1→0], (Fig. 8, node Q) [2: 1→2], (Fig. 8, node R) [88: 0→1].

Commented [WGP12]: What is supporting this placement? What ever it is would finally show that overall squamosal morphology (i.e. isolated squamosals) cannot be used to separate Leptosuchus/Smilosuchus from Machaeroprotopus as utilized by Ballew, Long & Murry, Parker and Irmis, etc.... Protome has a Smilosuchus/Leptosuchus type squamosal.

854

855 **Conflicting relationships**

856 As discussed above, relationships among the non-Mystriosuchinae taxa are almost entirely
857 consistent across all four trees with the exception of ‘*Paleorhinus*’ *parvus*, ‘*Paleorhinus*’ *sawini* and
858 *Ebrachosuchus neukami* (Fig. 8). The relationships between these taxa are poorly supported statistically
859 and variable, and the three form a polytomy together with Mystriosuchinae in the strict consensus trees of
860 the D and DC analyses (Figs. 4, 5). In the DM and DCM analyses (Figs. 6, 7) the relationships are
861 consistent, if not well supported. ‘*Paleorhinus*’ *parvus* is the sister taxon of Mystriosuchinae, with
862 *Ebrachosuchus neukami* and ‘*Paleorhinus*’ *sawini* forming successively more distant sister groups.

863 Those non-Mystriosuchini members of Leptosuchomorpha in this analysis comprise species
864 assigned to the genera *Smilosuchus*, *Leptosuchus*, ‘*Phytosaurus*’, *Pravusuchus*, *Nicrosaurus* and
865 *Coburgosuchus*. Relationships between these taxa are entirely consistent in the DC and DCM trees (Figs.
866 5, 7). However, the D and DM trees each show different topologies (Figs. 4, 6). In the DC and DCM trees,
867 ‘*Smilosuchus*’ *lithodendrorum* is the most basal taxon in Leptosuchomorpha. Within Leptosuchomorpha
868 there are two clades: one containing all species of *Leptosuchus* and *Nicrosaurus*, in addition to
869 *Pravusuchus hortus*, *Coburgosuchus goeckeli* and PEFO 34852; and one containing ‘*Phytosaurus*’
870 *doughtyi*, *Smilosuchus adamanensis*, *Smilosuchus gregorii*, *Protome* and Mystriosuchini.

871 In the D tree, all the aforementioned taxa with the exception of *Smilosuchus gregorii* form an
872 unnamed clade (Fig. 4, node 14), which forms a sister relationship within Leptosuchomorpha with
873 *Smilosuchus gregorii* + Mystriosuchini. The basalmost taxon within this unnamed clade is *Smilosuchus*
874 *adamanensis*, which in the other three trees presented here is recovered as a branch just basal to *S.*
875 *gregorii*; the next taxon in the clade, ‘*Phytosaurus*’ *doughtyi*, also falls closer to *S. gregorii* than
876 *Leptosuchus* in the DC, DM and DCM trees. Above ‘*Phytosaurus*’ *doughtyi*, two distinct clades are

877 present as sister taxa. One of these (Fig. 4, node 17) contains *Leptosuchus* spp., plus '*Smilosuchus*'
878 *lithodendrorum* and PEFO 34852; the second (Fig. 4, node 20) contains *Pravusuchus hortus*, *Nicrosaurus*
879 spp. and *Coburgosuchus goeckeli*. Relationships in both clades have weak Bremer support, with the
880 exception of the node uniting *Nicrosaurus kapffi*, *N. meyeri* and *C. goeckeli* (Fig. 4, node 21), in which
881 frequency supports are generally better.

882 The topology for this region of the DM tree is very different from that of the D tree (to which it is
883 very similar in most other respects). The taxa that form a distinct clade in the D tree (Fig. 4, node 14)
884 instead form a largely pectinate series of outgroups to *Mystriosuchini* in the DM tree (Fig. 6, nodes 15–
885 25). The most basally branching taxon is *Leptosuchus studeri*, which falls outside of *Leptosuchomorpha*
886 in this tree. At the base of *Leptosuchomorpha* is a relatively poorly supported (according to frequency
887 supports) clade including '*Phytosaurus*' *doughtyi*, *Leptosuchus crosbiensis*, and a sister taxon relationship
888 between '*Smilosuchus*' *lithodendrorum* and PEFO 34852 (Fig. 6, node 17). *Pravusuchus hortus*,
889 *Smilosuchus adamanensis* and *Smilosuchus gregorii* form a series of outgroups to a clade consisting of
890 *Mystriosuchini* and the *Nicrosaurus* + *Coburgosuchus* clade. In the DM tree the *Nicrosaurus* species are
891 sister taxa (Fig. 6, node 25). In this topology, *Nicrosaurus* occupies a position consistent with that
892 recovered in previous analyses of *Mystriosuchini* (Hungerbühler, 2002; Hungerbühler *et al.*, 2013) and
893 with the group's previous definition (Kammerer *et al.*, 2015).

894 The main inconsistency within *Mystriosuchini* is the fluctuating position of the *Mystriosuchus*
895 clade (*Mystriosuchus* spp. plus NHMW 1986 0024 0001 and MB. R. 2747). In both trees incorporating
896 continuously scored data (DC, DCM) this group is recovered as highly derived within *Mystriosuchini*
897 (Figs. 5, 7), as has previously been found by Stocker (2010, 2012, 2013), Butler *et al.* (2014) and
898 Kammerer *et al.* (2015) (Figs. 2B; 3A, B). In the D and DM coding treatments, however, the
899 *Mystriosuchus* clade forms the sister group to *Protome batalaria* + *Machaeroprotopus* (Figs. 4, 6), as has

900 been found by Hungerbühler (2002), Parker and Irmis (2006) and Hungerbühler *et al.* (2013) (Figs. 1A;
901 2A, C).

902 Relationships among other species within Mystriosuchini are highly variable, though the general
903 pattern is of a highly ladderred series of sequentially more derived terminals. Although the order of OTUs
904 varies considerably, there are some similarities across different coding treatments; taxa in the less derived
905 positions are generally *Protome batalaria* and *Machaeroprosoopus andersoni*, which are then followed by
906 *Machaeroprosoopus pristinus*, *Machaeroprosoopus buceros* and *Machaeroprosoopus lottorum* and then a
907 clade containing both species of ‘*Redondasaurus*’ (Fig. S2).

908 As previously mentioned, the two conflicting hypotheses regarding the position of *Mystriosuchus*
909 (basal or derived within Mystriosuchini) split the results of the four coding methods into two alternative
910 topological hypotheses. The positions of *Machaeroprosoopus mccauleyi* and *Machaeroprosoopus*
911 *jablonskiae* also consistently differ between these topologies. In the trees in which *Mystriosuchus*
912 occupies a derived position within Mystriosuchini (DC, DCM), *Machaeroprosoopus mccauleyi* and
913 *Machaeroprosoopus jablonskiae* form successive sister taxa, basal to the clade comprising
914 *Machaeroprosoopus pristinus*, *Machaeroprosoopus buceros* and *Mystriosuchus*. In topologies where
915 *Mystriosuchus* is recovered basal to *Machaeroprosoopus* (D, DM), *Machaeroprosoopus mccauleyi* and
916 *Machaeroprosoopus jablonskiae* are more derived than the clade composed of *Machaeroprosoopus*
917 *pristinus*, *Machaeroprosoopus buceros* and *Machaeroprosoopus lottorum*, forming successive sister taxa to
918 ‘*Redondasaurus*’.

919 The position of *Machaeroprosoopus zunii* is more consistent; in three trees (D, DC and DM) it is
920 recovered basal to the clade composed of *Machaeroprosoopus pristinus*, *Machaeroprosoopus buceros*, and
921 all more derived taxa. In the DCM results *Machaeroprosoopus zunii* is placed more derived than than

922 *Machaeroprosoopus pristinus* and *Machaeroprosoopus buceros*, but less derived than *Machaeroprosoopus*
923 *lottorum*.

924 *Machaeroprosoopus lottorum* is another taxon which varies consistently between the two broad
925 topological hypotheses presented. In the trees incorporating continuously scored data, in which
926 *Mystriosuchus* is highly derived (DC, DCM), *Machaeroprosoopus lottorum* forms a clade with NMMNHS-
927 P 31094 (Figs. 5, 7), closely related to ‘*Redondasaurus*’ and *Mystriosuchus*, as was found by
928 Hungerbühler *et al.* (2013). In the alternative topologies (D, DM) *Machaeroprosoopus lottorum* nests with
929 *Machaeroprosoopus pristinus*, to the exclusion of *Machaeroprosoopus buceros* (Figs. 4, 6). Both positions
930 are similarly poorly supported by Bremer analyses, but possess relatively good frequency scores. In this
931 topology NMMNHS-P 31094 is consistently found within ‘*Redondasaurus*’, as the sister taxon of
932 ‘*Redondasaurus*’ *gregorii*, to the exclusion of ‘*Redondasaurus*’ *bermani*.

933

934 **Accuracy and validity**

935 **Bremer supports.** With poorly supported nodes collapsed below Bremer values of 0.08, the DM
936 condition produced greatest tree resolution, retaining 23 nodes; however, its mean Bremer score is one of
937 the lowest among the four trees, suggesting that the additional nodes supported in this tree only exceed the
938 cut-off by a small amount (Table 6). When using the mean step length of a single character (0.11) as a cut-
939 off for node-collapsing, the DM and DCM conditions were found to perform more poorly than the D and
940 DC conditions in terms of nodes retained and total Bremer support. Mean Bremer values for the retained
941 nodes remained almost consistent across all trees (Table 6).

942 When broken down into regions, it appears that the extra support in the DM tree is added in
943 regions three and four, which are almost consistently the worst supported in all trees. Despite this extra

Commented [WGP13]: Does not support proposed conspecific hypothesis for *M. pristinus* and *M. buceros* as sexual dimorphs.

944 support, relationships within these regions are still relatively poorly supported in the DM condition, and
945 the support for region one also becomes among the poorest in both GM trees (DM and DCM) (Table 7).

946 The best condition for overall Bremer support was the DC tree (Fig. 5), achieving the highest, or
947 equal highest support in all regions except three and four, with a sum of mean support equalling 0.75.
948 Conversely, despite maximizing support in the poorest regions of the tree, the DM condition scored
949 second worst for overall support, with a sum total of 0.60; this was followed by the DCM condition with a
950 score of 0.58 (Table 7).

951
952 **Frequency supports.** With a cut-off for node collapsing of <10, symmetric frequency support produced
953 broadly similar results for all the trees, with the DC condition producing a marginally higher resolution
954 and mean support value. Conversely to the results from Bremer supports, the DM condition was the
955 poorest supported topology based on symmetric resampling, although the difference between ‘best’ and
956 ‘worst’ is minor (Table 6).

957 Split into regions, the overall sum of mean supports follows the same trend as that of the Bremer
958 supports; DC is best, with a sum of 240.56, then D (229.47), DM (213.16) and finally DCM (199.11). The
959 DC tree holds the highest mean support compared to the other trees in regions one, three and five. The
960 DM tree only holds the highest support value in region four; however this is one of the two poorest
961 supported regions (three and four), and is therefore important in achieving the best possible resolution in
962 all parts of the tree (Table 8).

963
964 **Stratigraphic congruence.** All tree topologies recovered under the four data conditions tested in this
965 analysis were found to be significantly better correlated with stratigraphy than would be expected of
966 random data. Among the raw results from each correlation metric, there is no consistent trend indicating

one or more of the four topologies are optimal. The SCI metric suggests the D and DM topologies (in which *Mystriosuchus* is basal to *Machaeroprotopus*) to be better stratigraphically correlated than the DC and DCM topologies (in which *Mystriosuchus* is the most derived member of Mystriosuchini); however, this finding is not borne out by any other metric. Among the other three metrics the only consistent trend is the slightly worse performance of the two datasets incorporating GM characters (DM and DCM); however, the difference in fit is almost negligible (Table 9).

The previous phylogenetic analyses of Parker & Irmis (2006) and Kammerer *et al.* (2015) (based respectively on the original matrices of Hungerbühler [2002] and Stocker [2010]), also correlate well with the stratigraphic data used in this study, generally achieving significance values equal to those of the current study. The topologies of Hungerbühler *et al.* (2013) were found to correlate poorly with stratigraphy and were not statistically differentiable from random data; however the analysis of Hungerbühler *et al.* (2013) focuses only on one area of the tree, roughly corresponding to ‘region four’ in this study. This region is poorly supported in terms of accuracy and robusticity. The poor stratigraphic correlation of the analysis of Hungerbühler *et al.* (2013) may indicate that this region has poor stratigraphic support, but this is masked in the stratigraphic correlations of other studies by good correlation overall in other areas of the tree.

983

984 **Tree choice**

In order to carry out further investigations into the effects of alternative, or previously reported topologies, it was decided to select only two of the four topologies presented above to avoid unnecessarily long comparisons of fit between multiple alternative taxonomic relationships within multiple tree topologies. As there is a general dichotomy in tree topology within the four trees, it would be inappropriate to arbitrarily favour one topology over the other, so a representative of each topology was chosen.

990 The DC condition exhibits an almost identical topology to the DCM condition, but consistently
991 outperforms the latter in the various robusticity analyses described above. Comparisons of topological
992 similarity do not assist in selecting one of these topologies over the other as they are shown to be almost
993 identical, with neither being more representative of all topologies.

994 The D and DM conditions are less similar to each other than are the DC and DCM conditions,
995 though they show largely the same topology. Between the Bremer and frequency analyses the D and DM
996 conditions outperform each other in various aspects; when the trees are regionalized the DM condition
997 generally provides slightly better support in the worst-supported areas of the tree, but is poorly supported
998 in most other areas. The sum of Robinson-Foulds distances for the D tree in comparison to all others
999 suggests that it is the most representative topology of the four trees recovered in this study; this was never
1000 found to be the case with the DM topology.

1001 Ultimately the D and DC trees (Figs. 4, 5) were selected for further analysis based partially on the
1002 above metrics, but partially due to the relative difficulty of undertaking multiple further GM analyses.
1003 Continuous and discrete characters boast substantial advantages in analysis duration, and the comparative
1004 simplicity of data acquisition and processing, over GM characters. Because of these reasons continuous
1005 and discrete data are far more accessible and provide a better basis on which future studies can build.

1006

1007 **Alternative taxonomic relationships**

1008 The consistent recovery of a sister-relationship between *Rutiodon carolinensis* and the genus
1009 *Angistorhinus* makes the decision of whether or not to synonymize these taxa entirely arbitrary (see
1010 below); therefore, to test for their synonymy would also be meaningless and as such these taxa were
1011 excluded from these analyses.

1012 *Nicrosaurus* was previously found as the basal-most member of Mystriosuchini (Hungerbühler,
1013 2002; Hungerbühler *et al.*, 2013) and was therefore used as an internal specifier for the previous
1014 phylogenetic definition of the clade (Kammerer *et al.*, 2016); however, as described in the introduction
1015 little data has been provided to support this. Here we find *Nicrosaurus* to group closer to *Leptosuchus* than
1016 to *Mystriosuchus* or *Machaeroprotopus*, and thus outside of Mystriosuchini according to our redefinition
1017 of the clade (Table 2). We tested the previously proposed position of *Nicrosaurus*, i.e. as the most basal
1018 group within Mystriosuchini (Kammerer *et al.*, 2016). To achieve this, the clade of *Nicrosaurus* and
1019 *Coburgosuchus* was constrained to its previous position in relation to Mystriosuchini, such that all
1020 members of *Machaeroprotopus* and *Mystriosuchus* fell in a more derived position. Additionally
1021 *Pravusuchus hortus* was constrained as the basal sister taxon to *Nicrosaurus*, *Coburgosuchus* and
1022 Mystriosuchini, to replicate the previous hypothesis that *Pravusuchus* is the immediate sister taxon to
1023 Mystriosuchini (Stocker, 2010). Under these topological constraints tree character fit worsened by 0.693
1024 in the D condition, and 1.013 in the DC condition.

1025 The tree topology resulting from the D condition places *Mystriosuchus* as the sister clade to
1026 *Machaeroprotopus*; for this analysis we constrained *Mystriosuchus* to nest within *Machaeroprotopus* as
1027 found by Stocker (2010), although its exact position within the clade was left flexible. Under this
1028 condition the tree-fit worsens by 0.584. In contrast, in the DC condition *Mystriosuchus* was found to
1029 occupy a position within the *Machaeroprotopus* clade; therefore, we constrained it as sister to this clade,
1030 leading to a decline in tree fit by 0.714.

1031 Unlike the findings of Hungerbühler *et al.* (2013), in our phylogenies the two species of
1032 ‘*Redondasaurus*’ do appear to form a sister taxon relationship; however, in accordance with their findings
1033 and those of other studies (Ballew, 1989; Hungerbühler, Chatterjee & Cunningham, 2003; Stocker, 2010;
1034 Butler *et al.*, 2014; Kammerer *et al.*, 2015) ‘*Redondasaurus*’ remains nested within *Machaeroprotopus*.

Commented [WGP14]: For Pseudopalatinae.

1035 When the two genera are forced into a sister group relationship the tree fit deteriorated considerably by a
1036 score of 0.857 under the D condition, and 1.004 in the DC condition.

1037

1038 **Discussion**

1039

1040 **Higher-level taxonomy**

1041 The recently revived family-level name Parasuchidae Lydekker, 1885, (Kammerer *et al.*, 2015) was
1042 suggested by Stocker *et al.* (2017) to exclude the proposed basal phytosaur *Diandongosuchus fuyuanensis*.
1043 Our analysis corroborates the hypothesis of Stocker *et al.* (2017) that *Diandongosuchus* is the most basal
1044 phytosaur, and the only taxon to fall outside of Parasuchidae but within Phytosauria using current
1045 definitions.

1046 The taxonomic content of Mystriosuchinae von Huene, 1915, defined as the last common ancestor
1047 of *Angistorhinus grandis* and *Mystriosuchus planirostris* and all its descendants by Kammerer *et al.*
1048 (2015), is largely compatible between the phylogenetic hypotheses presented here and that presented by
1049 Kammerer *et al.* (2015). However, in the phylogeny of Kammerer *et al.* (2015) ‘*Paleorhinus*’ *sawini* falls
1050 within Mystriosuchinae whereas here it is excluded from this clade.

1051 Stocker (2010) erected the clade Leptosuchomorpha, defined as the most recent common ancestor
1052 of *Leptosuchus studei* and *Machaeroprotopus pristinus*, and all descendants thereof. In the D and DM
1053 trees presented here this definition is perfectly compatible with previous definitions of the clade; however
1054 in the DC and DCM conditions ‘*Smilosuchus*’ *lithodendrorum* is recovered in a more basal position than
1055 all other previous members of Leptosuchomorpha, and would thus be excluded from the group based on
1056 the definition of Stocker (2010), despite exhibiting numerous similarities with other members. We
1057 therefore redefine Leptosuchomorpha such that it includes the latest common ancestor of ‘*Smilosuchus*’

1058 *lithodendrorum*, *Leptosuchus studeri* and *Machaeroprotopus pristinus*, and all of its descendants (Table
1059 2). In addition, *Protome batalaria* and '*Machaeroprotopus*' *zunii* are consistently recovered within
1060 Leptosuchomorpha in the analyses presented here, whereas they were previously excluded (Stocker, 2010;
1061 Butler *et al.*, 2014; Kammerer *et al.*, 2015).

1062 The definition of Mystriosuchini von Huene, 1915 proposed by Kammerer *et al.* (2015) is
1063 problematic with regard to the results presented here, due to our general result that *Nicrosaurus* is deeply
1064 nested with taxa such as *Leptosuchus* and *Smilosuchus* that are traditionally excluded from
1065 Mystriosuchini. This problem is especially pronounced in the D tree (Fig. 4), in which the previous
1066 definition of Mystriosuchini renders the group entirely synonymous with Leptosuchomorpha; the DC and
1067 DCM trees produce a very similar result, though excluding '*Smilosuchus*' *lithodendrorum* from
1068 Mystriosuchini (Figs. 5, 7). In the DM tree (Fig. 6) the taxonomic content of Mystriosuchini using the
1069 previous phylogenetic definition is essentially the same as in previous studies, with the inclusion of a few
1070 additional taxa such as *Protome batalaria*.

1071 To resolve this taxonomic issue we propose that *Nicrosaurus kapffi* is removed from the definition
1072 of Mystriosuchini due to its conflicting phylogenetic position, and is replaced with *Machaeroprotopus*
1073 *jablonskiae* to stabilize the taxonomic content of the clade (see above; Table 2). Without the addition of
1074 *Machaeroprotopus jablonskiae* as a specifier, *Machaeroprotopus mccauleyi* and *Machaeroprotopus*
1075 *jablonskiae* would be variably excluded from Mystriosuchini, despite consistent previous findings of their
1076 inclusion in the clade. A number of other taxa would also be variably included in Mystriosuchini, leading
1077 to increased instability of the clade.

1078 *Machaeroprotopus jablonskiae* is recovered in a similar position to that found by previous
1079 phylogenetic analyses (Parker & Irmis, 2006; Hungerbühler *et al.*, 2013; Butler *et al.*, 2014; Kammerer *et*
1080 *al.*, 2015) in all of our trees. In the DC and DCM trees *Machaeroprotopus jablonskiae* is recovered as one

1081 of the most basal taxa within *Machaeroprosoopus* (Figs. 5, 7), as in the studies of Parker & Irmis (2006)
1082 and Hungerbühler *et al.* (2013) (Fig. 2A,C). In the D and DM trees *Machaeroprosoopus jablonskiae* is
1083 placed in a more derived position in the *Machaeroprosoopus* clade (Figs. 4, 6), similar to the findings of
1084 Butler *et al.* (2014) and Kammerer *et al.* (2015) (Fig. 3A,B); however, as this coincides with the migration
1085 of *Mystriosuchus* to a more basal position with respect to *Machaeroprosoopus*, the taxa retained in
1086 Mystriosuchini remain largely identical among our four trees. Crucially, *Machaeroprosoopus jablonskiae*
1087 consistently nests within Mystriosuchini in previous studies (Parker & Irmis, 2006; Hungerbühler *et al.*,
1088 2013; Butler *et al.*, 2014; Kammerer *et al.*, 2015), and in this sense our proposed definition errs on the
1089 side of caution in ensuring the definition of Mystriosuchini used here is as compatible as possible with the
1090 phylogenetic topologies of previous studies. This being the first investigation of this dataset, it seems
1091 likely that future analyses of this data could disagree with our findings, in which case a definition that
1092 maximizes compatibility between recent studies may be the most useful. We therefore tentatively suggest
1093 Mystriosuchini should henceforth be defined as the most recent common ancestor of *Mystriosuchus*
1094 *planirostris*, *Machaeroprosoopus jablonskiae* and *Machaeroprosoopus buceros*, and all its common
1095 ancestors (Table 2).

1096

1097 **Lower-level taxonomy**

1098 **Synonymy of *Rutiodon* and *Angistorhinus*.** The results of this analysis depart from both previously
1099 proposed hypotheses of the relative phylogenetic positions of these taxa: that *Rutiodon* occupies a derived
1100 position within the monophyletic clade of *Angistorhinus* (Hungerbühler and Sues, 2001), or that *Rutiodon*
1101 sits in a more derived position than *Angistorhinus*, closer to *Leptosuchus* (Hungerbühler, 1998; Stocker,
1102 2010). Supporting character data was not provided for the proposal of synonymy made by Hungerbühler
1103 & Sues (2001), which was published in an abstract only. In our results the two taxa form a monophyletic

1104 group, supported by two synapomorphies common to all four best-fit trees [22: 2→1; 92: 0→1]. However,
1105 the fact that *Rutiodon* consistently forms the sister group to *Angistorhinus* makes the decision of whether
1106 or not to synonymize the genera entirely arbitrary. Unfortunately we were unable to study any material of
1107 *Brachysuchus megalodon*, which has been suggested to be synonymous with *Angistorhinus* (Long &
1108 Murry, 1995), but which was also found to be distinct by Stocker (2010).

1109
1110 ***Angistorhinus*.** In her discussion of the relationships of *Angistorhinus*, Stocker (2010) advocated the
1111 necessity for future in-depth analysis of *Angistorhinus* and its affinities. We do not present a detailed
1112 analysis or redescription of any species within *Angistorhinus*; however, our analysis is only the second to
1113 include more than one species (Hungerbühler, 1998), and the first to incorporate further specimens that
1114 have been identified previously as *Angistorhinus*. Our results provide a stable and consistently well-
1115 supported phylogenetic position for *Angistorhinus* that future descriptive and taxonomic work can build
1116 on. Furthermore we provide additional synapomorphies for both the *Angistorhinus* clade, and
1117 relationships within it.

1118 The *Angistorhinus* clade (Figs. 4, 5, node 9; Figs. 6, 7, node 11) is distinguished by two
1119 unambiguous synapomorphies common to all trees, pertaining to the parietal/squamosal bars being
1120 medially convex, and at least as wide as the postorbital/squamosal bars [56: 0→1; 58: 0→1]. Both of
1121 these characters have previously been suggested to be diagnostic features of *Angistorhinus* Mehl, 1913
1122 (Mehl, 1915; Gregory, 1962; Stocker, 2010) or ‘Angistorhininae’ Camp, 1930 (Long & Murry, 1995).

1123 The next most inclusive clade contains *Angistorhinus talanti*, *A. grandis*, TMM 31100-1332 and
1124 USNM V 21376. This group is distinguished by the presence of a sulcus running longitudinally along the
1125 postorbital/squamosal bar [42: 0→1], and the partial or total squaring of the medial rim of the
1126 postorbital/squamosal bar and posterior process [51: 0→1].

1127 The next most inclusive clade excludes *A. talaini*, leaving only *A. grandis*, TMM 31100-1332 and
1128 USNM V 21376. This clade is well supported by four unambiguous synapomorphies, though within the
1129 clade the basal-most member (TMM 31100-1332) shows no autapomorphies and the sister grouping of *A.*
1130 *grandis* with USNM V 21376 is supported by only one synapomorphy [69: 2→1] and displays poor
1131 support values. Given the strong support for the wider clade, but the relatively poor differentiation of the
1132 OTUs within it, there may be a case for referring both TMM 31100-1332 and USNM V 21376 to *A.*
1133 *grandis*. The synapomorphies of this clade are: the division of the narial openings into an anterior
1134 ‘anteriorly opening’ section and a posterior ‘dorsally opening’ section [12: 0→1]; the raising of the
1135 external nares above the level of the skull roof [17: 0→1]; the posttemporal fenestra being moderately
1136 wide and dorsoventrally compressed [66: 0→1]; and the presence of an anteroposteriorly oriented ridge
1137 on the midline of the basioccipital between the basitubera [70: 0→1].

1138 Based on these results we suggest *A. grandis* to be one of the most derived members of
1139 *Angistorhinus*, and *A. talaini* to be less derived. At face value there does not appear to be any clear
1140 relationship between palaeogeography and phylogeny; *A. talaini*, from Morocco, nests amongst the
1141 specimens known from the west and south central USA. This finding should be expected as these
1142 locations were placed at broadly similar palaeolatitudes and were closely connected in the Late Triassic.

1143
1144 **Monophyly of *Leptosuchus*.** Stocker (2010) found a strongly supported monophyletic relationship
1145 between *Leptosuchus crosbiensis* and *Leptosuchus studeri*; here, we found almost all nodes relating to
1146 *Leptosuchus*-grade taxa were extremely poorly supported in each tree. Only in the D tree did we find an
1147 arrangement approaching a monophyletic *Leptosuchus* (Fig. 4, node 17), though with the addition of
1148 ‘*Smilosuchus lithodendrorum*’ and PEFO 34852 as a sister clade to *L. crosbiensis*. In the DC and DCM
1149 trees *Leptosuchus studeri* forms the sister group to a clade containing *Leptosuchus crosbiensis*, but also

1150 *Pravusuchus*, *Coburgosuchus* and *Nicrosaurus* (Fig. 5, node 15; Fig. 7, node 17). Support values are
1151 generally poor. In the DM tree *Leptosuchus*-grade taxa occur as a paraphyletic grade of sequentially more
1152 derived branches (Fig. 6).

1153 Stocker (2010) found one synapomorphy to support the monophyly of *Leptosuchus* and one
1154 further potential apomorphy under DELTRAN optimization.

1155 *Distal end of paroccipital process of opisthotic rounded, distal edge is curved rather than straight*
1156 (36: 1→2). This character was excluded from analysis here as the associated morphology appears to be
1157 highly variable both inter- and intraspecifically, is often subject to damage, and scoring may change
1158 depending on small differences in viewing angle.

1159 *Jugal contributing to antorbital fenestra (4: 0→1) (potential apomorphy under DELTRAN)*. In our
1160 analysis this character state is optimized as basal to the entire tree, and is found in the vast majority of
1161 taxa. In this position the character does not provide unambiguous support for the monophyly of
1162 *Leptosuchus*.

1163

1164 **Monophyly of *Smilosuchus*.** The previously proposed taxonomic content of *Smilosuchus* is not
1165 monophyletic in any of our best-fit trees. In the D tree (Fig. 4) all three species are found in different
1166 locations: *S. adamanensis* forms the basal-most taxon in a clade containing all leptosuchomorph taxa
1167 excluded from Mystriosuchini except *S. gregorii* (Fig. 4, node 14); '*S.* *lithodendrorum*' is deeply nested
1168 within this group, forming a close relationship with *Leptosuchus crosbiensis* (Fig. 4, node 18); *S. gregorii*
1169 forms its own distinct branch forming a sister relationship with Mystriosuchini (Fig. 4, node 23).

1170 In none of the trees presented here does '*Smilosuchus*' *lithodendrorum* form a close relationship
1171 with any other member of *Smilosuchus*. Instead, its relationships are divergent, being recovered in two
1172 trees as the most basal member of the newly defined Leptosuchomorpha (DC & DCM; Figs. 5, 7) and in

1173 the other two nesting closely with *Leptosuchus crosbiensis* (D & DM; Figs. 4, 6). The similarity to
1174 *Leptosuchus crosbiensis* has previously been noticed, leading Long & Murry (1995) to regard 'S'.
1175 *lithodendrorum* as a junior synonym of the former taxon, though without a written justification (see
1176 Appendix 1 for more details). We do not here revise the taxonomy of 'S'. *lithodendrorum*, as the
1177 instability of its position does not allow any consistent hypothesis of its relationships to be reached.
1178 Instead, we consider the phylogenetic position of this taxon as uncertain pending a more detailed
1179 investigation into its similarity to *L. crosbiensis*.

1180 In Stocker's (2010) analysis, the monophyly of *Smilosuchus* was supported on the basis of two
1181 synapomorphies and a further possible apomorphy under ACCTRAN optimization.

1182 *Ventral margin of squamosal gently sloping anteroventrally from posterior edge of posterior*
1183 *process to opisthotic process (28: 1→0)*. In contrast to the scorings of Stocker (2010), no specimen of 'S'.
1184 *lithodendrorum* was found with a gently sloping posteroventral squamosal margin. This state was,
1185 however, found to be present in both *S. adamanensis* and *S. gregorii*. The latter taxon displays
1186 polymorphism for this character as AMNH D. VP. 3060 displays a morphology that is neither a gentle
1187 slope, nor a sharp shelf, but sits somewhere between.

1188 In the D and DM trees (Figs. 4, 6) *S. adamanensis* and *S. gregorii* apparently gain this character
1189 state (0) independently, though because the latter taxon is polymorphic for this character, the ancestral
1190 state (1) is partially retained. In the DC and DCM trees (Figs. 5, 7) the ancestral state is polymorphic;
1191 therefore, depending on the tree in question this character is either partially consistent or inconsistent with
1192 the hypothesis of monophyly between *S. adamanensis* and *S. gregorii*.

1193 Interestingly, if *S. gregorii* is scored as '0' rather than as polymorphic, both taxa consistently form
1194 a monophyly in the D tree, whereas they were previously relatively distant phylogenetically from each
1195 other. This was also tested in the DC tree (which shares the same relative phylogenetic positions of *S.*

1196 *adamanensis* and *S. gregorii* as in the DM and DCM trees). However, the phylogenetic positions of these
1197 two taxa were not modified, and state ‘0’ was also reconstructed as ancestral to the clade including
1198 *Protome batalaria* and *Mystriosuchini*.

1199 *Squamosal fossa extends to posterior edge of squamosal* (30: 1→0). The scores for this character
1200 in the current analysis are inconsistent with those of Stocker (2010); we observed a polymorphic state in
1201 both ‘*S. lithodendrorum*’ (TMM 31173-121: 0; UCMP 26688: 1) and *S. gregorii* (UCMP 27200: 0;
1202 AMNH 3060: 1). Our character optimization is inconsistent with the hypothesis of a monophyletic
1203 *Smilosuchus*, given that character state ‘0’ is ancestral to the majority of taxa (excluding many basal taxa
1204 for which the character is inapplicable and most species of *Machaeroprotopus*) in all four of our trees.

1205 *Lateral border of posttemporal fenestra formed by the contact of the parietal process of the*
1206 *squamosal and the paroccipital process of the opisthotic* (37: 1→0) (potential apomorphy under
1207 ACCTRAN). Our scoring for this character differs from that of Stocker (2010); we concur that ‘*S.*
1208 *lithodendrorum*’ displays state ‘0’, whereas both *S. adamanensis* and *S. gregorii* are scored as possessing a
1209 thin lamina of squamosal that slightly undercuts the border of the fenestra ventrolaterally (character state
1210 ‘2’). The latter condition is ancestral to both species of *S. adamanensis* and *S. gregorii*, all species of
1211 *Machaeroprotopus* and closely related taxa in all four trees (though in the D tree the ancestral state is
1212 polymorphic ‘0, 2’). In trees D, DC and DCM character state ‘2’ independently characterizes the clade
1213 formed by *Nicrosaurus* and *Coburgosuchus*. Character state ‘0’ is the ancestral condition for
1214 ‘*Smilosuchus*’ *lithodendrorum* in all four trees presented here. None of the optimizations of this character
1215 presented here support the monophyly of *Smilosuchus*.

1216
1217 **Position of *Pravusuchus hortus*.** *Pravusuchus hortus* has previously been indirectly implied to
1218 potentially form a close relationship with *Nicrosaurus*: *Pravusuchus* was found to form the immediate

Commented [WGP15]: Is this really *S. lithodendrorum*?
Based on whose assessment?

1219 outgroup to Mystriosuchini by Stocker (2010), while *Nicrosaurus* has long been hypothesized to form a
1220 close relationship with *Mystriosuchus* and *Machaeroprotopus* (Ballew, 1989) as the most basal taxon
1221 within Mystriosuchini (Long & Murry, 1995; Hungerbühler, 2002; Parker & Irmis, 2006; Hungerbühler *et*
1222 *al.*, 2013). Thus our a priori assumption was that these taxa would be closely related. Our results
1223 corroborate this view, with *Pravusuchus* forming the outgroup to a clade containing *Nicrosaurus* and
1224 *Coburgosuchus* in three of the four analyses (D, DC, DCM); however, these taxa are found here to nest
1225 deeply within a clade of non-Mystriosuchini leptosuchomorph taxa in all but the DM analysis.

1226 The analysis of Stocker (2010) identified a single synapomorphy in support of a clade containing
1227 *Pravusuchus*, *Machaeroprotopus mccauleyi*, *Machaeroprotopus pristinus* and *Mystriosuchus westphali*.
1228 In the three trees in which *Pravusuchus* is the immediate outgroup of *Nicrosaurus* we found two
1229 consistent synapomorphies supporting the clade of *Pravusuchus*, *Nicrosaurus* and *Coburgosuchus*:
1230 presence of an infranasal recess, and absence of a furrow or ridge on the lateral surface of the
1231 squamosal/post-orbital bar [21: 0→1; 29: 1→0]. The synapomorphy identified by Stocker (2010) is
1232 discussed below.

1233 *Subsidiary opisthotic process of the squamosal present (29: 0→1)*. Our scores for this character
1234 are partially inconsistent with those of Stocker (2010); we found *Pravusuchus* to be polymorphic for this
1235 character (PEFO 31218: 0; AMNH FR. 30646:1), as was the case in *Machaeroprotopus mccauleyi*
1236 (UCMP 126999: 0; PEFO 31219: 1), *Machaeroprotopus pristinus* (PEFO 382: 0; MU 525: 1; AMNH FR.
1237 7222: 1; NMMNHS P50040: 1), and *Mystriosuchus westphali* (AMNH FR. 10644: 0; GPIT 261/001: 1).

1238 In all four trees presented here, the most exclusive clade that contains *Pravusuchus* is not
1239 supported by the synapomorphy of Stocker (2010); instead, character optimization finds the absence of
1240 the subsidiary opisthotic process [47: 0] to be symplesiomorphic for this clade. Here we find that the
1241 presence of a subsidiary opisthotic process of the squamosal [47: 1] primarily optimizes in two alternative

Commented [WGP16]: Preservation?

positions depending on tree topology. In the D and DM trees (in which *Mystriosuchus* is basal within Mystriosuchini), the presence of this character is a synapomorphy of the clade formed by USNM v 17098 and all more derived taxa. This clade includes *Machaeroprotopus mccauleyi* and *Machaeroprotopus pristinus*, but excludes *Mystriosuchus westphali* and *Pravusuchus hortus*. Therefore in these topologies, this synapomorphy is partially consistent with the aforementioned clade of Stocker (2010), though fundamentally excludes *Pravusuchus* and therefore does not provide support for its position in our trees. In the DC and DCM trees (in which *Mystriosuchus westphali* occupies a more derived position within the *Machaeroprotopus* clade), the presence of a subsidiary opisthotic process is optimized as polymorphic for the clade that includes *Machaeroprotopus mccauleyi* and all more derived taxa (including *Machaeroprotopus pristinus* and *Mystriosuchus westphali*, but excluding *Pravusuchus*). At the node one step more derived, (thus excluding *Machaeroprotopus mccauleyi*) the character is optimized as ‘present’ (1) however cannot be regarded as a synapomorphy due to the uncertain optimization of the previous node. This is also partially consistent with the optimization of this character by Stocker (2010); however, the clade supported by this character state excludes *Pravusuchus*, and is inconsistent with the phylogenetic hypothesis of Stocker (2010).

Position of *Nicrosaurus*. The most recent novel cladistic analysis to investigate the position of *Nicrosaurus* was that of Hungerbühler (2002). The analysis found *Nicrosaurus* as the sister taxon to a clade formed by *Mystriosuchus*, ‘*Redondasaurus*’ and *Machaeroprotopus* - congruent with the later definition of Mystriosuchini by Kammerer *et al.* (2015); however, no synapomorphies were reported in support of this clade.

In three of the four trees identified in this study (D, DC, DCM) *Nicrosaurus* groups more closely with a number of non-Mystriosuchini leptosuchomorph taxa than with Mystriosuchini. *Nicrosaurus*

differs from *Mystriosuchini* in all trees due to the possession of a relatively long free-section of the postorbital/squamosal bar, rather than a short bar as is synapomorphic for the latter clade [43: 2→0] (although *Nicrosaurus meyeri* independently acquires a short postorbital/squamosal bar). Character optimization suggests that the relatively long ‘free-section’ is plesiomorphic to almost all phytosaurs. This character therefore provides no support for the hypothesized position of *Nicrosaurus* suggested by Hungerbühler (2002).

Position of *Mystriosuchus*. The dichotomy of topologies regarding the position of *Mystriosuchus*, as presented in the results section, reflects the dichotomy seen in the literature. The two most recent hypotheses of the position of *Mystriosuchus*, based on independent datasets, are those of Hungerbühler (2002) and Stocker (2010), which respectively place *Mystriosuchus* in the less and more derived positions found in this analysis.

Less derived position. In the analysis of Hungerbühler (2002), the clade in which *Mystriosuchus* is the basal member is diagnosed with three synapomorphies.

Presence of a pre-infratemporal shelf (18: 1). We find this character in three trees (D, DC, DCM) to be a synapomorphy of the clade containing *Mystriosuchus*, ‘*Redondasaurus*’ and many members of *Machaeroprotopus* - generally matching the clade membership of *Mystriosuchini* as it was previously defined in both Hungerbühler (2002) and Stocker (2010). This character is therefore largely unaffected by the placement of *Mystriosuchus*, and thus supports both hypotheses.

Presence of the pre-infratemporal shelf is restricted in our analysis almost exclusively to the clade discussed above, however this character state independently arises as a polymorphic state in *Nicrosaurus* and *Pravusuchus*, and also in *Parasuchus hislopi*.

1288 *Presence of a parietal ledge (21: 2).* This character was not included in this analysis as the
1289 morphology described is dependent on the morphology of the depressed squamosal processes of the
1290 parietal, which is scored elsewhere (character 75). The morphology of this area of the skull is partially
1291 considered in character 74, which scores the ratio of width to length of the parietals between the
1292 supratemporal fenestrae. Regardless, this morphology appears to be present in all leptosuchomorph
1293 phytosaurs, and would thus be unlikely to support the clade detailed above.

1294 *Parieto/squamosal bar is strongly depressed (23: 2).* We find this character to be synapomorphic
1295 for a more inclusive group than that of Hungerbühler (2002), consisting of *Smilosuchus gregorii*,
1296 *Mystriosuchus planirostris*, their common ancestor and all its descendants [49: 1→2]. In three of the trees
1297 presented here (D, DC and DCM) this transformation independently occurs in *Nicrosaurus* and
1298 *Coburgosuchus*, whereas in the DM tree *Nicrosaurus* and *Coburgosuchus* are included in the clade
1299 described above. This character distribution therefore is not found here to support the clade described by
1300 Hungerbühler (2002).

1301 No synapomorphies were listed by Hungerbühler (2002) for the clade from which *Mystriosuchus*
1302 was immediately excluded; therefore, we are unable to comment of the consistency of our
1303 synapomorphies with those of Hungerbühler (2002), for a clade containing *Machaeroprotopus* and
1304 ‘*Redondasaurus*’ but excluding *Mystriosuchus*. The characters supporting this phylogenetic arrangement
1305 in our study are detailed in the results section.

1306

1307 **More derived position.** Stocker (2010) identified eight synapomorphies (and two potential
1308 synapomorphies under ACCTAN) supporting a clade consisting of *Machaeroprotopus mccauleyi*,
1309 *Machaeroprotopus pristinus* and *Mystriosuchus westphali*, which, in her analysis, represented
1310 Mystriosuchini.

1311 *Interpremaxillary fossa present - narrow slit (8: 1→2)*. Here this character state is restricted only
1312 to *Mystriosuchus* and NHMW 1986 0024 0001, which consistently sits within the same clade as
1313 *Mystriosuchus* (and probably represents an unnamed species within this this genus), and is a
1314 synapomorphy of the node uniting these taxa in all four trees [2: 1→2]. It therefore provides no support
1315 for the topology hypothesized by Stocker.

1316 *Alveolar ridges not visible in lateral view (9: 0→1)*. We find this character to optimize as a
1317 synapomorphy in multiple locations across our four trees; however, these are mostly inconsistent with
1318 Stocker's hypothesis of this character's optimization.

1319 In both trees which present the same topological hypothesis of the relationships of *Mystriosuchus*
1320 as Stocker (2010) (DC, DCM), this character is found as a synapomorphy of a clade containing
1321 *Machaeroprotopus pristinus*, *Machaeroprotopus buceros*, *Machaeroprotopus lottorum*, both species of
1322 'Redondasaurus', and *Mystriosuchus* [3: 0→1]. This synapomorphy, however, describes a morphological
1323 reversal, i.e. state 1→0, rather than 0→1 as suggested by Stocker. In the two trees in which *Mystriosuchus*
1324 occupies a more basal position (D, DM), this character is optimized as a 0→1 synapomorphy, as
1325 suggested by Stocker (2010), of a clade similar to that described above, though differing by containing all
1326 members of *Machaeroprotopus* and excluding *Mystriosuchus*. In summary, we find this character to
1327 contradict the hypothesized optimization of Stocker (2010), in that a 0→1 change is only found when
1328 *Mystriosuchus* is one of the sister taxa to *Machaeroprotopus*, rather than nesting within the clade.

1329 *Postorbital squamosal articulation approximately transverse (22: 1→2)*. The distribution of
1330 character state (2) is here restricted to members of *Machaeroprotopus*, *Mystriosuchus* and
1331 'Redondasaurus', though it twice arises independently in the *Leptosuchus*-grade OTUs PEFO 34852 and
1332 *Coburgosuchus*. Despite its restricted occurrence, this trait change [33: 1→2] is not optimized as a
1333 synapomorphy here, though the change from 0→1 is optimized in two trees (DC, DCM) as a

1334 synapomorphy of the node linking *Smilosuchus adamanensis* with all more derived members of
1335 Leptosuchomorpha. In the DM tree a 0→1 change is a defining feature of the most recent node linking the
1336 clade of *Nicrosaurus* and *Coburgosuchus* with all more derived members of Leptosuchomorpha.

1337 Although not optimized as a synapomorphy, the distribution of this character state is broadly
1338 supportive of not only the hypothesis of Stocker (2010), but also that of Hungerbühler (2002), as in both
1339 topologies, character state (2) is optimized as being plesiomorphic to the clade containing
1340 *Machaeroprotopus* and *Mystriosuchus*.

1341 *Lateral ridge from postorbital/squamosal bar continues strongly on lateral surface of squamosal*
1342 *as two raised ridges (23: 1→2)*. This character state was removed from the analysis as it could not be
1343 reliably identified in any species of phytosaur. A similar character state was added by Butler *et al.* (2014),
1344 referring specifically to the bifurcation of the lateral ridge in species of *Parasuchus*, though this state has
1345 not been observed in any other phytosaurs. Here we find the presence of a ridge to occur sporadically
1346 throughout the tree, though with a greater frequency in more derived members of *Machaeroprotopus*. In
1347 *Mystriosuchus* a ridge is only found as a polymorphism within *Mystriosuchus westphali*, and it is
1348 otherwise entirely absent within the genus. In topologies in which *Mystriosuchus* is a sister group of
1349 *Machaeroprotopus* the absence state is plesiomorphic to the group. When *Mystriosuchus* is found within
1350 *Machaeroprotopus*, the clade containing *Machaeroprotopus mccauleyi*, *Machaeroprotopus pristinus* and
1351 *Mystriosuchus westphali* is plesiomorphically polymorphic for this character. Furthermore, the presence
1352 of any form of ridge is only found as a synapomorphy of derived members of *Machaeroprotopus* in the D
1353 tree; in this topology *Mystriosuchus* is in any case excluded from the *Machaeroprotopus* clade.

1354 *Posterior process of squamosal dorsoventrally expanded in lateral view (25: 2→1)*. This character
1355 was altered to use the terminology of Ballew (1989) and Hungerbühler (2002) for the ‘knob-like’

1356 posterior process found in *Machaeroprotopus pristinus*, *Machaeroprotopus buceros* and some specimens
1357 of *Machaeroprotopus mccauleyi*; this was done to reduce ambiguity in character scoring.

1358 This character is not optimized as a synapomorphy of any node close to either the base of
1359 *Mystriosuchus* or *Machaeroprotopus* in any of the trees presented here. State (1) (which here refers to the
1360 same morphology as Stocker's character) is here found to be more frequent in derived members of
1361 *Machaeroprotopus*, (excluding *Machaeroprotopus pristinus* and *Machaeroprotopus buceros* which are
1362 characterized by a state change of 1→2) and is plesiomorphic for the clade. Although the general
1363 character distribution generally supports Stocker's (2010) topological hypothesis for all other members of
1364 Stocker's 'Pseudopalatus' clade, this character does not convey any information regarding the position of
1365 *Mystriosuchus* as the taxon lacks a posterior process and optimization of this character at the base of
1366 *Mystriosuchus* relies entirely on its position in the phylogeny. This character therefore provides no
1367 support for the inclusion of *Mystriosuchus* within *Machaeroprotopus*.

1368 *Supratemporal fenestrae fully depressed, posterior process of parietal and entire*
1369 *parietal/squamosal bar below level of skull roof (32: 1→2)*. Rather than forming a synapomorphy of only
1370 the *Mystriosuchini* clade used by Stocker (2010), we find this character to be synapomorphic for the node
1371 uniting *Smilosuchus gregorii* with all more derived taxa (D, DC: node 23; DM: node 22; DCM: node 25)
1372 [49: 1→2]. *Mystriosuchus* is included within this clade regardless of its position with respect to
1373 *Machaeroprotopus*, thus this character does not provide any support for the inclusion of *Mystriosuchus*
1374 within *Machaeroprotopus*.

1375 *Border of posttemporal fenestra formed laterally and slightly ventrally by process of squamosal*
1376 *that extends onto paroccipital process (37: 1→2)*. *Mystriosuchus* is scored here as polymorphic for this
1377 character. In the trees in which it occupies a more derived position *Mystriosuchus* forms a sister group to
1378 'Redondasaurus', which consistently displays character state (0); the plesiomorphic state is, in this

1379 situation, also polymorphic - providing only limited support for the hypothesis of a derived placement for
1380 *Mystriosuchus*. This character is more consistent here with the hypothesis that *Mystriosuchus* is sister to
1381 *Machaeroprotopus*, as character state (2) alone is plesiomorphic for *Mystriosuchus* in this position, and
1382 forms a synapomorphy in three of our trees (DC, DM and DCM) for the clade formed by all descendants
1383 of the common ancestor of *Smilosuchus adamanensis* and *Mystriosuchus planirostris* [67: 0→2].

1384 *Skull shape boxy in posterior view, width across squamosals approximately equal to width across*
1385 *ventral edge of quadrates (38: 1→0)*. This character was excluded in this analysis as it is extremely
1386 sensitive to taphonomic distortion, and is highly subjective. The most basal taxon in Mystriosuchini
1387 identified by Stocker (2010) is *Machaeroprotopus mccauleyi*, which contrary to Stocker's scoring would
1388 here be considered to possess a trapezoidal skull shape, as would *Machaeroprotopus buceros* and all taxa
1389 in '*Redondasaurus*', none of which were included in Stocker's analysis. Despite the exclusion of this
1390 character, the inclusion of multiple additional taxa in this analysis may have affected the optimization of
1391 synapomorphies in the clade.

1392 *Rostral crest present, continuous and sloping steeply anteroventrally from nares to terminal*
1393 *rosette (19: 0→1) (Possibly additional apomorphy under ACCTRAN)*. The above character was altered
1394 slightly in this analysis (Appendix 2); however, character state (1) of Stocker (2010) is still represented by
1395 character state (2) here. We find a wide range of synapomorphy optimizations of this character in our
1396 trees, none of which are consistent with the results of Stocker (2010).

1397 In the DCM tree a clade containing *Mystriosuchus*, '*Redondasaurus*' and more derived members
1398 of *Machaeroprotopus* are partially defined by this character as a synapomorphy; however,
1399 *Machaeroprotopus mccauleyi* is excluded from the group and the state transformation is from the
1400 presence of a steep, continuous slope posteriorly from the terminal rosette, to the presence of a narial crest

1401 - the relatively abrupt rise from a thin, tubular snout to the nares [7: 2→1]. Within this clade,
1402 ‘*Redondasaurus*’ undergoes a state reversal back to the morphology of a steep, continuous crest [7: 1→2].

1403 The D and DM trees both optimize this character as a synapomorphy of a clade including all
1404 species of *Machaeroprotopus* and ‘*Redondasaurus*’; in these trees, the state transformation is from the
1405 presence of a narial crest, to the presence of a partial rostral crest [7: 1→4]. A more exclusive clade within
1406 the former, containing *Machaeroprotopus mccauleyi*, *Machaeroprotopus jablonskiae* and
1407 ‘*Redondasaurus*’ again features this character as a synapomorphy, with a state change from a partial
1408 rostral crest, to presence of a continuous steep slope [7: 4→2]. *Mystriosuchus*, however, occurs in none of
1409 these clades in the two trees and this character is not found to support any relatively exclusive clade
1410 containing *Mystriosuchus*.

1411 In the DC tree this character is not found to define any clade in which *Mystriosuchus* is placed;
1412 within close proximity to *Mystriosuchus* the only clade featuring this as a synapomorphy is
1413 ‘*Redondasaurus*’, displaying a change from a narial crest to a continuous, steep rostral crest [7: 1→2].

1414 *Supratemporal fenestrae mostly covered/completely closed dorsally, at most only anteromedial*
1415 *corners of supratemporal fenestrae visible in dorsal view (33: 1→2) (Possible additional apomorphy*
1416 *under ACCTRAN)*. In the trees in which *Mystriosuchus* is recovered in a derived position this character
1417 was only found as a synapomorphy of the clade of *Mystriosuchus* + NHMW 1986 0024 0001 + MB.R.
1418 2747; specifically, the synapomorphy denotes a character transformation from state (2) to state (1) [57:
1419 2→1]. This does not provide support for the hypothesis of relationships within Mystriosuchini proposed
1420 by Stocker (2010); however, the majority of nodal optimizations and scorings for this character in the
1421 other members of Mystriosuchini (and for all those included in Stocker’s analysis), display character state
1422 (2). The state change observed by Stocker (2010) is likely not found here due to a polymorphic
1423 optimization of states (1) and (2) at the base of the *Machaeroprotopus* clade (*Machaeroprotopus*

Commented [WGP17]: Crest is not preserved in the holotype specimen.

1424 *andersoni* and all more derived taxa); at the node one step more derived (*Machaeroprotopus jablonskiae*
1425 and all more derived taxa) the character is optimized as state (2), as are the majority of following nodes. It
1426 is therefore likely that a state change of (1) to (2) [57: 1→2] is synapomorphic at the base of
1427 *Machaeroprotopus* which, in the DC and DCM topologies, is consistent with the phylogenetic hypothesis
1428 of Stocker's 'Mystriosuchini' clade.

1429 In the D and DM trees (i.e. where *Mystriosuchus* occupies a less derived position), this character is
1430 only optimized as a synapomorphy of 'Redondasaurus' + NMMNHS P31094, as a state change from the
1431 supratemporal fenestrae being mostly covered (state 2), to being fully covered (state 3). However, the
1432 synapomorphy suggested by Stocker (2010) is probably again suppressed due to two nodes optimized as
1433 polymorphisms bracketing the base of *Machaeroprotopus*. Using the D tree as an example: the two nodes
1434 directly basal to *Machaeroprotopus* (Fig. 4, nodes 28, 29) are optimized as state (1) and (1 or 2)
1435 respectively; in the following node (the most basal in *Machaeroprotopus* [node 30]), this character is
1436 again optimized as (1 or 2). In the next node (node 31) the character is optimized as state (2), as are the
1437 majority of other nodes within the clade. Therefore, we suggest that the topology in the D and DM trees is
1438 also mostly consistent with the reduction in supratemporal fenestra visibility identified by Stocker (2010),
1439 except that *Mystriosuchus* is excluded from the supported clade in the D and DM trees.

1440 Relatively few of the synapomorphies identified in previous analyses to support particular clades
1441 containing *Mystriosuchus* are corroborated here, despite the dichotomy of tree topologies presented in this
1442 analysis being broadly consistent with each of the previous studies discussed above.

1443
1444 **Monophyly of 'Redondasaurus'**
1445 'Redondasaurus' was originally diagnosed by Hunt & Lucas (1993) solely on the basis of the lack of
1446 visibility of the supratemporal fenestrae in dorsal view. The genus was re-diagnosed by Spielmann &

1447 Lucas (2012) with a broader complement of characters: 1) supratemporal fenestrae concealed in dorsal
1448 view; 2) reduced antorbital fenestrae; 3) a prominent pre-infratemporal shelf at the anteroventral margin
1449 of the lateral temporal fenestra; 4) septomaxillae wrap around the outer margin of the external narial
1450 opening; 5) thickened orbital margin; 6) inflated posterior nasal behind the external narial opening; 7)
1451 thickened dorsal osteoderms.

1452 Hungerbühler *et al.* (2013) were unable to recover ‘*Redondasaurus*’ *gregorii* and ‘*Redondasaurus*’
1453 *bermani* as a monophyletic group in any of their trees; however, we find a monophyletic ‘*Redondasaurus*’
1454 (albeit nested within *Machaeroprotopus*) in all of our trees. Many of the characters proposed by
1455 Spielmann & Lucas (2012) were not implemented in the analysis of Hungerbühler *et al.* (2013); however,
1456 in this analysis we included some of these characters that were used in previous phylogenetic studies and
1457 independently identified others which overlap to a considerable extent with those proposed
1458 synapomorphies of ‘*Redondasaurus*’. The consistency of the characters included in our analysis with the
1459 hypothesis of a monophyletic ‘*Redondasaurus*’ are discussed below.

1460 *Supratemporal fenestrae concealed in dorsal view.* As was briefly mentioned above, this character
1461 is found as a synapomorphy of the ‘*Redondasaurus*’ clade in all trees presented in this study [57: 2→3],
1462 and is therefore entirely consistent with the hypothesis of Hunt & Lucas (1993). This character state
1463 occurs in no other taxon, though is found in NMMNHS P31094 (referred to ‘*Redondasaurus*’ *gregorii* by
1464 Spielmann & Lucas 2012), which in the D and DM trees is included within the ‘*Redondasaurus*’ clade,
1465 but in the other trees is recovered as the sister taxon of *Machaeroprotopus lottorum*, the character state
1466 having arisen independently of ‘*Redondasaurus*’.

1467 *Anteriormost border of pre-infratemporal shelf terminates anterior of the posteriormost corner of*
1468 *the antorbital fenestra.* The presence of this character state is restricted almost entirely to
1469 ‘*Redondasaurus*’ and *Mystriosuchus*; unsurprisingly, where these two groups form a clade this character

1470 is consistently optimized as a synapomorphy. However, in the D and DM trees, where *Mystriosuchus* is
1471 placed basally, distant from ‘*Redondasaurus*’, the character only constitutes a synapomorphy for
1472 *Mystriosuchus* rather than ‘*Redondasaurus*’; this may be due to the polymorphic condition of
1473 ‘*Redondasaurus*’ *gregorii* for this character. Despite this inconsistency between trees the distribution of
1474 this character still broadly supports a monophyletic ‘*Redondasaurus*’.

1475 The diagnostic characters proposed by Spielmann & Lucas (2012) for ‘*Redondasaurus*’ but not
1476 included in our analysis are discussed briefly below. We agree that several of these support a sister taxon
1477 relationship between ‘*Redondasaurus*’ *gregorii* and ‘*Redondasaurus*’ *bermani*, and are therefore
1478 consistent with our results.

1479 *Reduced antorbital fenestrae*. Whether or not the antorbital fenestrae are substantially reduced
1480 may be subjective; in more robust specimens of ‘*Redondasaurus*’ (NMMNHS P-4256) the antorbital
1481 fenestra does appear smaller than in closely related taxa. However, in more gracile specimens (YPM
1482 3294) the fenestra appears similar in proportions to those of other phytosaurs such as *Mystriosuchus*. The
1483 antorbital fenestrae do appear to exhibit a unique shape in most specimens of ‘*Redondasaurus*’; the
1484 general shape is roughly triangular, as is common in *Mystriosuchus* and *Machaeroprotopus*, but the
1485 anterior- and posterior-most corners of the fenestra are sharp angles, rather than smooth curves.

1486 *Septomaxillae wrap around the outer margin of the external narial opening*. No taxon studied was
1487 observed to possess ‘septomaxillae’ that extend onto the lateral surface of the external nares. Stocker
1488 (2010) noted the presence of this character state in ‘*Redondasaurus*’ and suggested it may also occur in
1489 *Pravusuchus hortus*; however, upon inspection of the holotype and referred specimens of *Pravusuchus*
1490 *hortus* it seems equally likely that the morphology described by Stocker pertains to cracks on the
1491 holotype, with the true sutures covered by iron oxide. Rather than a lateral extension of the

1492 ‘septomaxillae’ the feature identified in ‘*Redondasaurus*’ and *Pravusuchus* may represent the paranasals,
1493 identified in *Machaeroprotopus lottorum* by Hungerbühler *et al.* (2013).

1494 *Thickened orbital margin.* We here concur with Spielmann & Lucas (2012); in all specimens of
1495 ‘*Redondasaurus*’ examined by us, the descending process of the postorbital appears to be greatly
1496 thickened to an extent not seen in any other group. For this particular character Spielmann & Lucas (2012)
1497 suggested it is also shared with *Coburgosuchus*; however, we see no observable expansion of the
1498 postorbital in the latter taxon to distinguish it from the condition present in most other phytosaurs. The
1499 descending process of the postorbital in *Coburgosuchus* has a roughly rectangular cross-section, with the
1500 external face relatively thin, but facing anterolaterally. If Spielmann and Lucas (2010) measured this
1501 feature in *Coburgosuchus* diagonally between the anterolateral and posteromedial corners (i.e. the full
1502 width observable in direct lateral view), this could account for the increased width, especially given the
1503 oblique angle of the process in direct lateral view. As this morphology is measured in all other taxa based
1504 on only the flat lateral-most face of the descending process, this procedure should also be applied here to
1505 preserve homology within the character.

1506 *Inflated posterior nasal behind the external narial opening.* Although this entire area of skull is
1507 missing in the type specimen of ‘*Redondasaurus*’ *gregorii* (YPM 3294), it is common to a variable extent
1508 in many other specimens referred to the genus by Spielmann & Lucas (2012). This feature is not,
1509 however, restricted to ‘*Redondasaurus*’, as the morphology of specimens from other taxa frequently
1510 overlap with the range of variation observed in ‘*Redondasaurus*’. Examples include: *Nicrosaurus kapffi*
1511 (SMNS 4379), *Machaeroprotopus mccauleyi* (PEFO 31219) and *Machaeroprotopus lottorum* (TTU-P
1512 10076). It may be valid to say that ‘*Redondasaurus*’ is the only taxon in which this character state
1513 consistently occurs; however, its variability makes the taxonomic utility of this feature unclear. Given the
1514 variable presence of this character in more than one species of *Machaeroprotopus*, this character is likely

1515 to support the hypothesis that ‘*Redondasaurus*’ is nested within *Machaeroprosoopus*, though verification
1516 would require the inclusion of this character in phylogenetic analyses.

1517 *Thickened dorsal osteoderms.* The osteoderms of some large phytosaur taxa are also strongly
1518 thickened, e.g.e.g. *Smilosuchus gregorii* (AMNH 3060); however, we have not carried out any
1519 sufficiently detailed study of osteoderms to fully assess this proposed synapomorphy. Until more detailed
1520 work emerges on phytosaur osteoderm variation we tentatively accept this character, though emphasize
1521 that potential size correlation should be borne in mind.

1522

1523 **Synonymy with *Machaeroprosoopus***

1524 Hungerbühler *et al.* (2013) presented three lines of reasoning in support of the synonymization of
1525 ‘*Redondasaurus*’ into *Machaeroprosoopus*. First, they argued that *Machaeroprosoopus lottorum* ‘bridges
1526 the morphological gap’ between other members of *Machaeroprosoopus* and ‘*Redondasaurus*’ *gregorii* and
1527 ‘*Redondasaurus*’ *bermani* in a number of features, and possesses a combination of characters formerly
1528 considered exclusive to one or other group. Second, in all trees recovered by Hungerbühler *et al.* (2013),
1529 both species of ‘*Redondasaurus*’ were found within the clade of *Machaeroprosoopus*; in analyses that were
1530 constrained to recover ‘*Redondasaurus*’ as a monophyletic sister group to *Machaeroprosoopus*, tree fit
1531 lengthened by five extra steps. Third, they did not find ‘*Redondasaurus*’ *gregorii* and ‘*Redondasaurus*’
1532 *bermani* to form a clade to the exclusion of species of *Machaeroprosoopus* in any of their trees; instead, the
1533 two taxa were interspersed with members of *Machaeroprosoopus*, with ‘*Redondasaurus*’ *gregorii* being
1534 recovered in a substantially more derived position than ‘*Redondasaurus*’ *bermani* in every tree.

1535 The first two points are consistent with our results; however, with regard to their third point we
1536 find the exact opposite - that these taxa are always monophyletic to the exclusion of species of
1537 *Machaeroprosoopus*. In all trees this clade is supported by two to four synapomorphies, with one

(supratemporal fenestra completely obscured in dorsal view) consistently present in all trees. Despite this, we agree with the suggestions of Long & Murry (1995) and Hungerbühler *et al.* (2013) that ‘*Redondasaurus*’ should be synonymized with *Machaeroprotopus*.

Effects of scoring method

CI and RI. The consistency indices calculated for the four character coding variables (D, DC, DM and DCM) were broadly similar; though as noted above, those which incorporated continuous data produced slightly better scores than the others. Regardless, all CI values displayed a significantly higher consistency than expected of random data (for a dataset of 43 taxa and between 90 and 94 characters), based on comparisons with simulated data in Klassen, Mooi & Locke (1991). Differences in the retention indices (RI) were marginal between all conditions, indicating that despite the increased homoplasy in GM datasets, the same proportion of synapomorphic information was retained as in datasets excluding GM data. As the RIs of the continuous and non-continuous datasets are almost identical, it is unlikely that the difference in homoplasy indicated by CI between the datasets can be ascribed to a greater proportion of uninformative or autapomorphic characters in the continuous dataset.

Tree length. When comparing the tree-length (weighted homoplasy) produced by datasets with equal numbers of characters, trees that incorporate continuous data are consistently shorter than those which exclude it. The D tree (94 characters) produced a tree-length of 31.90, whereas the DC tree (94 characters) produced a length of 27.46. Likewise, the DM tree (90 characters) recovered a length of 30.52, while the DCM (90 characters) tree-length was 25.44.

The effects of including GM data cannot be interpreted in the same way as above; the base D dataset contains more characters than the DM dataset, and we would therefore naturally assume that the

DM tree would be shorter just by virtue of having fewer characters. It is, however, possible to say that the continuous characters in this study do have a shortening effect on tree-length when compared to the standard discrete data tree (D vs DC tree-length). Furthermore, the incorporation of continuous data into the DM dataset (DM vs DCM tree-length) resulted in a greater reduction in tree length than was produced by the combined effect of incorporating GM data into the D dataset and the associated reduction in the number of characters (D vs DM). This may indicate that the continuous characters in this dataset produced a stronger influence on tree length than the GM characters. Additionally, as extended implied weighting was in effect the shorter tree lengths equate to reduced homoplasy. Considering the higher consistency index of the continuous datasets, it is unsurprising that the continuous datasets also produce the shortest tree lengths when compared to D and DM, as under implied weighting, the ‘length’ of each character is partially calculated using the same technique as the consistency index. The overall tree-length is an ensemble score of estimated homoplasy within the dataset - similarly the CI measures ensemble consistency.

Topological similarity. In analyses of topological similarity (maximum agreement subtrees, SPR distances and Robinson-Foulds distance) the DC tree differed from the base discrete data tree by 37.2%, 32.5% and by 0.45122 in each respective metric, whereas the DM tree only differed from the base tree by 23.3%, 15% and 0.23171 respectively. This suggests that the incorporation of continuous characters into the base dataset altered the topology of the output tree to a greater extent than by incorporating GM characters.

Within our overall dataset, continuous characters appear to exert a stronger influence on tree topology and tree length than GM characters, and the incorporation of continuous rather than GM

1583 characters produces a tree that is found to be slightly less homoplastic by consistency index and implied
1584 weighting.

1585 It should be noted that the elevated influence of continuous data may be related to variations in our
1586 dataset rather than an inherent property of the scoring method. For example, in the DC condition
1587 continuous data accounted for 10.64% of the characters used, but in the DM condition GM data only
1588 accounted for 5.56% of the total characters; therefore, continuous data may have more influence as it
1589 constituted a greater proportion of the data. Alternatively, it is possible that the characters scored as
1590 continuous data may, by chance, have been less homoplastic than those scored using GM techniques. It
1591 should also be noted that these two influences are not mutually exclusive.

1592
1593 **Support metrics.** A slightly different finding to the above was obtained when investigating Bremer and
1594 frequency supports. When collapsing nodes with Bremer scores less than that of the average character step
1595 length (0.11), the datasets incorporating GM data (DM and DCM) produced consistently poorer total
1596 Bremer support for the collapsed tree, and retained less nodes than the non-GM datasets (D and DC). The
1597 mean Bremer support values for nodes exceeding the cut-off were almost entirely consistent between all
1598 four data treatments, whereas at the lower cut-off (0.08) these means were more variable. This suggests
1599 that the cut-off of 0.11 largely retained the nodes for which the Bremer support values were more resistant
1600 to the effects of data treatment.

1601 In contrast to Bremer scores, frequency supports performed more consistently between scoring
1602 techniques in terms of number of nodes retained; however, similarly to the results of Bremer supports, the
1603 DCM treatment produced the worst results. The pattern of summed frequency values matched the general
1604 trend of the Bremer supports, i.e. the GM conditions produced lower total support for the collapsed tree;
1605 although, the mean frequency supports across the four collapsed trees were again relatively constant.

1606 When the Bremer and frequency support values were averaged in five tree regions and summed
1607 within each tree, in both metrics the DC condition produced the best values and the two GM conditions
1608 produced the worst.

1609

1610 **Conclusions**

1611

1612 To broadly summarize our findings - for our dataset it appears that continuous characters consistently
1613 exert a greater influence over the results than GM characters, and in comparison to datasets excluding
1614 continuous characters, they also appear to reduce homoplasy. GM characters in this study produced trees
1615 with generally worse nodal support values, and despite the lack of polytomies within the best-fit trees,
1616 when collapsing nodes to adjust for over-resolution of the tree the GM datasets retained fewer nodes at a
1617 reasonable cut-off value than the continuous and discrete trees.

1618 A potential drawback of using GM data in particular is the relative difficulty, in comparison to
1619 discrete characters, of interpreting morphological changes in a way that is useful for producing written
1620 diagnoses. For synapomorphic continuous characters it is possible to express the character ‘state’ of a
1621 taxon or group as a numerical range and transformations as shifts from one range to another; however,
1622 describing subtle, but apparently phylogenetically relevant changes in shape according to geometric
1623 morphometrics necessitates either multiple diagrams of landmark displacements at supported nodes, or
1624 long breakdowns of morphology, and an elevation of analytical complexity for relatively little gain (at
1625 least in the case of this dataset). An example of the perplexity caused by GM data may be seen in the
1626 nodal synapomorphies in the treatments which incorporate GM data (Appendix 3); in both trees (DM and
1627 DCM) almost all GM characters are optimized as synapomorphies for almost every node.

1628 A further obstacle to incorporating substantial amounts of GM data into phylogenetic analyses is
1629 that in palaeontological datasets, and especially with phytosaurs, it is relatively uncommon to find the
1630 pristine, non-deformed morphologies necessary for geometric morphometric comparisons. Furthermore,
1631 GM characters may inherently encompass multiple discrete characters; if one aspect of a morphological
1632 feature is deformed (thus rendering the feature unusable for GM), all associated morphological features to
1633 be scored by the same configuration of landmarks would also have to be excluded from the analysis. In
1634 this sense, the addition of GM characters into a dataset may actually increase the quantity of missing data
1635 in a dataset where the characters could be alternatively scored with discrete or continuous methods.

1636 For the various reasons outlined above we prefer the D and DC trees as they either incorporate
1637 continuous data, exclude GM data, or both. These trees are also representative of the two conflicting
1638 topologies found in this study and are generally consistent with previous analyses of ingroup Phytosauria.
1639 Therefore, we recommend use of these datasets and their resultant trees in future phylogenetic analyses of
1640 the clade.

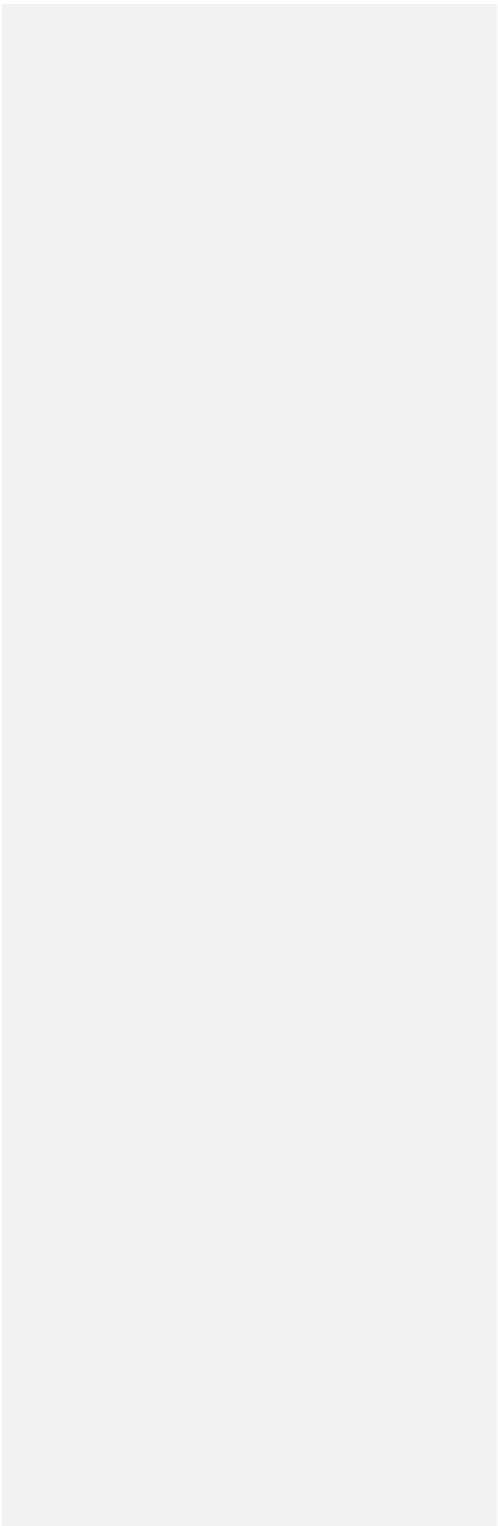
1642 **Acknowledgements**

1643
1644 We thank the following people for access to, and assistance with, specimens in their care: Carl Mehling
1645 (AMNH), Oliver Rauhut (BSPG), William Simpson (FMNH), Philippe Havlik and Davit Vasilyan (GPIT),
1646 Daniela Schwarz and Thomas Schossleitner (MB), Ronan Allain (MNHN), Casey Holliday and James
1647 Schiffbauer (MU), Lorna Steel (NHMUK), Ursula Göhlich (NHMW), Eckhard Mönning (NMC), Amanda
1648 Cantrell (NMMNHS), William Parker and Matthew Smith (PEFO), Rainer Schoch (SMNS), Kenneth
1649 Bader and Matthew Brown (TMM), Bill Mueller (TTU-P), Patricia Holroyd (UCMP), Michael Brett-
1650 Surman (USNM), Daniel Brinkman (YPM), and Robert Bronowicz and Tomasz Sulej (ZPAL). We are

Commented [WGP18]: I think the Strict Consensus tree of all four analyses demonstrates the issues we still have with phytosaur taxonomy and phylogeny, especially regarding the non-pseudopalatine leptosuchomorphs which historically have been shuffled between the genera *Rutiodon*, *Leptosuchus*, and *Smilosuchus*. Essentially they could all be redefined as monospecific genera. Could you please briefly address this. Protome batalaria within *Machaerops*/*Redondasaurus* is problematic because that negates to use of isolated phytosaur squamosals in vertebrate biostratigraphy (e.g., Long and Murry, 1995; Irmis & Parker, 2006; Parker, 2006; Parker and Martz, 2011) as *P. batalaria* has a *Leptosuchus*/*Smilosuchus* type squamosal.

1651 also grateful to Pablo Goloboff for TNT script suggestions and bug fixes, and to Octavio Mateus for
1652 useful discussion of phylogenetic characters.

1653



1654 **References**

1655

1656 **Adams, D. C., & Otárola-Castillo, E.** 2013. Geomorph: an R package for the collection and analysis of
1657 geometric morphometric shape data. *Methods in Ecology and Evolution*, **4**, 393–399 DOI:
1658 10.1111/2041-210X.12035

1659

1660 **Ballew, K. L.** 1989. *A phylogenetic analysis of Phytosauria (Reptilia: Archosauria) from the Late*
1661 *Triassic of the western United States*. Unpublished MA thesis, University of California, Berkeley, 73
1662 pp.

1663

1664 **Bell, M. A., & Lloyd, G. T.** 2014. strap: an R package for plotting phylogenies against stratigraphy and
1665 assessing their stratigraphic congruence. *Palaeontology*, **58**, 379–389 DOI: 10.1111/pala.12142

1666

1667 **Benton, M. J., & Clark, J. M.** 1988. Archosaur phylogeny and the relationships of the Crocodylia. Pp.
1668 295–338 in M. J. Benton (ed.) *The Phylogeny and Classification of the Tetrapods, Volume 1:*
1669 *Amphibians, Reptiles, Birds*. Clarendon Press, Oxford.

1670

1671 **Benton, M. J., & Storrs, G. W.** 1994. Testing the quality of the fossil record: paleontological knowledge
1672 is improving. *Geology*, **22**, 111–114 DOI: 10.1130/0091-7613(1994)022<0111:TTQOTF>2.3.CO;2

1673

1674 **Benton, M. J., Hitchin, R., & Wills, M. A.** 1999. Assessing congruence between cladistic and
1675 stratigraphic data. *Systematic Biology*, **48**, 581–596.

1676

1677 **Bookstein, F. L.** 1996. Landmark methods for forms without landmarks: localizing group differences in
1678 outline shape. *Mathematical Methods in Biomedical Image Analysis, 1996, Proceedings of the*
1679 *Workshop on Mathematical Methods in Biomedical Image Analysis*, 279–289.

1680

1681 **Brusatte, S. L., Butler, R. J., Niedźwiedzki, G., Sulej, T., Bronowicz, R., & Satkūnas, J.** 2013. First
1682 record of Mesozoic terrestrial vertebrates from Lithuania: phytosaurs (Diapsida: Archosauriformes) of
1683 probable Late Triassic age, with a review of phytosaur biogeography. *Geological Magazine*, **150**, 110–
1684 122 DOI: 10.1017/S0016756812000428

1685

1686 **Buffetaut, E.** 1993. Phytosaurs in time and space. *Paleontolol Lombarda Nuova serie*, **2**, 39–44.

1687

1688 **Butler, R. J., Rauhut, O. W., Stocker, M. R., & Bronowicz, R.** 2014. Redescription of the phytosaurs
1689 *Paleorhinus* (‘*Francosuchus*’) *angustifrons* and *Ebrachosuchus neukami* from Germany, with
1690 implications for Late Triassic biochronology. *Zoological Journal of the Linnean Society*, **170**, 155–208
1691 DOI: 10.1111/zoj12094

1692

1693 **Camp, C. L.** 1930. A study of the phytosaurs with description of new material from western North
1694 America. *Memoirs of the University of California*, **10**, 1–174.

1695

1696 **Case, E. C.** 1920. Preliminary description of a new suborder of phytosaurian reptiles with a description of
1697 a new species of *Phytosaurus*. *The Journal of Geology*, **28**, 524–535 DOI: 10.1086/622732

1698

1699 **Case, E. C.** 1922. New reptiles and stegocephalians from the Upper Triassic of western Texas. *Carnegie*
1700 *Institute of Washington Publication*, **321**, 1–84.

1701

1702 **Case, E. C.** 1929. Description of the skull of a new form of phytosaur: with notes on the characters of
1703 described North American phytosaurs. *University of Michigan Studies, Memoirs of the University of*
1704 *Michigan Museums*, **2**, 1–56.

1705

1706 **Case, E. C., & White, T. E.** 1934. Two new specimens of phytosaurs from the Upper Triassic of western
1707 Texas. *Contributions from the Museum of Paleontology, University of Michigan*, **4**, 133–142.

1708

1709 **Catalano, S. A., Goloboff, P. A., & Giannini, N. P.** 2010. Phylogenetic morphometrics (I): the use of
1710 landmark data in a phylogenetic framework. *Cladistics*, **26**, 539–549 DOI: 10.1111/j.1096-
1711 0031.2010.00302.x

1712

1713 **Chappill, J. A.** 1989. Quantitative characters in phylogenetic analysis. *Cladistics*, **5**, 217–234 DOI:
1714 10.1111/j.1096-0031.1989.tb00487.x

1715

1716 **Chatterjee, S.** 1978. A primitive parasuchid (phytosaur) reptile from the Upper Triassic Maleri Formation
1717 of India. *Palaeontology*, **21**, 83–127.

1718

1719 **Chatterjee, S.** 2001. *Parasuchus hislopi* Lydekker, 1885 (Reptilia, Archosauria): Proposed replacement
1720 of the lectotype by a neotype. *Bulletin of Zoological Nomenclature*, **58**, 34–36.

1721

1722 **Colbert, E. H.** 1947. Studies of the phytosaurs *Machaeroprosoopus* and *Rutiodon*. *Bulletin of the*
1723 *American Museum of Natural History*, **88**, 53–96.

1724

1725 **Congreve, C. R., & Lamsdell, J. C.** 2016. Implied weighting and its utility in palaeontological datasets:
1726 a study using modelled phylogenetic matrices. *Palaeontology*, **59**, 447–462 DOI: 10.1111/pala.12236

1727

1728 **Cope, E. D.** 1881. *Belodon* in New Mexico. *American Naturalist*, **15**, 922–923.

1729

1730 **Cranston, P. S., & Humphries, C. J.** 1988. Cladistics and computers: a chironomid
1731 conundrum? *Cladistics*, **4**, 72–92 DOI: 10.1111/j.1096-0031.1988.tb00469.x

1732

1733 **Crisp, M. D., & Weston, P. H.** 1987. Cladistics and legume systematics, with an analysis of the
1734 Bossiaceae, Brongniartieae and Mirbelieae. *Advances in Legume Systematics*, **3**, 65–130.

1735

1736 **Dodson, P.** 1975. Taxonomic implications of relative growth in lambeosaurine hadrosaurs. *Systematic*
1737 *Biology*, **24**, 37–54 DOI: 10.1093/sysbio/24.1.37

1738

1739 **Dutuit, J. M.** 1977. *Paleorhinus magnoculus*, phytosaure du Trias supérieur de l’Atlas
1740 marocain. *Géologie Méditerranéenne*, **4**, 255–268.

1741

1742 **Eaton, T. H. Jr** 1965. A new Wyoming phytosaur. *The University of Kansas Paleontological*
1743 *Contributions*, **2**, 1–6.

1744

1745 **Ezcurra, M. D.** 2016. The phylogenetic relationships of basal archosauromorphs, with an emphasis on
1746 the systematics of proterosuchian archosauriforms. *PeerJ*, **4**, e1778 DOI: 10.7717/peerj.1778
1747

1748 **Fara, E., & Hungerbühler, A.** 2000. *Paleorhinus magnoculus* from the Upper Triassic of Morocco: a
1749 juvenile primitive phytosaur (Archosauria). *Comptes Rendus de l'Académie des Sciences-Series IIA-*
1750 *Earth and Planetary Science*, **331**, 831–836 DOI: 10.1016/S1251-8050(00)01481-6
1751

1752 **Farris, J. S.** 1970. Methods for computing Wagner trees. *Systematic Biology*, **19**, 83–92 DOI:
1753 10.1093/sysbio/19.1.83
1754

1755 **Farris, J. S.** 1990. Phenetics in camouflage. *Cladistics*, **6**, 91–100 DOI: 10.1111/j.1096-
1756 0031.1990.tb00528.x
1757

1758 **Felsenstein, J.** 1988. Phylogenies and quantitative characters. *Annual Review of Ecology and*
1759 *Systematics*, **19**, 445–471 DOI: 10.1146/annurev.es.19.110188.002305
1760

1761 **Garcia-Cruz, J., & Sosa, V.** 2006. Coding quantitative character data for phylogenetic analysis: a
1762 comparison of five methods. *Systematic Botany*, **31**, 302–309 DOI: 10.1600/036364406777585739
1763

1764 **Gift, N., & Stevens, P. F.** 1997. Vagaries in the delimitation of character states in quantitative variation—
1765 an experimental study. *Systematic Biology*, **46**, 112–125 DOI: 10.1093/sysbio/46.1.112
1766

1767 **Goloboff, P. A.** 1993. Estimating character weights during tree search. *Cladistics*, **9**, 83–91 DOI:
1768 10.1111/j.1096-0031.1993.tb00209.x
1769

1770 **Goloboff, P. A., Mattoni, C. I., & Quinteros, A. S.** 2006. Continuous characters analyzed as
1771 such. *Cladistics*, **22**, 589–601 DOI: 10.1111/j.1096-0031.2006.00122.x
1772

1773 **Goloboff, P. A., Carpenter, J. M., Arias, J. S., & Esquivel, D. R. M.** 2008a. Weighting against
1774 homoplasy improves phylogenetic analysis of morphological data sets. *Cladistics*, **24**, 758–773 DOI:
1775 10.1111/j.1096-0031.2008.00209.x
1776

1777 **Goloboff, P. A., Farris, J. S., & Nixon, K. C.** 2008b. TNT, a free program for phylogenetic
1778 analysis. *Cladistics*, **24**, 774–786 DOI: 10.1111/j.1096-0031.2008.00217.x
1779

1780 **Goloboff, P. A., & Catalano, S. A.** 2011. Phylogenetic morphometrics (II): algorithms for landmark
1781 optimization. *Cladistics*, **27**, 42–51 DOI: 10.1111/j.1096-0031.2010.00318.x
1782

1783 **Goloboff, P. A., & Catalano, S. A.** 2016. TNT version 1.5, including a full implementation of
1784 phylogenetic morphometrics. *Cladistics*, **32**, 221–238 DOI: 10.1111/cla.12160
1785

1786 **Gregory, J. T.** 1962. The genera of phytosaurs. *American Journal of Science*, **260**, 652–690 DOI:
1787 10.2475/ajs.260.9.652
1788

1789 **Gregory, J. T.** 1969. Evolution und interkontinentale Beziehungen der Phytosauria
1790 (Reptilia). *Paläontologische Zeitschrift*, **43**, 37–51 DOI: 10.1007/BF02987926
1791

1792 **Holloway, W. L., Claeson, K. M., & O'keefe, F. R.** 2013. A virtual phytosaur endocast and its
1793 implications for sensory system evolution in archosaurs. *Journal of Vertebrate Paleontology*, **33**, 848–
1794 857 DOI: 10.1080/02724634.2013.747532
1795

1796 **Huelsenbeck, J. P.** 1994. Comparing the stratigraphic record to estimates of
1797 phylogeny. *Paleobiology*, **20**, 470–483 DOI: 10.1017/S009483730001294X
1798

1799 **Huene, F. von.** 1915. On reptiles of the New Mexican Trias in the Cope Collection. *Bulletin of the*
1800 *American Museum of Natural History*, **34**, 485–507.
1801

1802 **Hungerbühler, A.** 1998. *Cranial anatomy and diversity of the Norian phytosaurs of Southwestern*
1803 *Germany*. Unpublished PhD thesis, University of Bristol, 464 pp.
1804

1805 **Hungerbühler, A.** 2002. The Late Triassic phytosaur *Mystriosuchus westphali*, with a revision of the
1806 genus. *Palaeontology*, **45**, 377–418 DOI: 10.1111/1475-4983.00242
1807

1808 **Hungerbühler, A., & Sues, H. D.** 2001. Status and phylogenetic relationships of the Late Triassic
1809 phytosaur *Rutiodon carolinensis*. *Journal of Vertebrate Paleontology*, **21**, 64A.
1810

1811 **Hungerbühler, A., Chatterjee, S., & Cunningham, D. P.** 2003. A new phytosaur species from the
1812 Triassic of west Texas: new information on cranial anatomy, taxonomy, and sexual dimorphism in
1813 Pseudopalatinae. *Journal of Vertebrate Paleontology*, **23**, 63A-64A.

1814

1815 **Hungerbühler, A., Mueller, B., Chatterjee, S. & Cunningham, D. P.** 2013. Cranial anatomy of the
1816 Late Triassic phytosaur *Machaeroprosoopus*, with the description of a new species from West Texas.
1817 *Earth and Environmental Science Transactions of the Royal Society of Edinburgh*, **103**, 269–312 DOI:
1818 10.1017/S1755691013000364

1819

1820 **Hunt, A. P., & Lucas, S. G.** 1989. New genotype designations for the phytosaurs *Mystriosuchus* and
1821 *Rutiodon* with a discussion of the taxonomic status of *Mystriosuchus*, *Clepsysaurus* and *Rutiodon*. Pp.
1822 340–348 in S. G. Lucas & A. P. Hunt (eds) *Dawn of the Age of Dinosaurs in the American Southwest*.
1823 New Mexico Museum of Natural History and Science, Albuquerque.

1824

1825 **Hunt, A. P., & Lucas, S. G.** 1991. The *Paleorhinus* biochron and the correlation of the non-marine
1826 Upper Triassic of Pangaea. *Palaeontology*, **34**, 487–501.

1827

1828 **Hunt, A. P., & Lucas, S. G.** 1993. A new phytosaur (Reptilia: Archosauria) genus. *New Mexico*
1829 *Museum of Natural History and Science Bulletin*, **3**, 193–196.

1830

1831 **ICZN 2003.** *Parasuchus hislopi* Lydekker, 1885 (Reptilia, Archosauria): lectotype replaced by a neotype.
1832 *Bulletin of Zoological Nomenclature*, **60**, Opinion 2045.

1833

1834 **Irmis, R. B.** 2007. Axial skeleton ontogeny in the Parasuchia (Archosauria: Pseudosuchia) and its
1835 implications for ontogenetic determination in archosaurs. *Journal of Vertebrate Paleontology*, **27**, 350–
1836 361 DOI: 10.1671/0272-4634(2007)27[350:ASOITP]2.0.CO;2
1837
1838 **Jaeger, G. F.** 1828. *Über die fossilen Reptilien, welche in Württemberg aufgefunden worden*
1839 *sind*. Metzler, Stuttgart, 48 pp.
1840
1841 **Jaekel O.** 1910. Über einen neuen Belodonten aus dem Buntsandstein von Bernberg. *Sitzungsberichte*
1842 *Gesellschaft naturforschender Freunde zu Berlin*, **5**, 197–229.
1843
1844 **Juul, L.** 1994. The phylogeny of basal archosaurs. *Palaeontologia africana*, **31**, 1–38.
1845
1846 **Kammerer, C. F., Butler, R. J., Bandyopadhyay, S., & Stocker, M. R.** 2015. Relationships of the
1847 Indian phytosaur *Parasuchus hislopi* Lydekker, 1885. *Papers in Palaeontology*, **2**, 1–23 DOI:
1848 10.1002/spp2.1022
1849
1850 **Klassen, G. J., Mooi, R. D., & Locke, A.** 1991. Consistency indices and random data. *Systematic*
1851 *Biology*, **40**, 446–457 DOI: 10.1093/sysbio/40.4.446
1852
1853 **Koch, N. M., Soto, I. M., & Ramírez, M. J.** 2015. First phylogenetic analysis of the family Neriidae
1854 (Diptera), with a study on the issue of scaling continuous characters. *Cladistics*, **31**, 142–165 DOI:
1855 10.1111/cla.12084
1856

1857 **Kuhn, O. 1936.** Weitere Parasuchier und Labyrinthodonten aus dem Blasensandstein des mittleren
1858 Keuper von Ebrach. *Palaeontographica Abteilung A*, **83**, 61–98.
1859
1860 **Langston, W. 1949.** A new species of *Paleorhinus* from the Triassic of Texas. *American Journal of*
1861 *Science*, **247**, 324–341 DOI: 10.2475/ajs.247.5.324
1862
1863 **Lautenschlager, S., & Butler, R. J. 2016.** Neural and endocranial anatomy of Triassic phytosaurian
1864 reptiles and convergence with fossil and modern crocodylians. *PeerJ*, **4**, e2251 DOI:
1865 10.7717/peerj.2251
1866
1867 **Li, C., Wu, X. C., Zhao, L. J., Sato, T., & Wang, L. T. 2012.** A new archosaur (Diapsida,
1868 Archosauriformes) from the marine Triassic of China. *Journal of Vertebrate Paleontology*, **32**, 1064–
1869 1081 DOI: 10.1080/02724634.2012.694383
1870
1871 **Long, R. A., & Ballew, K. L. 1985.** Aetosaur dermal armor from the Late Triassic of southwestern North
1872 America, with special reference to material from the Chinle Formation of Petrified Forest National
1873 Park. *Museum of Northern Arizona Bulletin*, **47**, 45–68.
1874
1875 **Long, R. A., & Murry, P. A. 1995.** Late Triassic (Carnian and Norian) tetrapods from the southwestern
1876 United States. *New Mexico Museum of Natural History and Science Bulletin*, **4**, 1–254.
1877
1878 **Lucas, S.G. 1998.** Global Triassic tetrapod biostratigraphy and biochronology. *Palaeogeography*,
1879 *Palaeoclimatology, Palaeoecology*, **143**, 347–384 DOI: 10.1016/S0031-0182(98)00117-5

1880

1881 **Lucas, S. G.** 2010. The Triassic timescale based on nonmarine tetrapod biostratigraphy and

1882 biochronology. *Geological Society, London, Special Publications*, **334**, 447–500 DOI:

1883 10.1144/SP334.15

1884

1885 **Lucas, S. G., & Hunt, A. P.** 1993. Tetrapod biochronology of the Chinle Group. *New Mexico Museum of*

1886 *Natural History and Science Bulletin*, **3**, 327–329.

1887

1888 **Lydekker, R.** 1885. The Reptilia and Amphibia of the Maleri and Denwa groups. *Palaeontologia Indica*,

1889 *Series 1*, **1**, 1–38.

1890

1891 **Mehl, M. G.** 1913. *Angistorhinus*, a new genus of Phytosauria from the Trias of Wyoming. *The Journal*

1892 *of Geology*, **21**, 186–191 DOI: 10.1086/622049

1893

1894 **Mehl, M. G.** 1915. The Phytosauria of the Trias. *The Journal of Geology*, **23**, 129–165 DOI:

1895 10.1086/622217

1896

1897 **Mehl, M. G.** 1916. New or little known phytosaurs from Arizona. Pp. 5–28 in M. G. Mehl, W. C.

1898 Toepelmann and G. M. Schwartz (eds) *New or Little Known Reptiles from the Trias of Arizona and*

1899 *New Mexico with Notes on the Fossil Bearing Horizons near Wingate, New Mexico*. Quarterly Bulletin

1900 of the University of Oklahoma, New Series, **103**, 5–44.

1901

1902 **Mehl, M. G.** 1928. The Phytosauria of the Wyoming Triassic. *Journal of the Denison University*
1903 *Laboratories, Denison University*, **23**, 141–172.

1904

1905 **Meyer, H. von.** 1860. Briefliche Mittheilung an Prof. Bronn. *Neues Jahrbuch für Mineralogie,*
1906 *Geognosie, Geologie und Petrefakten-Kunde*, 556–560.

1907

1908 **Meyer, H. von.** 1863. Der Schädel des Belodon aus dem Stubensandstein des oberen Keupers.
1909 *Palaeontographica*, **10**, 227–246.

1910

1911 **Mickevich, M. F., & Johnson, M. S.** 1976. Congruence between morphological and allozyme data in
1912 evolutionary inference and character evolution. *Systematic Zoology*, **25**, 260–270 DOI:
1913 10.2307/2412494

1914

1915 **Nesbitt, S. J.** 2011. The early evolution of archosaurs: relationships and the origin of major clades.
1916 *Bulletin of the American Museum of Natural History*, **352**, 1–292 DOI: 10.1206/352.1

1917

1918 **Parker, W. G., & Irmis, R. B.** 2006. A new species of the Late Triassic phytosaur *Pseudopalatus*
1919 (Archosauria: Pseudosuchia) from Petrified Forest National Park, Arizona. *Museum of Northern*
1920 *Arizona Bulletin*, **62**, 126–143.

1921

1922 **Parker, W. G., Hungerbühler, A., & Martz, J. W.** 2012. The taxonomic status of the phytosaurs
1923 (Archosauriformes) *Machaeroprotopus* and *Pseudopalatus* from the Late Triassic of the western

1924 United States. *Earth and Environmental Science Transactions of the Royal Society of Edinburgh*, **103**,
1925 265–268 DOI: 10.1017/S1755691013000339
1926
1927 **Parrish, J. M.** 1993. Phylogeny of the Crocodylotarsi, with reference to archosaurian and crurotarsan
1928 monophyly. *Journal of Vertebrate Paleontology*, **13**, 287–308 DOI: 10.1080/02724634.1993.10011511
1929
1930 **Parrish, J. M., & Carpenter, K.** 1986. A new vertebrate fauna from the Dockum Formation (Late
1931 Triassic) of eastern New Mexico. Pp. 151–160 in K. Padian (ed) *The Beginning of the Age of*
1932 *Dinosaurs: Faunal Change Across the Triassic-Jurassic Boundary*. Cambridge University Press,
1933 Cambridge.
1934
1935 **Perrard, A., Lopez- Osorio, F., & Carpenter, J. M.** 2016. Phylogeny, landmark analysis and the use of
1936 wing venation to study the evolution of social wasps (Hymenoptera: Vespidae: Vespinae). *Cladistics*,
1937 **32**, 406–425 DOI: 10.1111/cla.12138
1938
1939 **Pimentel, R. A., & Riggins, R.** 1987. The nature of cladistic data. *Cladistics*, **3**, 201–209 DOI:
1940 10.1111/j.1096-0031.1987.tb00508.x
1941
1942 **Poe, S., & Wiens, J. J.** 2000. Character selection and the methodology of morphological phylogenetics.
1943 Pp. 20–36 in J. J. Wiens (ed) *Phylogenetic Analysis of Morphological Data*. Smithsonian Institution
1944 Press, Washington, D.C.
1945

1946 **Pol, D., & Norell, M. A.** 2001. Comments on the Manhattan stratigraphic measure. *Cladistics*, **17**, 285–
1947 289 DOI: 10.1111/j.1096-0031.2001.tb00125.x
1948
1949 **Pol, D., & Norell, M. A.** 2006. Uncertainty in the age of fossils and the stratigraphic fit to
1950 phylogenies. *Systematic Biology*, **55**, 512–521 DOI: 10.1080/10635150600755446
1951
1952 **Rae, T. C.** 1998. The logical basis for the use of continuous characters in phylogenetic
1953 systematics. *Cladistics*, **14**, 221–228 DOI: 10.1111/j.1096-0031.1998.tb00335.x
1954
1955 **R Core Team.** 2016. *R: A language and environment for statistical computing*. R Foundation for
1956 Statistical Computing, Vienna, Austria. Updated at: <https://www.R-project.org/>, accessed 11 January
1957 2018.
1958
1959 **Rohlf, F. J.** 2015. The tps series of software. *Hystrix, the Italian Journal of Mammalogy*, **26**, 9–12.
1960
1961 **Romer, A. S.** 1972. The Chañares (Argentina) Triassic reptile fauna. XVI. Thecodont
1962 classification. *Breviora*, **395**, 1–24.
1963
1964 **Rozhdestvensky, A. K.** 1965. Growth changes in Asian dinosaurs and some problems of their
1965 taxonomy. *Palaeontologicheskii Zhurnal*, **3**, 95–109.
1966

1967 **Sampson, S. D., Ryan, M. J., & Tanke, D. H.** 1997. Craniofacial ontogeny in centrosaurine dinosaurs
1968 (Ornithischia: Ceratopsidae): taxonomic and behavioral implications. *Zoological Journal of the*
1969 *Linnean Society*, **121**, 293–337 DOI: 10.1111/j.1096-3642.1997.tb00340.x
1970
1971 **Scannella, J. B., & Horner, J. R.** 2010. *Torosaurus* Marsh, 1891, is *Triceratops* Marsh, 1889
1972 (Ceratopsidae: Chasmosaurinae): synonymy through ontogeny. *Journal of Vertebrate*
1973 *Paleontology*, **30**, 1157–1168 DOI: 10.1080/02724634.2010.483632
1974
1975 **Sereno, P. C.** 1991. Basal archosaurs: phylogenetic relationships and functional implications. *Journal of*
1976 *Vertebrate Paleontology*, **11**(S4), 1–53 DOI: 10.1080/02724634.1991.10011426
1977
1978 **Sereno, P. C., & Arcucci, A. B.** 1990. The monophyly of crurotarsal archosaurs and the origin of bird
1979 and crocodile ankle joints. *Neues Jahrbuch für Geologie und Paläontologie, Abhandlungen*, **180**, 21–
1980 52.
1981
1982 **Siddall, M. E.** 1996. Stratigraphic consistency and the shape of things. *Systematic Biology*, **45**, 111–115
1983 DOI: 10.2307/2413516
1984
1985 **Siddall, M. E.** 1998. Stratigraphic fit to phylogenies: a proposed solution. *Cladistics*, **14**, 201–208 DOI:
1986 10.1111/j.1096-0031.1998.tb00333.x
1987
1988 **Sookias, R. B.** 2016. The relationships of the Euparkeriidae and the rise of Archosauria. *Royal Society*
1989 *open science*, **3**, 150674 DOI: 10.1098/rsos.150674

1990

1991 **Spielmann, J. A., & Lucas, S. G.** 2012. Tetrapod fauna of the Upper Triassic Redonda Formation, east-

1992 central New Mexico: the characteristic assemblage of the Apachean land-vertebrate faunachron. *New*

1993 *Mexico Museum of Natural History and Science Bulletin*, **55**, 1–119.

1994

1995 **Stevens, P. F.** 1991. Character states, morphological variation, and phylogenetic analysis: a

1996 review. *Systematic Botany*, **16**, 553–583 DOI: 10.2307/2419343

1997

1998 **Stocker, M. R.** 2010. A new taxon of phytosaur (Archosauria: Pseudosuchia) from the Late Triassic

1999 (Norian) Sonsela Member (Chinle Formation) in Arizona, and a critical reevaluation of *Leptosuchus*

2000 Case, 1922. *Palaeontology*, **53**, 997–1022 DOI: 10.1111/j.1475-4983.2010.00983.x

2001

2002 **Stocker, M. R.** 2012. A new phytosaur (Archosauriformes, Phytosauria) from the Lot's Wife beds

2003 (Sonsela Member) within the Chinle Formation (Upper Triassic) of Petrified Forest National Park,

2004 Arizona. *Journal of Vertebrate Paleontology*, **32**, 573–586 DOI: 10.1080/02724634.2012.649815

2005

2006 **Stocker, M. R.** 2013. A new taxonomic arrangement for *Paleorhinus scurriensis*. *Earth and*

2007 *Environmental Science Transactions of the Royal Society of Edinburgh*, **103**, 1–13 DOI:

2008 10.1017/S1755691013000340

2009

2010 **Stocker, M. R., & Butler, R. J.** 2013. Phytosauria. *Geological Society, London, Special*

2011 *Publications*, **379**, 91–117 DOI: 10.1144/SP379.5

2012

2013 **Stocker, M. R., Zhao, L. J., Nesbitt, S. J., Wu, X. C., & Li, C.** 2017. A short-snouted, Middle Triassic
2014 phytosaur and its implications for the morphological evolution and biogeography of
2015 Phytosauria. *Scientific Reports*, **7**, 46028 DOI: 10.1038/srep46028
2016
2017 **Stovall, J. W., & Wharton Jr, J. B.** 1936. A new species of phytosaur from Big Spring, Texas. *The*
2018 *Journal of Geology*, **44**, 183–192 DOI: 10.1086/624416
2019
2020 **Swofford, D., Olsen, G., Paddell, P., & Hills, D.** 1996. Phylogenetic inference. Pp. 407–514 in D. Hillis,
2021 C. Moritz, & B. Mable (eds) *Molecular Systematics*. Sinauer, Sunderland, Massachusetts.
2022
2023 **Thiele, K.** 1993. The holy grail of the perfect character: the cladistic treatment of morphometric
2024 data. *Cladistics*, **9**, 275–304 DOI: 10.1111/j.1096-0031.1993.tb00226.x
2025
2026 **Thorpe, R. S.** 1984. Coding morphometric characters for constructing distance Wagner
2027 networks. *Evolution*, **38**, 244–255 DOI: 10.1111/j.1558-5646.1984.tb00282.x
2028
2029 **Tschopp, E., Mateus, O., & Benson, R. B. J.** 2015. A specimen-level phylogenetic analysis and
2030 taxonomic revision of Diplodocidae (Dinosauria, Sauropoda). *PeerJ*, **3**, e857 DOI: 10.7717/peerj.857
2031
2032 **Tsuihiji T, Watabe M, Tsogtbaatar K, Tsubamoto T, Barsbold R, Suzuki S, Lee AH, Ridgely RC,**
2033 **Kawahara Y, Witmer LM.** 2011. Cranial osteology of a juvenile specimen of *Tarbosaurus bataar*
2034 (Theropoda, Tyrannosauridae) from the Nemegt Formation (Upper Cretaceous) of Bugin Tsav,
2035 Mongolia. *Journal of Vertebrate Paleontology*, **31**, 497–517 DOI: 10.1080/02724634.2011.557116

2036

2037 **Upchurch, P., Tomida, Y., & Barrett, P. M.** 2004. A new specimen of *Apatosaurus ajax* (Sauropoda:

2038 Diplodocidae) from the Morrison Formation (Upper Jurassic) of Wyoming, USA. *National Science*

2039 *Museum Monographs*, **26**, 1–118.

2040

2041 **Walker, A. D.** 1968. *Protosuchus*, *Proterochampsia*, and the origin of phytosaurs and

2042 crocodiles. *Geological Magazine*, **105**, 1–14 DOI: 10.1017/S0016756800046434

2043

2044 **Westphal, K. W.** 1979. Missing holotype of *Machaeroprotopus validus* (Mehl, 1916). *Journal of*

2045 *Paleontology*, **53**, 741.

2046

2047 **Wiens, J. J.** 1998. Testing phylogenetic methods with tree congruence: phylogenetic analysis of

2048 polymorphic morphological characters in phrynosomatid lizards. *Systematic Biology*, **47**, 427–444

2049 DOI: 10.1080/106351598260806

2050

2051 **Wiens, J. J.** 2001. Character analysis in morphological phylogenetics: problems and solutions. *Systematic*

2052 *Biology*, **50**, 689–699 DOI: 10.1080/106351501753328811

2053

2054 **Wills, M. A.** 1999. Congruence between phylogeny and stratigraphy: randomization tests and the gap

2055 excess ratio. *Systematic Biology*, **48**, 559–580 DOI: 10.1080/106351599260148

2056

2057 **Wills, M. A., Barrett, P. M., & Heathcote, J. F.** 2008. The modified gap excess ratio (GER*) and the
2058 stratigraphic congruence of dinosaur phylogenies. *Systematic Biology*, **57**, 891–904 DOI:
2059 10.1080/10635150802570809
2060
2061 **Zelditch, M., Swiderski, D. L., & Sheets, H. D.** 2012. *Geometric Morphometrics for Biologists: A*
2062 *Primer*. Academic Press.

1 **Appendix 1: Taxonomic list**

2

3 **Institutional abbreviations**

4 **AMNH**: American Museum of Natural History, New York, USA; **BSPG**: Bayerische Staatssammlung für
5 Paläontologie und Geologie, Munich, Germany; **CMNH**: Carnegie Museum of Natural History,
6 Pittsburgh, USA; **FMNH**: Field Museum of Natural History, Chicago, USA; **GPIT**: Institut für Geologie
7 und Paläontologie Tübingen, Tübingen, Germany; **GR**: Ruth Hall Museum of Paleontology, Ghost Ranch,
8 Abiquiu, USA; **ISI**: Indian Statistical Institute, Kolkata, India; **MB**: Museum für Naturkunde, Berlin,
9 Germany; **MBSN**: Museo Civico di Scienze naturali 'E. Caffi', Bergamo, Italy; **MCZ**: Harvard
10 University Museum of Comparative Zoology, Cambridge, USA; **MNA**: Museum of Northern Arizona,
11 Flagstaff, USA; **MNH**: Muséum National d'Histoire Naturelle, Paris, France; **MSM**: Arizona Museum
12 of Natural History (previously Mesa Southwest Museum), Mesa, USA; **MU**: University of Missouri,
13 Columbia, Missouri, USA; **NHMUK**: Natural History Museum, London, UK; **NHMW**: Naturhistorisches
14 Museum Wien, Vienna, Austria; **NMC**: Naturkundemuseum Coburg, Coburg, Germany; **NMMNHS**:
15 New Mexico Museum of Natural History and Science, Albuquerque, USA; **OMNH**: Oklahoma Museum
16 of Natural History, Norman, USA; **PEFO**: Petrified Forest National Park, Arizona, USA; **PPHM**:
17 Panhandle Plains Historical Museum West Texas A&M University, Canyon, USA; **SMF**:
18 Forschungsinstitut und Natur-Museum Senckenberg, Frankfurt/Main, Germany; **SMNS**: Staatliches
19 Museum für Naturkunde Stuttgart, Stuttgart, Germany; **TMM**: Texas Memorial Museum, Austin, USA;
20 **TTU-P**: Museum of the University of Texas Tech, Lubbock, USA; **UCM**: University of Colorado
21 Museum, Boulder, USA; **UCMP**: University of California Museum of Paleontology, Berkeley, USA;
22 **UMMP**: University of Michigan Museum of Paleontology, Ann Arbor, USA; **USNM**: National Museum
23 of Natural History, Washington D.C., USA; **UW**: University of Wisconsin Geological Museum, Madison,

24 USA; **YPM**: Yale Peabody Museum, New Haven, USA; **ZMNH**: Zhejiang Museum of Natural History,
25 Hangzhou, China; **ZPAL**: Instytut Paleobiologii PAN, Warsaw, Poland.

26

27 *Diandongosuchus fuyuanensis* Li *et al.*, 2012

28 **Age**: Ladinian (c. 242–237 Mya)

29 **Occurrences**: Zhuganpo Member, Falang Formation, southeast Fuyuan County, Yunnan Province, China

30 **Holotype**: ZMNH M8770, largely complete skeleton missing many caudal vertebrae

31 **Previously Referred Specimens**: Additional specimen under preparation (personal communication with
32 X.-C. Wu cited by Griffin *et al.* [2017])

33 **Specimen(s) Used for Scoring**: ZMNH M8770

34 **Key References**: Li *et al.* (2012); Stocker *et al.* (2017)

35 **Most Recent Diagnosis**:

36 Stocker *et al.* (2017) distinguished *D. fuyuanensis* from all other phytosaurs using the following
37 characters: 1) Anterodorsal (nasal) process of premaxilla extending well posterior of external naris; 2)
38 Presence of a fossa expanded in anteroventral corner of external naris; 3) Jugal with pronounced
39 longitudinal ridge on lateral surface; 4) Anterior process of jugal much broader than the posterior process
40 underlying anterior process of quadratojugal; 5) Premaxilla with nine teeth; 6) More than one set of
41 paramedian osteoderms dorsal to the cervical series.

42 **Comments**: *D. fuyuanensis* was originally described as a rauisuchian archosaur (Li *et al.*, 2012), and was
43 subsequently reassessed as the most basal phytosaur (Stocker *et al.*, 2017), using the following characters:
44 1) Posterodorsal process of premaxilla strongly sutured to maxilla; 2) More than six premaxillary teeth; 3)
45 Facial portion of maxilla anterior to anterior edge of antorbital fenestra equal in length or longer than
46 portion posterior to anterior edge of fenestra; 4) Entire anterior margin of scapula straight/convex or

47 partially concave; 5) Anterior portion of coracoid distinctly hooked; 6) Ectepicondylar flange of humerus
48 present; 7) Obturator foramen of the pubis modified into a notch that opens medioventrally; 8) medial side
49 of distal tarsal 4 with foramen/foramina; 9) Articular surface for the fibula on the calcaneum convex and
50 hemicylindrical shaped; 10) Osteoderms covering the appendages; 11) Retroarticular process of the
51 articular and surangular well ventral to the articulation with the quadrate; 12) Lateral margin of the
52 humerus straight from midshaft to proximal portion. The hypothesis that *D. fuyuanensis* is the most basal
53 known phytosaur was not explicitly tested by Stocker *et al.* (2017); its position within Phytosauria is
54 assessed for the first time in this study.

55

56

57 ***Wannia scurriensis*** (Langston, 1949)

58 **Age:** late Carnian–early Norian (*c.* 232–225 Mya)

59 **Occurrences:** Camp Springs Formation, Dockum Group, Scurry County, Texas, USA

60 **Holotype:** TTU-P 00539, partial skull

61 **Previously Referred Specimens:** TTU-P 11422 (Stocker 2010)

62 **Specimen(s) Used for Scoring:** TTU-P 00539

63 **Key References:** Langston (1949); Stocker (2013)

64 **Most Recent Diagnosis:** Stocker (2013) diagnosed *Wannia scurriensis* on the basis of the following
65 proposed autapomorphies: 1) Basitubera that are widely separated mediolaterally; 2) Presence of a ridge
66 on the lateral surface of the jugal; 3) Presence of a thickened shelf along the posteroventral edge of an
67 expanded pterygoid-quadrate wing; 4) ‘Septo-maxillae’ that do not contact one another and do not form
68 part of the internarial septum; 5) Presence of a nasal swelling posterior to the posterior border of the nares.
69 In addition to these autapomorphies, Stocker (2013) also provided a differential diagnosis outlining non-
70 autapomorphic characters that distinguish *W. scurriensis* from other phytosaurs.

71 **Modified Diagnosis:** Here, we diagnose *Wannia scurriensis* using the following unique combination of
72 characters: 1) Presence of an anteroposteriorly oriented ridge on the lateral surface of the jugal,
73 positioned toward the middle or ventral edge of the jugal posterior process; 2) Presence of a nasal
74 swelling posterior to the posterior border of the nares; 3) Posterior rim of nares smooth (not rugose); 4)
75 Absence of paired depressions posterior to the posterior narial rim.

76 **Comments:** Some of the characters (1, 2, 3, 5) used by Stocker (2013) to diagnose *Wannia scurriensis*
77 also occur in species of *Parasuchus* and cannot, therefore, be considered autapomorphic. As noted by
78 Stocker (2013), the separation of the basitubera (character 1) is the same as that in *Parasuchus*
79 *angustifrons*; however, Stocker suggested that the basitubera in *Parasuchus angustifrons* are not as
80 rounded as those of *W. scurriensis*. Based on our examination of specimens of both taxa, this distinction
81 seems subjective and questionable, particularly given that the holotype of *Parasuchus angustifrons*
82 (BSPG 1931 X 502) has been subjected to dorsoventral compression. Stocker (2013) also noted that the
83 narial swelling (character 5) is also present in *Parasuchus angustifrons* (and is, therefore, also not
84 autapomorphic), although the latter species can be differentiated from *W. scurriensis* as it possesses paired
85 depressions just posterior to the external nares and a rugose posterior narial rim (BSPG 1931 X 502;
86 Butler *et al.* 2014).

87 The thickened pterygoid-quadrato shelf (character 3) appears to also be present in TMM 31100-
88 101, a specimen referable to *Parasuchus bransoni* on the basis of its narial morphology (see below).
89 Moreover, the majority of the quadrato is missing in *W. scurriensis*, making character 3 difficult to assess.
90 There are difficulties in scoring character 4 accurately for *W. scurriensis* because interpretative lines have
91 been incorrectly drawn onto the specimen to supposedly mark the positions of the ‘septo-maxillae’, and
92 the dorsal surface of the septum is damaged. On close side-by-side inspection of the holotype and a cast
93 (TTU-P 14911, which lacks the interpretative lines), the septomaxillae do seem to form a midline contact,

94 and do not therefore differ in any significant regard from those of *Parasuchus hislopi*, *Parasuchus*
95 *bransoni* and *Parasuchus angustifrons*.

96 An additional partial skull (TTU-P 11422) was considered referable to *W. scurriensis* by Stocker
97 (2010); however, as noted by Stocker (2013), no characters are preserved that would allow this specimen
98 to be diagnosed, and as such this specimen should be classified as an indeterminate parasuchid excluded
99 from Mystriosuchinae.

100

101

102 ***Parasuchus bransoni*** (Williston, 1904)

103 **Age:** late Carnian–early Norian (c. 232–225 Mya)

104 **Occurrences:** Popo Agie Formation, Chugwater Group, Wyoming, USA; Colorado City Formation,
105 Dockum Group, Texas, USA

106 **Holotype:** FMNH UC 632, skull

107 **Previously Referred Specimens:** TTU-P 00539 (holotype of *Wannia scurriensis*); TMM 31025-172;
108 TMM 31100-8; TMM 31100-101; TMM 31100-175; TMM 31100-418; TMM 31100-419; TMM 31100-
109 453; TMM 31185-11; TMM 31185-38 (Long & Murry, 1995)

110 **Specimen(s) Used for Scoring:** FMNH UC 632; TMM 31100-101; TMM 31100-418 and 419 (these two
111 specimens likely represent an associated skull and mandible).

112 **Key References:** Williston (1904); Lees (1906); Long & Murry (1995); Butler *et al.* (2014); Kammerer *et*
113 *al.* (2015)

114 **Most Recent Diagnosis:** Long & Murry (1995) diagnosed *Parasuchus bransoni* with the following
115 combination of characters: 1) Skull low; 2) Orbit directed dorsolaterally; 3) Rostrum moderately long,
116 prenarial length equals postnarial length; 4) Maxilla with straight ventral margin; 5) Posterior portion of

maxilla not flared laterally; 6) Interpterygoid vacuity small or absent; 7) Homodont dentition; 8) Alveoli circular throughout; 9) Posterior premaxillary alveolae normal; 10) Upper dentition with 36–45 teeth.

Modified Diagnosis: A combination of the three *Parasuchus* characters identified by Butler *et al.* (2014) and Kammerer *et al.* (2015) and one character of Kammerer *et al.* (2015) to distinguish *Parasuchus bransoni* from *Parasuchus hislopi* and *Parasuchus angustifrons*: 1) Presence of an anterior frontal depression; 2) Bifurcated lateral ridge on the squamosal; 3) Row of nodes on the lateral surface of the jugal; 4) Possession of high ‘triangular’ nares.

Comments: Long & Murry (1995) used a combination of nine characters to diagnose *Parasuchus bransoni*. Characters such as their 1, 2, 5, 7 and 9 have been criticized for being subjective, vague and prone to taphonomic distortion (Hungerbühler, 1998; Stocker, 2010). Character 6 appears to have been generated based on the distorted morphology of the holotype. All non-Mystriosuchinae members of Parasuchidae have an interpterygoid vacuity which extends anteroposteriorly along at least 50% of the palatal vault, and which only becomes restricted in more derived taxa. This proposed diagnostic character is actually therefore plesiomorphic for Mystriosuchinae. Character 7 is problematic as the assessment of dentition used by Long & Murry (1995) was based on empty alveolae and, therefore, may be unreliable. In any case, some degree of heterodonty has now been recognized in all phytosaurs. Character 9 (here inferred to relate to the increase in size of the posterior two or three premaxillary alveolae in many taxa) is also problematic; although the increase in posterior premaxillary alveolar size is subtler in *Parasuchus bransoni* than in many taxa, it does still occur. Several of the characters are probably plesiomorphic for Phytosauridae (3, 4, 5, 7, 8, and probably 9) and/or are widespread (1, 2, 8, 10) in basal members of the clade.

Parasuchus hislopi Lydekker, 1885

140 **Age:** late Carnian–early Norian (c. 232–225 Mya)

141 **Occurrences:** Lower Maleri Formation, Pranhita Godavari Valley, Telangana, India; Tiki Formation,
142 Madhya Pradesh, India

143 **Holotype:** ISI R 42 (neotype), almost complete skeleton including cranium and mandible.

144 **Previously Referred Specimens:** ISI R 43; ISI R 44; ISI R 45; ISI R 46; ISI R 47; ISI R 160; ISI R 161
145 (Chatterjee, 1978)

146 **Specimen(s) Used for Scoring:** ISI R 42; ISI R 43

147 **Key References:** Lydekker (1885); Chatterjee (1974, 1978); Kammerer *et al.* (2015)

148 **Most Recent Diagnosis:** Kammerer *et al.* (2015) diagnosed *Parasuchus hislopi* as follows: a species of
149 *Parasuchus* that is 1) distinguished from *Parasuchus bransoni* by a relatively low narial eminence with a
150 raised, rugose posterior margin of the naris (a ‘narial rim’); 2) Distinguished from *Parasuchus*
151 *angustifrons* by the absence of paired depressions on the anterior portions of the nasals; 3) Tentatively
152 distinguished from ‘*Pal. ~~Magnoculus~~’-magnoculus’ by the posterior confluence of the raised margins of
153 the nares.*

154

155 ***Parasuchus angustifrons*** (Kuhn, 1936)

156 **Age:** late Carnian (c. 232–228 Mya)

157 **Occurrences:** Blasensandstein (lateral equivalent of Hassberge Formation), Middle Keuper Subgroup,
158 northern Bavaria, Germany; Middle Keuper Subgroup, Opole province, Poland

159 **Holotype:** BSPG 1931 X 502, partial skull

160 **Previously Referred Specimens:** None, although the phytosaur material from Krasiejów in Opole,
161 southwest Poland, was considered highly similar to *Parasuchus angustifrons* by Butler *et al.* (2014), and

one of these specimens, ZPAL AbIII 200, was noted to be ‘probably referable to *Parasuchus*
angustifrons’ by Kammerer *et al.* (2015).

Specimen(s) Used for Scoring: BSPG 1931 X 502; ZPAL AbIII 111; ZPAL AbIII 200

Key References: Kuhn (1936); Butler *et al.* (2014); Kammerer *et al.* (2015)

Most Recent Diagnosis: Butler *et al.* (2014) diagnosed *Parasuchus angustifrons* on the basis of the following proposed autapomorphies: 1) Stepped lateral rim of external naris that is strongly swollen and rugose at posterior end; 2) Paired depressions on the anterior portions of the nasals (immediately posterior to the external nares) and anterior portions of the frontals; 3) Foramen in ectopterygoid enlarged and subcircular in outline; 4) Suborbital foramen elongate and boomerang-shaped; 5) Large postparietal foramen at junction of supraoccipital and parietal.

Modified Diagnosis: Species of *Parasuchus* with the following autapomorphies: 1) Paired depressions on the anterior portions of the nasals; 2) Large postparietal foramen at junction of supraoccipital and parietal.

Comments: Of the characters proposed by Butler *et al.* (2013) as autapomorphic for *Parasuchus angustifrons*, characters 1 and 3 are both present in other members of *Parasuchus*: the laterally stepped and posteriorly rugose nares are also present in *Parasuchus hislopi* (ISI R42), while the enlarged ectopterygoid foramen is visible in the holotype of *Parasuchus bransoni* (FMNH UC 632). Character 4, an elongate and boomerang-shaped suborbital foramen, may be variable within the species, given that it appears to be absent in ZPAL AbIII 200. However, the degree of variability of this character among basal phytosaurs is difficult to assess, given the paucity of well-preserved palates generally within the genus *Parasuchus*. Given this uncertainty, character 4 should not be considered diagnostic until sufficient comparative material is available to assess its usefulness.

185 ***‘Paleorhinus’ parvus*** Mehl, 1928

186 **Age:** late Carnian–early Norian (c. 232–225 Mya)

187 **Occurrences:** Popo Agie Formation, Fremont County, Wyoming, USA

188 **Holotype:** MU 530, rostral/mandibular fragments and partial postcrania

189 **Previously Referred Specimens:** None

190 **Specimen(s) Used for Scoring:** MU 530

191 **Key References:** Mehl (1928); Kammerer *et al.* (2015)

192 **Most Recent Diagnosis:** Mehl (1928) did not provide a list of distinct autapomorphies; however, the

193 morphology of *‘Paleorhinus’ parvus* was discussed in relation to other phytosaurs, and a number of

194 distinctive features were highlighted, which are discussed below.

195 **Modified Diagnosis:** Diagnosable on the basis of a unique combination of characters: 1) Anterior tip of

196 the rostrum abruptly downturned; 2) Steep anterodorsally concave curve to the nares; 3) Anterior border

197 of nares anterior to the antorbital fenestra; 4) Subnarial facial portion of the maxilla is dorsoventrally

198 extensive.

199 **Comments:** *‘Paleorhinus’ parvus* was interpreted by Mehl (1928) to possess a proportionately shorter

200 prenarial rostrum than that of *Parasuchus bransoni*. The postnarial portion of the skull of *‘Paleorhinus’*

201 *parvus* is not preserved; therefore, Mehl based his calculations on a partial mandible associated with the

202 cranial remains, which he used to estimate total skull length. Mehl’s measurements suggest that the snout

203 constituted 42.4% of total cranial length, which is indeed proportionately short compared to *Parasuchus*

204 *bransoni*, for which values are approximately 50% (TMM 31100-101, 31100-418). This character should

205 be treated with caution, however, as Mehl’s calculations of skull length based on the mandible may be

206 somewhat inaccurate. Mehl also suggested that the rostrum of *‘Paleorhinus’ parvus* is more slender than

207 that of *Parasuchus bransoni*; however, it is uncertain whether this is due to mediolateral compression of
208 the former.

209 The anterior tip of the rostrum was suggested by Mehl (1928) suggested to be more abruptly
210 downturned than in *Parasuchus bransoni*. We concur with this assessment: the rostrum of ‘*Paleorhinus*’
211 *parvus* is more abruptly downturned than all species of *Parasuchus*, ‘*Paleorhinus*’ *sawini* and
212 *Ebrachosuchus neukami*, and more closely approximates the rostral morphology of *Brachysuchus* and
213 *Angistorhinus*. Mehl also noted that the nares of ‘*Paleorhinus*’ *parvus* are more steeply curved
214 anterodorsally than *Parasuchus bransoni*, but considered the narial development to be suspect and ‘not
215 dependable’. However, we concur with Kammerer *et al.* (2015) that there is no reason to suspect that the
216 morphology of the narial region is not genuine, even considering lateral compression. Kammerer *et al.*
217 (2015) also noted that the ‘subnarial facial portion of the maxilla’ is well preserved and ‘has greater
218 relative height than that of *Parasuchus hislopi*’. We agree with this assessment, and find that this is also
219 true when compared with all other members of *Parasuchus*.

220

221 ‘*Paleorhinus*’ *sawini* Long & Murry, 1995

222 **Age:** late Carnian–early Norian (c. 232–225 Mya)

223 **Occurrences:** ‘Pre-Tecovas Horizon’, Dockum Group, Borden County, Texas, USA

224 **Holotype:** TMM 31213-16, skull and possibly associated isolated postcrania

225 **Previously Referred Specimens:** None

226 **Specimen(s) Used for Scoring:** TMM 31213-16

227 **Key References:** Long & Murry (1995); Stocker (2010)

228 **Most Recent Diagnosis:** Long & Murry (1995) diagnosed ‘*Paleorhinus*’ *sawini* on the basis of the

229 following combination of characters: 1) Skull high; 2) Rostrum short and robust; 3) Prenarial length less

230 than postnarial length; 4) Maxilla with strongly convex ventral margin; 5) Posterior portion of maxilla
231 with prominent lateral flare; 6) Probable heterodont dentition; 7) Posterior maxillary alveoli enlarged and
232 transversely rectangular; 8) Posterior premaxillary enlarged; 9) Upper dentition with 38 teeth.

233 **Modified Diagnosis:** A non-leptosuchomorph phytosaur with the following unique character complex: 1)
234 Rostrum short and robust; 2) Prenarial length less than postnarial length; 3) Posterior premaxillary alveoli
235 enlarged; 4) Upper dentition with 38 teeth; 5) Parietal/squamosal bars are medially bowed.

236 **Comments:** Characters 1, 4 and 5 of Long & Murry (1995) may be related to general large size and
237 robusticity, but this has yet to be tested through ontogenetic studies of early phytosaurs. In particular, the
238 height of the skull in proportion to its width does not appear to differ considerably from other species of
239 early phytosaur such as *Parasuchus bransoni* (TMM 31100-8, 31100-101) or *Parasuchus angustifrons*
240 (ZPAL Ab III 111, Ab III 200). Characters 6 and 7 are based on incomplete or missing morphology. No
241 teeth remain in the skull, thus estimations of heterodonty are based solely on the shapes and relative sizes
242 of empty alveolae. Given that some degree of heterodonty is present in all phytosaurs and the roots of
243 even mediolaterally compressed phytosaur teeth are approximately circular, it is difficult to make
244 meaningful statements about heterodonty without preservation of the actual dentition. Similarly, the
245 posterior maxillary alveolae are heavily reconstructed with plaster, making character 7 questionable. It is
246 unclear how intraspecifically variable tooth counts are in phytosaurs; however, specimens of *Parasuchus*
247 *bransoni* and *Parasuchus hislopi* consistently have more than 40 teeth in the upper jaw (TMM 31100-101,
248 31100-239, ISI R42), whereas *Parasuchus angustifrons* appears to possess a similar number to
249 ‘*Paleorhinus*’ *sawini* (ZPAL Ab III 200). This character is therefore retained, as further study may reveal
250 it to contain taxonomic value.

251 Stocker (2010) noted two further characters that she proposed distinguish ‘*Paleorhinus*’ *sawini*
252 from *Parasuchus*: 1) Shares medially-bowed parietal-squamosal bars with *Angistorhinus*; 2) The

253 antorbital fossa is highly reduced or absent. It is, however, debatable how reduced in size the antorbital
254 fossa was; upon close examination it appears possible that the fossa may have been broken up to its outer
255 rim, i.e. to the extent of the concavity of the fossa. There is evidence of a thin lamina extending from the
256 interior edge of the purported fenestra in TMM 31213-16, but all of its edges are broken away; this may
257 be the remnants of the original antorbital fossa.

258

259 ***Ebrachosuchus neukami*** Kuhn, 1936

260 **Age:** late Carnian (c. 232–228 Mya)

261 **Occurrences:** Blasensandstein (lateral equivalent of Hassberge Formation), Middle Keuper Subgroup,
262 northern Bavaria, Germany

263 **Holotype:** BSPG 1931 X 501

264 **Previously Referred Specimens:** None

265 **Specimen(s) Used for Scoring:** BSPG 1931 X 501

266 **Key References:** Kuhn (1936); Long & Murry (1995); Butler *et al.* (2014)

267 **Most Recent Diagnosis:** Butler *et al.* (2014) diagnosed *E. neukami* based on six autapomorphies: 1)
268 Preorbital length more than 3.8 times that of the orbit + postorbital length; 2) More than 50 teeth in the
269 premaxilla and maxilla combined; 3) Pronounced, sharp flange extending along the lateral surface of the
270 dorsal (postorbital) process of the jugal and the ventral (jugal) process of the postorbital that is continuous
271 posteriorly with the lateral margin of the postorbital-squamosal bar; 4) Infratemporal fenestra is
272 substantially longer anteroposteriorly than deep dorsoventrally, terminates anteriorly beneath the midpoint
273 of the orbit; 5) Quadrate foramen very large, approximately two-thirds of width of foramen magnum; 6)
274 Alveolar ridges absent from the anterior maxilla and only poorly developed on the premaxilla.

275

276 ***Rutiodon carolinensis*** Emmons, 1856

277 **Age:** early Norian (c. 228–218 Mya)

278 **Occurrences:** Cumnock Formation, Deep River Coal Field, near Gulf, North Carolina, USA; Cumnock

279 Formation, New Egypt coal mine, Chatham County, North Carolina, USA

280 **Neotype:** USNM PAL 214513 (formerly ‘Williams College unnumbered specimen’)

281 **Previously Referred Specimens:** Emmons’ original material (isolated, assorted postcrania, the location

282 and accession numbers of which are unknown); 17 vertebrae and associated ribs (holotype of

283 ‘*Clepsysaurus leai*’, location and accession numbers unknown); teeth, referred to various taxa by Emmons

284 (1856) (location and accession numbers unknown); USNM 5373 (holotype of ‘*Rhytidodon rostratus*’

285 Marsh, 1896); AMNH 1 (semi-complete skull plus composite skeleton); AMNH 2 (skull roof); AMNH 3

286 (right posterior portion of skull roof including squamosal and supratemporal fenestra); AMNH 4 (rostral

287 fragment including partial nares and partial antorbital fenestra); AMNH 5 (Skull roof including left

288 supratemporal region, quadrate and quadratojugal) (Gregory, 1962).

289 **Specimen(s) Used for Scoring:** USNM PAL 214513; USNM V 5373; AMNH 1–5

290 **Key References:** Emmons (1856; 1860); Marsh (1896); McGregor (1906); Colbert (1947); Gregory

291 (1962); Hunt & Lucas (1989); Stocker (2010)

292 **Most Recent Diagnosis:** Stocker (2010) suggested the following diagnostic characters with reference to

293 the neotype specimen: 1) Slender rounded premaxillae that lack a rostral crest; 2) Nares placed posteriorly

294 between the antorbital fenestrae with borders above the level of the skull roof. To enable distinction

295 between *Rutiodon carolinensis* and *Angistorhinus*, Stocker added a further character based on preserved

296 temporal regions referred to *Rutiodon carolinensis* in the AMNH collections (AMNH 1–5): 3) Semi-

297 depressed parietal-squamosal bars.

298 **Comments:** Hunt & Lucas (1989) designated a neotype for *Rutiodon carolinensis* and proposed four
299 diagnostic characters that were centred around the temporal region of the skull. Stocker (2010) noted that
300 none of the characters included in the diagnosis of Hunt & Lucas (1989) were observable in their
301 designated neotype due to the temporal region not being preserved. Instead, the diagnostic appear to be
302 based on USNM and AMNH material that was referred to *Rutiodon carolinensis* by Gregory (1962).

303 Characters 1 and 2 of the diagnosis of Stocker (2010) are observable in the neotype; however, if
304 only these characters are considered it is not possible to differentiate *Rutiodon carolinensis* from
305 *Angistorhinus*. Stocker also therefore used the referred AMNH material to provide a further character and
306 a more robust diagnosis.

307 It should be noted that the elevation of the nares (character 2 of Stocker, 2010) may not be entirely
308 reliable, as the orbital and narial portions of the neotype do not articulate together meaning there is no
309 way to be certain that the nares would have been elevated above the level of the skull roof. Furthermore,
310 Gregory (1962) noted that in the neotype the nares were inferred to be elevated, while those of AMNH 1
311 are not, suggesting a degree of variability in this feature.

312

313 *Angistorhinus talaini* Dutuit, 1977

314 **Age:** late Carnian–early Norian (c. 232–225 Mya)

315 **Occurrences:** Timezgadiouine Formation, Western Moroccan Atlas, Morocco

316 **Holotype:** MNHN TAL 1–11 (syntypes), three skulls plus four partial mandibles and mandibular
317 fragments

318 **Previously Referred Specimens:** None

319 **Specimen(s) Used for Scoring:** MNHN TAL 1; MNHN TAL 2

320 **Key References:** Mehl (1913); Dutuit (1977); Long & Murry (1995)

321 **Most Recent Diagnosis:** Long & Murry (1995) felt the placement of *A. talainti* within the genus
322 *Angistorhinus* was unjustified and therefore considered it as referable to a new and currently unnamed
323 genus within the subfamily ‘Angistorhininae’ Camp, 1930. They considered it to be diagnosed by the
324 following combination of characters: 1) Supratemporal fenestra extremely elongate and narrow, crescentic
325 in dorsal view and extending to posterolateral corner of squamosal; 2) Postorbital portion of the skull
326 elongate with parietals long, narrow and fused for most of their length; 3) Postfrontal not in contact with
327 supratemporal fenestra; 4) Occiput with shallow posterior emargination; 5) Posterior process of squamosal
328 well developed and terminally convex; 6) Parietal extensions not present; 7) Opisthotic process short and
329 paddle shaped.

330 **Modified Diagnosis:** *A. talainti* can be diagnosed from other phytosaurs using a combination of
331 characters that includes generic *Angistorhinus* characters and characters recognized in previous studies
332 (Dutuit, 1977; Long & Murry, 1995): 1) Parietal/squamosal bars equal to, or greater than the thickness of
333 the postorbital/squamosal bars; 2) Parietal/squamosal bars curve medially; 3) Supratemporal fenestrae
334 narrow and short; 4) Postorbital portion of the skull elongate with parietals long, narrow and fused for
335 most of their length; 5) Posterior process of squamosal well developed and terminally convex; 6)
336 Posterolaterally curving groove extends from the supratemporal fenestra to the posterolateral corner of the
337 squamosal; 7) Prominent ridge runs along the anterior dorsolateral edge of the postorbital-squamosal bar;
338 8) Parietals diverge posterior to the main vacuity of the supratemporal fenestra.

339 **Comments:** The interpretation of the supratemporal fenestra of *A. talainti* in character 1 of Long & Murry
340 (1995) contradicts the description of Dutuit (1977), who stated in his diagnosis that the supratemporal
341 fenestrae are narrow and short. The figures in Dutuit (1977) superficially show an elongate fenestra, as
342 suggested by Long & Murry (1995); however, Long & Murry did not distinguish between the dorsal
343 opening of the fenestra and a posterior groove which grades from the posterior corner of the fenestra onto

the posterolateral corner of the squamosal. It is difficult to delimit the fenestra due to the presence of this groove, but we agree with Dutuit (1977), that the actual opening of the fenestra is relatively short. Characters 3 and 4 of Long & Murry (1995) appear to be shared by all members of *Angistorhinus* observed in this study, and character 5 is present in multiple specimens from Texas and New Mexico, such as TMM 31100-1332, TMM 31100-164, TMM 31100-298 and NMMNHS-P 4781. Character 6 is difficult to interpret - the terms ‘parietal extensions’ and ‘horizontal parietal extensions’ are used in Long & Murry’s revised diagnosis of ‘Angistorhinae’; however, no further explanation of these features is given. We assume that this terminology refers to the posterior thickening of the parietal/squamosal bars that is observed throughout *Angistorhinus*. The parietals of *A. talaini* are expanded posteriorly in a horizontal plane to a greater extent than other species and specimens of *Angistorhinus* mentioned by Long & Murry (1995).

355

356

357 ***Angistorhinus grandis*** Mehl, 1913

358 **Age:** late Carnian–early Norian (c. 232–225 Mya)

359 **Occurrences:** Popo Agie Formation, between Squaw and Baldwin Creeks, Fremont County, Wyoming,
360 USA

361 **Holotype:** FMNH UC 631, Skull and associated partial mandible

362 **Previously Referred Specimens:** None

363 **Specimen(s) Used for Scoring:** FMNH UC 631

364 **Key References:** Mehl (1913); Long & Murry (1995)

365 **Most Recent Diagnosis:** Long & Murry (1995) diagnosed *A. grandis* as a species of *Angistorhinus* with
366 the following characters: 1) Posterior process of squamosal very short, but deep with straight posterior

margin; 2) No cleft between posterior process and descending process of the squamosal; 3) Parietal extension ?short; 4) Rostrum delicate; 5) Alveoli circular throughout with posterior premaxillary alveoli not enlarged (this region of snout is not swollen); 6) Ventral margin of maxilla not laterally flared; 7) Orbits directed more dorsally than laterally.

Modified Diagnosis: We diagnose *A. grandis* as a species of *Angistorhinus* with the following unique character combination: 1) Ventral margin of maxilla not laterally flared; 2) Supratemporal fenestrae wide and triangular in shape; 3) Lateral temporal fenestra large and more sub-triangular than rectangular; 4) U-shaped emargination between the supratemporal fenestrae at the posterior border of the parietals in dorsal view.

Comments: We suggest that characters 1 and 2 of Long & Murry (1995) should be treated with caution, or potentially rejected, as the posterior process of the squamosal is not actually preserved in *A. grandis*. The morphology of the posterior process was reconstructed in plaster from a supposed impression of the medial surface of the process preserved in the matrix with the skull; however, no photographs or diagrams exist of this impression, and its described morphology differs from the rounded morphology of the posterior process of the squamosal observed in all other specimens of *Angistorhinus*.

Characters 3 and 4 of Long & Murry (1995) are phrased ambiguously and are therefore difficult to objectively assess. Alongside character 5, these characters are also present in all other specimens of *Angistorhinus* that were examined, and are therefore not useful for a diagnosis at specific level. Character 7 reports the orientation of the orbit; however, phytosaur skulls are often mediolaterally or dorsoventrally compressed meaning that the orientation of the orbits can vary widely both inter- and intraspecifically, and should not be used for diagnostic or phylogenetic purposes (Chatterjee, 1978; Hungerbühler, 1998).

388

389

390 *Smilosuchus gregorii* (Camp, 1930)

391 **Age:** early Norian (c. 225–220 Mya)

392 **Occurrences:** Blue Mesa Member, Chinle Formation, near Round Rock, Apache County, Arizona, USA

393 **Holotype:** UCMP 27200, slightly dorsoventrally compressed skull and mandibles

394 **Previously Referred Specimens:** UCMP A270/27192; UCMP A270/27195 (Camp, 1930); AMNH

395 D.VP. 3060 (Colbert, 1947); USNM V 18313; UCMP 63921; UCMP 35737; UMMP 14366; PPHM WT

396 3217; PPHM WT 3214; PPHM WT 3230 (Long & Murry, 1995).

397 **Specimen(s) Used for Scoring:** UCMP 27200; AMNH D.VP. 3060

398 **Key References:** Camp (1930); Colbert (1947); Long & Murry (1995)

399 **Most recent diagnosis:** Long & Murry (1995) diagnosed the new genus *Smilosuchus* and the sole species

400 that they referred to it, *S. gregorii*, based on the following character combination: 1) Extreme heterodonty;

401 2) Posterior premaxillary teeth (except last three) abruptly and very greatly enlarged, causing a swelling of

402 the premaxilla in this region; 3) Tooth pattern posteriorly shifted; 4) Ventral margin of the maxilla greatly

403 flared laterally; 5) Rostral crest fully developed; 6) Anterior portion of rostrum very heavy and massive;

404 7) Posterior portion of the skull considerably wider than in *Leptosuchus*, with lateral temporal fenestra

405 facing dorsolaterally; 8) Orbit directed dorsolaterally.

406 **Modified Diagnosis:** *S. gregorii* is diagnosed on the basis of the following unique character combination:

407 1) Full rostral crest; 2) Greatly dorsoventrally expanded posterior process of the squamosal.

408 **Comments:** Characters ~~four~~4, ~~six~~6 and ~~seven~~7 of Long & Murry (1995) may be size-correlated, which is

409 both undesirable and problematic (Irmis, 2005); ~~seven~~7 and ~~eight~~8 are highly prone to taphonomic

410 distortion and the phrasing of character ~~three~~3 is ambiguous.

411 Of the remaining characters, ~~two~~2 and ~~five~~5 are consistently present only in *S. gregorii* rather than ‘*S*’.

412 *adamanensis* or ‘*S*’. *lithodendrorum* and may therefore be useful in defining the species. Character one

Commented [WGPI]: Use numerals to stay consistent through this section.

413 (extreme heterodonty) is present in all current species of *Smilosuchus* and is therefore not of diagnostic
414 use for *S. gregorii*.

415

416 ‘*Smilosuchus*’ *adamanensis* (Camp, 1930)

417 **Age:** early Norian (c. 225–220 Mya)

418 **Occurrences:** Blue Mesa and lower Sonsela Members, Chinle Formation, near Adamana Petrified Forest

419 National Park, Apache County, Arizona, USA

420 **Holotype:** UCMP 26699, skull and mandibles

421 **Previously Referred Specimens:** All phytosaur material from UCMP/PEFO localities 7038PFV 122,

422 7039PFV 120, 7040PFV 121, 7044PFV 142, 7046-PFV 157 and 7047-PFV 155 (Camp, 1930; Parker,

423 2002); (UCMP 26696, 26697, 26698, 26706, 26717, 26718, 26720, 26725, 26727, 26729, 26730, 26731,

424 26756, 27070, 27093, 27094, 27104 and 27106 referred as paratypes (Camp, 1930)); UCMP 27099,

425 27006, 27007, 27008, 27010, 27011, 27013, 27014, 27015, 27025, 27026, 27027 (Camp, 1930); UCMP

426 27446; MNA Pl.V-3024; MNA Pl.V-3025; MNA Pl.V-2675; MNA V3698; UCMP 27444; UCMP 27185;

427 UCMP 27036 (holotype of ‘*M*. *zunii*’); UCMP 27060; UCMP 126991; USNM 15841; UCMP 124957;

428 USNM (NPS 72-39 in part); AMNH (EHC 1946-23); UCMP 26688 (holotype of ‘*S*. *lithodendrorum*’);

429 UMMP 7523 (holotype of ‘*Leptosuchus imperfecta*’) (Long & Murry, 1995). PEFO 34852 (Griffin et al.,

430 2017).

431 **Specimen(s) Used for Scoring:** UCMP 26699; UCMP 170166

432 **Key References:** Camp (1930); Long & Murry (1995); Stocker (2010)

433 **Most Recent Diagnosis:** Long & Murry (1995) differentiated ‘*S*. *adamanensis*’ from other *Leptosuchus*-

434 grade phytosaurs on the basis the following character combination: 1) Posterior process of squamosal is a

435 deep vertical plate with moderate posterior elongation beyond paroccipital process; 2) Post-fenestral

Commented [WGP2]: Petrified Forest National Park

Commented [WGP3]: Petrified Forest Vertebrate locality

Commented [WGP4]: Please use the official PEFO locality numbers.

Commented [WGP5]: Parker, W. G. 2002. Correlation of locality numbers for vertebrate fossil sites in Petrified Forest National Park, Arizona. New Mexico Museum of Natural History and Science Bulletin 21:37-42.

Commented [WGP6]: P1 designation for vertebrates is no longer used.

Commented [WGP7]: Griffin, C.T., Stefanic, C.M., Parker, W.G., Hungerbuhler, A., and M. R. Stocker 2017. Sacral anatomy of the phytosaur *Smilosuchus adamanensis*, with implications for pelvic girdle evolution among Archosauriformes. Journal of Anatomy 231:886-905.

436 portion of squamosal wide and abruptly truncated when viewed dorsally, though the extra-fenestral
437 portion of the bar is narrow.

438 **Comments:** Both characters of Long & Murry are accurate; however, character 1 is somewhat variable in
439 other early leptosuchomorph taxa e.g., *Leptosuchus crosbiensis* (UMMP 7522, TMM 31173-120), and
440 character 2 is based on heavily distorted morphology in the holotype. The lack of either a rostral or narial
441 crest in ‘*S.*’ *adamanensis* distinguishes it from other putative members of the genus *Smilosuchus* and
442 members of *Leptosuchus*, though it is unclear whether or not this feature is plesiomorphic.

443 ‘*S.*’ *adamanensis* suffers the same problem as ‘*S.*’ *lithodendrorum* (see below); the majority of
444 material referred to this species by Camp (1930) was referred based on geographical and stratigraphical
445 proximity. As such, previous definitions of the taxon may be chimeric; subsequent analyses should
446 therefore treat referred specimens with caution or rely only on the holotype. A thorough re-examination
447 and redescription of the holotype of ‘*S.*’ *adamanensis* may bring further diagnostic characters to light;
448 however, such work is beyond the scope of the current study.

450 ‘*Smilosuchus*’ *lithodendrorum* (Camp, 1930)

451 **Age:** Norian (c. 219–217 Mya)

452 **Occurrences:** ~~Lot’s Wife beds~~ ~~Lower Carrizo fossil horizon~~, Sonsela Member, Chinle Formation, ~~near~~
453 ~~Adamana~~ Petrified Forest National Park, Navajo County, Arizona, USA; Tecovas Formation, Dockum
454 Group, Crosby County, Texas, USA

455 **Holotype:** UCMP 26688, poorly preserved, fragmentary and compressed left half of skull, and almost
456 complete mandibles.

457 **Previously Referred Specimens:** All phytosaur material from UCMP/UCMP-PEFO localities ~~A-258~~ PFV
458 108, 7034PFV 096, 7037PFV 172, 7042-PFV 146 and 7044-PFV 161 (Camp, 1930; Parker, 2002);

Commented [WGP8]: Parker and Martz, 2011.

Formatted: Font: Not Bold

Commented [WGP9]: Petrified Forest National Park

Commented [WGP10]: Please use the official PEFO locality numbers.

Commented [WGP11]: Parker, W. G. 2002. Correlation of locality numbers for vertebrate fossil sites in Petrified Forest National Park, Arizona. New Mexico Museum of Natural History and Science Bulletin 21:37-42.

459 (UCMP 26683, 26684, 26719, 27179, 27189, 27181 and 27182 referred as paratypes (Camp, 1930));
460 UCMP 27151, 26693, 26694, 27017, 27183, 27184, 27149 (Camp, 1930); TMM 31173-121 (Stocker,
461 2010).

462 **Specimen(s) Used for Scoring:** UCMP 26688; TMM 31173-121

463 **Key References:** Camp (1930); Long & Murry (1995); Stocker (2010)

464 **Most Recent Diagnosis:** Stocker (2010) proposed that '*Smilosuchus*' *lithodendrorum* should be
465 diagnosed as a species of *Smilosuchus* with the following characters: 1) A highly angled rostrum that
466 continues anteroventrally in a smooth descent; 2) The posterior process of the squamosals grade
467 anteroventrally into the opisthotic process; 3) Very slight medial flange on the dorsal edge of the
468 squamosal.

469 **Comments:** The validity of '*S.*' *lithodendrorum* has previously been questioned; it was synonymized with
470 *Leptosuchus crosbiensis* by Long & Murry (1995) with no justification given. Stocker (2010) suggested
471 that this may have been due to the narrow postorbital/squamosal bar, which is a prominent feature of
472 *Leptosuchus crosbiensis* and *Leptosuchus studei*. It is also possible that the synonymization was due to
473 extensive morphological variation exhibited in the specimens referred to '*S.*' *lithodendrorum* by Camp
474 (1930). Camp's assignments of lectotypes and referred specimens were based on geographical and
475 stratigraphical proximity of specimens to the holotype, rather than morphology; as a result, a number of
476 smaller, non-crested skulls (between 678 and 965 mm in length) were assigned to this species as juveniles
477 of '*S.*' *lithodendrorum* (UCMP 26684, 26719, 27179, 27181). These specimens lack the full rostral crest
478 reported in larger individuals of '*S.*' *lithodendrorum*, instead their crests extend anterior of the nares
479 before descending to form tubular rostra close to the most anterior extent of the maxillae. This
480 morphology, combined with the size range of the specimens and aforementioned similarities between *L.*
481 *crosbiensis* and '*S.*' *lithodendrorum*, seemingly makes them indistinguishable from the holotype of *L.*

482 *crobiensis*. Conversely, the crest morphology in larger specimens of both ‘*S.*’ *lithodendrorum* and *L.*
483 *crobiensis* does differ substantially. In larger specimens of ‘*S.*’ *lithodendrorum* (e.g., UCMP 26688;
484 TMM 31173-121) the rostrum is fully crested, with the crest forming a straight diagonal gradient from the
485 nares to the tip of the premaxillae. However, in larger specimens of *L. crobiensis* (e.g., TMM 43684,
486 43684-8) the morphology remains unchanged from smaller specimens such as TMM 31173-120, with a
487 partial rostral crest extending from the nares to the most anterior extent of the maxillae, and a separate
488 premaxillary crest at approximately the mid-point of the premaxillae. A more detailed examination of all
489 material potentially referable to these taxa may help to quantify the morphological variation associated
490 with these taxa, and disentangle their diagnoses. Stocker (2010) did tentatively identify some subtle
491 differences between ‘*S.*’ *lithodendrorum* and *L. crobiensis*, although her diagnosis does not take into
492 account the intermediate morphologies present in some specimens. However, a full redescription and re-
493 evaluation of the species is beyond the remit of this paper. We therefore use the diagnosis of Stocker
494 (2010).

495

496 ‘*Phytosaurus*’ *doughty* Case, 1920

497 **Age:** early Norian (c. 225–220 Mya)

498 **Occurrences:** Tecovas Formation, Dockum Group, Texas, USA

499 **Holotype:** AMNH FR. 4919, right posterior portion of skull

500 **Previously Referred Specimens:** Possibly MSM 92-023.001 (Stocker, 2010).

501 **Specimen(s) Used for Scoring:** AMNH FR. 4919

502 **Key References:** Case (1920); Stocker (2010)

503 **Most Recent Diagnosis:** Case (1920) was able to identify two characters to separate ‘*Phytosaurus*’
504 *doughtyi* from other *Leptosuchus*-grade phytosaurs: 1) No evidence of the opisthotic process posterior to
505 the quadrate; 2) The nares rise at their posterior rim.

506 **Comments:** Character 2 of Case (1920) is present in referred specimens of *Leptosuchus crobiensis*
507 (TMM 31173-120 and TTU-P 09230); despite this, Stocker (2010) tentatively suggested the referral of
508 MSM 92-023.001 to ‘*Phytosaurus*’ *doughtyi* based in part on the presence of a deep saddle between the
509 orbits and external nares. It may therefore be the case that the differences in this character are more
510 nuanced between *L. crobiensis* and ‘*Phytosaurus*’ *doughtyi*, rather than being simply present or absent.
511 Character 1 of Case (1920) appears to be an autapomorphy of ‘*Phytosaurus*’ *doughtyi*, and this is
512 supported by our first-hand study of the holotype specimen.

513

514 ***Leptosuchus studei*** Case & White, 1934

515 **Age:** early Norian (c. 225–220 Mya)

516 **Occurrences:** Tecovas Formation, Dockum Group, Cerita de la Cruz Creek, Potter County, Texas USA;

517 ~~Lower Petrified Forest~~ Blue Mesa Member, Chinle Formation, Arizona, USA

518 **Holotype:** UMMP 14267, skull

519 **Previously Referred Specimens:** None

520 **Specimen(s) Used for Scoring:** UMMP 14267

521 **Key References:** Case & White (1934); Stocker (2010)

522 **Most Recent Diagnosis:** Stocker (2010) used two characters to diagnose *L. studei*: 1) Posterior edges of
523 the posterior processes [of the squamosals] curl inwards in *L. studei*, differing from the straight posterior
524 processes of *L. crobiensis*; 2) Small dorsally convex area on the dorsal surface of the mid-premaxillae.

525 **Comments:** At the time of writing the holotype and referred specimens of *L. studei* were unavailable to
526 study, so our observations are tentative and brief. It seems possible that character 1 of Stocker (2010)
527 could be due to taphonomic distortion, although the morphology is present on both posterior processes,
528 and to the same degree. Character 2 of Stocker (2010) is also present in *Leptosuchus crosbiensis*,
529 appearing in a line-drawing of the holotype (Case, 1922), and is visible in multiple other specimens
530 (TMM 31173-120, 43684, 43684-8; TTU-P 00902, 09230, 09234, 10001). The shape of the premaxillary
531 crest does, however, appear to be different to that of *L. crosbiensis*. The crest of *L. crosbiensis* is
532 anteroposteriorly symmetrical and forms a smooth ‘hump’, whereas in *L. studei* the anterior portion of
533 the crest slopes gently and the posterior slightly more steeply; the apex of the crest is therefore sharper. A
534 partially prepared specimen at Petrified Forest National Park (field no. RLG 11/07-3) also displays this
535 crest morphology, and the posterior process of the squamosal is also identical in lateral view to *L. studei*.

536

537 ***Leptosuchus crosbiensis*** Case, 1922

538 **Age:** early Norian (c. 225–220 Mya)

539 **Occurrences:** Tecovas Formation, Dockum Group, Crosby County, Texas, USA

540 **Holotype:** UMMP 7522, skull

541 **Previously Referred Specimens:** USNM 15481 (Stocker, 2010); PPHM WT 3243; UCMP 27179;

542 UCMP 27181; UCMP 26688 (Holotype of ‘*S. lithodendrorum*’); UCMP 126992; UCMP 126988; UCMP

543 126745; UCMP 27195; UCMP 27192; MSM 92-023.001; UMMP 14267 (Holotype of *L. studei*); UMMP

544 14366; UMMP 12198; TTU-P ‘383’; TMM 1010-5; TMM 31173-120; TMM 31173-121 (Long & Murry,

545 1995).

546 **Specimen(s) Used for Scoring:** UMMP 7522; TMM 31173-120; USNM V 15841; TTU-P 09230

547 **Key References:** Case (1922); Long & Murry (1995); Stocker (2010)

548 **Most Recent Diagnosis:** Stocker (2010) listed diagnostic features of *L. crosbiensis* in comparison to other
549 *Leptosuchus*-grade taxa: 1) An overall slenderness of the skull; 2) Supratemporal fenestrae that are
550 completely visible in dorsal view; 3) Supratemporal fenestrae are bounded anterolaterally by
551 mediolaterally narrow dorsal edges of the squamosals.

552 **Modified Diagnosis:** 1) An overall slenderness of the skull; 2) Supratemporal fenestrae that are
553 completely visible in dorsal view; 3) Supratemporal fenestrae are bounded anterolaterally by
554 mediolaterally narrow dorsal edges of the squamosals; 4) Dorsally rounded crest on the anterior portion of
555 the premaxilla; 5) Partial rostral crest extends approximately level from the nares and descends at a point
556 level with the anterior-most extent of the maxillae.

557 **Comments:** We suggest two additional characters (4 and 5 in the above modified diagnosis), to reinforce
558 the diagnosis of *L. crosbiensis*. See '*Smilosuchus lithodendrorum*' for further discussion of this taxon.

559

560 ***Pravusuchus hortus*** Stocker, 2010

561 **Age:** Norian (c. 219–217 Mya)

562 **Occurrences:** White 'hoodoo' sandstone, ~~2Jasper Forest Bed/Rainbow Forest Bed~~Kellogg Butte

563 Sandstone, Sonsela Member, Chinle Formation, Devil's Playground, Petrified Forest National Park,

564 Arizona, USA; ~~2~~Monitor Butte Member, Chinle Formation, Fry Canyon, Utah, USA

565 **Holotype:** AMNH FR. 30646, dorsoventrally crushed postnarial portion of skull and separate

566 mediolaterally compressed right half of rostrum

567 **Previously Referred Specimens:** PEFO 31218; PEFO 34239 (Stocker, 2010); ~~unnumbered specimen~~

568 from Utah (McCormack & Parker, 2017).

569 **Specimen(s) Used for Scoring:** AMNH FR. 30646; PEFO 31218; PEFO 34239

570 **Key References:** Stocker (2010); McCormack & Parker (2017)

Commented [WGP12]: Parker and Martz, 2011.

Commented [WGP13]: This is a Utah Museum of Natural History Specimen. UMNH 28293.

571 **Most Recent Diagnosis:** Stocker (2010) identified one autapomorphy for *Pravusuchus hortus* (the
572 ‘septomaxilla’ forms part of the lateral rim of the external nares) and a unique character combination: 1)
573 Absence of antorbital fossa; 2) broad and rounded interpremaxillary fossa; 3) Alveolar ridges visible in
574 lateral view; 4) Fully crested rostrum; 5) Long posterior process of squamosal; 6) Posterior process of
575 squamosal is greatly dorsoventrally expanded; 7) Possession of a subsidiary opisthotic process of the
576 squamosal; 8) Supratemporal fenestrae partially depressed; 9) Supratemporal fenestrae that are mostly
577 visible in dorsal view.

578 **Comments:** In relation to the ‘septomaxillary’ autapomorphy of *Pravusuchus hortus* Stocker (2010)
579 stated that ‘dorsal examination of the narial region shows a possible dorsolateral process of the
580 ‘septomaxilla’ on the lateral border of the naris’. Upon first-hand examination of the holotype and other
581 specimens we suggest that a lateral extension of the ‘septomaxilla’ is unlikely; rather, the suture identified
582 by Stocker may represent the lateral border of the paranasal, as described by Hungerbühler *et al.* (2013).
583 As noted in the holotype by Stocker (2010), ‘iron oxide covers potential ‘septomaxilla’-premaxilla
584 sutures’; however, amongst the iron oxide a distinct groove extends from the anterior narial border,
585 occupying the same position as the ‘septomaxillary’ suture in most phytosaurs. Therefore, we suggest that
586 *Pravusuchus hortus* is diagnosed using only the unique character combination proposed by Stocker
587 (2010), until the lateral extent of the ‘septomaxillae’ can be unambiguously verified in additional
588 specimens.

589

590 *Nicrosaurus kapffi* (Meyer, 1860)

591 **Age:** middle–late Norian (c. 216–209 Mya)

592 **Occurrences:** Löwenstein Formation (middle Stubensandstein), Middle Keuper Subgroup, Baden-
593 Württemberg, Germany

594 **Holotype:** SMNS 4060/4060a, poorly preserved rostral fragment and associated symphyseal-
595 postsymphyseal mandibular fragment, and uncat. No. 15, left maxillary and jugal fragment that fits with
596 4060 (all lectotype); SMNS 54708, anterior fragment of left premaxilla (paralectotype)
597 **Previously Referred Specimens:** SMNS 4378; SMNS 4379; SMNS 5725; SMNS 5726, SMNS 5727;
598 SMNS 13078; SMNS 54706; SMNS 56989; SMNS uncat. No. 12; SMNS 4380; SMNS 5730; SMNS
599 uncat. No. 9; SMNS 54708; NHMUK 38036; NHMUK 38043; NHMUK 42743; NHMUK 42744; GPIT
600 2223.000; GPIT uncat. No. 399 (Hungerbühler, 1998).
601 **Specimen(s) Used for Scoring:** SMNS 4378; SMNS 4379; SMNS 5726; SMNS 5727; NHMUK 42743
602 **Key References:** Meyer (1860, 1861, 1863, 1865); Hungerbühler (1998); Hungerbühler & Hunt (2000)
603 **Most Recent Diagnosis:** Hungerbühler (1998) presented a unique character combination for *N. kapffi*
604 based largely on characters from Long & Murry (1995) and Ballew (1989). The unique combination is
605 composed of the following two characters: 1) Presence of a continuous prenarial crest reaching just
606 behind the downturned tip of the snout; 2) Top of prenarial crest straight or slightly convex.
607
608 *Nicrosaurus meyeri* Hungerbühler & Hunt (2000)
609 **Age:** middle–late Norian (c. 216–209 Mya)
610 **Occurrences:** Löwenstein Formation (middle Stubensandstein), Middle Keuper Subgroup, Baden-
611 Württemberg, Germany
612 **Holotype:** SMNS 12593, dorsoventrally compressed skull in two pieces
613 **Previously Referred Specimens:** SMNS 4059, 12593/2 & SMNS uncat. No. 11; NHMUK 38038 &
614 42745; GPIT 261/001 & GPIT 2070.001 (Hungerbühler & Hunt, 2000).
615 **Specimen(s) Used for Scoring:** SMNS 12593; SMNS 4059; NHMUK 38038; NHMUK 42745; GPIT
616 2070.001

617 **Key References:** Meyer (1861); Hunt (1994a); Hungerbühler (1998); Hungerbühler & Hunt (2000)

618 **Most Recent Diagnosis:** Hungerbühler & Hunt (2000) identified *N. meyeri* as a species of *Nicrosaurus*,
619 differentiated from *N. kapffi* on the basis of the following characters: 1) Rostrum slender and gracile; 2)
620 Prenarial crest absent or over posterior part of the snout only; 3) Septomaxilla terminates at the level of
621 the anterior tip of the nasal; 4) Anterior part of the internasal septum may be prominent and visible in
622 lateral view; 5) Sculpture of the pre-orbital region prominent; 6) Cheek region (quadratojugal + jugal)
623 always with a well developed longitudinal depression; 7) Craniomandibular facet of the quadrate less
624 wide and lateral condyle offset from the cheek; 8) Postorbital-squamosal bar broader; 9) Supratemporal
625 fenestra less wide; 10) In dorsal view the posterior process of the squamosal is continuously broad, the
626 medial rim is angular; 11) Posterior process of the squamosal terminates with a pointed tip; 12)
627 Paroccipital process of the squamosal ('hooklike process') small; 13) Alveolar ridges more prominent,
628 prechoanal part of the vomers mostly slender and tapering; 14) Upper jaw dentition moderately
629 heterodont; 15) Premaxillary teeth set more laterally; 16) Mandibular symphysis equals ~50% of the total
630 mandibular length (rather than 40% as in *Nicrosaurus kapffi*).

631

632 ***Coburgosuchus goeckeli*** Heller, 1954

633 **Age:** middle-late Norian (c. 216–209 Mya)

634 **Occurrences:** Upper Burgsandstein (lateral equivalent of the Löwenstein Formation), Untersiema,
635 Baden-Württemberg, Germany

636 **Holotype:** NMC 15436, postnarial portion of skull

637 **Previously Referred Specimens:** None

638 **Specimen(s) Used for Scoring:** NMC 15436

639 **Key References:** Heller (1954)

640 **Most Recent Diagnosis:** Heller (1954) originally described this specimen in German; however, since then
641 this taxon has been largely ignored. Heller (1954) diagnosed the genus as a phytosaur of similar size to
642 *Nicrosaurus kapffi*, though differentiated by an even greater development of the squamosals and more
643 laterally oriented orbits.

644 **Comments:** As with many other diagnoses, we doubt the utility of orbital orientation as a reliable
645 diagnostic character; however, the substantially more pronounced lateral curvature of the squamosals does
646 appear to be valid and distinguishes *Coburgosuchus goeckeli* from *Nicrosaurus kapffi*. We are currently
647 preparing a redescription of *Coburgosuchus*, and as such we do not present further diagnostic characters at
648 this time.

649

650 **'Machaeroprotopus' zunii** Camp, 1930

651 **Age:** early Norian (c. 225–220 Mya)

652 **Occurrences:** ~~Mesa Redondo~~/Blue Mesa Member, Chinle Formation, Arizona, USA

653 **Holotype:** UCMP 27036, partial braincase and postcrania

654 **Previously Referred Specimens:** All specimens from UCMP localities 7307, 7308, 7309, 7310 & A 255;
655 UCMP 27041, 27044, 27054, 27154, 27155, 27156, 27189, 27158, 27056, 27057, 27159, 27048 & 27189
656 (Camp, 1930).

657 **Specimen(s) Used for Scoring:** UCMP 27159

658 **Key References:** Camp (1930); Stocker (2010)

659 **Most Recent Diagnosis:** Camp (1930) produced a diagnosis of '*M. zunii*' based on various referred
660 specimens. Due to the arbitrary referral of many of the specimens (see below) the characters presented
661 may constitute a mosaic from multiple species: 1) Rostrum very long, slender; 2) Nasals large, extending
662 forward beyond nares and entering dorsal border of antorbital fenestra; 3) Posterior squamosal process

Commented [WGP14]: Not in the Mesa Redondo Member.
Lucas et al. 1997 erroneously considered the Placerias
Quarry to be low down in the Chinle Formation.

663 very large, broad, flat, and expanded vertically; 4) Parietals small, anterior suture lies well behind
664 posterior border of orbits; 5) Posterior parietal process Y-shaped; 6) Anterior border of supratemporal
665 fenestra very wide and not excavated forward to or nearly to middle of parietals; 7) Postorbito-squamosal
666 bar narrow.

667 **Comments:** Camp (1930) presented the holotype of '*M. zunii*' as a partial braincase and postcrania, thus
668 containing little to no material of diagnostic utility. However, a number of specimens containing cranial
669 material, such as UCMP 27048, 27189, 27159 were also referred to '*M. zunii*', of which UCMP 27159
670 was also used in the matrix of Stocker (2010). As the type material is undiagnostic the rest of the referred
671 specimens are referred on the basis of stratigraphic and geographic proximity to the type and should
672 therefore be treated cautiously or altogether excluded. '*M. zunii*' is included here and scored based on
673 only one of Camp's referred specimens. A specimen in the Smithsonian Institution (USNM V17098) is
674 catalogued as '*M. zunii*' and appears to share a similar morphology to that of the specimens referred by
675 Camp; we include this specimen as a separate OTU to test the credibility of its referral and this taxon in
676 general, to judge whether it warrants more detailed investigation.

677

678 ***Protome batalaria*** Stocker, 2012

679 **Age:** early Norian (c. 220–218 Mya)

680 **Occurrences:** Upper Lot's Wife beds, Sonsela Member, Chinle Formation, Petrified Forest National
681 Park, Arizona, USA

682 **Holotype:** PEFO 34034, pre-narial rostrum with narial fragments, post-narial skull roof with squamosals,
683 basioccipital and left mandible.

684 **Previously Referred Specimens:** None

685 **Specimen(s) Used for Scoring:** PEFO 34034

686 **Key References:** Stocker (2012)

687 **Most Recent Diagnosis:** Stocker (2012) presented three autapomorphies and a unique character
688 combination for *Protome batarialia*. Due to the length of the unique character combination we only
689 present the autapomorphies here: 1) Presence of a flat ventral surface on the basitubera; 2) Posterior
690 prongs from the exoccipitals dorsal to the foramen magnum; 3) Fossa surrounding the anterior corner of
691 the external mandibular fenestra.

692 **Comments:** These autapomorphies all appear valid, although the posterior exoccipital prongs mentioned
693 in character 2 may also be present in *Coburgosuchus*, but further study is required to verify this.

694

695 **‘Machaeroprotopus’ andersoni** Mehl, 1922

696 **Age:** late Norian (c. 218–208 Mya)

697 **Occurrences:** Bull Canyon Formation, Dockum Group, near Santa Rosa, Guadalupe County, New
698 Mexico, USA

699 **Holotype:** FMNH UC 396, heavily reconstructed skull

700 **Previously Referred Specimens:** None

701 **Specimen(s) Used for Scoring:** FMNH UC 396

702 **Key References:** Mehl (1922); Long & Murry (1995)

703 **Most Recent Diagnosis:** Mehl (1922) suggested that ‘*M*’. *andersoni* shares a close affinity with
704 ‘*Machaeroprotopus validus*’ and distinguished it using the following characters: 1) Postero-median
705 border of supra-temporal fenestrae not completely depressed; 2) Anterior border of nares not elevated; 3)
706 Terminal expansion of rostrum gradual; 4) Nasals extending some distance in front of anterior border of
707 nares; 5) Greatest length of maxillae at alveolar margin; 6) Approximately ninety-four teeth in upper

708 dentition; 7) Four large teeth in terminal expansion of rostrum; 8) Alveolae not crowded; 9) Lateral
709 expansion of rostrum at posterior end of premaxillae.

710 **Comments:** '*M. andersoni*' was synonymized with *Machaeroprotopus buceros* by Long & Murry
711 (1995); however, upon inspection of their diagnosis of *Machaeroprotopus buceros* it is clear that many
712 characters are inappropriate for, or are not preserved in the holotype (and only specimen) of '*M.*
713 *andersoni*'. Two characters pertain to the squamosals, which are not preserved in '*M. andersoni*', three
714 characters are unnecessarily used to describe the same morphology of the pre-narial crest, and the
715 majority of the remaining characters do not distinguish either taxon from many others, even when the
716 characters are taken in combination.

717 Aside from the problem that the characters of Mehl (1922) may not differentiate '*M. andersoni*
718 from all current species of *Machaeroprotopus*, they are also based on comparison with
719 '*Machaeroprotopus validus*' which has subsequently been lost and also found not to be the type species
720 of *Machaeroprotopus*. This taxon requires reanalysis and thorough comparison to *Machaeroprotopus*
721 *buceros* (the valid type species) and other members of *Machaeroprotopus*; however, this is beyond the
722 scope of the current study.

723

724 *Machaeroprotopus jablonskiae* Parker & Irmis, 2006

725 **Age:** late Norian (c. 218–216 Mya)

726 **Occurrences:** ~~Basal~~ Jim Camp Wash beds, Sonsela Member, Chinle Formation, Petrified Forest National
727 Park, Arizona, USA

728 **Holotype:** PEFO 31207, skull roof with squamosals

729 **Previously Referred Specimens:** None

730 **Specimen(s) Used for Scoring:** PEFO 31207

Commented [WGP15]: Found to be in the upper part of the Jim Camp Wash beds. Parker and Martz, 2011.

731 **Key References:** Parker & Irmis (2006)

732 **Most Recent Diagnosis:** Parker & Irmis (2006) noted a single autapomorphy of *Machaeroproso-*

733 *jablonskiae*: Distinct smooth bevelled edge on the antero-medial edge of the postorbital-squamosal bar that

734 forms a supratemporal fossa lateral to the supratemporal fenestra. Alongside this they presented a unique

735 character combination as follows: 1) Apomorphic characters for *Pseudopalatus* [*Machaeroproso-*

736 *clade*; 2) Squamosal tips that are not knob-like as in *Machaeroproso-* *buceros* + *Machaeroproso-*

737 *pristinus*; 3) Thin oar-like paroccipital process of the opisthotic that is fused to the internal squamosal

738 process as in *Machaeroproso-* *buceros* + *Machaeroproso-* *mccauleyi*; 4) Anterior process of the

739 squamosal enters the lateral wall of the braincase as in *Mystriosuchus westphali* and *S. gregorii*; 5) No

740 lateral groove or ridge on the squamosal; 6) Squamosals are strongly anteroposteriorly shortened.

Commented [WGP16]: This may also be in *Machaeroproso-* *lottorum*.

742 *Machaeroproso-* *mccauleyi* (Ballew, 1989)

Commented [WGP17]: Should actually be *mccauleiorum*

743 **Age:** late Norian–early Rhaetian (c. 213–207 Mya)

744 **Occurrences:** ~~Upper Petrified Forest~~ *Martha’s Butte beds, Sonsela* Member, Chinle Formation, ~~Billings~~

745 ~~Gap~~ *Petrified Forest National Park*, Apache County, Arizona, USA

746 **Holotype:** UCMP 126999, skull missing anterior rostrum, mandibles present

747 **Previously Referred Specimens:** USNM 15839 (Ballew, 1989); PEFO 31219 (Stocker, 2010);

748 NMMNHS-P 4239, 4256; YPM 3293 (Hunt *et al.*, 2006).

749 **Specimen(s) Used for Scoring:** UCMP 126999; PEFO 31219; ~~PEFO unnumbered~~

Commented [WGP18]: Probably numbered now.

750 **Key References:** Ballew (1989); Hunt *et al.* (2006)

751 **Most Recent Diagnosis:** Ballew (1989) diagnosed *Machaeroproso-* *mccauleyi* based on the following

752 autapomorphies: 1) Squamosal with distinct triangular outline without knob-like process; 2) Lateral

753 portion of opisthotic thin and elongate; 3) Posttemporal fenestra large because of a medial expansion; 4)
754 Basioccipital head relatively large; 5) Basioccipital neck relatively short.

755 **Modified Diagnosis:** 1) Squamosal with distinct triangular outline without knob-like process; 2) rostrum
756 is completely crested in lateral view; 3) Ventral expansion of the alveolar rim at the border of the
757 premaxillae and maxillae 4) Pre-infratemporal shelf does not extend under the posterior corner of the
758 antorbital fenestra; 5) Anteroposterior corners of the antorbital fenestra rounded; 6) Anteromedial portion
759 of the supratemporal fenestrae remain visible in dorsal view.

760 **Comments:** Characters 2, 3, 4 and 5 of Ballew (1989) do not appear to be different to those in other
761 specimens of *Machaeroprotopus*. Character 1 does appear to be valid, but may be subject to intraspecific
762 variability; PEFO 31219 (referred by Stocker, 2010) does possess a short, robust terminal knob on the
763 posterior process of the squamosal, though in all other respects greatly resembles UCMP 126999 (the
764 holotype).

765 Hunt *et al.* (2006) referred three specimens from Bull Canyon, New Mexico to *Machaeroprotopus*
766 *mccauleyi* and cited three characters which link them to the holotype. The first character is the same as
767 character 1 of Ballew (1989), the others are: 2) In posterior view, the lateral margins of the skull flare at
768 about 60°; 3) In lateral view, the rostrum is completely crested (inferred from the gradient of the holotype
769 of *Machaeroprotopus mccauleyi* which lacks the distal rostrum). Character 2 of Hunt *et al.* (2006) is not
770 diagnostic, being present in all robust species of *Machaeroprotopus* and may be prone to taphonomic
771 distortion, and/or ontogenetic changes. Character 3 is useful as no other current species of
772 *Machaeroprotopus* share this character. Neither character 1 of Ballew (1989), nor character 3 of Hunt *et*
773 *al.* (2006) allow distinction of *Machaeroprotopus mccauleyi* from '*Redondasaurus bermani*'; therefore,
774 we suggest four further characters (our characters 3–6) to allow this differentiation.

775

Commented [WGP19]: Do you agree with this assignment?

776 ***Machaeroprosoopus buceros*** (Cope, 1881)

777 **Age:** late Norian–early Rhaetian (c. 213–207 Mya)

778 **Occurrences:** Petrified Forest Member, Chinle Formation, Orphan Mesa, New Mexico, USA; ~~Upper~~

779 Petrified Forest Member, Chinle Formation, Canjilon Quarry, New Mexico, USA; ~~Upper~~-Petrified Forest

780 Member, Chinle Formation, Snyder Quarry, New Mexico, USA

781 **Holotype:** AMNH FR. 2318, poorly preserved skull missing anterior end of rostrum

782 **Previously Referred Specimens:** UCMP 27228, 34246 & 34258; MNA V3478, CMNH 69727 (holotype

783 of ‘*Redondasaurus*’ *bermani*) (Ballew, 1989); UCMP 27149 & 34250; UW 3807; MNA ~~PL~~-V-25;

784 NMMNHS-P 18191, 31292, 33662, 33667, 33846, 33849, 33935, 35366, 35444, 35982, 36000, 36051,

785 36829, 37283, 37894 & 39700; FMNH UC 396 (holotype of ‘*Machaeroprosoopus*’ *andersoni*); YPM

786 3293; TTU-P 09234 (Long & Murry, 1995); UCMP 27231, 27234, 34245 & 34249; GR 147 (Zeigler *et*

787 *al.*, 2003a).

788 **Specimen(s) Used for Scoring:** AMNH FR. 2318; TTU-P 11423; UCMP 34250; NMMNHS-P 39700

789 **Key References:** Cope (1881); Ballew (1989); Long & Murry (1995); Lucas *et al.* (2002); Zeigler *et al.*

790 (2003a, b)

791 **Most Recent Diagnosis:** Long & Murry (1995) diagnosed *Machaeroprosoopus buceros* as a ‘heavy-

792 skulled’ ‘pseudopalatine’ with the following combination of characters: 1) Squamosal with posterior

793 process elongated, but deeper and shorter than that of *Pseudopalatus* [*Machaeroprosoopus pristinus*],

794 tapering into a blunt apex; 2) Descending process of squamosal large; 3) Rostrum partially crested; 4)

795 Length shorter than posterior portion of skull; 5) Snout does not descend abruptly immediately anterior to

796 external nares; 6) The latter are raised above the level of the skull roof as in *Pseudopalatus*

797 [*Machaeroprosoopus pristinus*]; 7) Crest sharp-edged with no sculpturing; 8) Dentition heterodont; 9)

798 Alveoli closely spaced; 10) Enlarged anteriormost teeth and with dagger-like teeth at mid-length of
799 premaxilla; 11) Crest deepest posteriorly.

800 **Modified Diagnosis:** In this study, we diagnose *Machaeroprotopus buceros* on the basis of the following
801 unique character combination: 1) Posterior process of the squamosal is elongate and knob-like; 2) Tubular
802 anterior portion of the rostrum has a triangular, rather than semi-circular, cross-section (amended from
803 Balley [1989] character 56); 3) Rostrum partially crested; 4) Snout does not descend abruptly
804 immediately anterior to external nares.

805 **Comments:** Characters 1, 2, 4, 6, 8 and 9 of Long & Murry (1995) present problems; characters 1 and 2
806 describe morphologies that vary between specimens of *Machaeroprotopus buceros* (AMNH FR. 2318,
807 TTU-P 11423, UCMP 34250). The morphologies described by characters 4 and 6 disagree with the first-
808 hand observations made in this study; with the rostrum measured from the most anterior point of the snout
809 to the anterior border of the nares, no specimens observed here possessed a rostrum shorter in length than
810 the narial + postnarial region of the skull - including even the holotype in which the most anterior section
811 of the snout is lost. As in other species of *Machaeroprotopus* such as *Machaeroprotopus pristinus* and
812 *Machaeroprotopus mccauleyi*, we found no evidence for the nares exceeding the height of the skull roof.
813 Characters 8 and 9 describe features that are common to some extent in many, if not most,
814 leptosuchomorph phytosaurs, and within *Machaeroprotopus* they are shared with *Machaeroprotopus*
815 *mccauleyi*.

816 In their revision of North American phytosaurs, Long & Murry (1995) erected the new genus
817 ‘*Arribasuchus*’, referring to it both *Machaeroprotopus buceros* and *Machaeroprotopus mccauleyi*. In a
818 similar manner to their diagnosis of *Smilosuchus* the diagnostic character combination for the genus
819 ‘*Arribasuchus*’ is the same as that for the type species, in this case *Machaeroprotopus buceros*.
820 *Machaeroprotopus mccauleyi* was tentatively retained in ‘*Arribasuchus*’ by Long & Murry (1995),

821 despite characters such as ‘rostrum partially crested’ being directly inconsistent with the species diagnosis
822 of *Machaeroprotopus mccauleyi* given by Ballew (1989) (also used by Long & Murry to diagnose
823 *Machaeroprotopus mccauleyi*).
824 Subsequent analyses have suggested that ‘*Arribasuchus*’ is paraphyletic (Hungerbühler, 2002;
825 Hungerbühler *et al.*, 2013; Parker & Irmis, 2006), and should be considered a junior synonym of
826 *Machaeroprotopus* (Hungerbühler *et al.*, 2013).
827
828 ***Machaeroprotopus pristinus*** (Mehl, 1928)
829 **Age:** late Norian–early Rhaetian (c. 213–207 Mya)
830 **Occurrences:** Chinle Formation, Petrified Forest National Park, Apache County, Arizona, USA; ~~Upper~~
831 Petrified Forest Member, Chinle Formation, Canjilon Quarry, New Mexico, USA; ~~Upper~~ Petrified Forest
832 Member, Chinle Formation, Snyder Quarry, New Mexico, USA
833 **Holotype:** MU 525, skull with many areas of plaster restoration
834 **Previously Referred Specimens:** UCMP 27018, 27235, 34245, 34249, 34251, 119436 & 131331;
835 AMNH FR. 7222; MNA V3495 (Ballew, 1989); NMMNHS-P 31292; AMNH/GR 1027; UCM 55163;
836 PEFO 4852; UCMP 27159 (referred to ‘*M.* *zunii*’ by Camp [1930] and used for scoring ‘*M.* *zunii*’ by
837 Stocker [2010]; however, in the latter study this specimen is also referred to *Machaeroprotopus pristinus*,
838 being mistakenly presented as the holotype of ‘*Machaeroprotopus tenuis*’. The correct specimen would
839 be UCMP 27018), UCMP 27231, UCMP 27234; YPM 3294 (holotype of ‘*Redondasaurus*’ *gregorii*)
840 (Long & Murry, 1995).
841 **Specimen(s) Used for Scoring:** MU 525; AMNH FR. 7222; NMMNHS-P 50040; PEFO 382; UCMP
842 137319; UCMP 27018 (‘*Machaeroprotopus tenuis*’ holotype)
843 **Key References:** Mehl (1928); Long & Murry (1995); Zeigler *et al.* (2002, 2003a, b)

844 **Most Recent Diagnosis:** Stocker (2010) used the following characters to diagnose *Machaeroprotopus*
845 *pristinus*: 1) Supratemporal fenestrae nearly completely closed in dorsal view by medially expanded
846 postorbital-squamosal bars, and the fenestrae are completely depressed below the level of the skull roof;
847 2) Squamosal process of the parietals immediately posterior to the main body of the parietals drop
848 ventrally before continuing on to articulate with the parietal processes of the squamosals; 3) The posterior
849 processes of the squamosals are expanded posteriorly as in *Leptosuchus*; however, there is no dorsoventral
850 expansion of this posterior process, which is usually described as ‘knob-like’ in this taxon.

851 **Modified Diagnosis:** We use a combination of characters from Stocker (2010), one modified from Ballew
852 (1989), and other novel characters: 1) Proportionally long rostrum (ratio of pre-narial to narial + post-
853 narial length [measured to the posterior extremity of the parietals] greater than or equal to 2.2); 2)
854 Subtriangular antorbital fenestra; anterior corner is pointed/acutely rounded and posterior border is taller
855 and straight/gently rounded; 3) Rostrum descends immediately anterior to external nares and remains low
856 and tubular for the majority of its length; 4) Tubular portion of rostrum is semi-circular in cross-section;
857 5) Weak heterodonty.

858 **Comments:** In her phylogenetic analysis, Stocker (2010) did not score *Machaeroprotopus pristinus* using
859 the holotype, and instead used UCMP 27159 and NMMNHS-P 31292. UCMP 27159 is a referred
860 specimen of ‘*M. zunii*’ (Camp, 1930) and was used as a referred specimen to phylogenetically score ‘*M.*
861 *zunii*’ in Stocker’s analysis; however, Stocker reported the same specimen number as the holotype of
862 *Machaeroprotopus tenuis*, which was referred to, and used to score *Machaeroprotopus pristinus*. We
863 assume this was a typographical error, and that Stocker actually scored and referred UCMP 27018 (actual
864 holotype of ‘*Machaeroprotopus tenuis*’) to *Machaeroprotopus pristinus*, as UCMP 27159 is clearly
865 different from *Machaeroprotopus pristinus* and UCMP 27018, based both on morphology and
866 preservation. The choice to refer, and use NMMNHS-P 31292 for scoring is puzzling; the skull displays a

867 partial rostral crest which rises above the level of the nares and abruptly descends approximately at the
868 midpoint of the external nares. No other referred specimen of *Machaeroprotopus pristinus* has a rostral
869 crest, and the crest morphology is unknown in any other species of phytosaur. The specimen has
870 previously been referred to *Machaeroprotopus buceros* (Zeigler *et al.*, 2002), to which
871 *Machaeroprotopus pristinus* was also referred as a junior synonym and may explain the use of
872 NMMNHS-P 31292 to define *Machaeroprotopus pristinus* by Stocker. However, Stocker clearly stated
873 that her analysis would not investigate the synonymy of these species, and in accordance used the
874 proposed junior synonym '*Machaeroprotopus pristinus*' in her analysis, demonstrating that no synonymy
875 was assumed. Furthermore, Zeigler *et al.* (2002) attributed the unusual crest of NMMNHS-P 31292 to
876 post-mortem deformation; however, upon close study we believe the morphology to be genuine, which if
877 true, casts uncertainty over the referral of this specimen to any currently known species.

878 The diagnosis of Stocker (2010) does not allow differentiation of *Machaeroprotopus pristinus* and
879 *Machaeroprotopus buceros*; in our revised diagnosis we therefore highlight that *Machaeroprotopus*
880 *pristinus* possesses only weak heterodonty, whereas *Machaeroprotopus buceros* is strongly heterodont.

881

882 *Machaeroprotopus lottorum* Hungerbühler *et al.*, 2013

883 **Age:** late Norian (c. 218–208 Mya)

884 **Occurrences:** Upper Cooper Canyon Formation, Dockum Group, Texas, USA

885 **Holotype:** TTU-P 10076, skull

886 **Previously Referred Specimens:** TTU-P 10077 (Hungerbühler *et al.*, 2013).

887 **Specimen(s) Used for Scoring:** TTU-P 10076; TTU-P 10077

888 **Key References:** Hungerbühler *et al.* (2013)

Commented [WGP20]: Hungerbühler *et al.* 2013 agreed with Zeigler's assessment that they are sexual dimorphs; however, this is difficult to support.

889 **Most Recent Diagnosis:** Hungerbühler *et al.* (2013) diagnosed *Machaeroprosopeus lottorum* with the
890 following characters: 1) Lateral rim of the naris broad, flat and rugose; 2) Supratemporal fenestra fully
891 closed in dorsal aspect, forming a shallow semi-circular indentation into the skull roof, with a strongly
892 bevelled rim that continues onto the parietal; 3) Free section of the postorbital/squamosal bar short; 4)
893 Strongly developed horizontal medial laminae of palatines, that almost close the posterior section of the
894 palatal vault in ventral view.

895 **Modified Diagnosis:** 1) Lateral rim of the naris broad, flat and rugose; 2) Supratemporal fenestra fully
896 closed in dorsal aspect, forming a shallow semi-circular indentation into the skull roof, with a strongly
897 bevelled rim that continues onto the parietal; 3) Strongly developed horizontal medial laminae of
898 palatines, that almost close the posterior section of the palatal vault in ventral view.

899 **Comments:** We generally agree with the characters proposed by Hungerbühler *et al.* (2013), with the
900 exception of their character 3. In TTU-P 10076 character 3 holds true i.e. the free section of
901 postorbital/squamosal bar is proportionately shorter than in almost all other phytosaur specimens studied.
902 However, in TTU-P 10077 the length of the free section of postorbital/squamosal bar is greater than in
903 some specimens of *Machaeroprosopeus pristinus* (UCMP 34249, 27231, 34228) including the holotype
904 (MU 525), but shorter than other referred specimens (NMMNHS P-50040; PEFO 382; AMNH FR 7222);
905 this character is also shorter in the majority of specimens of *Mystriosuchus planirostris*. This suggests the
906 feature may be more variable than previously realized in *Machaeroprosopeus lottorum* and is therefore
907 removed from the diagnosis.

908

909 **'Redondasaurus' gregorii** Hunt & Lucas, 1993

910 **Age:** Rhaetian (c. 208.5–201.3 Mya)

911 **Occurrences:** Redonda Formation, Dockum Group, Shark Tooth Hill, Quay County, New Mexico, USA

912 **Holotype:** YPM 3294, poorly preserved and compressed skull missing left quadrate area, dorsal narial
913 area and tip of rostrum

914 **Previously Referred Specimens:** OMNH 1250 (Hunt & Lucas, 1993).

915 **Specimen(s) Used for Scoring:** YPM 3294

916 **Key References:** Gregory (1972); Hunt & Lucas (1993); Hungerbühler *et al.* (2013)

917 **Most Recent Diagnosis:** Spielmann & Lucas (2012) built on the original diagnosis of Hunt & Lucas
918 (1993) and diagnosed *Redondasaurus gregorii* using the following character combination: 1)
919 Supratemporal fenestrae concealed in dorsal view; 2) Reduced antorbital fenestrae; 3) A prominent pre-
920 infratemporal shelf at the anteroventral margin of the lateral temporal fenestra; 4) Septomaxillae that wrap
921 around the outer margin of the external narial opening; 5) A thickened orbital margin; 6) An inflated
922 posterior nasal behind the external narial opening; 7) Thickened dorsal osteoderms.

923 **Modified Diagnosis:** We retain most of the characters proposed by Spielmann & Lucas (2012) but
924 reword them for more precise interpretation: 1) Supratemporal fenestrae concealed in dorsal view; 2)
925 Antorbital fenestra with a distinct sharp corner at the anterior-most and posterior-most extremities; 3) Pre-
926 infratemporal shelf projects anteriorly as a lobe reaching beneath the posterior corner of the antorbital
927 fenestra, and dorsally joins with a ventrally descending flange of the postorbital; 4) Posterior border of the
928 orbit equal to- or thicker than the dorsoventrally thinnest part of the posterior process of the jugal; 5) An
929 inflated posterior nasal behind the external narial opening; 6) Postorbital/squamosal bars wide; 7)
930 Thickened dorsal osteoderms.

931 **Comments:** We find issues with characters 2 and 4 of the diagnosis of Spielmann & Lucas (2012). The
932 reduction of the antorbital fenestra in '*Redondasaurus*' appears to be subjective based on the relative size
933 of the antorbital fenestra when compared to the robusticity and size of the skull. In large specimens such
934 as NMMNHS P-4256 and NMMNH P-31094 that have previously been referred to '*Redondasaurus*', the

935 antorbital fenestra appears small; however, in the holotype of ‘*Redondasaurus*’ *gregorii* (YPM 3294) the
936 antorbital fenestra appears of similar proportions relative to the skull as in other phytosaurs such as
937 *Mystriosuchus planirostris* or *Machaeroprotopus pristinus*. We suggest instead that the shape of the
938 antorbital fenestra is unique in ‘*Redondasaurus*’ as both its anterior and posterior apices are sharp, rather
939 than rounded; the antorbital fenestra only appears to be relatively small in specimens of ‘*Redondasaurus*’
940 *bermani* and is therefore used as a character for that species only. Although this is a generic feature of
941 ‘*Redondasaurus*’ it is retained in this species diagnosis in case ‘*Redondasaurus*’ is synonymized with
942 *Machaeroprotopus*. In such a scenario this character would be useful as part of a character combination to
943 differentiate the species from almost all other members of the genus. We find no evidence for
944 ‘septomaxillae’ that wrap around to the lateral side of the nares; Stocker (2010) found this feature to be
945 present in both ‘*Redondasaurus*’ and *Pravusuchus hortus*; however, in the holotype of the latter this area
946 is covered with iron oxide and may actually be the paranasal suture, which was identified in
947 *Machaeroprotopus lottorum* by Hungerbühler *et al.* (2013). Given the phylogenetic proximity of
948 *Machaeroprotopus lottorum* and ‘*Redondasaurus*’ it is likely that the feature described in
949 ‘*Redondasaurus*’ may also be the paranasal; as the feature is currently ambiguous it is excluded from the
950 diagnosis given here.

951

952 ‘*Redondasaurus*’ *bermani* Hunt & Lucas, 1993

953 **Age:** Rhaetian (c. 208.5–201.3 Mya)

954 **Occurrences:** ‘siltstone member’, Chinle Formation, ~~Bull Canyon, Quay~~*Coelophysis Quarry, County,*

955 New Mexico, USA

956 **Holotype:** CMNH 69727, skull

Commented [WGP21]: Holotype is from the Coelophysis Quarry at Ghost Ranch New Mexico.
Formatted: Font: Italic

957 **Previously Referred Specimens:** Hungerbühler (2002) used a silhouette of NMMNHS-P 4256 in their
958 phylogeny to denote ‘*Redondasaurus*’ *bermani*, but referred to as ‘NMMNHS-P 5246’. This appears to be
959 a typographical mistake. NMMNHS-P 4256 is included as a separate OTU to ‘*Redondasaurus*’ in this
960 study so its affinities can be tested.

961 **Specimen(s) Used for Scoring:** NMMNHS-P 4983

962 **Key References:** Hunt & Lucas (1993); Hunt *et al.* (2006); Hungerbühler (2002); Hungerbühler *et al.*
963 (2013)

964 **Most Recent Diagnosis:** Hunt & Lucas (1993) diagnosed ‘*Redondasaurus*’ *bermani* as a ‘*Redondasaurus*
965 species that differs from others in possessing a rostrum with a partial crest’.

966 **Modified Diagnosis:** A species of ‘*Redondasaurus*’ with the following characters: 1) Full rostral crest
967 extending from nares to the terminal rosette of the premaxilla; 2) Antorbital fenestra reduced in size
968 relative to other taxa of similar size and robusticity; 3) Length of the symphyseal portion of the mandible
969 approximately half that of the post-symphyseal region.

970 **Comments:** ‘*Redondasaurus*’ *bermani* was synonymized with *Machaeroprotopus buceros* by Long &
971 Murry (1995) as mentioned above, and was also synonymized with ‘*Redondasaurus*’ *gregorii* by
972 Spielmann & Lucas (2012) who concluded that it was the male sexual dimorph. Due to the lack of
973 evidence for synonymy we tentatively retain ‘*Redondasaurus*’ *bermani* as a distinct species, but a
974 thorough re-description of the species would be of great benefit.

975

976 ***Mystriosuchus westphali*** (Hungerbühler & Hunt 2000)

977 **Age:** middle–late Norian (c. 216–209 Mya)

978 **Occurrences:** Löwenstein Formation (middle Stubensandstein), Middle Keuper Subgroup, Baden-
979 Württemberg, Germany

980 **Holotype:** GPIT 261/001, skull with left side slightly distorted

981 **Previously Referred Specimens:** GPIT 261/17/7 (Hungerbühler & Hunt, 2000); GPIT 2145.000,
982 2146.000 & 2156.000 (provisionally included) (Hungerbühler, 2002).

983 **Specimen(s) Used for Scoring:** GPIT 261/001; AMNH 10644

984 **Key References:** Huene (1909; 1911); Hungerbühler (1998; 2002); Hungerbühler & Hunt (2000)

985 **Most Recent Diagnosis:** Hungerbühler (2002) listed eight autapomorphies for *Mystriosuchus westphali*
986 as follows: 1) Discrete snout crest at midlength of the premaxillae; 2) Semicylindrical alveolar ridges; 3)
987 Posterior process of the squamosal absent; 4) Squamosal contacts the prootic anteriorly; 5) Supraoccipital
988 reaches the post-temporal fenestra and borders its dorsomedial half; 6) Lobate extension of the vertically
989 descending squamosal process of the parietal; 7) Post-temporal fenestra is reduced to a narrow slit; 8)
990 Presence of a discrete ossification (orbitosphenoid) anterior to the laterosphenoid.

991 **Modified Diagnosis:** 1) Discrete snout crest at midlength of the premaxillae; 2) Squamosal contacts the
992 prootic anteriorly; 3) Supraoccipital reaches the post-temporal fenestra and borders its dorsomedial half;
993 4) Post-temporal fenestra is reduced to a narrow slit; 5) Presence of a discrete ossification
994 (orbitosphenoid) anterior to the laterosphenoid; 6) A sharp corner of bone extends into the antorbital
995 fenestra at approximately the midpoint of the posterior border, giving the posterior border a ‘stepped’
996 appearance.

997 **Comments:** Based on subsequent analyses and first-hand examination of specimens, we exclude
998 characters 2, 3 and 6 of Hungerbühler (2002) from this diagnosis. Character 2 is present in almost all
999 phytosaurs; characters 3 and 6 are both observed in the holotype of *Mystriosuchus westphali*. However, a
1000 specimen found in the collections of the AMNH (AMNH 10644), which is referable to *Mystriosuchus*
1001 *westphali* (as a species of *Mystriosuchus* that possesses a distinct sharp crest at the midlength of the
1002 premaxilla and lacks the abrupt concave rise of the rostrum into a narial crest), differs in displaying

1003 neither of these states. In AMNH 10644 the posterior process of the squamosal shares the same
1004 morphology as *Mystriosuchus planirostris* and the ‘lobate extensions’ on the squamosal process of the
1005 parietal are absent. Furthermore, these lobate extensions have been found in an indeterminate specimen of
1006 *Machaeroprotopus* (either *Machaeroprotopus pristinus*, *Machaeroprotopus buceros* or
1007 *Machaeroprotopus lottorum*) by Hungerbühler *et al.* (2013), but not in any others, suggesting this state is
1008 likely intraspecifically variable in multiple taxa. A further character, relating to the antorbital fenestra, is
1009 added which is found in both the holotype and AMNH 10644 but in no specimens of *Mystriosuchus*
1010 *planirostris*.
1011
1012 ***Mystriosuchus planirostris*** (Meyer, 1863)
1013 **Age:** middle–late Norian (c. 216–209 Mya)
1014 **Occurrences:** Löwenstein Formation (middle Stubensandstein), Middle Keuper Subgroup, Baden-
1015 Württemberg, Germany; Zorzino Limestone, Lombardy, Italy
1016 **Holotype:** MCZ 1018, fragment of right pre-orbital (lectotype); MCZ 1019A, 1019B, 1019C; MCZ
1017 1022A, 1022B, rostral and skull fragments, partial caudal centrum (paralectotypes)
1018 **Previously Referred Specimens:** SMNS 9134 (Fraas, 1896); SMNS 10260 (McGregor, 1906); SMNS
1019 11126(1) (Huene, 1911); GPIT 249/002 (Huene, 1909); AMNH 10644 (Witmer, 1997); SMF uncat
1020 (Drevermann, 1918); MBSN 2 (Pinna, 1987); NHMW 1986 0024 0001 (Buffetaut, 1993); SMNS 13007,
1021 13240, uncat 180, uncat 183, uncat 184 (possibly SMNS 9900); SMNS uncat 397, uncat 205;, 2074.000,
1022 2149.002, 2149.003, 2150.000; MB.I.008.05 (Hungerbühler, 1998).
1023 **Specimen(s) Used for Scoring:** SMNS 10260; SMNS 9900; SMNS 9134; SMNS 13240; SMNS 91574
1024 **Key References:** Meyer (1863); Fraas (1896); Hungerbühler (1998; 2002); Hungerbühler & Hunt (2000)

1025 **Most Recent Diagnosis:** Hungerbühler (2002) listed six autapomorphic characters to distinguish
1026 *Mystriosuchus westphali* from *Mystriosuchus planirostris*: 1) The rostrum is extremely elongated; 2) A
1027 subvertical slope results in a concave profile of the prenasal area from side to side; 3) The external nasal
1028 opening is subdivided into a posterior section facing dorsally, and a strongly inclined anterior section that
1029 opens anteriorly; 4) The raised anterior border of the supratemporal fenestra extends along the medial rim
1030 of the squamosal; 5) The parieto-squamosal bar is depressed by more than 30 per cent of the skull height;
1031 6) A larger quadrate foramen is present in a round recess formed by quadratojugal and quadrate.
1032 **Comments:** Hungerbühler (2002) provided a detailed and useful discussion of characters previously used
1033 to diagnose *Mystriosuchus planirostris*, giving reasons why they should now be excluded.

1035 **Specimen-level OTUs**

1037 **NMMNHS-P 4781**

1038 **Age:** early Norian (c. 225–218 Mya)

1039 **Occurrence:** Los Esteros Member, Santa Rosa Formation, Santa Fe County, New Mexico, USA

1040 **Notes:** This specimen consists of the right orbital plus postorbital region of a skull, though lacking any of
1041 the interior or posterior elements such as the braincase, occipitals or palatines. Hunt *et al.* (1993) assigned
1042 this specimen to *Angistorhinus* sp. based on a combination of features: 1) Supratemporal fenestrae at the
1043 level of the skull roof; 2) Squamosals project posteriorly; 3) Squamosal process (parietal/squamosal bar)
1044 is rounded.

1046 **TMM 31100-1332**

1047 **Age:** late Carnian–early Norian (c. 232–225 Mya)

1048 **Occurrence:** ‘Otis Chalk Quarry 3’, Colorado City Formation, Dockum Group, Howard County, Texas,
1049 USA

1050 **Notes:** Stocker (2013) mentioned this specimen in reference to ‘*Angistorhinus*-like specimens from the
1051 Otis Chalk localities’. The specimen consists of a complete cranium, infilled with sediment, though
1052 lacking an associated mandible. Although the surface preservation is relatively good, there are many
1053 cracks through the skull, which cause slight displacements in areas such as the rostrum. The temporal
1054 region of the skull is slightly compressed dorsoventrally, causing the squamosal posterior processes and
1055 parietal/squamosal bars to curve posteroventrally.

1056
1057 **USNM v 21376**

1058 **Age:** late Carnian–early Norian (c. 232–225 Mya)

1059 **Occurrence:** Base of the Dockum Group, three miles North of Otis Chalk, Howard County, Texas, USA

1060 **Notes:** This specimen was figured in lateral view by Stocker & Butler (2013) (Figure 5d), as an example
1061 of the genus *Angistorhinus*. The preorbital portion of the specimen is preserved, as is an area of skull roof
1062 including the prefrontals, frontals and the anterior parts of the postfrontals and parietals. The posterior
1063 processes of the squamosals are also preserved, as is the occipital condyle and ventral parts of the
1064 quadrates; however almost all of the postorbitals, jugals, quadratojugals and anterior and ventral parts of
1065 the squamosals are modelled with plaster. Due to the plaster reconstruction, the orientation of the
1066 supratemporal fenestrae is incorrect; the proximal remnants of the parietal/squamosal bars preserved on
1067 the squamosals have been aligned with the reconstructed postorbital/squamosal bars, whilst the
1068 parietal/squamosal bars are reconstructed entirely from plaster mimicking the depressed temporal
1069 morphology of *Mystriosuchus* or *Machaeropsopus*. The specimen also preserves the symphyseal region
1070 of the mandible, the anterior portions of the two rami including approximately the anterior third of the

mandibular fenestra, and part of the left articular and retroarticular process. The nares appear to be elevated well above the level of the skull roof, although their posterior extremity appears to be damaged and the skull roof may be slightly crushed. The specimen may also be slightly mediolaterally compressed.

PEFO 34852

Age: early Norian (c. 225–220 Mya)

Occurrence: Blue Mesa Member, Chinle Formation, Petrified Forest National Park, Arizona, USA

Notes: This specimen consists of a complete cranium which has been crushed laterally at an oblique angle such that the external elements of the left half of the skull retain their original morphology, whereas the right half is strongly dorsoventrally compressed.

Griffin *et al.* (2017) referred this specimen to *Smilosuchus adamanensis* based on the following characters from the matrix of Kammerer *et al.* (2015): 1) An antorbital fossa is absent (3-3); 2) A rostral crest is present but not continuous (18-1); 3) The interorbital-nasal area is concave (21-1); 4) There is a moderate posterior process of the squamosal (24-1); 5) The posterior process of the squamosal is expanded in lateral view, but not rounded (25-1); 6) The squamosal fossa extends to the posterior edge of the squamosal (30-0); 7) The supratemporal fenestrae are partially depressed (32-1); 8) The supratemporal fenestrae are mostly visible in dorsal view (33-1).

However, upon first-hand comparison of these character scorings with the holotype of *S. adamanensis* and specimens of other non-mystriosuchin leptosuchomorph taxa, we find that all the above character scorings, aside from number 5, may equally refer to *Leptosuchus crosbiensis*. Furthermore, we find that the score for character 2 does not reflect the rostral morphology of either the holotype of *S. adamanensis* or our referred specimen UCMP 170166; in both specimens there is no evidence of any rostral crest, i.e. the rostrum forms an unbroken, straight slope from the posterior border of the nares to the

1094 premaxillae, whereupon the rostrum becomes tubular. However, in PEFO 34852, previously referred
1095 specimens of *L. crosbiensis* (USNM 15481, TMM 31173-120, TTU-P 09230), the holotype of *L.*
1096 *crosbiensis* (subtly) and the holotype of *Leptosuchus studei* (the sister taxon to *L. crosbiensis* in the
1097 analysis of Stocker (2010)), the narial openings extend horizontally from their posterior border, and
1098 directly anterior to the nares the rostrum either continues horizontally or slopes slightly ventrally, before
1099 dipping more strongly ventrally and levelling out to form a tubular rostrum. Therefore, from the
1100 characters presented it is unclear whether this specimen actually represents *S. adamanensis*; for this
1101 reason we include the specimen here as a separate OTU so its affinities can be tested phylogenetically.

1102

1103 **NMMNHS-P 4256**

1104 **Age:** late Norian (c. 218–208 Mya)

1105 **Occurrence:** lower Bull Canyon Formation, ~~Chinle~~Dockum Group, Barranca Badlands, Quay County,
1106 New Mexico, USA

1107 **Notes:** This specimen consists of a large skull, missing the majority of its right postnarial region, the
1108 entire palate and the posterior section of the right mandibular ramus. Similarly to PEFO 34852, the skull
1109 has been compressed at an oblique dorsolateral angle leaving the left half relatively free from
1110 deformation, whilst the right half is strongly compressed and sheared dorsally.

1111 According to Heckert *et al.* (2001) this specimen was originally referenced in the PhD thesis of
1112 Hunt (1994b) as a ‘robust morph’ of ‘*Redondasaurus*’ *gregorii*. Subsequently it was used in the
1113 phylogeny of Hungerbühler (2002) to exemplify ‘*Redondasaurus*’ *bermani*, rather than the unnumbered
1114 Carnegie Museum specimen assigned as the holotype of ‘*Redondasaurus*’ *bermani* by Hunt & Lucas
1115 (1993). Hunt *et al.* (2006) then referred this specimen to *Machaeropsopus mccauleyi*, as a male sexual
1116 dimorph of the species due to the difference in skull size and rostral robusticity between this specimen and

Formatted: Font: Italic

1117 the holotype of *Machaeroprosoopus mccauleyi*. Their species referral was based on three characters: 1)
1118 Posterior squamosal process is sub-triangular and lacks a knob-like termination; 2) In posterior view, the
1119 lateral margins of the skull flare at about 60 degrees; 3) In lateral view the rostrum is completely crested.
1120 All of these characters (regardless of their legitimacy or usefulness) can also be found in ‘*Redondasaurus*’
1121 *bermani*; however, Hunt *et al.* also based their identification on an assumption that two species of
1122 ‘brachyrostral’ phytosaurs were unlikely to have occurred simultaneously geographically and temporally.
1123 As detailed earlier, the genus ‘*Redondasaurus*’ was redefined by Spielmann & Lucas (2012), and more
1124 diagnostic characters were added; again, disregarding the legitimacy of these characters, many of them are
1125 applicable to NMMNHS-P 4256, suggesting the need for the placement of this specimen to be tested more
1126 thoroughly.

1127

1128 **USNM v 17098**

1129 **Age:** early Norian (c. 221–219 Mya)

1130 **Occurrence:** Bluewater Creek Member, Chinle Formation, Apache County, Arizona, USA

1131 **Notes:** USNM v 17098 is a poorly preserved partial skull and mandible that are dorsoventrally
1132 compressed. The skull lacks most of the left lateral postnarial elements, though preserves much of the
1133 right half, the palate and braincase. The mandible is largely complete, though aspects are fragmentary and
1134 lacks the anterior-most portion of the terminal rosette.

1135 This specimen was referred to *Leptosuchus* sp. by Long & Murry (1995) and again by Heckert &
1136 Lucas (2003); however, the label with the specimen identifies it as *Machaeroprosoopus zunii*, though no
1137 justification has been provided for any of these three identifications. By scoring this specimen
1138 phylogenetically it may be possible to more definitively constrain its position.

1139

Commented [WGP22]: Possibly. Hard to get into David Ranch these days, but it is pretty low in the Chinle.

1140 **NMMNHS-P 31094**

1141 **Age:** Rhaetian (c. 208.5–201.3 Mya)

1142 **Occurrence:** Redonda Formation, Dockum Group, Apache Canyon, Quay County, New Mexico, USA

1143 **Notes:** This specimen consists of an extremely robust cranium, missing the majority of the premaxillae

1144 and the anterior extremities of the maxillae. The skull is slightly dorsoventrally crushed and slightly

1145 sheared. Heckert *et al.* (2001) provided a short description of the skull, referring the specimen to

1146 ‘*Redondasaurus*’ sp. on the basis of comparisons with other taxa, which we summarize as four characters:

1147 1) Supratemporal fenestrae that are depressed and concealed in dorsal view; 2) Antorbital fenestra ‘tiny’

1148 relative to narial length; 3) Postorbital/squamosal bars are anteroposteriorly short; 4)

1149 Postorbital/squamosal bars are broad.

1150

1151 **MB.R. 2747**

1152 **Age:** Rhaetian (c. 208.5–201.3 Mya)

1153 **Occurrence:** lower Exter Formation, near Salzgitter, Lower Saxony, Germany

1154 **Notes:** MB.R. 2747 represents the largest phytosaur specimen found in Europe, and consists of a strongly

1155 deformed skull preserved in 11 articulating and non-articulating fragments, a partial mandible preserved

1156 in four articulating fragments, multiple vertebrae and centra, partial scapulae and coracoids, a humerus,

1157 and a set of articulated osteoderms. The skull retains the majority of the rostrum up to the anterior corner

1158 of the antorbital fenestrae, the posterior process of the right maxilla and the main bodies of the left and

1159 right jugals with the anterior corners of the lateral temporal fenestrae, a postnarial portion of the skull roof

1160 including a section of the posterior narial border and a dorsal part of the right orbital rim, a relatively

1161 complete, but crushed, braincase with dorsal portions of the parietals preserved and a fragment of the left

1162 postorbital/squamosal bar. The mandible consists of a short posterior section of the symphysis, from

1163 which the two rami bifurcate; the left ramus extends posteriorly such that part of the mandibular fenestra
1164 is preserved, whilst the right ramus does not extend as far as the beginning of the fenestra. The surface
1165 preservation of the material is generally good, but is extensively fractured making sutures difficult to
1166 discern.

1167 This specimen was originally described by von Huene (1922) and was referred to the species
1168 ‘*Angistorhinopsis ruetimeyeri*’. This referral was based entirely on stratigraphic age and the size of the
1169 specimen, as the holotype of ‘*A. ruetimeyeri*’ consists of a partial phytosaur basioccipital, mandibular and
1170 postcranial fragments from a bonebed in Switzerland - none of which are diagnostic. The taxon ‘*A.*
1171 *ruetimeyeri*’ is therefore a nomen dubium; furthermore, MB.R. 2747 has never before been included in a
1172 phylogenetic analysis of phytosaurs. Its inclusion here will therefore provide a phylogenetic placement
1173 that may be useful in any future redescription of the specimen.

1174

1175 **NHMW 1986 0024 0001**

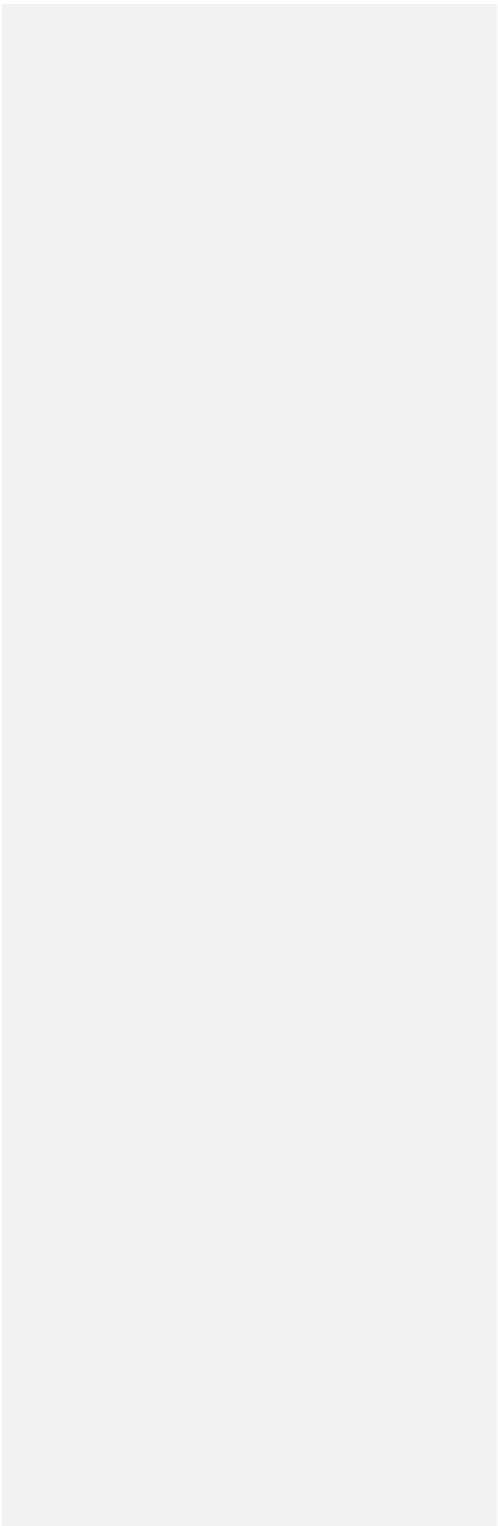
1176 **Age:** middle–late Norian (c. 216–209 Mya)

1177 **Occurrence:** Dachsteinkalk, Totes Gebirge, Styria, Austria

1178 **Notes:** This specimen is an undescribed right half of a phytosaur skull from Austria, with a possibly
1179 associated partial mandible and ilium, that was referred to *Mystriosuchus planirostris* by Buffetaut (1993).
1180 Aside from the anterior tip of the snout and the quadratojugal, the half skull is relatively complete and
1181 well preserved with some sutures discernible; however, it may be somewhat mediolaterally compressed.
1182 The mandible is more poorly preserved; its dorsal surface is heavily weathered and the posterior half of
1183 the left ramus is missing, although the ventral surface is retained, allowing a more accurate estimate of
1184 skull length. Approximately the posterior quarter of the right ramus is missing. Similarly to MB.R. 2747,

1185 this specimen has never before been analysed phylogenetically, and its inclusion may assist future
1186 descriptive work.

1187



1188 **Appendix 2: Character list**

1189

1190 It is important to note here that when incorporating continuous and geometric morphometric character
1191 scorings for analysis, the format of the TNT data file requires these characters to be presented first in the
1192 file. This differs from how the characters are ordered in the character list below. Our character list
1193 presents characters in the order in which they occur for the base discrete matrix; where a character
1194 possesses a continuous or GM variant this is flagged next to that character, as indicated below. It should
1195 also be noted that characters in a TNT file begin at zero, whereas we shift our characters such that the list
1196 begins at one.

1197

1198 * Character possesses a corresponding continuous variant

1199 † Character possesses a corresponding/partially corresponding GM variant

1200

1201 **1) Anterior end of premaxillae [from Stocker 2010, character 7]**

1202 0: In anteroposterior plane of posterior rostrum

1203 1: downturned

1204 Although the distal terminus of the rostrum is downturned in all phytosaurs, in some such as *Parasuchus* and some
1205 specimens of *Machaeroprotopus pristinus*, there is dorsoventral constriction of the rostrum just posterior to the
1206 terminal rosette subsequent to which the rostrum deepens again such that the ventral edge is approximately level
1207 with the downturned anterior tip.

1208

- 1209
- 2) Interpremaxillary fossa [Hungerbühler 2002, character 43; Stocker 2010, character 8]
- 1210
- 0: Absent
- 1211
- 1: Present, broad and rounded
- 1212
- 2: Present, narrow slit
- 1213
- Only species of *Mystriosuchus* display a narrow, slit-like fossa between the alveolar ridges; all other phytosaurs
- 1214
- possess a broadly rounded fossa.
- 1215
-
- 1216
- 3) Alveolar ridges [modified from Stocker 2010, character 9]
- 1217
- 0: Continuously visible in lateral view
- 1218
- 1: Inconsistently visible, or entirely hidden in lateral view
- 1219
- Modified such that the state differences reflect the development of any kind of ventral overhang of the ventral
- 1220
- rostral margin, rather than separating only those taxa in which such a ventral overhang is complete from those that
- 1221
- display either an intermediate state or no overhang.
- 1222
-
- 1223
- 4) Ventral alveolar bulge between premaxilla and maxilla [modified from Hungerbühler *et al.* 2013,
- 1224
- character 2]
- 1225
- 0: Absent
- 1226
- 1: Present
- 1227
- Wording modified for clarity. This ventral bulge of the tooth-row is consistently visible in *Smilosuchus gregorii* and
- 1228
- most robust members of *Machaeroprotopus*. In some other taxa such as *Smilosuchus lithodendrorum*, *Pravusuchus*
- 1229
- hortus* and ‘*Redondasaurus*’ *gregorii* the bulge is not present in all specimens.

1230

1231 **5) Alveolar rim of maxilla [modified from Hungerbühler 2002, character 3; Stocker 2010, character 10]**

1232 0: Horizontal or subconvex

1233 1: Strongly ventrally convex

1234 Wording altered slightly for clarity.

1235

1236 **6) Premaxillary crest [modified from Hungerbühler 2002, character 48]**

1237 0: Absent

1238 1: Present, rounded

1239 2: Present, sharp

1240 In the majority of phytosaurs an isolated premaxillary crest is absent, however *Mystriosuchus westphali* possesses a
1241 premaxillary crest with a sharp dorsal edge, giving the rostrum a more triangular coronal cross-section through the
1242 crest. *Leptosuchus studeri* and *crobiensis* both also display an isolated premaxillary crest, however the dorsal edge
1243 is rounded, maintaining a curved dorsal profile in cross-section. This character is modified here to account for the
1244 different crest morphologies.

1245

1246 **7) Rostral crest [modified from Stocker 2010, characters 17, 18, 19]**

1247 0: Absent

1248 1: Narial crest a relatively abrupt rise to the nares interrupting a straight profile from rostrum to orbit

1249 2: A straight steep slope from the nares to the premaxilla

1250 3: Extends horizontally level from the nares for the majority of the crest with a terminal anterior slope

1251 4: Extends horizontally level from nares for less than half the rostral length then descends and becomes tubular

1252 This character was previously three separate characters, the first of which pertained to the morphology of the

1253 premaxilla, while the subsequent two scored the presence or absence of a ‘rostral crest’ and its morphology. Putting

1254 aside disputes over the cladistic usefulness of crest characters, these characters appear to overlap, risking artificial

1255 inflation of the influence of some traits. From the character state descriptions in the second and third characters, the

1256 ‘rostral crest’ appears to refer to the crest across both the premaxilla and maxilla. State zero of the first character

1257 (premaxilla dorsoventrally taller than mediolaterally wide) therefore directly overlaps with the second state of the

1258 next character (presence of a rostral crest). State one of the first character (tube-like morphology of the premaxilla)

1259 does not completely correlate with state zero of the next character (absence of rostral crest - rostrum tube-like for

1260 entire length) as morphologies exist (e.g., *Leptosuchus crosbiensis* and *Leptosuchus studei*) where the premaxilla is

1261 slender, but rises into a crest posterior to its contact with the maxilla; this would be described by a combination of

1262 state one in the first character, and state zero in the second. This morphology is, however, given a distinct state of

1263 its own in the third character: state zero (rostral crest partial or undulating from nares to terminal rosette); this state

1264 correlates exactly with a combination of states of the previous two characters. Furthermore, the third character is

1265 only applicable to taxa with rostral crests; un-crested taxa must therefore be scored as inapplicable which is treated

1266 as uncertainties during character optimization, resulting in their morphologies being ‘estimated’ for a trait they do

1267 not possess. Here we present a multi-state combination of the previously used characters, in which states are

1268 mutually exclusive and that is applicable to all taxa. An example of character state one is the abrupt rise to the nares

1269 in *Mystriosuchus planirostris*; state two is exemplified by *Smilosuchus gregorii*; state three is autapomorphic for

1270 *Nicrosaurus kapffi* and state four applies to taxa such as *Leptosuchus crosbiensis* and *studei*.

1271

1272 * [ORDERED] 8) Transverse width of the rostrum between the antorbital fenestrae in dorsal view [modified

1273 from Butler *et al.* 2014, character 46]

1274 0: Less than or equal to 1.20

1275 1: 1.21 to 1.59

1276 2: Greater than or equal to 1.60

1277 States are here modified to represent the greater range of morphologies measured in this study. Measured as the

1278 ratio of the width of the rostrum between the antorbital fenestrae at their midpoint, and the interorbital distance at its

1279 shortest point. State zero corresponds to a narrow width, state one to moderate, and state two to a large width.

1280

1281 **9) Suture between maxilla, premaxilla and nasal [from Hungerbühler 2002, character 2]**

1282 0: Slopes anteroventrally

1283 1: Dorsally convex lobe

1284

1285 **10) Posterior portion of maxilla lateral outline in dorsal view [from Hungerbühler 2002, character 4]**

1286 0: Straight/subconcave

1287 1: Convex

1288

1289 *** [ORDERED] 11) Ratio of rostral to narial plus post narial length [modified from Hungerbühler 2002,**

1290 **character 1; Stocker 2010, character 14]**

1291 0: Less than or equal to 1.50

1292 1: 1.51 to 1.99

1293 2: Greater than or equal to 2.00

1294 In previous analyses this character used the pre-orbital and orbital + post-orbital lengths; however, orbital + post-

1295 orbital length was measured to the posterior process of the squamosal - the morphology of which is highly variable,

1296 and the subject of a number of other characters in their matrices. To avoid mixing the signal of this character with
1297 those of characters pertaining to the squamosal, we use the posterior extremity of the parietals as our posterior
1298 measuring point. The nares are used here rather than the orbits as phylogenetic signal is either unclear or lost when
1299 pre-orbital length is compared to the orbital + postorbital length to the posterior tip of the parietals. This suggests
1300 that much of the signal previously found in this character may be linked to variation in the squamosals, combined
1301 with rostral variation. The position of the nares does shift between phytosaurs belonging to, and excluded from
1302 Mystriosuchinae and thus presents a partial correlation with one other character pertaining to this change in
1303 position. However this is here judged to be a more favourable option than correlation with the squamosals, which
1304 are far more variable than the position of the nares, are the subject of more characters and have traditionally been
1305 used as one of the main diagnostic features for different groups of phytosaurs.

1306

1307 **12) Narial openings [from Hungerbühler 2002, character 50]**

1308 0: Dorsally or anterodorsally

1309 1: Anterior section opens forward, posterior upward

1310

1311 **13) Narial openings B [from Sereno 1991, character P; Stocker 2010, character 1]**

1312 0: Directed laterally

1313 1: Directed dorsally

1314

1315 **[ORDERED] 14) Position of nares [from Hungerbühler 2002, character 10; Stocker 2010, character 2]**

1316 0: Terminal

1317 1: Non-terminal, posterior rim of nares in front of anterior rim of antorbital fenestra

- 13182: Non-terminal, posterior rim of nares behind anterior rim of antorbital fenestra
- 1319
- 132015) Anterior extent of septomaxillae [from Stocker 2010, character 12]
- 13210: Anterior to anterior tip of nasal
- 13221: Posterior to or at level with anterior tip of nasal
- 1323
- 132416) Narial outlets [from Hungerbühler et al. 2013, character 10]
- 13250: Absent
- 13261: Present
- 1327This character refers to grooves exiting the anterior extremity of the external nares, often resulting from the anterior
- 1328convergence of the lateral narial borders. Narial outlets are almost entirely pervasive throughout non-
- 1329leptosuchomorph phytosaurs, but only occur in a handful of more derived taxa; specifically in *Machaeroproso-*
- 1330*lottorum* and some specimens of *Nicrosaurus meyeri*, *Mystriosuchus planirostris* and *westphali* and
- 1331*Machaeroproso-*
pus pristinus.
- 1332
- 133317) Dorsal rim of nares [from Hungerbühler 2002, character 9; Stocker 2010, character 20]
- 13340: At or below level of skull roof
- 13351: Above level of skull roof
- 1336
- 133718) Narial wing [from Hungerbühler et al. 2013, character 11]
- 13380: Present

1339 1: Absent, narial opening closed anteriorly

1340 State zero refers to a raised lateral rim of the external nares, which descends prior to the anterior border of the nares,

1341 often abruptly, leaving a roughly 90 degree corner at the anterodorsal oint of the lateral narial rim, exemplified in

1342 *Mystriosuchus planirostris*.

1343

1344 **19) Interorbital nasal area lateral view [modified from Hungerbühler 2002, character 14; Stocker 2010,**

1345 **character 21]**

1346 0: Flat from orbit to nares

1347 1: Posterior border of nares and anterior border of orbits dip down into a concavity

1348 This character and the subsequent one were previously a single character, describing the morphology of the

1349 interorbital-nasal area. However the original description of the character and its states are confusing:

1350 ‘Interorbitonasal area: flat (0); convex (1). The area between the nares and the orbits is primitively flat and broad. In

1351 derived phytosaurs, the area is narrower, transversely round, and saddle-shaped because of the elevation of the

1352 nares and the orbital rims.’ Hungerbühler (2002). The character initially appears to be describing only the transverse

1353 profile of the interorbital-narial area, however at the end the phrase ‘saddle-shaped’ is used in relation to the

1354 concavity seen in some phytosaurs in lateral view caused by the raised posterior border of the nares and anterior

1355 border of the orbits. This suggests the character should be aimed at describing the full three-dimensional

1356 morphology of the area, however this laterally visible morphology is not represented in the character states. The

1357 character is split here, in order to allow representation of both the laterally visible profile (character 19) and

1358 transverse morphology (character 20).

1359 Additionally, whilst the states of character 20 are roughly similar to their original wording, their

1360 applicability to some taxa is different. Previously all derived taxa were stated to possess an interorbital-nasal area

1361 that ‘is narrower, transversely round’; however all members of Mystriosuchini excluding *Mystriosuchus* (and

1362 *Nicrosaurus* if included within Mystriosuchini) possess a much broader area between the nares and orbits than the

1363 more basal taxa, which is transversely flat, prior to its lateral descent. The cross section of this morphology is
1364 roughly rectangular in dorsal profile, rather than the inverted U-shape present in *Leptosuchus*-like phytosaurs,
1365 *Rutiodon* and *Angistorhinus*. In *Parasuchus*-grade phytosaurs, the large anteroposterior extent of the interorbital-
1366 nasal area results in a varied transverse morphology depending on the position at which it is sampled. We therefore
1367 tentatively exclude *Parasuchus*-grade phytosaurs from this character
1368

1369 **20) Interorbital nasal area cross section [modified from Hungerbühler 2002, character 14; Stocker 2010,**
1370 **character 21]**

1371 0: Flat and broad

1372 1: Dorsally curved in cross section

1373 [See notes for character 19]

1374

1375 **21) Infranasal recess [from Hungerbühler 2002, character 11]**

1376 0: Absent

1377 1: Present

1378

1379 **[ORDERED] 22) Antorbital fossa [from Hungerbühler 2002, character 12; Stocker 2010: character 3; Butler**
1380 ***et al.* 2014, character 3]**

1381 0: Present lacrimal jugal and maxillary fossae touching

1382 1: Present but reduced lacrimal jugal and maxillary fossae in contact dorsally but not ventrally

1383 2: Present but reduced lacrimal jugal and maxillary fossae not touching

1384 3: Absent

1385

1386 **23) Discrete row of anteroposteriorly extending nodes on the lateral surface of the jugal [from Butler *et al.***

1387 **2014, character 44]**

1388 0: Absent

1389 1: Present

1390

1391 **24) Jugal and antorbital fenestra [from Stocker 2010, character 4]**

1392 0: Excluded from antorbital fenestra

1393 1: Contributing to antorbital fenestra

1394

1395 *** [ORDERED] 25) Length of antorbital fenestra [modified from Hungerbühler *et al.* 2013, character 13]**

1396 0: Less than 1.9 times naris length

1397 1: Greater than or equal to 1.9 times naris length

1398 Modified to reflect the range of morphology sampled in this study. Measured as the ratio between the length of the

1399 antorbital fenestra and the length of the external nares. State zero scores a relatively shorter antorbital fenestra,

1400 while state one scores a relatively longer antorbital fenestra.

1401

1402 **26) Broad median depression on dorsal surface of frontals near border with nasals [from Kammerer *et al.***

1403 **2015, character 47]**

1404 0: Absent

1405 1: Present

1406

1407 **27) Posterolateral margins of nares [modified from Kammerer *et al.* 2015, character 48]**

1408 0: Relatively low without ornamentation or derived features

1409 1: Swollen and rugose creating a distinct narial rim

1410 2: Distinctly raised in lateral view forming a sharp triangular peak well above the surrounding skull roof

1411 State two is added here to reflect the morphology of *Parasuchus bransoni*, which deviates from the previous two

1412 states with the dorsally pronounced morphology of its posterior narial rim.

1413

1414 **28) Pre-orbital depression [from Hungerbühler 2002, character 15]**

1415 0: Absent

1416 1: Present

1417

1418 **29) Depression and flange in postorbital bar [from Hungerbühler *et al.* 2013, character 14]**

1419 0: Absent

1420 1: Small elongate depression posterior rim of postorbital may create a small flange behind orbit

1421 2: Strong elongate depression posterior rim of postorbital bar forms a distinct flange merging with po/sq bar

1422

1423 **30) Jugal and orbit [from Stocker 2010, character 5]**

1424 0: Excluded from orbit

- 14251: Contributing to orbit
- 1426In *Nicrosaurus kapffii*, both states of this character are present, with both states represented in individual specimens
- 1427in some cases (**Hungerbühler, 1998**).
- 1428
- 1429**31) Medial margins of orbits [from Stocker 2010, character 6]**
- 14300: Flat with skull roof
- 14311: Raised into orbital ridges
- 1432
- 1433**32) Deep sculpture of the skull roof [from Hungerbühler 2002, character 17]**
- 14340: Absent
- 14351: Present
- 1436
- 1437**33) Sutural articulation of squamosal and postorbital in dorsal view [from stocker 2010, character 22]**
- 14380: Slot like, posterior process of po fits into slot in sq
- 14391: Diagonal, sq forms anteromedial portion of po/sq bar and po forms posterolateral portion
- 14402: Approximately transverse
- 1441
- 1442**[ORDERED] 34) Most anterior extent of infra-temporal fenestra [from Butler *et al.* 2014, character 45]**
- 14430: Beneath the posterior corner of the orbit
- 14441: Extended anteriorly, reaches below the middle or anterior half of the orbit

1445 2: Anteroventral corner distinctly in front of anterior rim of orbit

1446

1447 **35) Pre-infratemporal shelf [from Hungerbühler 2002, character 18]**

1448 0: Absent

1449 1: Present

1450 The ‘pre-infratemporal shelf’ is an anteriorly convex, crescent-shaped ridge slightly anterior of the anterior border

1451 of the antero-ventral corner of the infratemporal fenestra. This morphology is present in all members of

1452 *Mystriosuchus*, *Machaeroprotopus* and ‘*Redondasaurus*’ to some degree, and also in some specimens of

1453 *Nicrosaurus*.

1454

1455 **36) Lateral ridge from post-orbital/squamosal bar [modified from Stocker 2010, character 23; Butler *et al.***

1456 **2014, character 23]**

1457 0: Absent

1458 1: Continues posteriorly onto squamosal as a horizontal ridge forming a shelf overhanging the infratemporal

1459 fenestra

1460 2: Bifurcates into two small ridges on lateral surface of squamosal

1461 The morphology of any ridge on the lateral surface of the postorbital/squamosal bar has previously been scored

1462 with considerable subjectivity. The original character on which this is based possesses a number of states which

1463 may be equally applicable to multiple taxa depending on interpretation. Here, the character is simplified to reflect

1464 the morphologies that were recognized in this study, including the absence of a ridge.

1465

1466 **37) Lateral ridge of postorbital squamosal bar continues as ridge onto posterior process of squamosal [from**
1467 **Hungerbühler *et al.* 2013, character 19]**

1468 0: Absent

1469 1: Present

1470

1471 * **[ORDERED] 38) Length of posterior process of squamosal in relation to postorbital length [modified from**
1472 **Hungerbühler 2002, character 31; Stocker 2010, character 24]**

1473 0: Absent or extremely short, posterior edge of squamosal does not extend or barely extends posteriorly beyond the
1474 distal end of the paroccipital process of the opisthotic

1475 1: Less than 3.60

1476 2: 3.60 to 4.99

1477 3: Greater than, or equal to 5.00

1478 Modified to reflect the measurements made for the greater range of taxa included in this study. The character is
1479 measured as the ratio of the distance from the posterior border of the orbit to the posteriormost point of the
1480 squamosal, and the distance from the posterior border of the paroccipital process to the tip of the squamosal. State
1481 one scores a long posterior process, state two a moderate process, and state three a short process.

1482

1483 † **39) Posterior process of squamosal [modified from Hungerbühler 2002, character 32; Stocker 2010,**
1484 **character 25]**

1485 0: Greatly dorsoventrally expanded

1486 1: Moderately dorsoventrally expanded

1487 2: Terminal knob

1488 Ballew (1989), character 50 references the presence of a ‘knob-like’ posterior process of the squamosal in

1489 *Machaeroprotopus pristinus* and *buceros*; this then became the ‘terminal knob’ of Hungerbühler (2002) and was

1490 subsequently used to describe this morphology. This character is modified to use this terminology, which is

1491 assumedly referenced by the ‘dorsally compressed’ state, used in previous versions of this character. Using this

1492 terminology makes the character less ambiguous.

1493

1494 † 40) Terminal knob [modified from Hungerbühler 2002, character 32; Hungerbühler *et al.* 2013, character

1495 24]

1496 0: Terminal knob raised distally above po/sq bar

1497 1: Terminal knob in plane of po/sq bar

1498 In some specimens the distal region of the terminal knob-like process of the squamosal is inflexed dorsally. The

1499 previous version of this character mentioned the posterior raising of the posterior process of the squamosal in

1500 reference to a greatly dorsoventrally expanded posterior process. This morphology was not recognized in any

1501 specimens in this study, whereas it was noted to be relatively common among individuals possessing a terminal

1502 knob.

1503

1504 41) Dorsal edge of squamosal [from Hungerbühler 2002, character 33; Stocker 2010, character 26]

1505 0: Straight and narrow, no medial expansion

1506 1: Expanded medially

1507 This character essentially scores the presence or absence of any size of medial flange of the postorbital/squamosal

1508 bar.

1509

1510 **42) Dorsal edge of squamosal B [from Stocker 2010, character 27]**

1511 0: Mediolaterally flat

1512 1: Ventral depression between medial and lateral edges of the dorsal edge of the squamosal

1513

1514 * **[ORDERED] 43) Length of free postorbital/squamosal bar [modified from Hungerbühler *et al.* 2013,**

1515 **character 17]**

1516 0: Less than 2.90

1517 1: 2.90 to 3.39

1518 2: Greater than or equal to 3.40

1519 Modified to reflect the measurements made for the greater range of morphologies in this study. The character is

1520 measured as the ratio between the distance from the most anterior point of the supratemporal fenestra and the

1521 posteriormost point of the squamosal, to the shortest distance between the posterior border of the orbit and the most

1522 anterior point of the supratemporal fenestra. State zero corresponds to ‘short’, one corresponds to ‘moderate’ and

1523 two to ‘long’.

1524

1525 **44) Medial extent of squamosal [modified from Hungerbühler 2002, character 30]**

1526 0: To mid length of parieto squamosal bar

1527 1: Enters base of supraoccipital shelf wedged between parietal and supraoccipital

1528 The character state ‘Enters rim of supraoccipital shelf dorsal to parietal’ has been removed as it was not recognized

1529 in any of the specimens examined in this study.

1530

1531 **45) Cross section of posterior half of postorbital squamosal bar [from Hungerbühler 2002, character 22]**

1532 0: Low, dorsoventrally compressed

1533 1: High, triangular

1534

1535 † **46) Ventral margin of squamosal [from Stocker 2010, character 28]**

1536 0: Gently sloping anteroventrally from posterior edge of posterior process to opisthotic process

1537 1: Distinct horizontal ventral edge between posterior edge of posterior process and opisthotic process

1538

1539 **47) Subsidiary opisthotic process of squamosal [from Hungerbühler 2002, character 35; Stocker 2010, character 29]**

1541 0: Absent

1542 1: Present

1543

1544 **48) Extent of squamosal fossa [from Stocker 2010, character 30]**

1545 0: Extends to posterior edge of sq

1546 1: Does not reach posterior edge of sq

1547

1548 **[ORDERED] 49) Orientation of supratemporal fenestra [from Stocker 2010, character 32]**

1549 0: Dorsally expressed parietal squamosal bar at level with skull roof

- 15501: Partially depressed parietal process of squamosal below level of skull roof
- 15512: Fully depressed posterior process of parietal and entire parietal squamosal bar below level of skull roof
- 1552
- 1553† 50) Mediolateral expansion of posterior process of squamosal [modified from Hungerbühler *et al.* 2013,
- 1554character 25]
- 15550: Tip of squamosal tapers strongly posteriorly
- 15561: Tip of squamosal tapers with a smooth lateral deflection distally
- 1557
- 155851) Face of medial rim of squamosal along supratemporal fenestra and posterior process [modified from
- 1559Hungerbühler *et al.* 2013, character 23]
- 15600: Entire rim rounded or sharp
- 15611: Rim entirely or in part squared
- 1562
- 156352) Extent of squaring of the squamosal rim [modified from Hungerbühler *et al.* 2013, character 23]
- 15640: Squared in posterior section
- 15651: Entire rim squared
- 1566
- 156753) Ridge around anterior and or medial edge of supratemporal fenestra [modified from Hungerbühler 2002,
- 1568character 20]
- 15690: Absent

1570 1: Present, medial only

1571 2: Present, anterior and medial

1572 The terminology used in the original character is quite vague ‘Anterior border of supratemporal fenestra... raised

1573 above skull roof’. This character is a reinterpretation of the original, with more specific terms. In state one, the ridge

1574 would only be present on the parietal ledge, whereas in state two the ridge may extend to the anterior border of the

1575 supratemporal fenestra.

1576

1577 * † [ORDERED] 54) Width of squamosal [modified from Hungerbühler *et al.* 2013, character 18]

1578 0: Less than or equal to 3.80

1579 1: Greater than 3.80

1580 Modified to reflect the greater range of morphologies measured in this study. Scored as the ratio between the length

1581 of the squamosal from the anteriormost point of the supratemporal fenestra to the posterior-most extent of the

1582 posterior process, and the width of the postorbital/squamosal bar at its approximate mid-point, or the point most

1583 representative of its general width. State zero corresponds to a wide postorbital/squamosal bar, state one denotes a

1584 relatively less wide bar.

1585

1586 † 55) Outline of medial rim of squamosal along supratemporal fenestra and posterior process [modified from

1587 Hungerbühler 2002, character 29]

1588 0: Sinuous

1589 1: Angular

1590 2: Straight

1591 3: Curved

1592 Character state three has here been added to represent the morphologies found in *Nicrosaurus* and *Coburgosuchus*,
1593 which we feel were not adequately described by the previous character states.

1594

1595 **56) Path of parietal/squamosal bars [from Stocker 2010, character 34]**

1596 0: Trending straight posteriorly to attachment on squamosals

1597 1: Curved medially convex before attaching on squamosals

1598

1599 **[ORDERED] 57) Visibility of supratemporal fenestrae in dorsal view [modified from Hungerbühler 2002,**
1600 **character 19; Stocker 2010, character 33]**

1601 0: Visible, STF completely open dorsally

1602 1: Mostly visible, posterolateral portions of STF covered in dorsal view

1603 2: Mostly covered dorsally, at most only anteromedial corners or medial slit of STF visible in dorsal view

1604 3: Lamella merges with parietal, STF obliterated in dorsal view

1605 This character combines those of Hungerbühler and Stocker. The wording used by Stocker is more inherently
1606 understandable, as Hungerbühler describes the visibility of the fenestra via the expansion of the squamosal, which is
1607 technically correct, but less intuitive. The final state of Hungerbühler’s character is, however, missing from
1608 Stocker’s and is useful in describing the morphology found in some extremely robust members of
1609 *Machaeroprotopus* and most specimens of ‘*Redondasaurus*’.

1610

1611 **58) Parietal/squamosal bars [from Stocker 2010, character 35]**

1612 0: Slender, narrower than the width of po/sq bars

1613 1: Wide, approximately the same mediolateral width as po/sq bars

1614

1615 **[ORDERED] 59) Dorsal edge of parietal/squamosal bar [from Hungerbühler 2002, character 26]**

1616 0: Horizontal

1617 1: Gently sloping

1618 2: Steeply sloping

1619 3: Either entirely, or in parts vertical

1620

1621 * **[ORDERED] 60) Parietal ledge, ratio of width to length [modified from Hungerbühler *et al.* 2013,**

1622 **character 30]**

1623 0: Less than 1.30

1624 1: 1.30 to 2.10

1625 2: Greater than 2.10

1626 Modified to reflect the greater range of morphologies sampled in this study. Width is measured either at the mid-

1627 point of the ledge, or the point that is most representative of its general width. Length is measured from the

1628 posterior-most extent of the ledge to the anterior-most point of the supratemporal fenestra (in phytosaurs where the

1629 parietal/squamosal bars are at the level of the skull roof, the posterior-most point of the ledge is measured at the

1630 midline of the parietals). State zero corresponds to a parietal ledge that is generally more anteroposteriorly

1631 prominent, whereas state two is very wide and hardly projects posteriorly.

1632

1633 **61) Medial half of parieto squamosal bar lateral wall of supraoccipital shelf [from Hungerbühler 2002,**
1634 **character 37]**

1635 0: High and thin

1636 1: Low, continuously thin

1637 2: Low, basally thickened

1638

1639 **62) Lobate extension on the vertical rim of the squamosal processes of the parietal [from Hungerbühler 2002,**
1640 **character 53]**

1641 0: Absent

1642 1: Present

1643

1644 **63) Depth and shape of supraoccipital shelf [from Hungerbühler 2002, character 36]**

1645 0: Shallow, longitudinal axis of shelf vertical

1646 1: Deep, axis of shelf straight and horizontal

1647 2: Deep axis of shelf with steep slope anteriorly and terminal horizontal deflection of shelf

1648

1649 **64) Top of parieto supraoccipital complex formed by squamosal processes of parietals [from Ballew 1989,**
1650 **character 19; Hungerbühler 2002, character 24]**

1651 0: Angular, inverted V shape

1652 1: Rounded, inverted U shape

1653 2: Rectangular

1654

1655 **65) Parietal prongs [from Hungerbühler 2002, character 25]**

1656 0: Absent

1657 1: Present

1658

1659 **66) Posttemporal fenestra [from Hungerbühler 2002, character 41]**

1660 0: Moderately wide and tall

1661 1: Moderately wide and compressed

1662 2: Extremely reduced in width and height to a slit

1663

1664 **67) Lateral border of posttemporal fenestra [Hungerbühler 2002, character 38; Stocker 2010, character 37]**

1665 0: Formed by contact of the parietal process of the squamosal and the paroccipital process of the opisthotic

1666 1: Formed laterally only by the paroccipital process

1667 2: Formed laterally and slightly ventrally by process of squamosal that extends onto paroccipital process

1668

1669 **68) Shape of quadratojugal [modified from Sereno 1991, character Q; Stocker 2010, character 31]**

1670 0: L shaped, anterior suture trends anteroventrally

1671 1: Subtriangular

1672 2: L shaped, anterior suture trends anterodorsally

1673

1674 **69) Anterior border of parabasisphenoid contribution to basitubera [from Stocker 2010, character 39]**

1675 0: Basitubera separated widely

1676 1: Basitubera separated narrowly with a ridge along their anterior border

1677 2: Basitubera connected tubera form a sharp ridge along their anterior border

1678

1679 **70) Morphology of basioccipital between tubera [from Stocker 2010, character 40]**

1680 0: Concave depression

1681 1: Anteroposteriorly oriented ridge on the midline

1682

1683 **71) Lateral extent of basitubera compared to basipterygoid processes in ventral view [from Stocker 2010,**
1684 **character 41]**

1685 0: Lateral extent of basitubera even with lateral extent of basipterygoid processes

1686 1: Lateral extent of basitubera more laterally expanded compared to basipterygoid processes

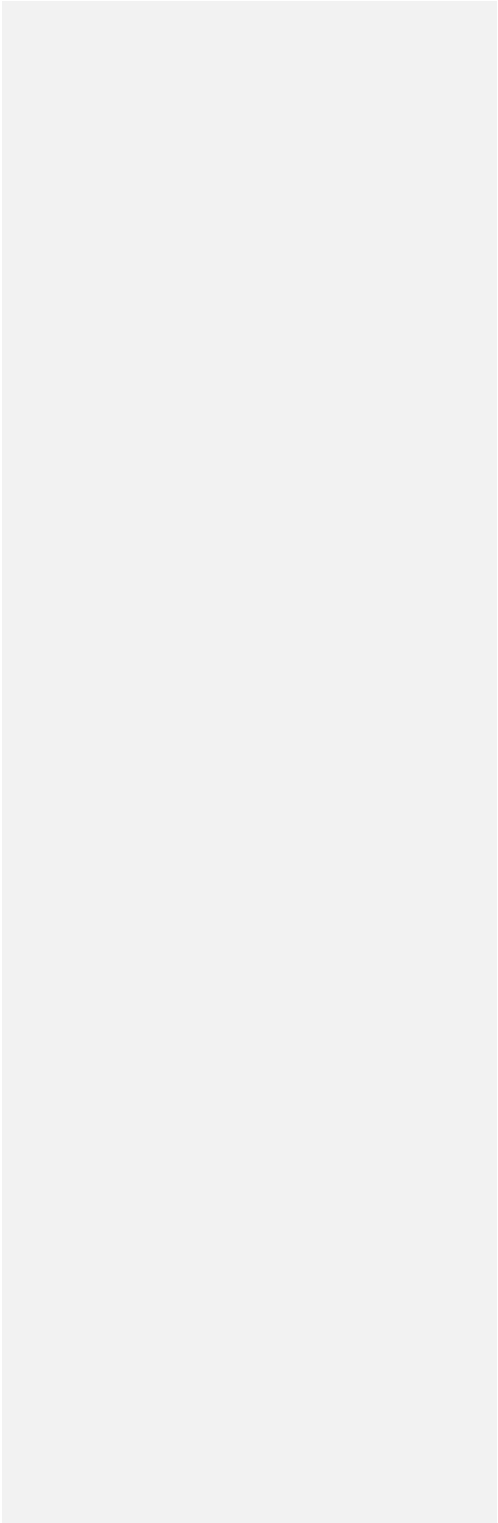
1687

1688 **72) Length of interpterygoid vacuity [from Chatterjee 1978, phenetic feature 7; Hungerbühler 2002,**
1689 **character 47]**

1690 0: Long, more than 50 per cent of length of palatal vault

1691 1: Tiny oval indentation at posterior rim of conjoined pterygoids

1692



- 1693
- 73) Suborbital foramen [from Hungerbühler 2002, character 46; Stocker 2010, character 43]
- 1694
- 0: Elongated, wide
- 1695
- 1: Elongated, slit-like
- 1696
- 2: Reduced to a single oval fenestra or subdivided into two or more small openings
- 1697
- 1698
- 74) Anterior extent of the palatine [from Hungerbühler 2002, character 44]
- 1699
- 0: Tip located behind the posterior rim of choana
- 1700
- 1: Tip extends forward beyond the posterior rim of choana
- 1701
- 2: Tip extends forward beyond the anterior rim of choana
- 1702
- 1703
- 75) Palatal ridge [from Hungerbühler *et al.* 2013, character 40]
- 1704
- 0: Low, rounded longitudinal elevation
- 1705
- 1: Prominent, sharp ventrally to ventromedially directed crest
- 1706
- 1707
- 76) Medial edge of palatine below posterior part of palatal vault [from Hungerbühler *et al.* 2013, character
- 1708
- 41]
- 1709
- 0: Sloping or vertical
- 1710
- 1: Horizontal flange may restrict the opening of the palatal vault significantly
- 1711
- 1712
- 77) Dorsal surface of surangular [from Mateus *et al.* 2014]

- 1713
- 0: Gently convex
- 1714
- 1: Gently concave rising to apex just posterior to dentary contact
- 1715
- 1716
- 78) Shape of retroarticular process in lateral view [from Mateus *et al.* 2014]**
- 1717
- 0: Distally sharply pointed or curved into a posterodorsally oriented hook
- 1718
- 1: Distally rounded or blunt
- 1719
- 1720
- 79) Snout dorsal surface cross sectional shape**
- 1721
- 0: Rounded, dorsal surface of snout is curved from side to side
- 1722
- 1: Triangular, sides of the snout are straight and slope up to the midline
- 1723
- 1724
- 80) Anterior separation of the septomaxillae**
- 1725
- 0: Septomaxillae separate posterior to level with the anterior narial border
- 1726
- 1: Septomaxillae separate distinctly anterior of the anterior narial border
- 1727
- 1728
- † 81) Shape of antorbital fenestra**
- 1729
- 0: oval
- 1730
- 1: Sausage-shaped
- 1731
- 2: Approximately triangular
- 1732
- 3: Approximately triangular - point posteriormost

Commented [WGP23]: What kind of sausage? This is not an adequate descriptive term.

1733

1734 **82) Lateral surface of maxilla and jugal ventral/posteroventral to AOF**

1735 0: Flat/laterally convex

1736 1: Concavity running along the length of the element

1737

1738 **83) Lateral surface of main body of jugal**

1739 0: Generally flat, element forms one dorsolaterally facing plane between its ventral and dorsal extremities

1740 1: Anteroposteriorly directed ridge running from below AOF towards ventral border of subTF splits jugal into a
1741 dorsolaterally facing facet and a laterally facing facet

1742 2: Anteroposterior ridge running along the centre of the jugal posterior process

1743 3: Anteroposterior ridge running toward ventral border of jugal posterior process

1744

1745 **84) Anterior extension of the sub temporal shelf**

1746 0: Anteriormost border of shelf is posterior to the posteriormost border of the antorbital fenestra

1747 1: Anteriormost border of shelf terminates anterior of the posteriormost corner of the antorbital fenestra

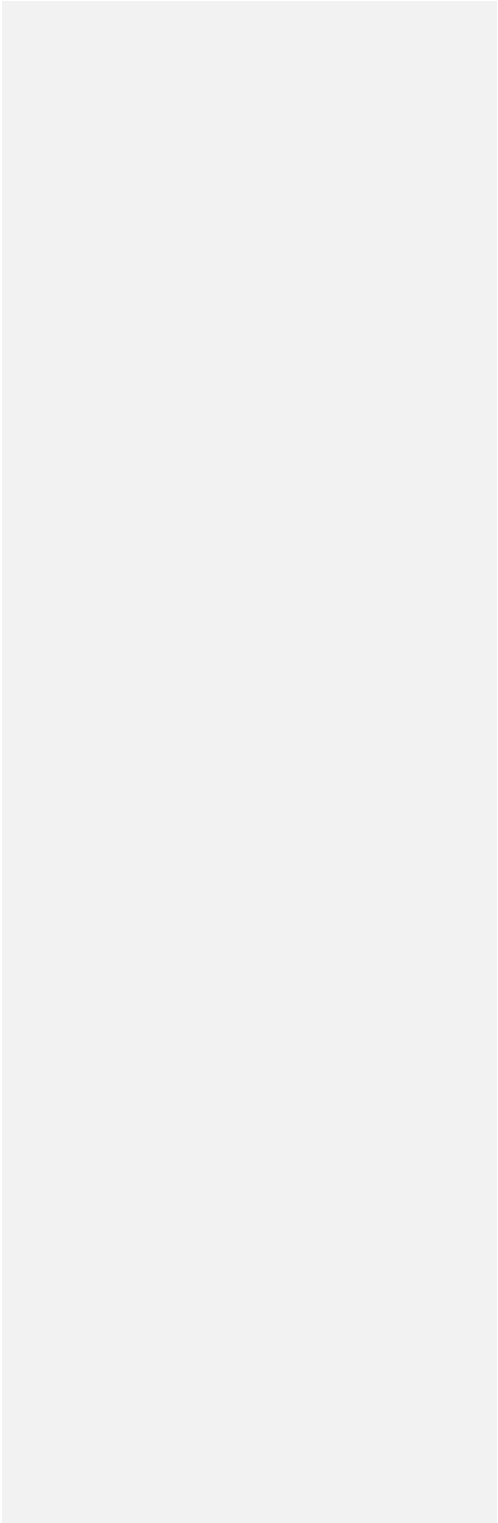
1748

1749 **85) Dorsal extension of sub temporal shelf**

1750 0: Merges dorsally into lateral surface of jugal

1751 1: Continues dorsally contributing to the posterior edge of the postorbital descending process

1752



- 1753
- 86) Jugal foramen in anteroventral corner of the sub temporal fenestra
- 1754
- 0: Visible only in medial view, not visible in lateral view
- 1755
- 1: Visible in lateral view
- 1756
- 1757
- * [ORDERED] 87) Relative robusticity of the jugal
- 1758
- 0: Less than 7.30
- 1759
- 1: 7.30-8.40
- 1760
- 2: Greater than 8.40
- 1761
- 1762
- 88) Proximal section of postorbital descending process where posterior border of orbit meets skull roof
- 1763
- 0: Flares anteroposteriorly creating a wide triangular connection
- 1764
- 1: Posterior border of orbit remains thin until it reaches skull roof
- 1765
- 1766
- * † [ORDERED] 89) Sub temporal fenestra diagonal aspect ratio
- 1767
- 0: Less than or equal to 2.30
- 1768
- 1: Greater than 2.30
- 1769
- 1770
- 90) Additional ridge on lateral surface of posterior process of squamosal below ridge or rugosity from po/sq
- 1771
- bar
- 1772
- 0: Absent

1773 1: Present

1774

1775 † **91) Posterior border of quadrate in lateral view**

1776 0: Straight anterodorsal line for majority of element

1777 1: Ventral section of border is anteroposteriorly concave

1778

1779 **92) Internarial septum**

1780 0: Restricted to between, or extends slightly anterior of the external nares

1781 1: Extends anterior of the nares by approximately the narial length

1782

1783 **93) Triangular projection ventral to articular condyle**

1784 0: Anterior border is straight, trending posteroventrally

1785 1: Ventral half of anterior border possesses an anteriorly projecting process

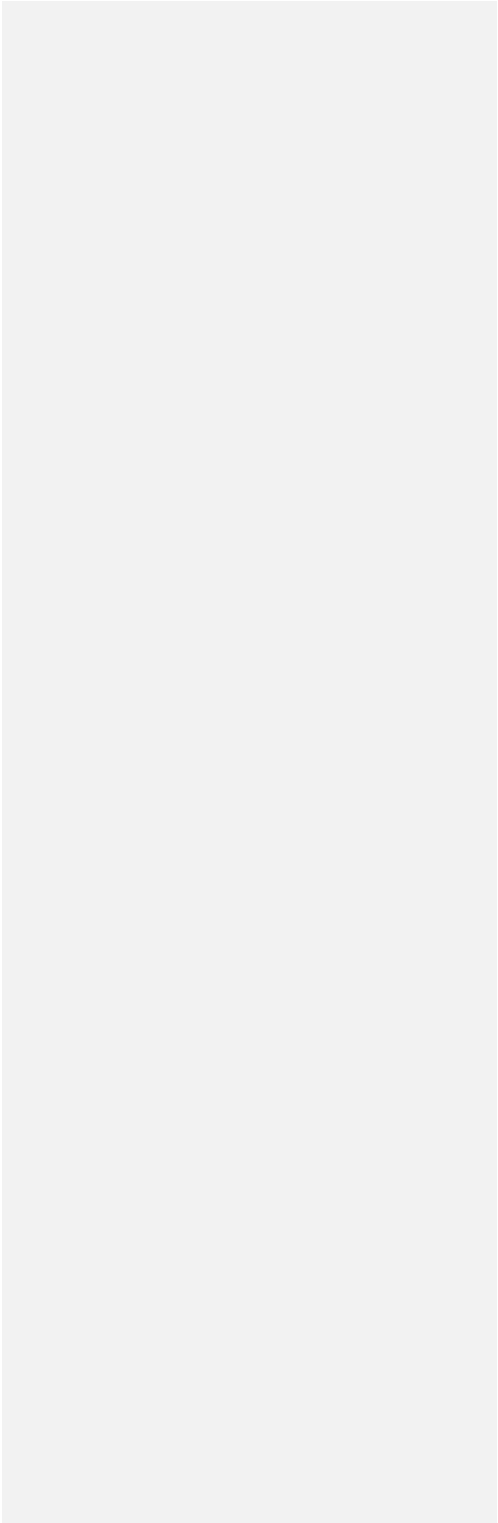
1786

1787 * **[ORDERED] 94) Relative length of mandibular symphysis**

1788 0: Less than 1.00

1789 1: Greater than or equal to 1.00

1790



1791 **Appendix 3: Nodal synapomorphies**

1792

1793 This list presents all synapomorphic character changes at every node of each of the four data treatments:

1794 discrete, discrete + continuous, discrete + GM, and discrete + continuous + GM.

1795

1796 **Discrete tree**

1797 1) No synapomorphies

1798

1799 2) 13: 0→1

1800 22: 0→1

1801

1802 3) 36: 0→1

1803 69: 0→1

1804

1805 4) 23: 0→1

1806 26: 0→1

1807 50: 0→1

1808

1809 5) 82: 0→1

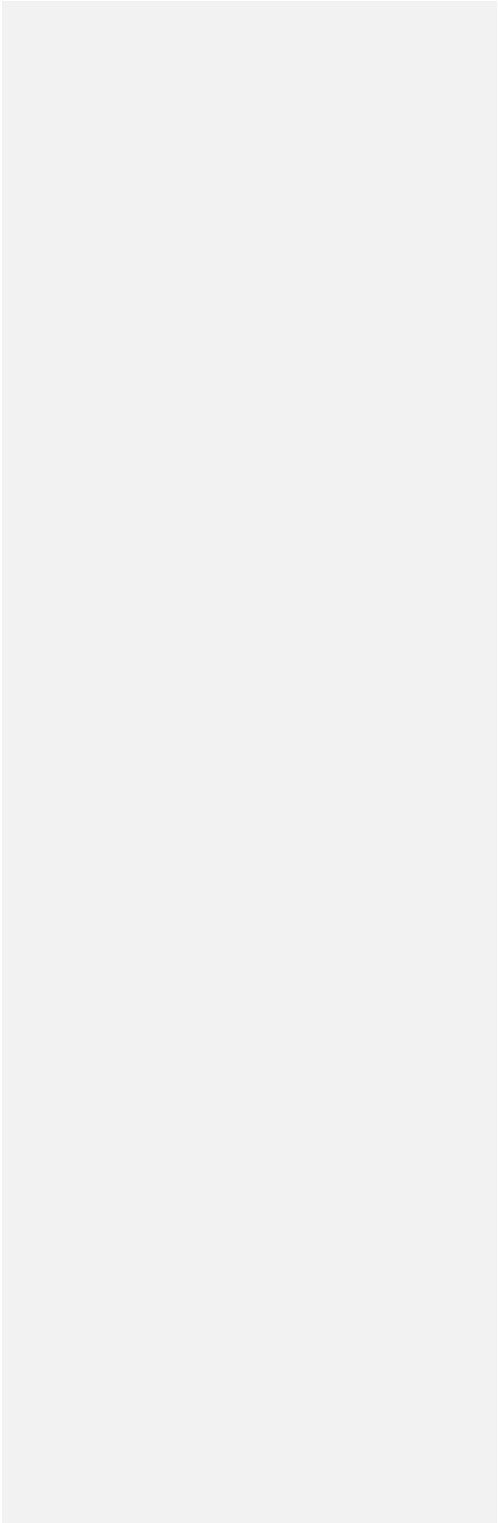
1810 91: 0→1

1811

1812 6) 1: 0→1

1813 22: 1→2

1814		73: 0→1
1815		83: 1→0
1816		
1817	7)	9: 0→1
1818		14: 1→2
1819		19: 0→1
1820		29: 0→1
1821		36: 1→0
1822		38: 0→2
1823		69: 1→2
1824		72: 0→1
1825		74: 1→2
1826		80: 0→1
1827		81: 0→2
1828		
1829	8)	22: 2→1
1830		60: 1→0
1831		92: 0→1
1832		
1833	9)	56: 0→1
1834		58: 0→1
1835		
1836	10)	42: 0→1



1837 51: 0→1

1838

1839 11) 12: 0→1

1840 17: 0→1

1841 66: 0→1

1842 70: 0→1

1843

1844 12) 69: 2→1

1845

1846 13) 8: 0→2

1847 16: 1→0

1848 25: 0→1

1849 41: 0→1

1850 44: 0→1

1851 49: 0→1

1852 57: 0→1

1853 59: 0→1

1854 88: 1→0

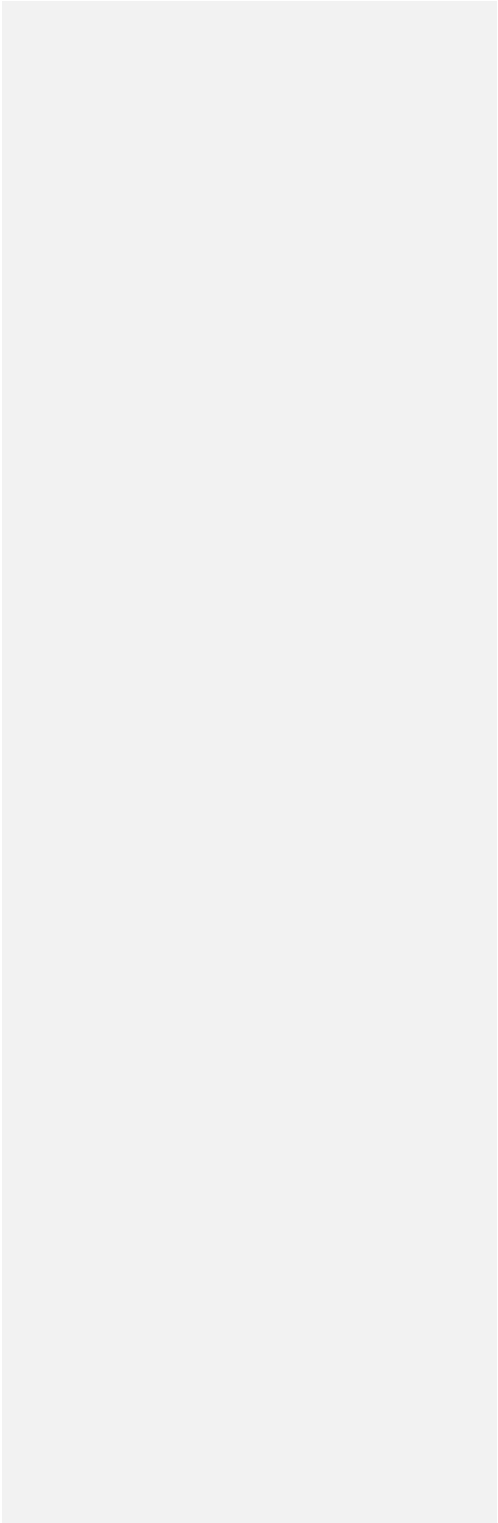
1855

1856 14) 81: 2→1

1857

1858 15) 90: 0→1

1859



186016)19: 1→0

186120: 0→1

186239: 0→1

1863

186417)7: 0→4

1865

186618)48: 0→1

1867

186819)3: 0→1

18697: 4→2

187033: 0→2

1871

187220)21: 0→1

187329: 1→0

1874

187521)49: 1→2

187653: 2→0

187754: 1→0

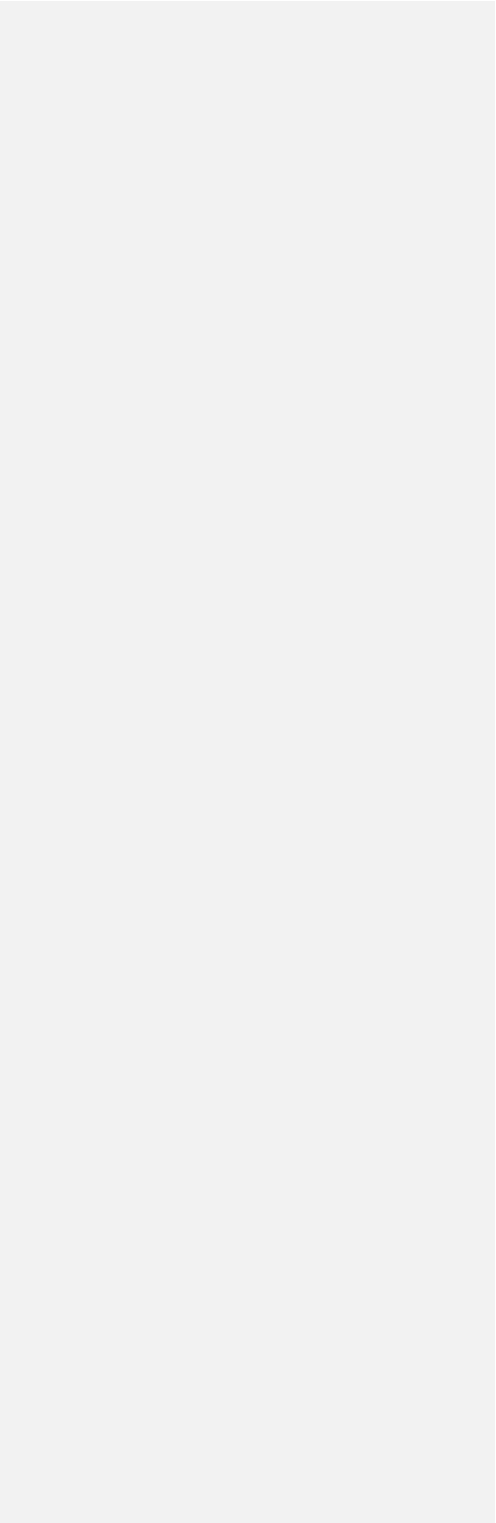
187857: 1→2

187967: 0→2

1880

188122)38: 2→3

1882



1883 23) 49: 1→2

1884

1885 24) 35: 0→1

1886 43: 2→0

1887 54: 1→0

1888 75: 0→1

1889 87: 0→1, 2

1890

1891 25) 59: 1, 2→3

1892 84: 0→1

1893 85: 1→0

1894

1895 26) 2: 1→2

1896 20: 0→1

1897

1898 27) 88: 0→1

1899

1900 28) 65: 0→1

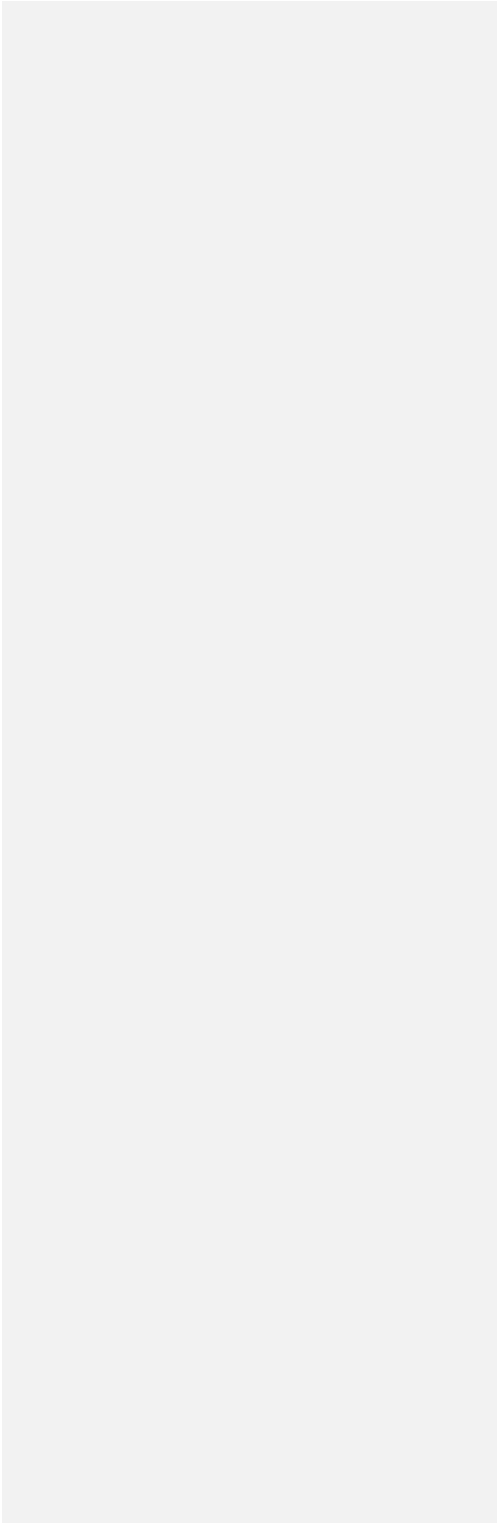
1901

1902 29) 3: 0→1

1903 4: 0→1

1904 7: 1→4

1905 46: 1→0



190647: 0→1

1907

190830)25: 1→0

190948: 0→1

1910

191131)30: 1→0

191236: 0→1

191351: 0→1

191460: 1→2

1915

191632)3: 1→0

19174: 1→0

191848: 0→1

191990: 0→1

1920

192133)7: 4→1

19228: 2→1

192389: 0→1

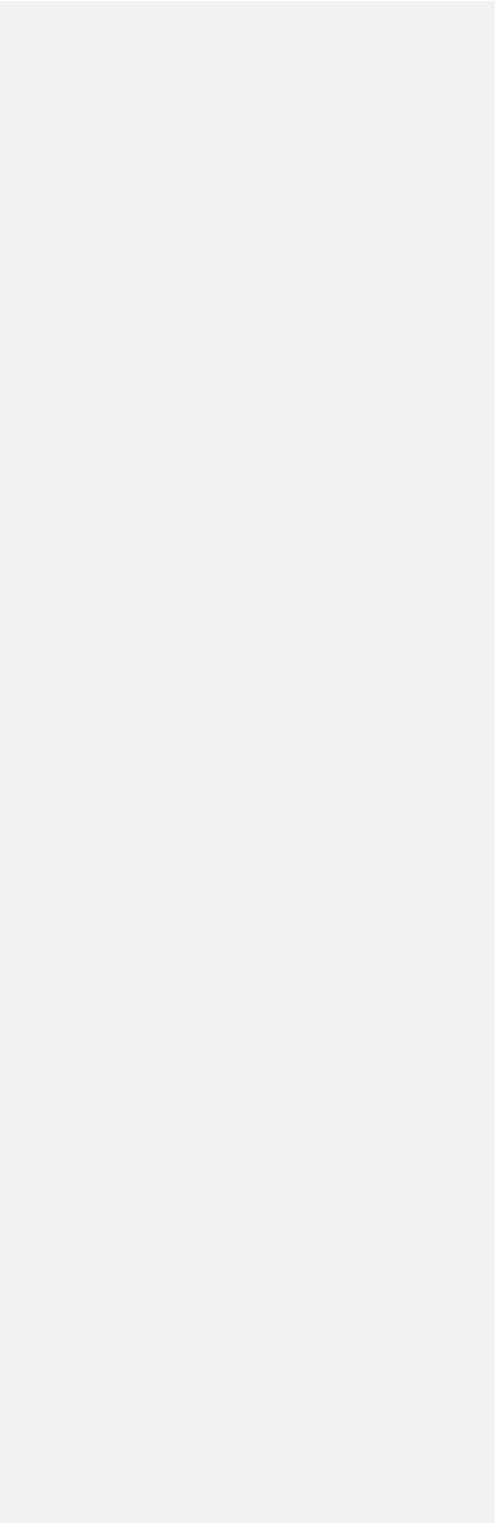
1924

192534)7: 4→2

192622: 2→3

1927

192835)11: 1→0



1929

1930 36) 48: 1→0

1931 53: 1→0

1932

1933 37) 19: 1→0

1934 57: 2→3

1935 59: 2→3

1936 63: 1→0

1937

1938 38) 89: 0→1

1939 **Discrete + continuous tree**

1940 1) No synapomorphies

1941

1942 2) 13: 0→1

1943 22: 0→1

1944

1945 3) 36: 0→1

1946 69: 0→1

1947

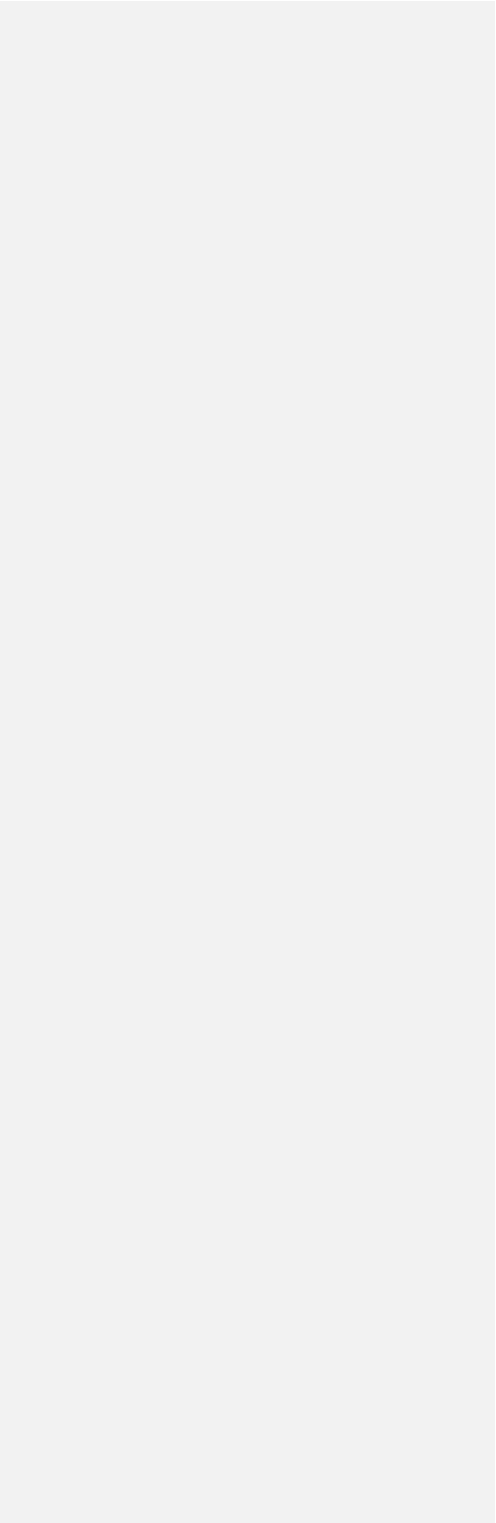
1948 4) 23: 0→1

1949 26: 0→1

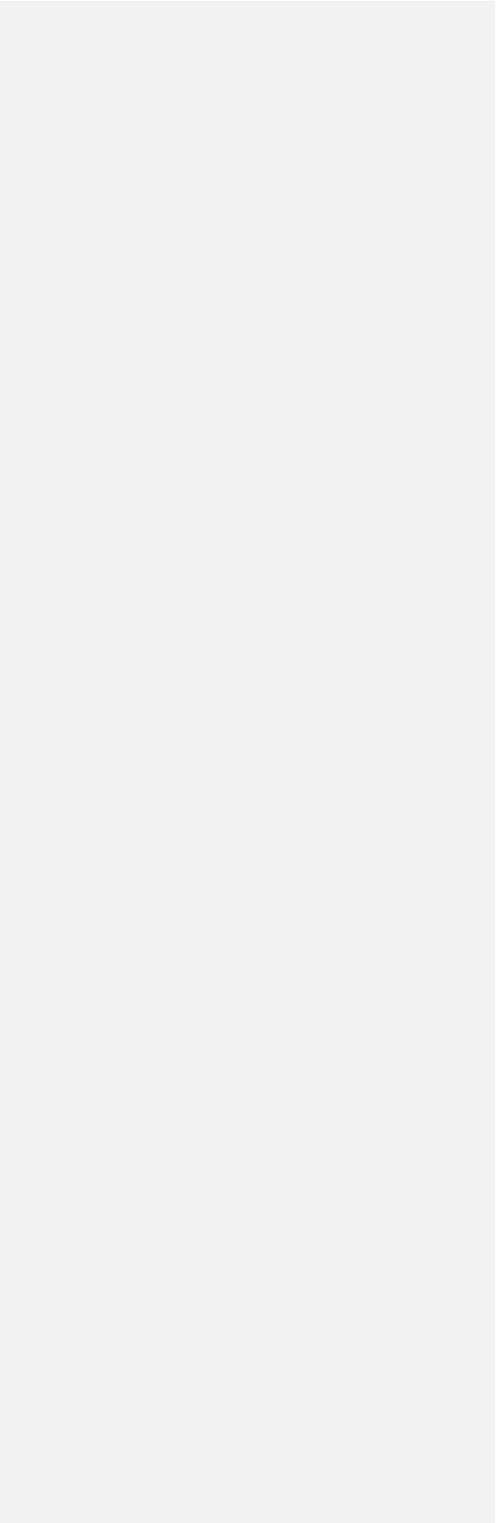
1950 50: 0→1

1951 54: 0.525-0.545 → 0.353-0.420

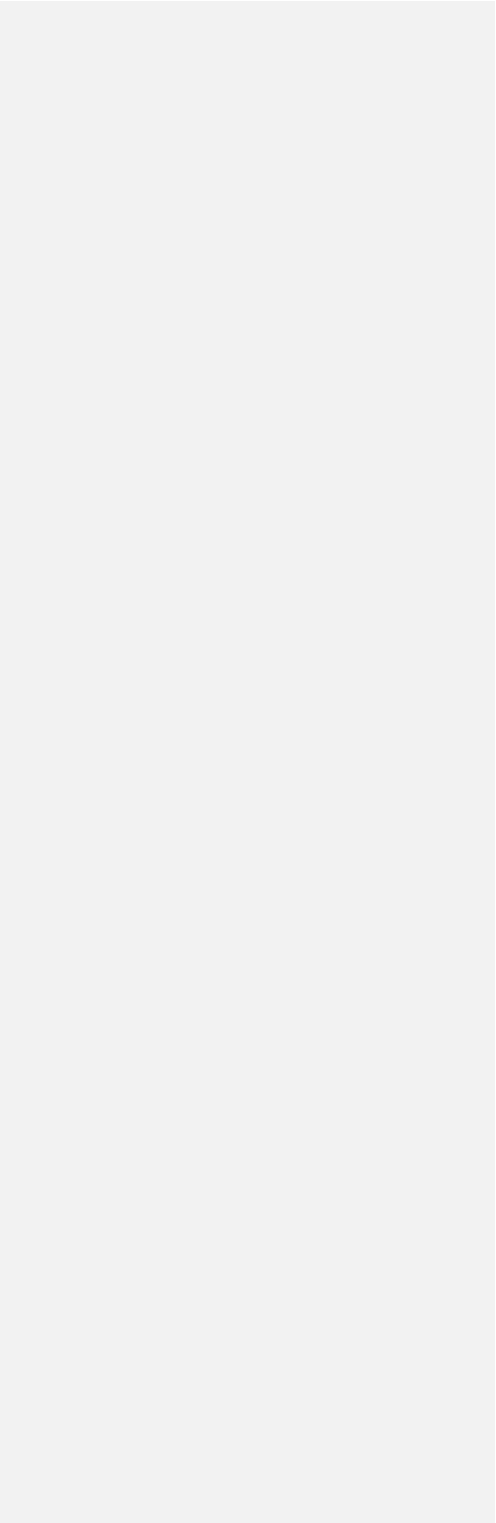
1952



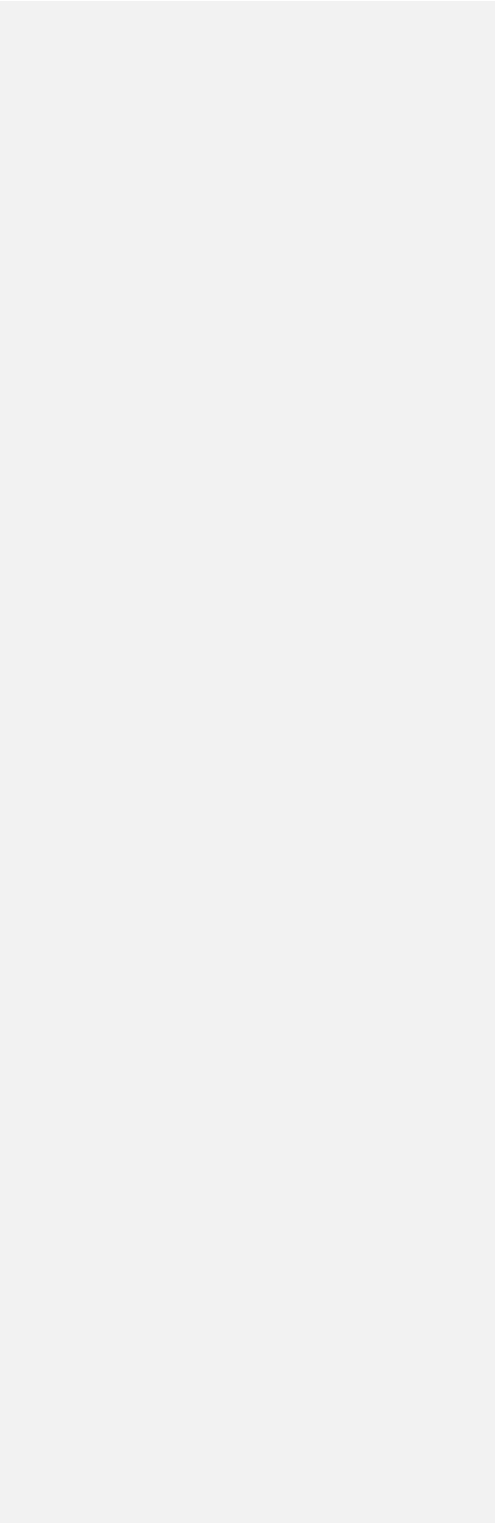
1953	5)	25: 0.452-0.470 \rightarrow 0.409-0.446
1954		82: 0 \rightarrow 1
1955		91: 0 \rightarrow 1
1956		
1957	6)	1: 0 \rightarrow 1
1958		11: 0.459-0.484 \rightarrow 0.490-0.686
1959		22: 1 \rightarrow 2
1960		25: 0.452-0.470 \rightarrow 0.514
1961		73: 0 \rightarrow 1
1962		83: 1 \rightarrow 0
1963		89: 0.244-0.272 \rightarrow 0.457-0.520
1964		
1965	7)	9: 0 \rightarrow 1
1966		14: 1 \rightarrow 2
1967		29: 0 \rightarrow 1
1968		36: 1 \rightarrow 0
1969		60: 0.060-0.090 \rightarrow 0.036-0.038
1970		69: 1 \rightarrow 2
1971		72: 0 \rightarrow 1
1972		74: 1 \rightarrow 2
1973		80: 0 \rightarrow 1
1974		
1975	8)	19: 0 \rightarrow 1



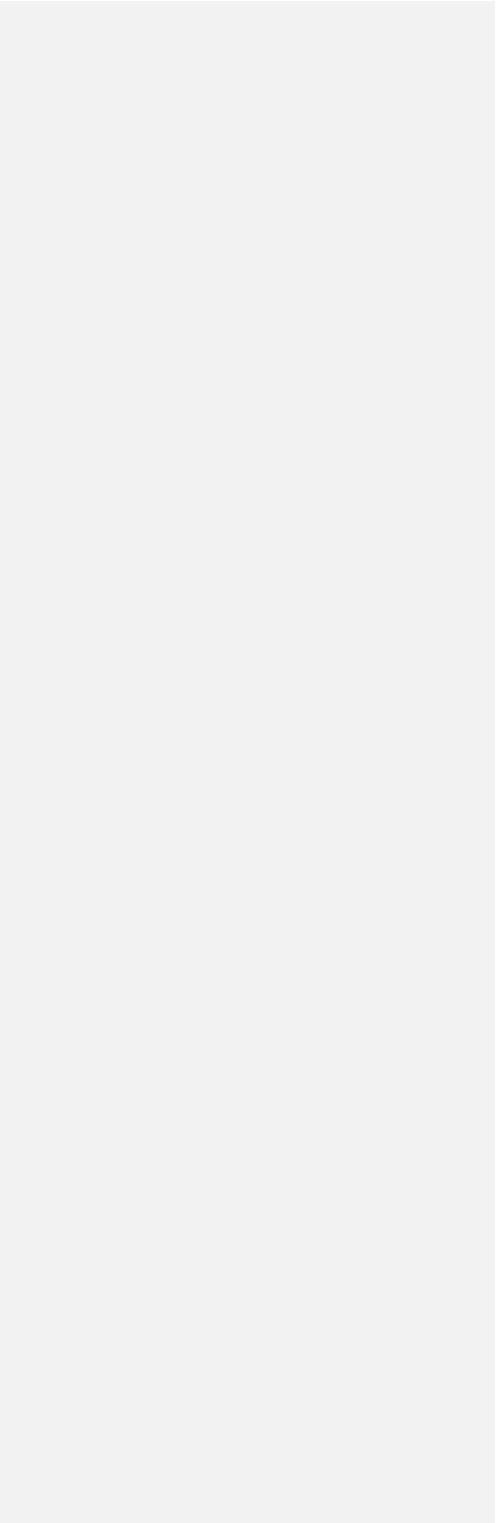
1976		22: 2→1
1977		25: 0.514 → 0.503
1978		92: 0→1
1979		
1980	9)	56: 0→1
1981		58: 0→1
1982		87: 0.106-0.110 → 0.103
1983		
1984	10)	42: 0→1
1985		51: 0→1
1986		
1987	11)	8: 0.240-0.253 → 0.274
1988		12: 0→1
1989		17: 0→1
1990		66: 0→1
1991		70: 0→1
1992		
1993	12)	69: 2→1
1994		
1995	13)	5: 0→1
1996		16: 1→0
1997		25: 0.514 → 0.684-0.718
1998		41:0→1



1999		88: 1→0
2000		90: 0→1
2001		
2002	14)	57: 0→1
2003		87: 0.106-0.110 → 0.117-0.132
2004		
2005	15)	10: 0→1
2006		79: 0→1
2007		
2008	16)	11: 0.678-0.686 → 0.729
2009		54: 0.525-0.545 → 0.395-0.406
2010		
2011	17)	48: 0→1
2012		89: 0.457 → 0.462
2013		
2014	18)	21: 0→1
2015		29: 1→0
2016		
2017	19)	49: 1→2
2018		54: 0.395-0.406 → 0.270
2019		57: 1→2
2020		67: 0→2
2021		



2022	20)	54: $0.270 \rightarrow 0.159$
2023		89: $0.457 \rightarrow 0.615-0.833$
2024		
2025	21)	19: $0 \rightarrow 1$
2026		20: $1 \rightarrow 0$
2027		
2028	22)	33: $0 \rightarrow 1$
2029		38: $0.281 \rightarrow 0.457$
2030		54: $0.525-0.545 \rightarrow 0.494$
2031		67: $0 \rightarrow 2$
2032		90: $1 \rightarrow 0$
2033		
2034	23)	49: $1 \rightarrow 2$
2035		54: $0.494 \rightarrow 0.383-0.399$
2036		
2037	24)	43: $0.106-0.118 \rightarrow 0.070$
2038		53: $2 \rightarrow 1$
2039		54: $0.383-0.399 \rightarrow 0.213$
2040		61: $0 \rightarrow 2$
2041		65: $0 \rightarrow 1$
2042		
2043	25)	59: $1 \rightarrow 2$
2044		60: $0.098-0.102 \rightarrow 0.125$



2045

2046 26) 60: 0.125 \rightarrow 0.236-0.267

2047

2048 27) 48: 0 \rightarrow 1

2049

2050 28) 35: 0 \rightarrow 1

2051 38: 0.457-0.751 \rightarrow 0.325-0.442

2052 89: 0.507 \rightarrow 0.550-0.582

2053

2054 29) 22: 3 \rightarrow 2

2055 75: 0 \rightarrow 1

2056

2057 30) 39: 1 \rightarrow 0

2058 53: 1 \rightarrow 2

2059

2060 31) 3: 1 \rightarrow 0

2061 4: 1 \rightarrow 0

2062

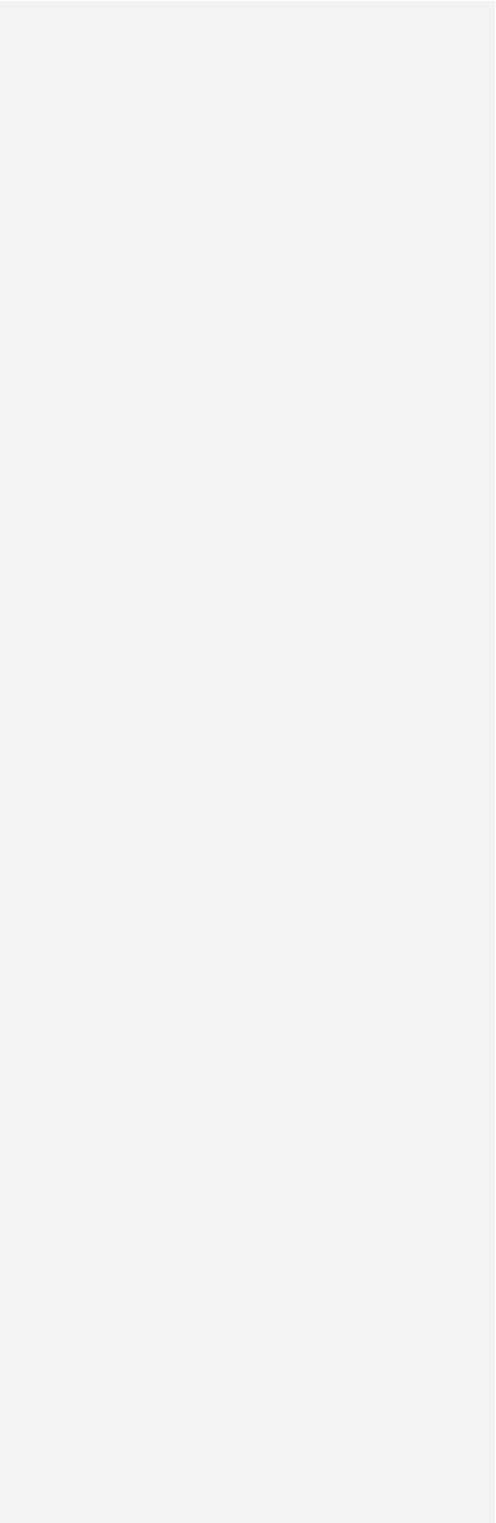
2063 32) 39: 1 \rightarrow 2

2064 90: 0 \rightarrow 1

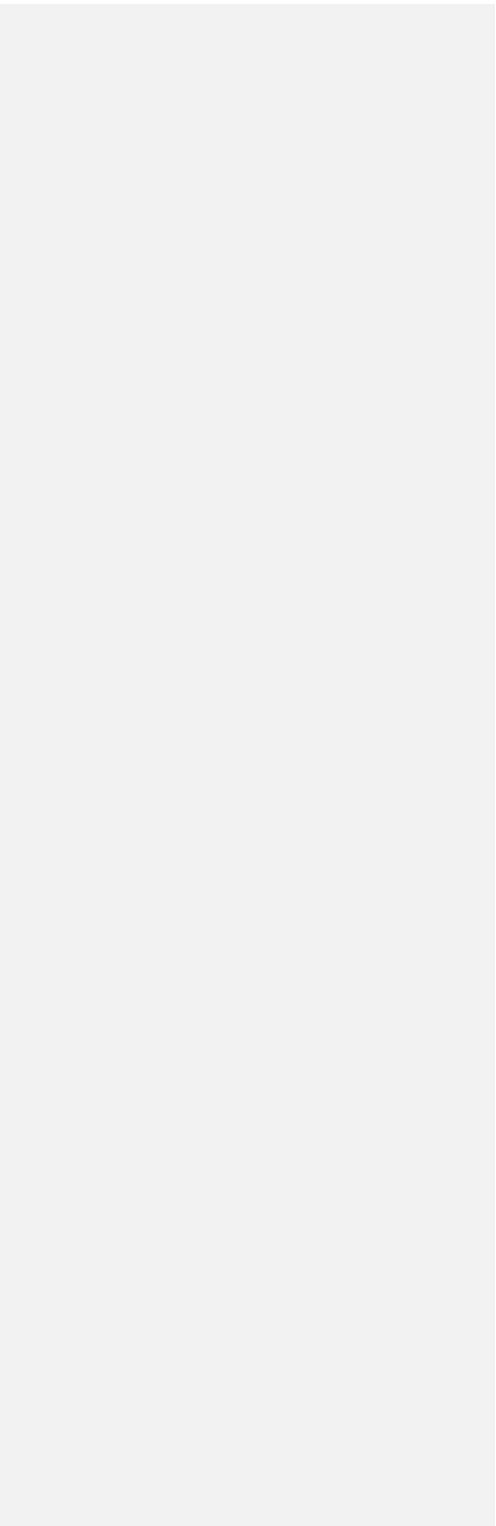
2065

2066 33) 43: 0.070 \rightarrow 0.034-0.043

2067 48: 1 \rightarrow 0



2068		59: 2→3
2069		86: 0→1
2070		
2071	34)	25: 0.439-0.514 → 0.113
2072		34: 1→2
2073		53: 1→0
2074		54: 0.180-0.197 → 0.039-0.095
2075		89: 0.550-0.620 → 0.710
2076		
2077	35)	84: 0→1
2078		87: 0.338-0.401 → 0.574-0.577
2079		
2080	36)	7: 1→2
2081		53: 1→2
2082		57: 2→3
2083		
2084	37)	57: 2→1
2085		61: 2→1
2086		85: 1→0
2087		
2088	38)	2: 1→2
2089		20: 0→1
2090		



2091 39) 19: 0→1

2092 88: 0→1

2093

2094 **Discrete + GM tree (excluding landmark ‘state changes’)**

2095 1) [39, 40, 46]: LANDMARK

2096 [50, 54, 55]: LANDMARK

2097 81: LANDMARK

2098 89: LANDMARK

2099 91: LANDMARK

2100

2101 2) 13: 0→1

2102 22: 0→1

2103 [39, 40, 46]: LANDMARK

2104 [50, 54, 55]: LANDMARK

2105 81: LANDMARK

2106 89: LANDMARK

2107 91: LANDMARK

2108

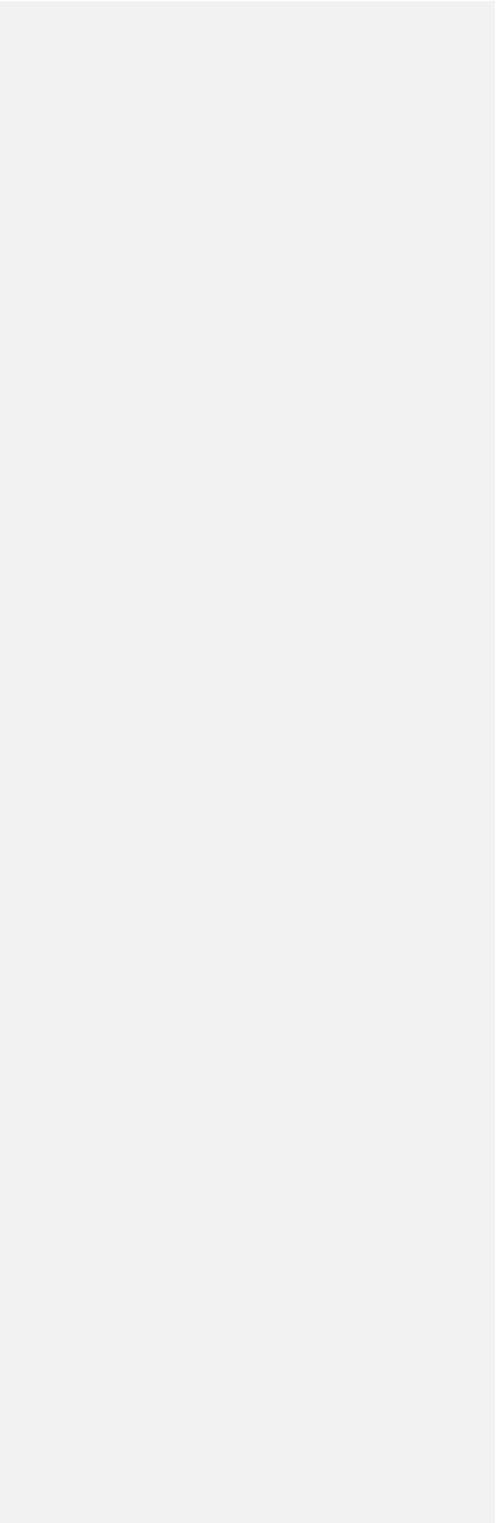
2109 3) 36: 0→1

2110 [39, 40, 46]: LANDMARK

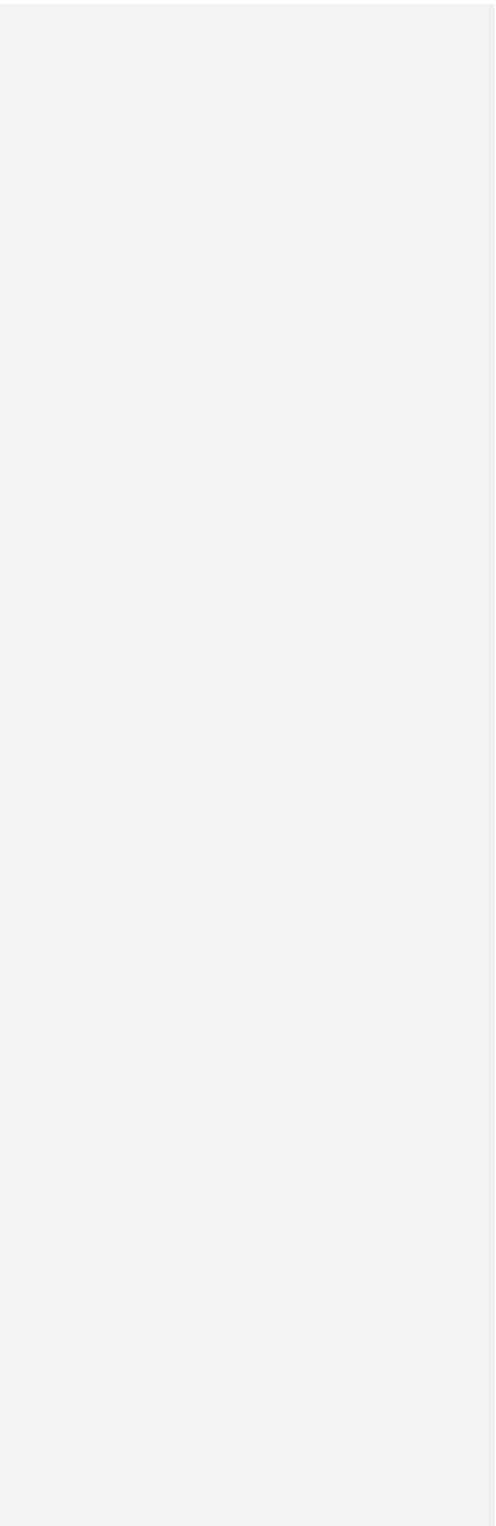
2111 [50, 54, 55]: LANDMARK

2112 69: 0→1

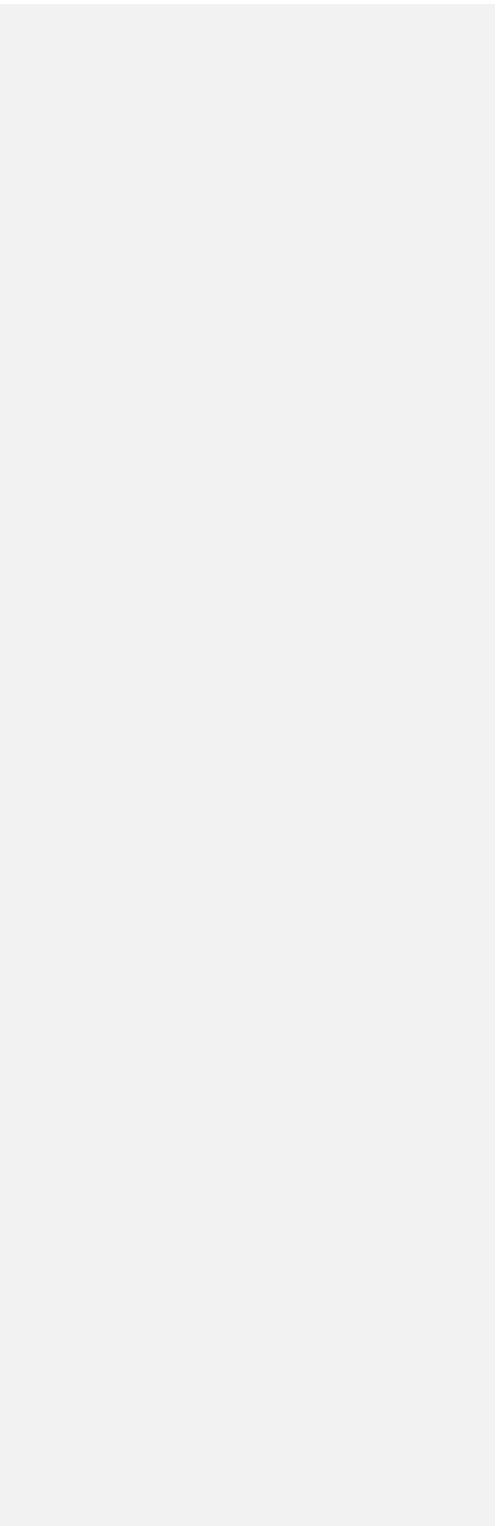
2113 81: LANDMARK



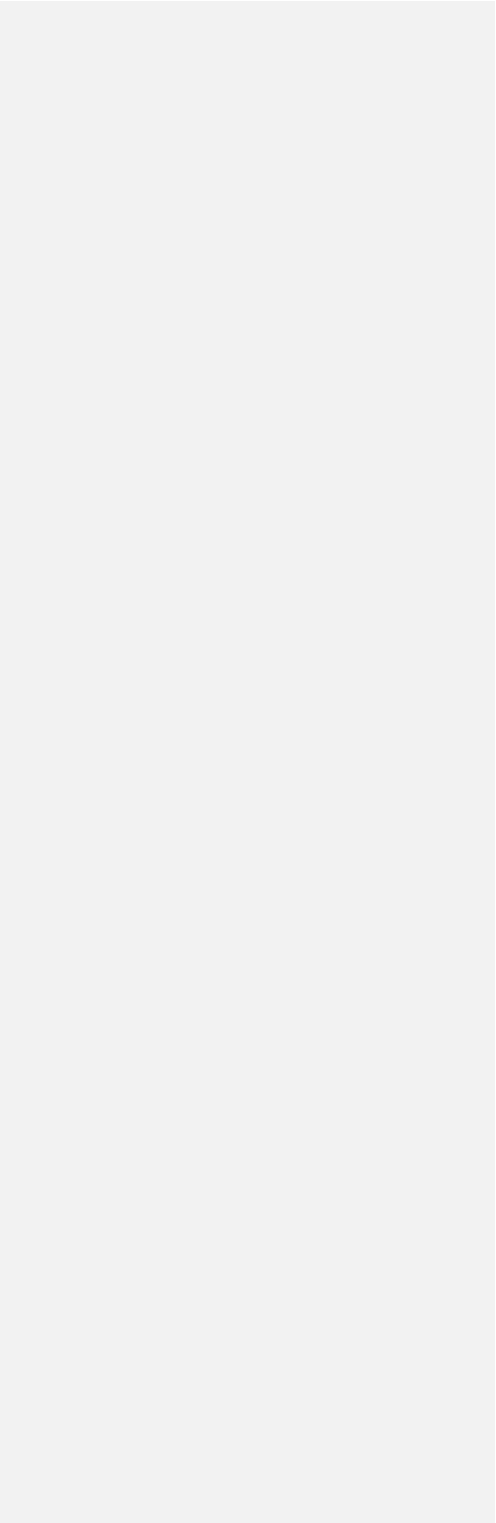
2114		89: LANDMARK
2115		91: LANDMARK
2116		
2117	4)	23: $0 \rightarrow 1$
2118		26: $0 \rightarrow 1$
2119		[39, 40, 46]: LANDMARK
2120		[50, 54, 55]: LANDMARK
2121		81: LANDMARK
2122		89: LANDMARK
2123		91: LANDMARK
2124		
2125	5)	[39, 40, 46]: LANDMARK
2126		[50, 54, 55]: LANDMARK
2127		81: LANDMARK
2128		82: $0 \rightarrow 1$
2129		89: LANDMARK
2130		91: LANDMARK
2131		
2132	6)	1: $0 \rightarrow 1$
2133		22: $1 \rightarrow 2$
2134		[39, 40, 46]: LANDMARK
2135		[50, 54, 55]: LANDMARK
2136		81: LANDMARK



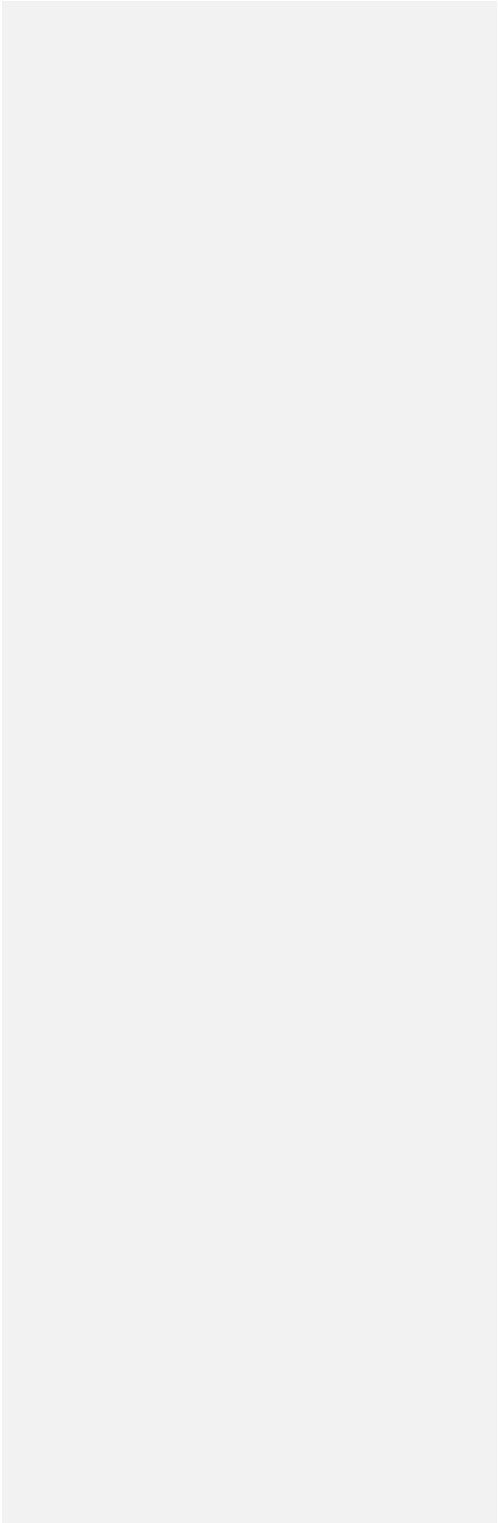
2137		83: $1 \rightarrow 0$
2138		89: LANDMARK
2139		91: LANDMARK
2140		
2141	7)	11: $0 \rightarrow 1,2$
2142		34: $0 \rightarrow 1$
2143		42: $1 \rightarrow 0$
2144		[39, 40, 46]: LANDMARK
2145		[50, 54, 55]: LANDMARK
2146		81: LANDMARK
2147		89: LANDMARK
2148		91: LANDMARK
2149		
2150	8)	[39, 40, 46]: LANDMARK
2151		[50, 54, 55]: LANDMARK
2152		81: LANDMARK
2153		89: LANDMARK
2154		91: LANDMARK
2155		
2156	9)	9: $0 \rightarrow 1$
2157		14: $1 \rightarrow 2$
2158		[39, 40, 46]: LANDMARK
2159		[50, 54, 55]: LANDMARK



2160		80: 0→1
2161		81: LANDMARK
2162		89: LANDMARK
2163		91: LANDMARK
2164		
2165	10)	19: 0→1
2166		22: 2→1
2167		[39, 40, 46]: LANDMARK
2168		81: LANDMARK
2169		89: LANDMARK
2170		91: LANDMARK
2171		92: 0→1
2172		
2173	11)	[39, 40, 46]: LANDMARK
2174		56: 0→1
2175		58: 0→1
2176		81: LANDMARK
2177		89: LANDMARK
2178		91: LANDMARK
2179		
2180	12)	42: 0→1
2181		[39, 40, 46]: LANDMARK
2182		51: 0→1



2183		81: LANDMARK
2184		89: LANDMARK
2185		91: LANDMARK
2186		
2187	13)	12: $0 \rightarrow 1$
2188		17: $0 \rightarrow 1$
2189		66: $0 \rightarrow 1$
2190		70: $0 \rightarrow 1$
2191		81: LANDMARK
2192		
2193	14)	69: $2 \rightarrow 1$
2194		81: LANDMARK
2195		
2196	15)	5: $0 \rightarrow 1$
2197		16: $1 \rightarrow 0$
2198		25: $0 \rightarrow 1$
2199		[39, 40, 46]: LANDMARK
2200		49: $0 \rightarrow 1$
2201		[50, 54, 55]: LANDMARK
2202		57: $0 \rightarrow 1$
2203		59: $0 \rightarrow 1$
2204		81: LANDMARK
2205		89: LANDMARK



220691: LANDMARK

2207

220816)41: 0→1

2209[39, 40, 46]: LANDMARK

2210[50, 54, 55]: LANDMARK

221181: LANDMARK

221289: LANDMARK

221391: LANDMARK

2214

221517)[39, 40, 46]: LANDMARK

221648: 0→1

2217[50, 54, 55]: LANDMARK

221881: LANDMARK

221989: LANDMARK

222090: 0→1

222191: LANDMARK

2222

222318)[39, 40, 46]: LANDMARK

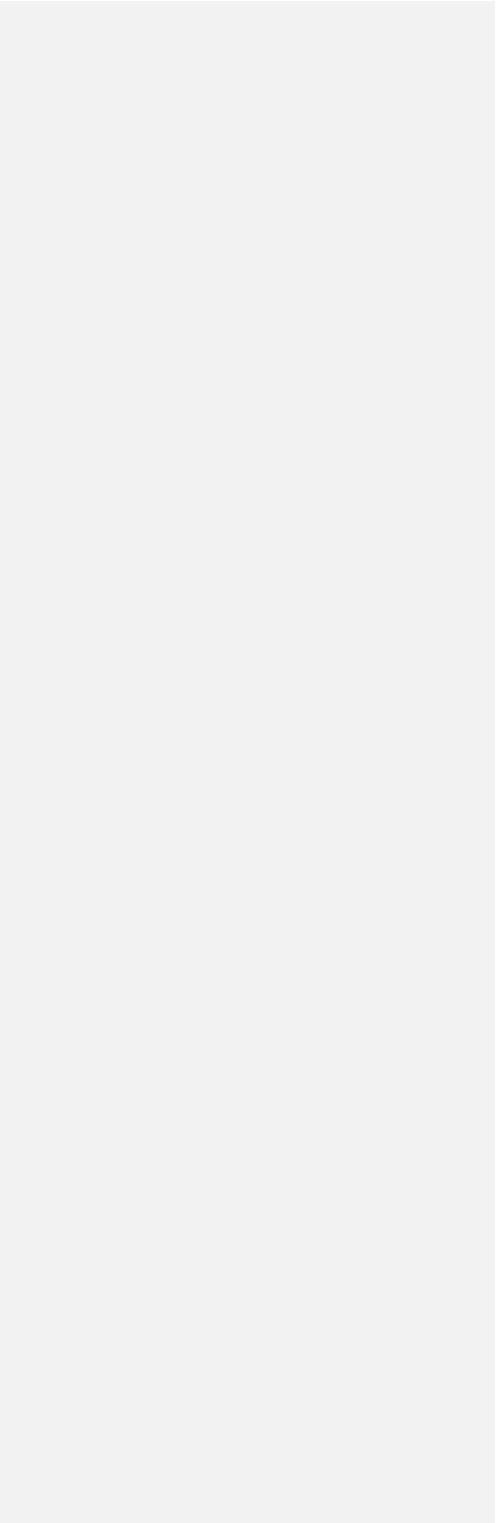
2224[50, 54, 55]: LANDMARK

222581: LANDMARK

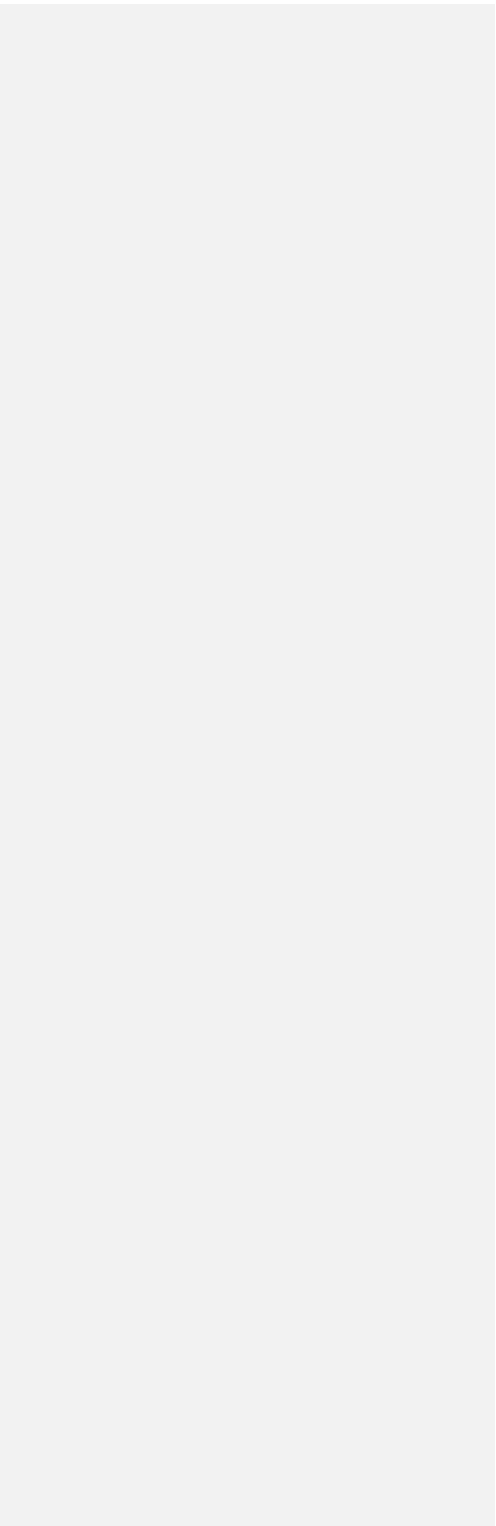
222689: LANDMARK

222791: LANDMARK

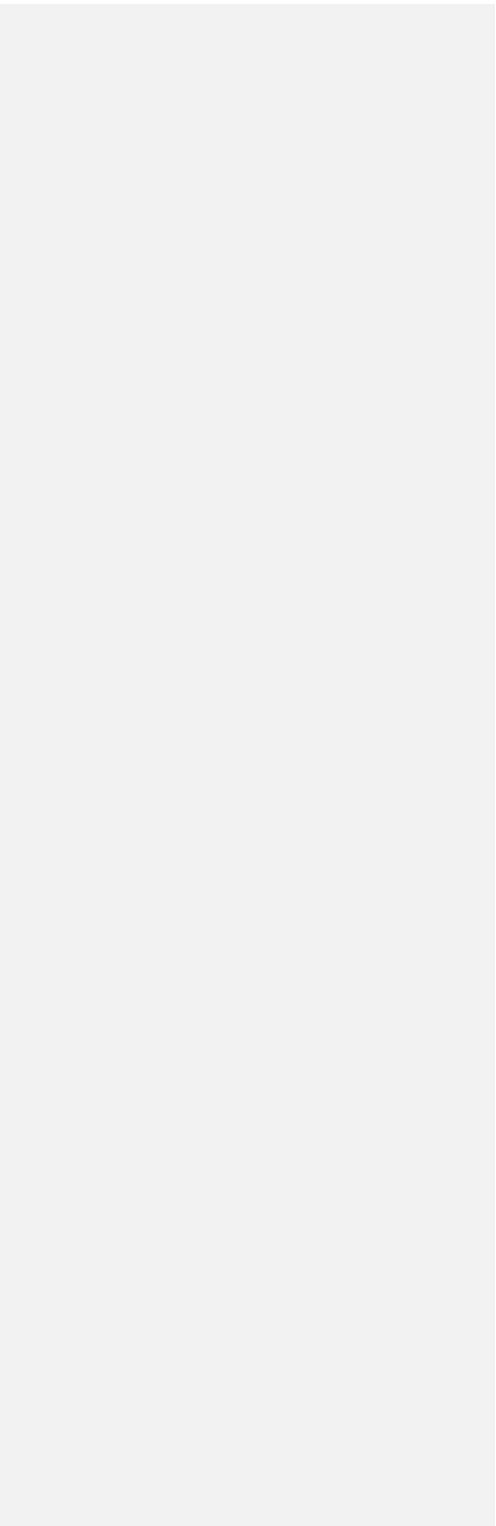
2228



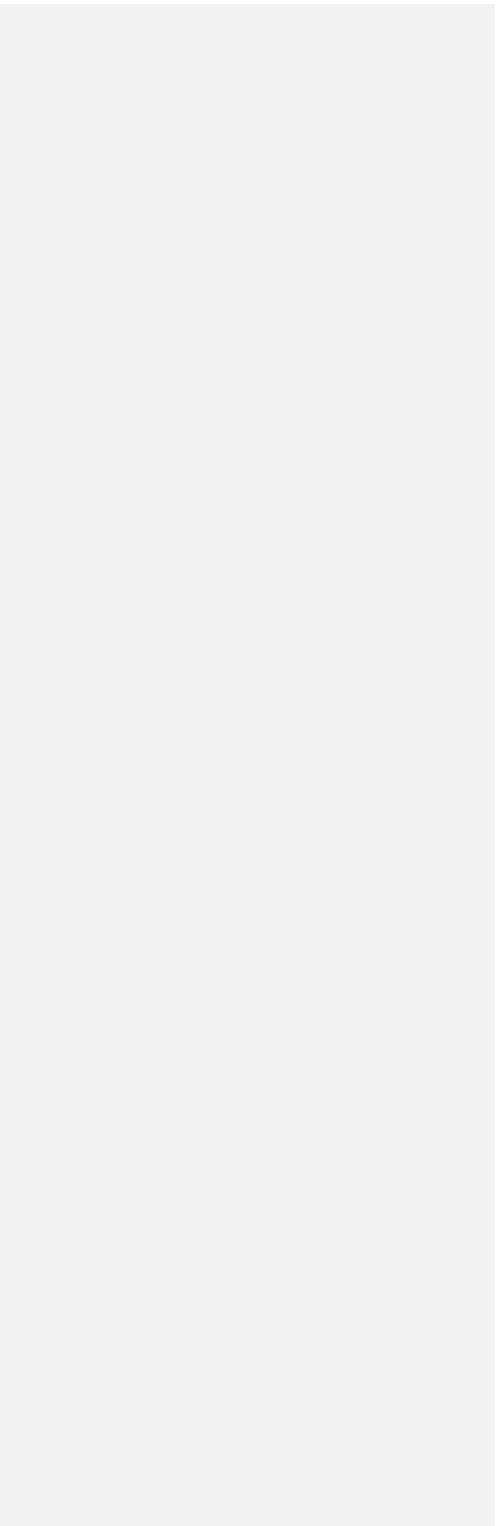
2229	19)	3: 0→1
2230		33: 0→2
2231		[39, 40, 46]: LANDMARK
2232		[50, 54, 55]: LANDMARK
2233		81: LANDMARK
2234		89: LANDMARK
2235		91: LANDMARK
2236		
2237	20)	29: 1→0
2238		33: 0→1
2239		[39, 40, 46]: LANDMARK
2240		[50, 54, 55]: LANDMARK
2241		81: LANDMARK
2242		89: LANDMARK
2243		91: LANDMARK
2244		
2245	21)	38: 2→3
2246		[39, 40, 46]: LANDMARK
2247		[50, 54, 55]: LANDMARK
2248		60: 0→1
2249		67: 0→2
2250		81: LANDMARK
2251		89: LANDMARK



2252		91: LANDMARK
2253		
2254	22)	[39, 40, 46]: LANDMARK
2255		49: 1→2
2256		[50, 54, 55]: LANDMARK
2257		81: LANDMARK
2258		89: LANDMARK
2259		91: LANDMARK
2260		
2261	23)	9: 1→0
2262		33: 1→2
2263		[39, 40, 46]: LANDMARK
2264		53: 2→1
2265		[50, 54, 55]: LANDMARK
2266		75: 0→1
2267		81: LANDMARK
2268		89: LANDMARK
2269		91: LANDMARK
2270		
2271	24)	[39, 40, 46]: LANDMARK
2272		[50, 54, 55]: LANDMARK
2273		57: 1→2
2274		81: LANDMARK



2275		89: LANDMARK
2276		90: $0 \rightarrow 1$
2277		91: LANDMARK
2278		
2279	25)	33: $2 \rightarrow 0$
2280		[39, 40, 46]: LANDMARK
2281		53: $1 \rightarrow 0$
2282		[50, 54, 55]: LANDMARK
2283		81: LANDMARK
2284		89: LANDMARK
2285		91: LANDMARK
2286		
2287	26)	38: $3 \rightarrow 2$
2288		43: $2 \rightarrow 0$
2289		[39, 40, 46]: LANDMARK
2290		[50, 54, 55]: LANDMARK
2291		64: $0 \rightarrow 1$
2292		81: LANDMARK
2293		87: $0 \rightarrow 1, 2$
2294		89: LANDMARK
2295		91: LANDMARK
2296		
2297	27)	[39, 40, 46]: LANDMARK



2298

[50, 54, 55]: LANDMARK

2299

59: 1, 2→3

2300

81: LANDMARK

2301

84: 0→1

2302

85: 1→0

2303

89: LANDMARK

2304

91: LANDMARK

2305

2306

28) 2: 1→2

2307

[39, 40, 46]: LANDMARK

2308

[50, 54, 55]: LANDMARK

2309

81: LANDMARK

2310

89: LANDMARK

2311

91: LANDMARK

2312

2313

29) 19: 0→1

2314

[39, 40, 46]: LANDMARK

2315

[50, 54, 55]: LANDMARK

2316

81: LANDMARK

2317

88: 0→1

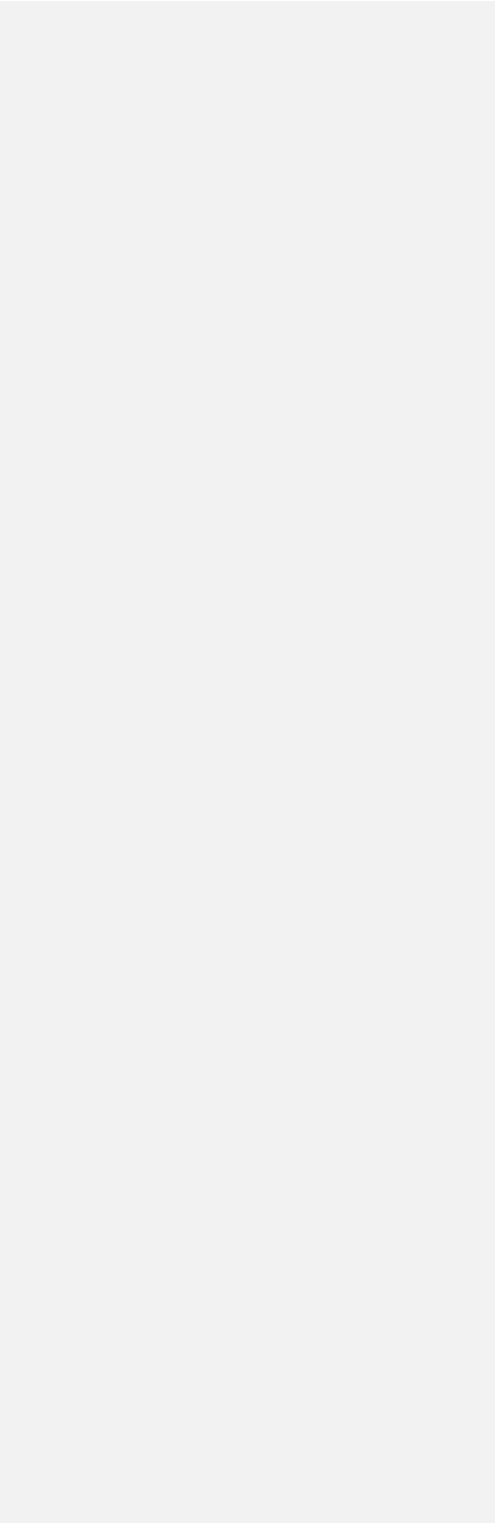
2318

89: LANDMARK

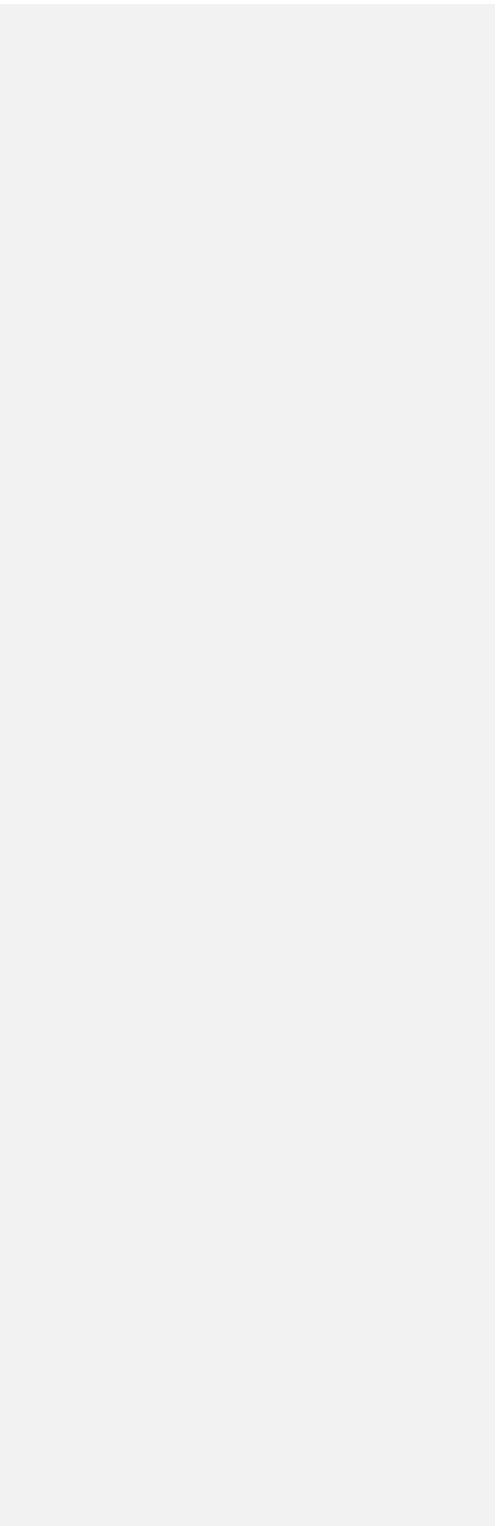
2319

91: LANDMARK

2320



2321	30)	29: 0→1
2322		[39, 40, 46]: LANDMARK
2323		[50, 54, 55]: LANDMARK
2324		65: 0→1
2325		81: LANDMARK
2326		89: LANDMARK
2327		91: LANDMARK
2328		
2329	31)	3: 0→1
2330		4: 0→1
2331		7: 1→4
2332		[39, 40, 46]: LANDMARK
2333		47: 0→1
2334		[50, 54, 55]: LANDMARK
2335		81: LANDMARK
2336		89: LANDMARK
2337		91: LANDMARK
2338		
2339	32)	[39, 40, 46]: LANDMARK
2340		48: 0→1
2341		[50, 54, 55]: LANDMARK
2342		81: LANDMARK
2343		89: LANDMARK



2344 91: LANDMARK

2345

2346 33) 19: $0 \rightarrow 1$

2347 [39, 40, 46]: LANDMARK

2348 [50, 54, 55]: LANDMARK

2349 81: LANDMARK

2350 89: LANDMARK

2351 91: LANDMARK

2352

2353 34) 30: $1 \rightarrow 0$

2354 [39, 40, 46]: LANDMARK

2355 [50, 54, 55]: LANDMARK

2356 60: $1 \rightarrow 2$

2357 81: LANDMARK

2358 89: LANDMARK

2359 91: LANDMARK

2360

2361 35) 3: $1 \rightarrow 0$

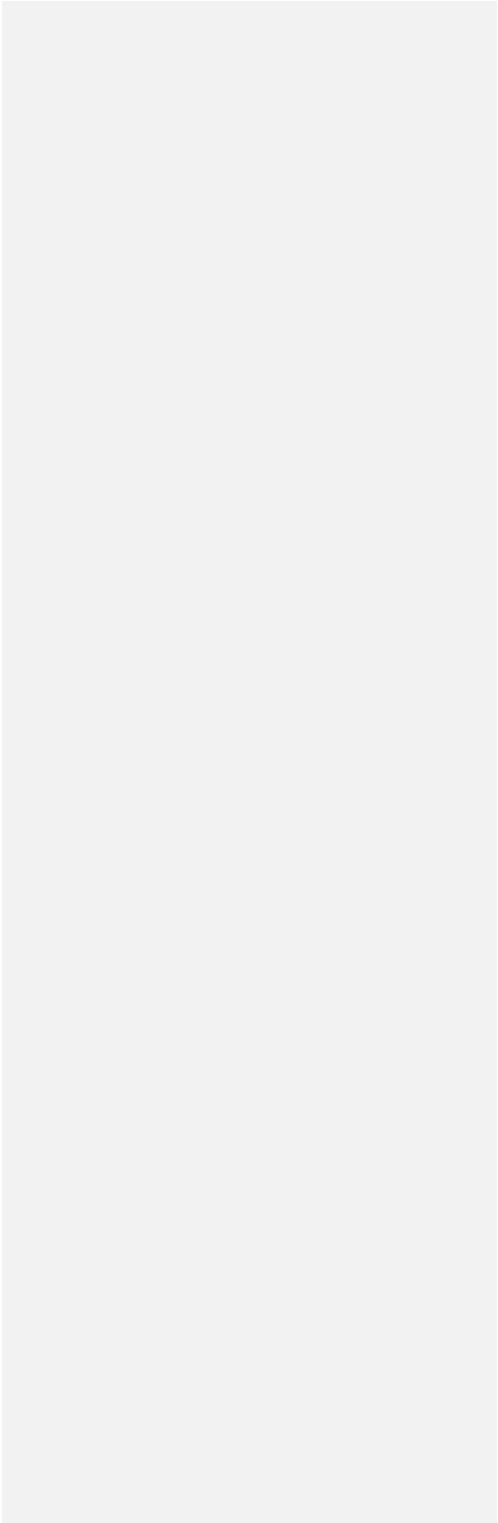
2362 4: $1 \rightarrow 0$

2363 [39, 40, 46]: LANDMARK

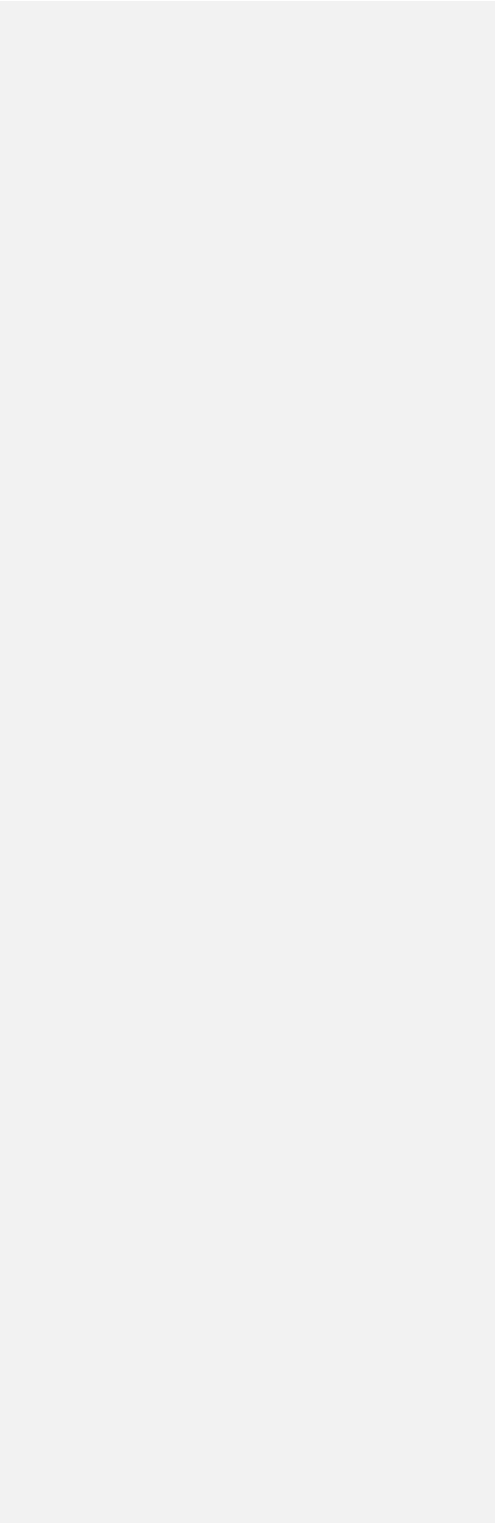
2364 [50, 54, 55]: LANDMARK

2365 81: LANDMARK

2366 89: LANDMARK



2367		90: $0 \rightarrow 1$
2368		91: LANDMARK
2369		
2370	36)	7: $4 \rightarrow 1$
2371		8: $2 \rightarrow 1$
2372		[39, 40, 46]: LANDMARK
2373		[50, 54, 55]: LANDMARK
2374		81: LANDMARK
2375		89: LANDMARK
2376		91: LANDMARK
2377		
2378	37)	7: $4 \rightarrow 2$
2379		22: $2 \rightarrow 3$
2380		[39, 40, 46]: LANDMARK
2381		[50, 54, 55]: LANDMARK
2382		81: LANDMARK
2383		89: LANDMARK
2384		91: LANDMARK
2385		
2386	38)	11: $1 \rightarrow 0$
2387		[39, 40, 46]: LANDMARK
2388		[50, 54, 55]: LANDMARK
2389		81: LANDMARK



239089: LANDMARK

239191: LANDMARK

2392

239339) [39, 40, 46]: LANDMARK

239448: 1→0

239553: 1→0

2396[50, 54, 55]: LANDMARK

239781: LANDMARK

239889: LANDMARK

239991: LANDMARK

2400

240140) 19: 1→0

2402[39, 40, 46]: LANDMARK

2403[50, 54, 55]: LANDMARK

240457: 2→3

240559: 2→3

240663: 1→0

240781: LANDMARK

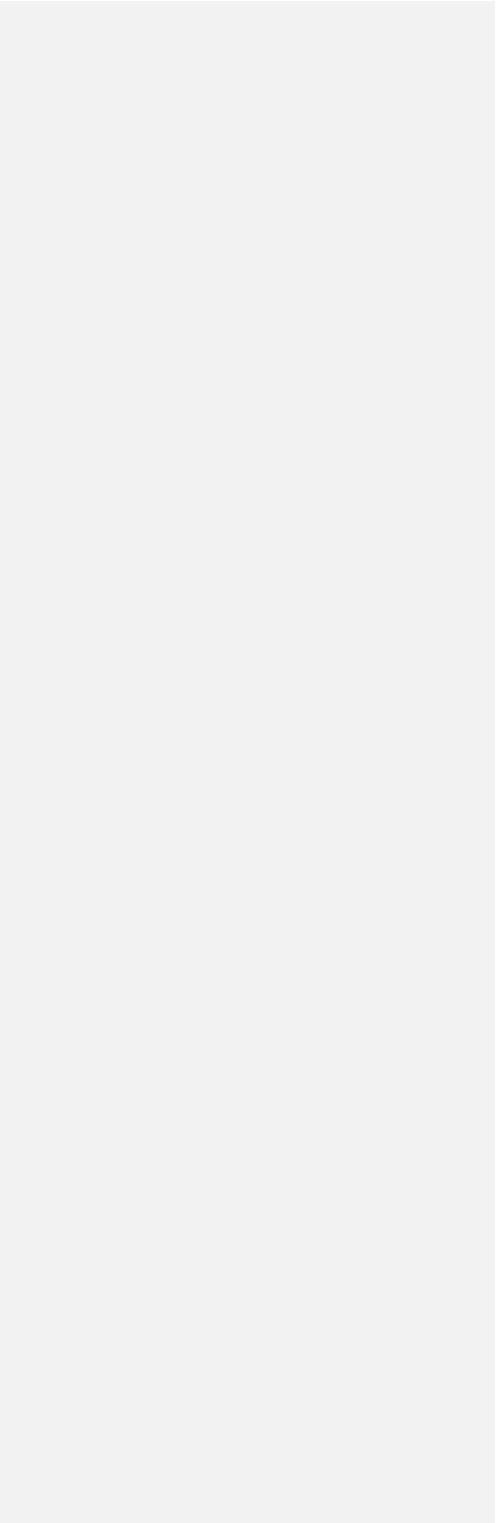
240889: LANDMARK

240991: LANDMARK

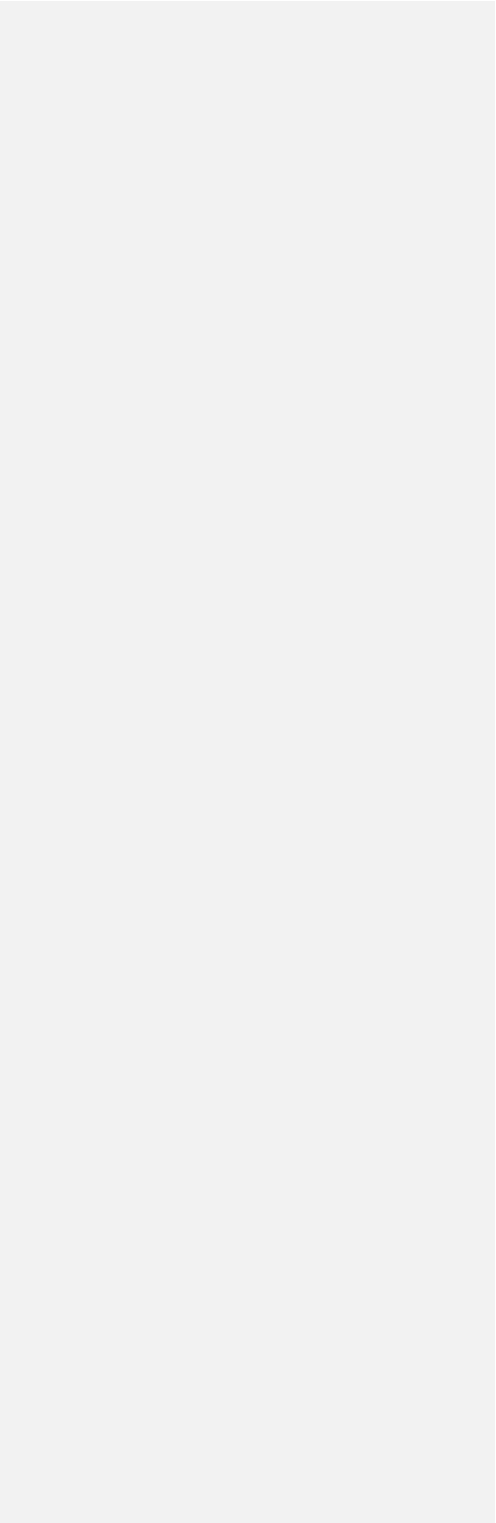
2410

241141) [39, 40, 46]: LANDMARK

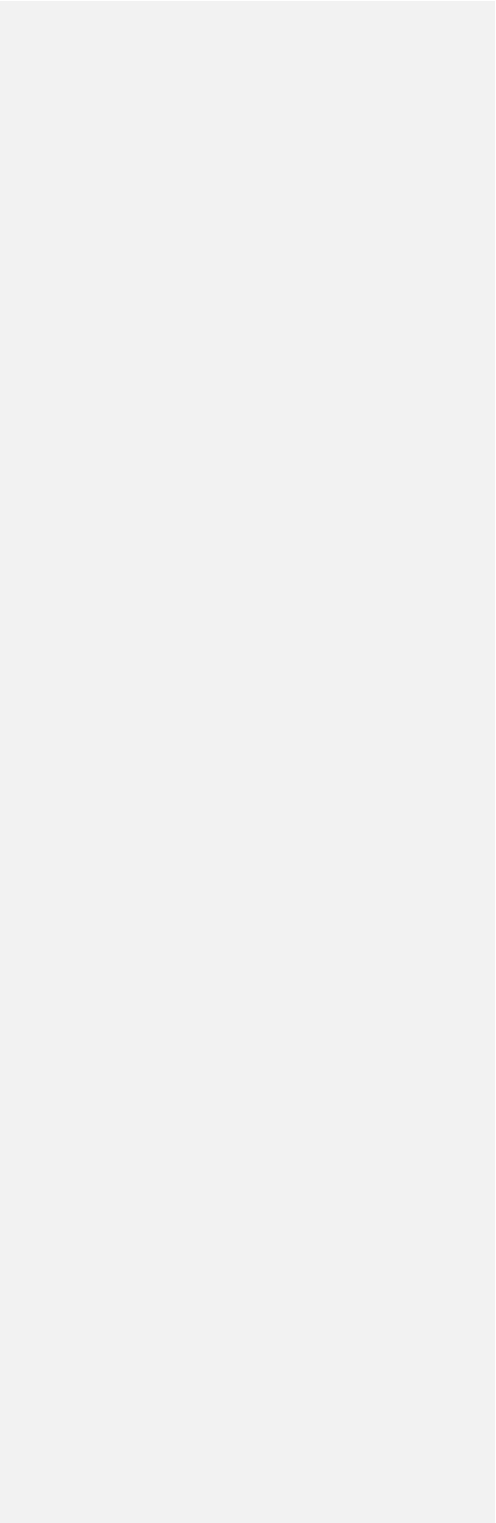
2412[50, 54, 55]: LANDMARK



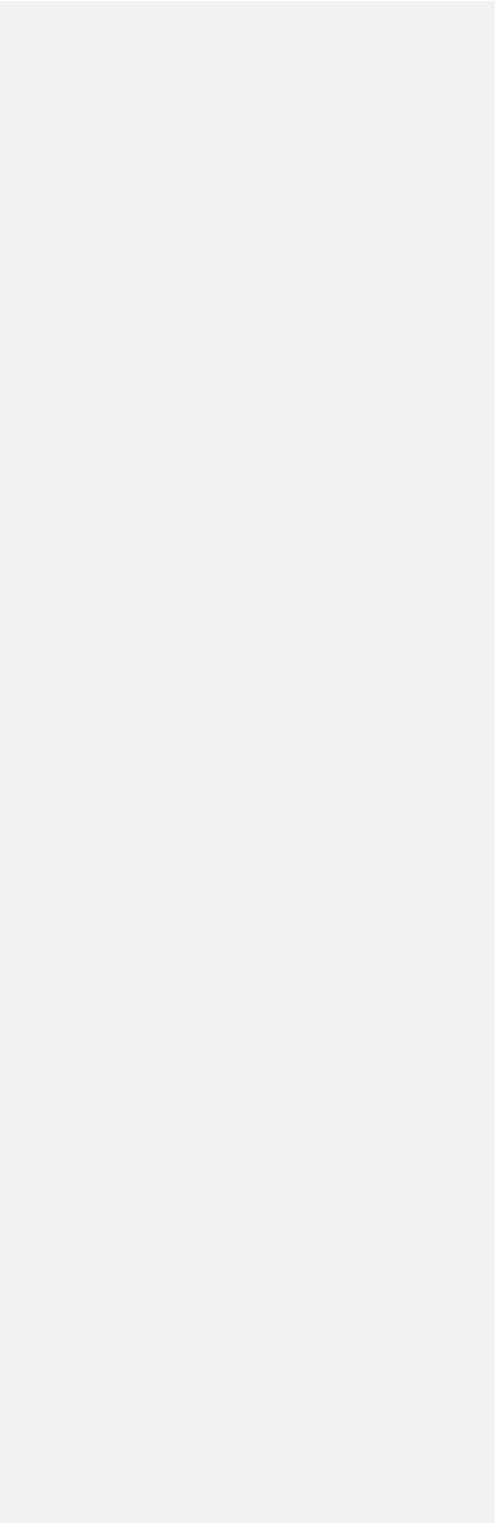
2413		81: LANDMARK
2414		89: LANDMARK
2415		91: LANDMARK
2416		
2417		Discrete + Continuous + GM tree (excluding landmark ‘state changes’)
2418	1)	[39, 40, 46]: LANDMARK
2419		[50, 54, 55]: LANDMARK
2420		81: LANDMARK
2421		89: LANDMARK
2422		91: LANDMARK
2423		
2424	2)	13: 0→1
2425		22: 0→1
2426		[39, 40, 46]: LANDMARK
2427		[50, 54, 55]: LANDMARK
2428		81: LANDMARK
2429		89: LANDMARK
2430		91: LANDMARK
2431		
2432	3)	36: 0→1
2433		[39, 40, 46]: LANDMARK
2434		[50, 54, 55]: LANDMARK
2435		69: 0→1



2436		81: LANDMARK
2437		89: LANDMARK
2438		91: LANDMARK
2439		
2440	4)	23: $0 \rightarrow 1$
2441		26: $0 \rightarrow 1$
2442		[39, 40, 46]: LANDMARK
2443		[50, 54, 55]: LANDMARK
2444		81: LANDMARK
2445		89: LANDMARK
2446		91: LANDMARK
2447		
2448	5)	25: $0.452\text{-}0.470 \rightarrow 0.409\text{-}0.446$
2449		[39, 40, 46]: LANDMARK
2450		[50, 54, 55]: LANDMARK
2451		81: LANDMARK
2452		82: $0 \rightarrow 1$
2453		89: LANDMARK
2454		91: LANDMARK
2455		
2456	6)	1: $0 \rightarrow 1$
2457		11: $0.459\text{-}0.484 \rightarrow 0.490$
2458		22: $1 \rightarrow 2$



2459		25: 0.452-0.470 \rightarrow 0.514
2460		[39, 40, 46]: LANDMARK
2461		[50, 54, 55]: LANDMARK
2462		81: LANDMARK
2463		83: 1 \rightarrow 0
2464		89: LANDMARK
2465		91: LANDMARK
2466		
2467	7)	8: 0.178-0.219 \rightarrow 0.253-0.616
2468		11: 0.490 \rightarrow 0.686-0.800
2469		34: 0 \rightarrow 1
2470		42: 1 \rightarrow 0
2471		43: 0.126-0.150 \rightarrow 0.104-0.106
2472		[39, 40, 46]: LANDMARK
2473		[50, 54, 55]: LANDMARK
2474		81: LANDMARK
2475		89: LANDMARK
2476		91: LANDMARK
2477		
2478	8)	[39, 40, 46]: LANDMARK
2479		[50, 54, 55]: LANDMARK
2480		81: LANDMARK
2481		89: LANDMARK



2482 91: LANDMARK

2483

2484 9) 9: 0→1

2485 14: 1→2

2486 [39, 40, 46]: LANDMARK

2487 [50, 54, 55]: LANDMARK

2488 80: 0→1

2489 81: LANDMARK

2490 89: LANDMARK

2491 91: LANDMARK

2492

2493 10) 19: 0→1

2494 22: 2→1

2495 25: 0.514 → 0.503

2496 [39, 40, 46]: LANDMARK

2497 81: LANDMARK

2498 89: LANDMARK

2499 91: LANDMARK

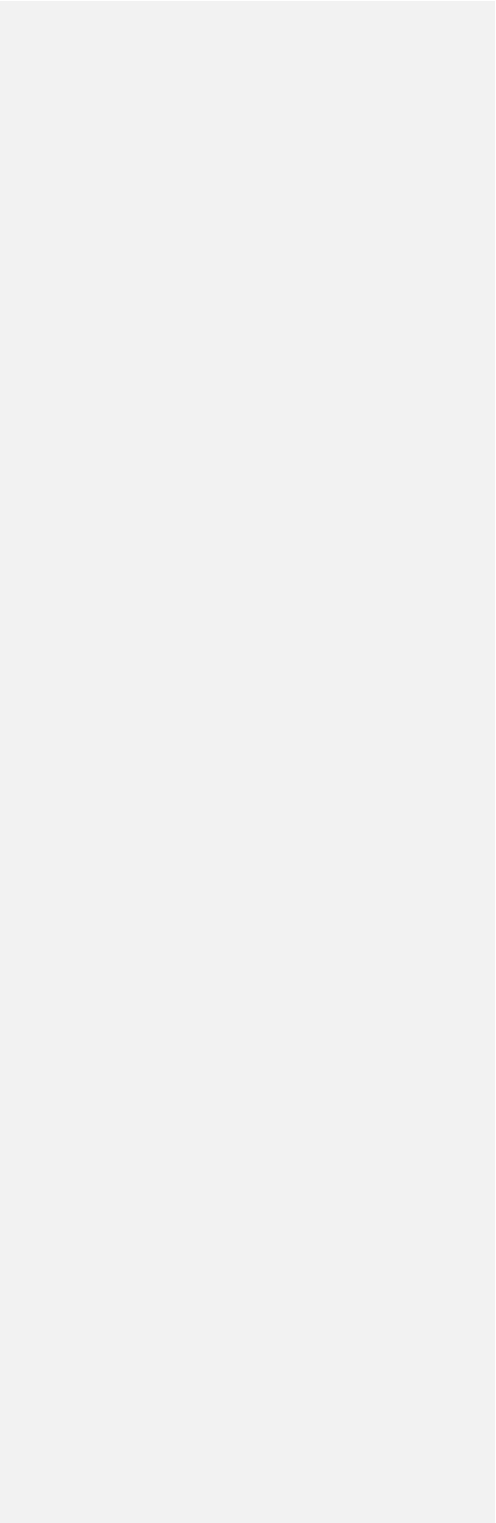
2500 92: 0→1

2501

2502 11) [39, 40, 46]: LANDMARK

2503 58: 0→1

2504 81: LANDMARK



2505 87: 0.106-0.132 → 0.103

2506 89: LANDMARK

2507 91: LANDMARK

2508

2509 12) 42: 0→1

2510 [39, 40, 46]: LANDMARK

2511 51: 0→1

2512 81: LANDMARK

2513 89: LANDMARK

2514 91: LANDMARK

2515

2516 13) 12: 0→1

2517 17: 0→1

2518 66: 0→1

2519 70: 0→1

2520 81: LANDMARK

2521

2522 14) 69: 2→1

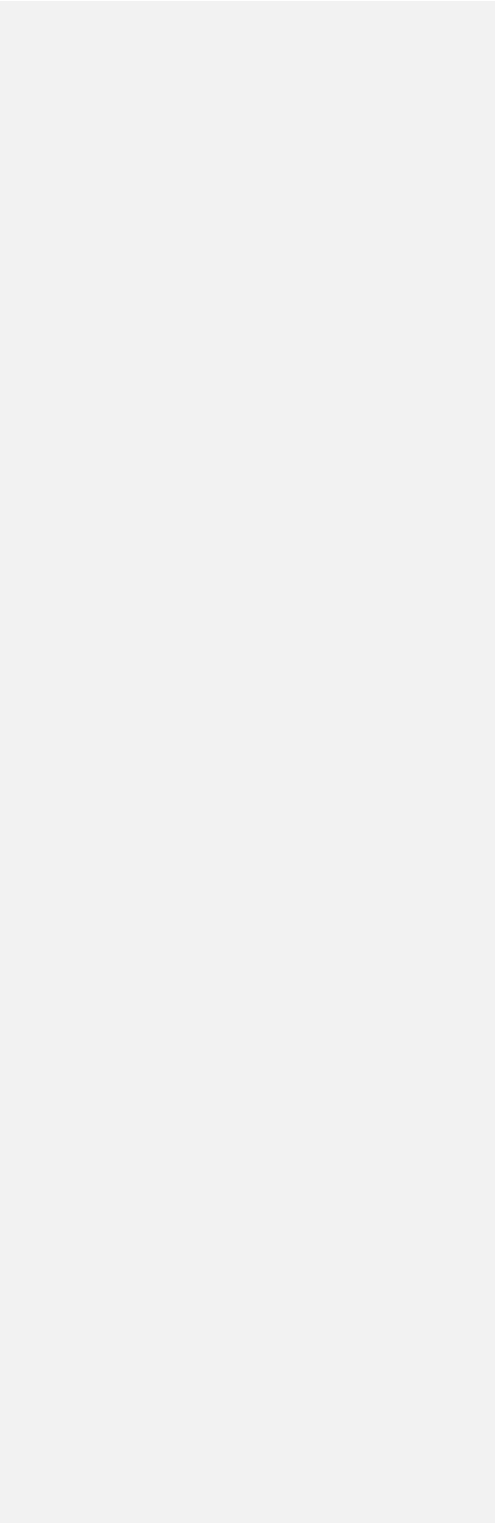
2523 81: LANDMARK

2524

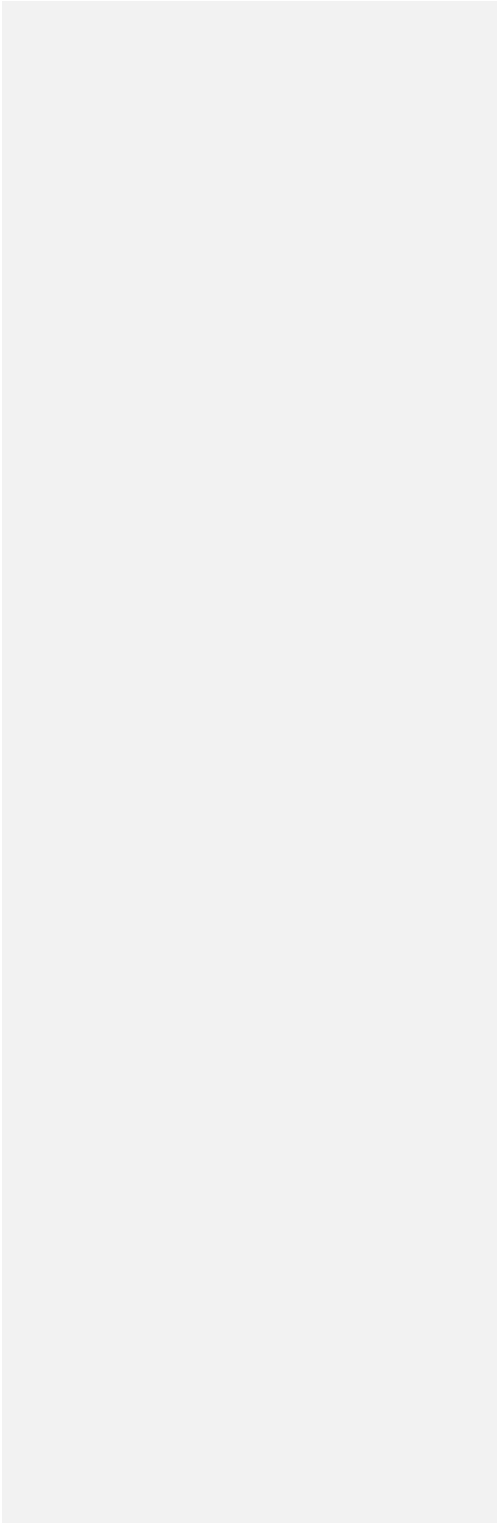
2525 15) 5: 0→1

2526 16: 1→0

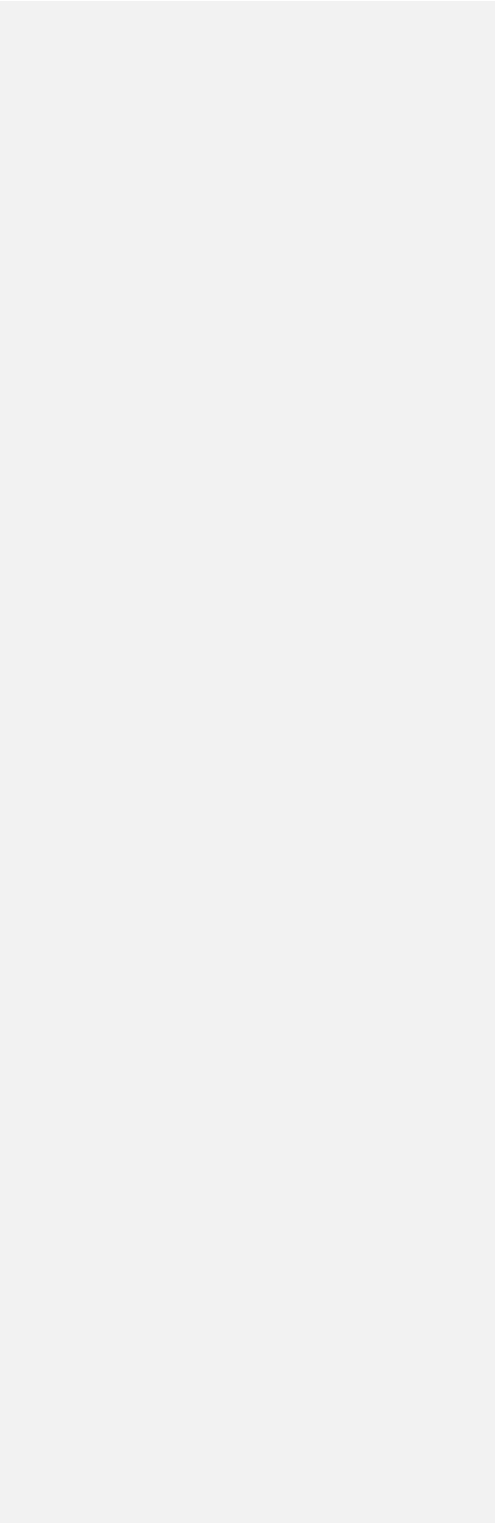
2527 25: 0.514 → 0.684-0.718



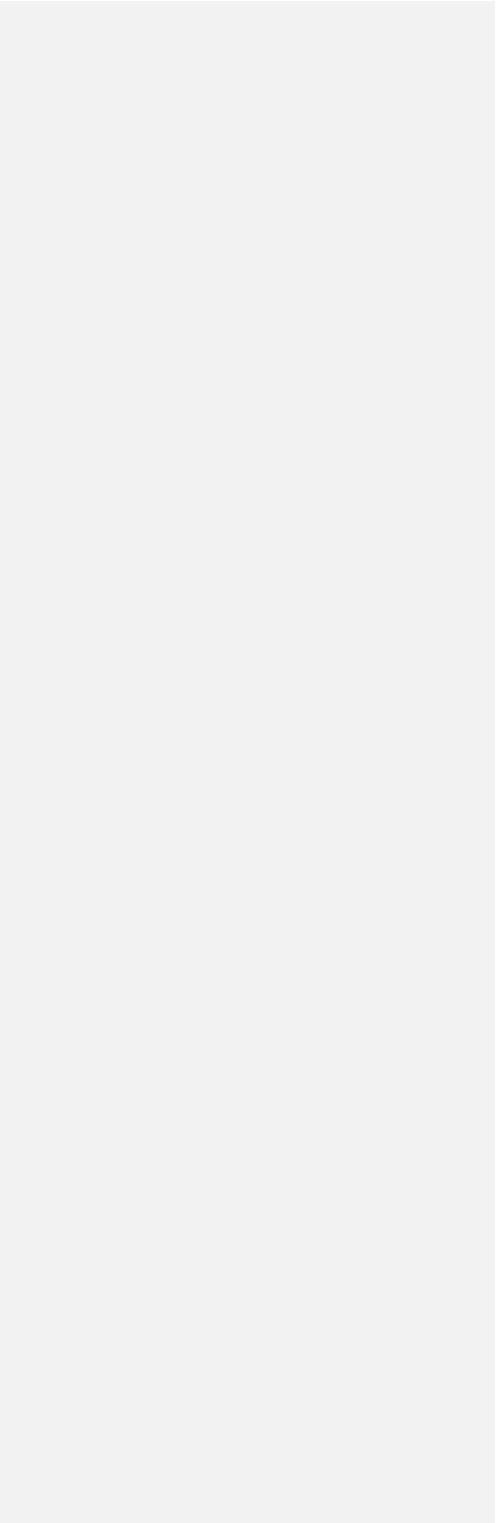
2528		41: $0 \rightarrow 1$
2529		[39, 40, 46]: LANDMARK
2530		[50, 54, 55]: LANDMARK
2531		81: LANDMARK
2532		89: LANDMARK
2533		90: $0 \rightarrow 1$
2534		91: LANDMARK
2535		
2536	16)	[39, 40, 46]: LANDMARK
2537		[50, 54, 55]: LANDMARK
2538		57: $0 \rightarrow 1$
2539		81: LANDMARK
2540		89: LANDMARK
2541		91: LANDMARK
2542		
2543	17)	10: $0 \rightarrow 1$
2544		[39, 40, 46]: LANDMARK
2545		[50, 54, 55]: LANDMARK
2546		79: $0 \rightarrow 1$
2547		81: LANDMARK
2548		87: $0.117\text{-}0.132 \rightarrow 0.145$
2549		89: LANDMARK
2550		91: LANDMARK



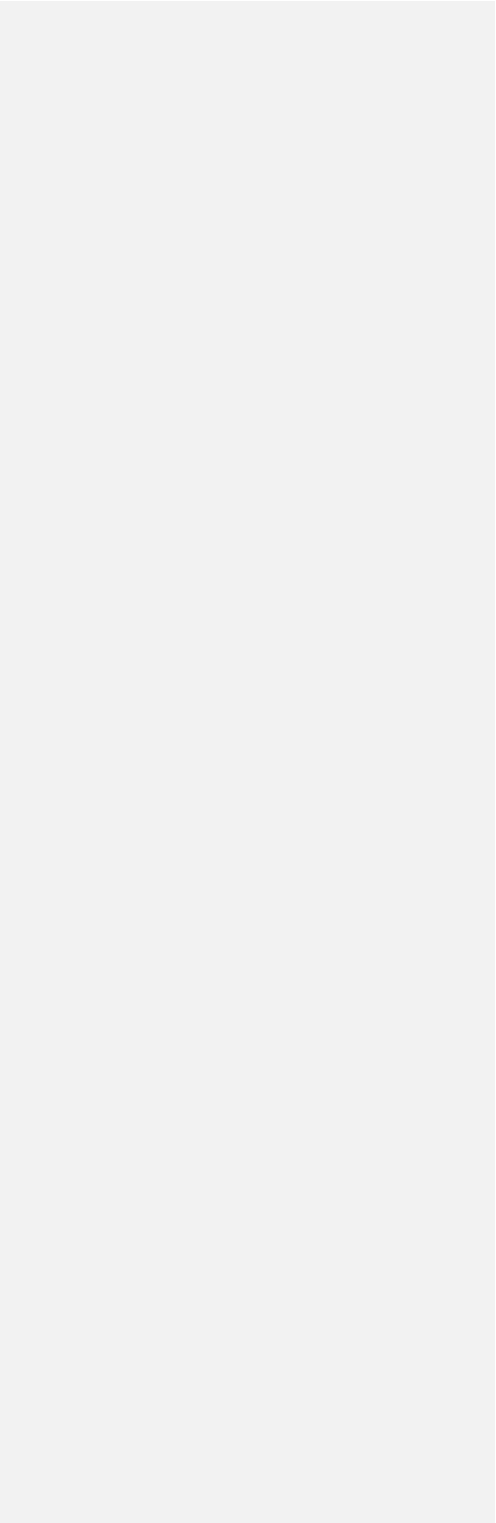
2551		
2552	18)	11:0.686-0.690 \rightarrow 0.729
2553		43: 0.104-0.106 \rightarrow 0.103
2554		[39, 40, 46]: LANDMARK
2555		[50, 54, 55]: LANDMARK
2556		81: LANDMARK
2557		89: LANDMARK
2558		91: LANDMARK
2559		
2560	19)	[39, 40, 46]: LANDMARK
2561		48: 0 \rightarrow 1
2562		[50, 54, 55]: LANDMARK
2563		81: LANDMARK
2564		89: LANDMARK
2565		91: LANDMARK
2566		
2567	20)	21: 0 \rightarrow 1
2568		29: 1 \rightarrow 0
2569		[39, 40, 46]: LANDMARK
2570		[50, 54, 55]: LANDMARK
2571		81: LANDMARK
2572		89: LANDMARK
2573		91: LANDMARK



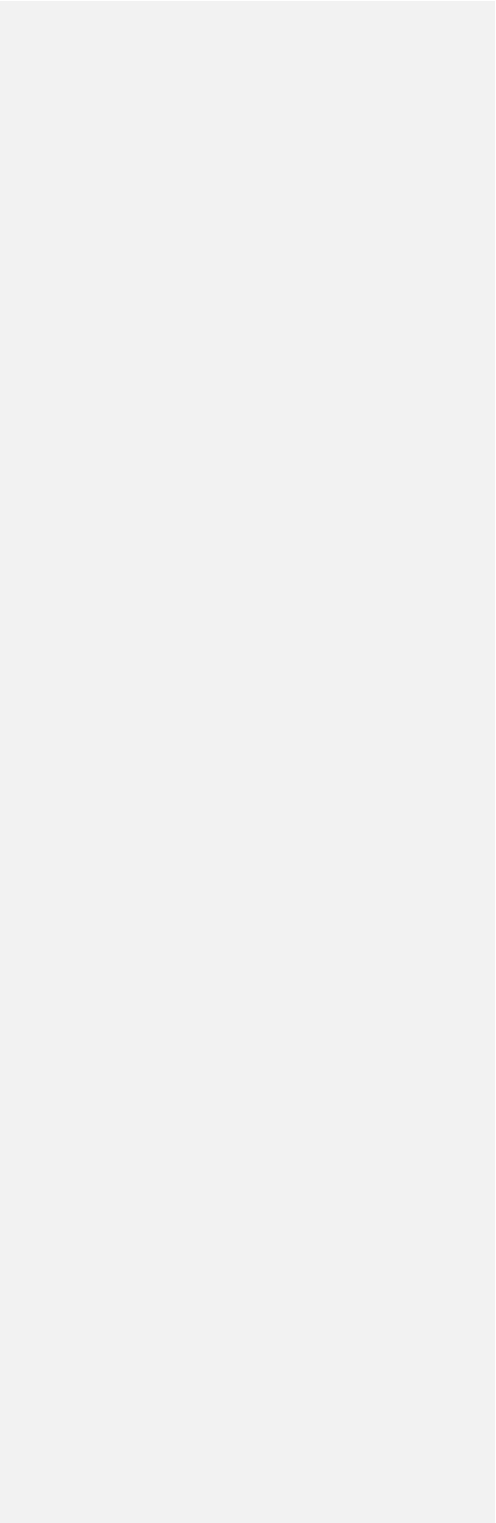
2574		
2575	21)	[39, 40, 46]: LANDMARK
2576		49: 1→2
2577		53: 2→0
2578		[50, 54, 55]: LANDMARK
2579		57: 1→2
2580		67: 0→2
2581		81: LANDMARK
2582		89: LANDMARK
2583		91: LANDMARK
2584		
2585	22)	38: 0.251 → 0.521
2586		[39, 40, 46]: LANDMARK
2587		[50, 54, 55]: LANDMARK
2588		81: LANDMARK
2589		89: LANDMARK
2590		91: LANDMARK
2591		
2592	23)	19: 0→1
2593		20: 1→0
2594		[39, 40, 46]: LANDMARK
2595		[50, 54, 55]: LANDMARK
2596		81: LANDMARK



2597		89: LANDMARK
2598		91: LANDMARK
2599		
2600	24)	33: $0 \rightarrow 1$
2601		38: $0.218 \rightarrow 0.442-0.457$
2602		[39, 40, 46]: LANDMARK
2603		[50, 54, 55]: LANDMARK
2604		67: $0 \rightarrow 2$
2605		81: LANDMARK
2606		89: LANDMARK
2607		90: $1 \rightarrow 0$
2608		91: LANDMARK
2609		
2610	25)	3: $0 \rightarrow 1$
2611		4: $0 \rightarrow 1$
2612		[39, 40, 46]: LANDMARK
2613		49: $1 \rightarrow 2$
2614		[50, 54, 55]: LANDMARK
2615		81: LANDMARK
2616		89: LANDMARK
2617		91: LANDMARK
2618		
2619	26)	43: $0.106-0.118 \rightarrow 0.070$



2620		[39, 40, 46]: LANDMARK
2621		[50, 54, 55]: LANDMARK
2622		73: 1→2
2623		76: 0→1
2624		81: LANDMARK
2625		89: LANDMARK
2626		91: LANDMARK
2627		
2628	27)	[39, 40, 46]: LANDMARK
2629		53: 2→1
2630		[50, 54, 55]: LANDMARK
2631		70: 0→1
2632		81: LANDMARK
2633		89: LANDMARK
2634		91: LANDMARK
2635		
2636	28)	[39, 40,46]:
2637		[50, 54, 55]: LANDMARK
2638		59: 1→2
2639		60: 0.098-0.102 → 0.125
2640		81: LANDMARK
2641		89: LANDMARK
2642		91: LANDMARK



2643

2644 29) [39, 40, 46]: LANDMARK

2645 [50, 54, 55]: LANDMARK

2646 60: 0.124 \rightarrow 0.236-0.267

2647 81: LANDMARK

2648 89: LANDMARK

2649 91: LANDMARK

2650

2651 30) [39, 40, 46]: LANDMARK

2652 48: 0 \rightarrow 1

2653 [50, 54, 55]: LANDMARK

2654 81: LANDMARK

2655 89: LANDMARK

2656 91: LANDMARK

2657

2658 31) 35: 0 \rightarrow 1

2659 [39, 40, 46]: LANDMARK

2660 [50, 54, 55]: LANDMARK

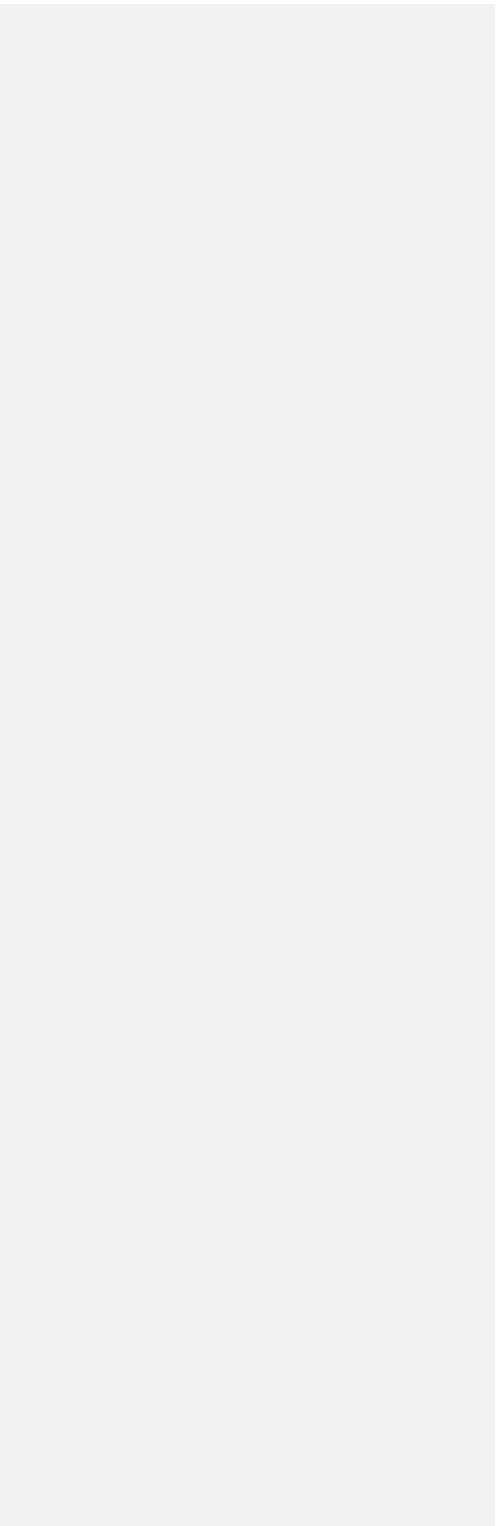
2661 81: LANDMARK

2662 89: LANDMARK

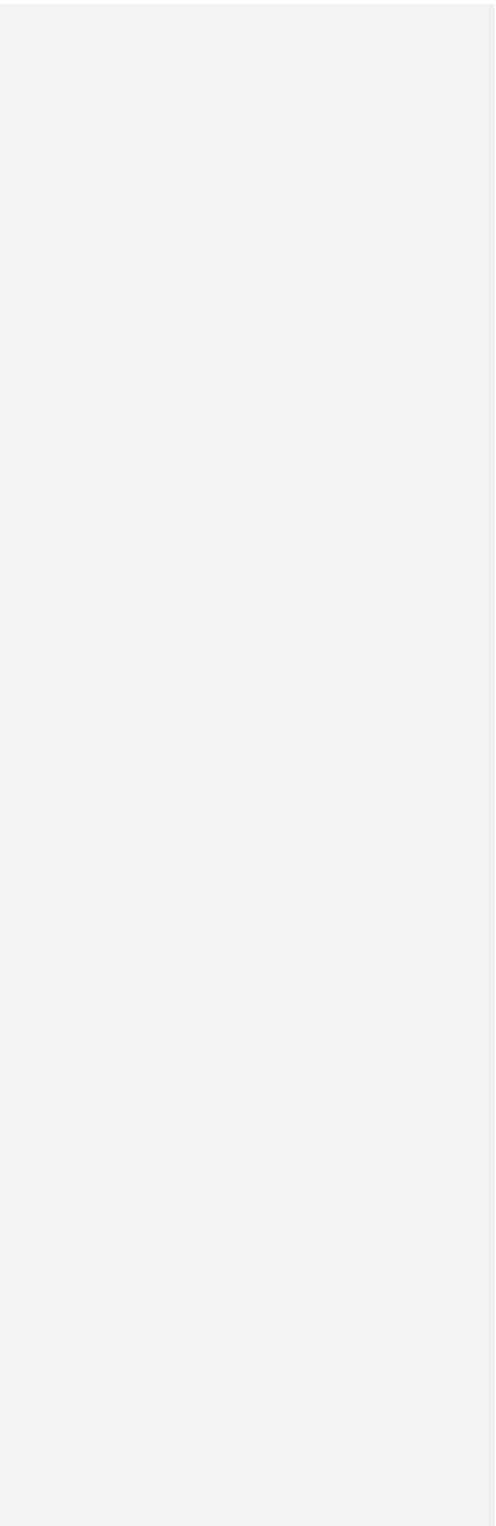
2663 91: LANDMARK

2664

2665 32) 3: 1 \rightarrow 0



2666		4: 1→0
2667		7: 2→1
2668		[39, 40, 46]: LANDMARK
2669		[50, 54, 55]: LANDMARK
2670		75: 0→1
2671		81: LANDMARK
2672		89: LANDMARK
2673		91: LANDMARK
2674		
2675	33)	38: 0.442-0.457 → 0.077-0.319
2676		[39, 40, 46]: LANDMARK
2677		[50, 54, 55]: LANDMARK
2678		81: LANDMARK
2679		89: LANDMARK
2680		90: 0→1
2681		91: LANDMARK
2682		
2683	34)	19: 1→0
2684		[39, 40, 46]: LANDMARK
2685		[50, 54, 55]: LANDMARK
2686		81: LANDMARK
2687		89: LANDMARK
2688		91: LANDMARK



2689

2690 35) [39, 40, 46]: LANDMARK

2691 48: 1→0

2692 [50, 54, 55]: LANDMARK

2693 81: LANDMARK

2694 86: 0→1

2695 89: LANDMARK

2696 91: LANDMARK

2697

2698 36) 25: 0.325-0.439 → 0.113

2699 34: 1→2

2700 [39, 40, 46]: LANDMARK

2701 53: 1, 2→0

2702 [50, 54, 55]: LANDMARK

2703 81: LANDMARK

2704 89: LANDMARK

2705 91: LANDMARK

2706

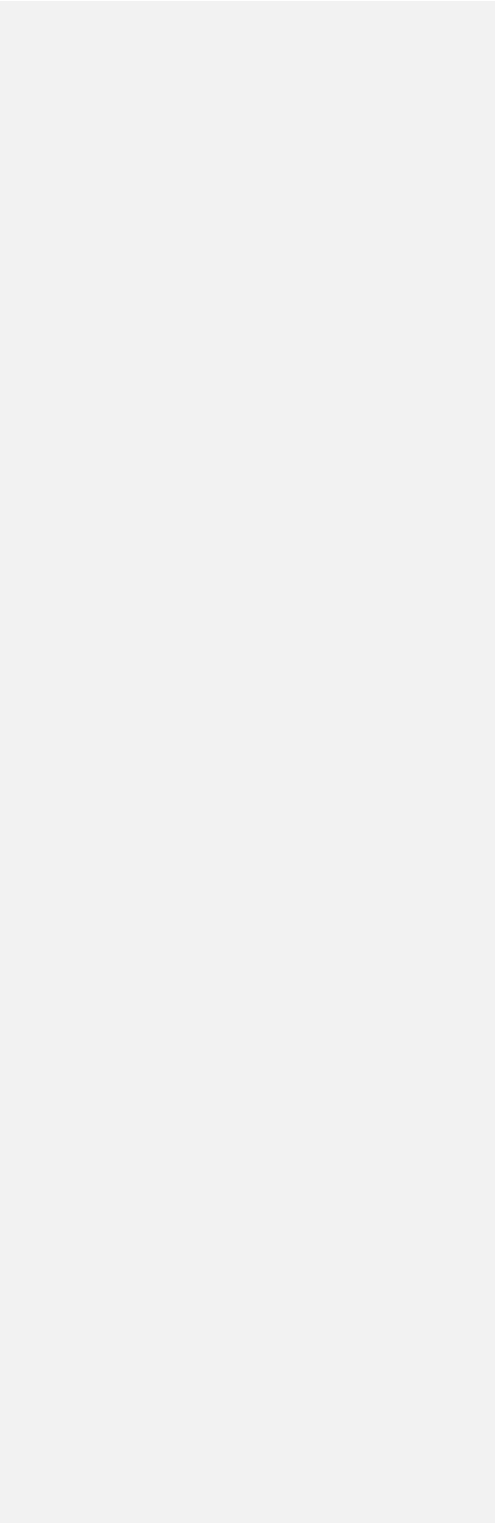
2707 37) [39, 40, 46]: LANDMARK

2708 [50, 54, 55]: LANDMARK

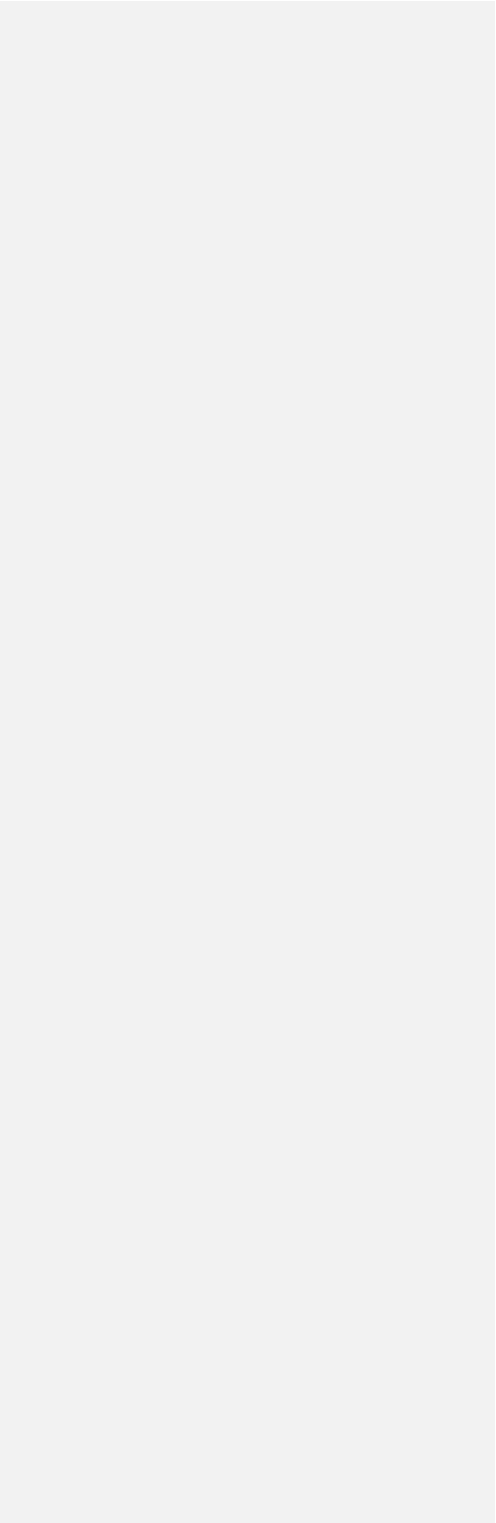
2709 81: LANDMARK

2710 84: 0→1

2711 87: 0.338-0.401 → 0.574-0.577



2712		89: LANDMARK
2713		
2714	38)	7: $1 \rightarrow 2$
2715		[39, 40, 46]: LANDMARK
2716		[50, 54, 55]: LANDMARK
2717		57: $2 \rightarrow 3$
2718		81: LANDMARK
2719		89: LANDMARK
2720		91: LANDMARK
2721		
2722	39)	[39, 40, 46]: LANDMARK
2723		[50, 54, 55]: LANDMARK
2724		57: $2 \rightarrow 1$
2725		61: $2 \rightarrow 1$
2726		81: LANDMARK
2727		85: $1 \rightarrow 0$
2728		89: LANDMARK
2729		91: LANDMARK
2730		
2731	40)	2: $1 \rightarrow 2$
2732		20: $0 \rightarrow 1$
2733		[39, 40, 46]: LANDMARK
2734		[50, 54, 55]: LANDMARK



2735 81: LANDMARK

2736 89: LANDMARK

2737 91: LANDMARK

2738

2739 41) 19: $0 \rightarrow 1$

2740 [39, 40, 46]: LANDMARK

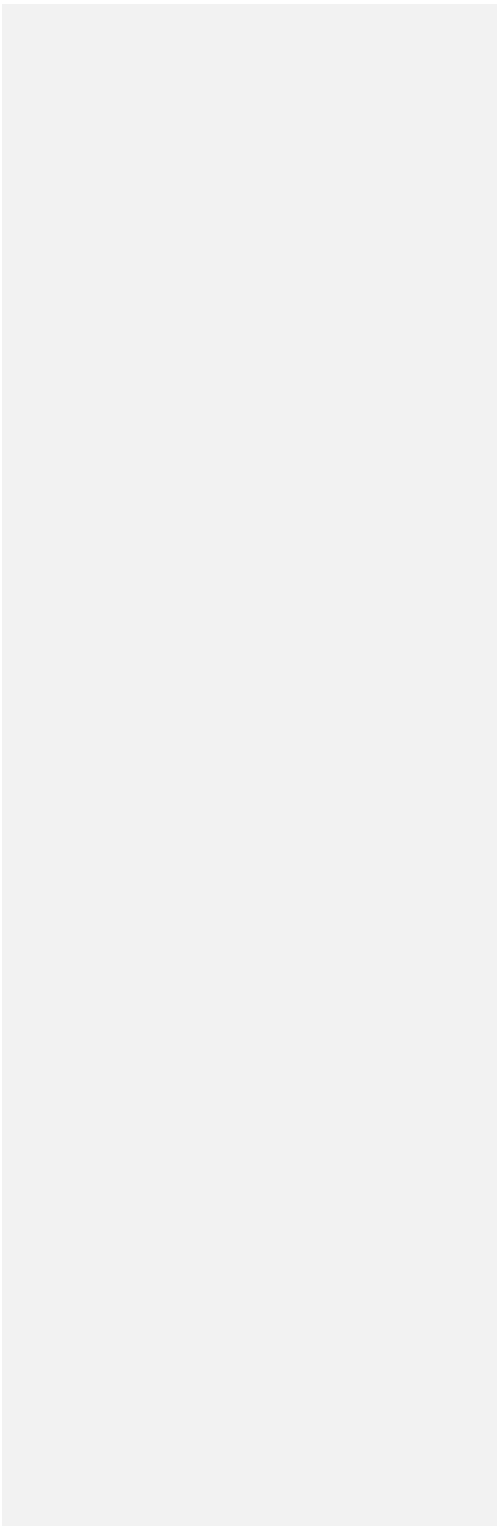
2741 [50, 54, 55]: LANDMARK

2742 81: LANDMARK

2743 88: $0 \rightarrow 1$

2744 89: LANDMARK

2745 91: LANDMARK



2746 **References**

2747

2748 **Ballew, K. L.** 1989. *A phylogenetic analysis of Phytosauria (Reptilia: Archosauria) from the Late Triassic of*
2749 *the western United States*. Unpublished MA thesis, University of California, Berkeley, 73 pp.

2750

2751 **Buffetaut, E.** 1993. Phytosaurs in time and space. *Paleontolol Lombarda Nuova serie*, **2**, 39-44.

2752

2753 **Butler, R. J., Rauhut, O. W., Stocker, M. R., & Bronowicz, R.** 2014. Redescription of the phytosaurs
2754 *Paleorhinus* ('*Francosuchus*') *angustifrons* and *Ebrachosuchus neukami* from Germany, with
2755 implications for Late Triassic biochronology. *Zoological Journal of the Linnean Society*, **170**, 155-208
2756 DOI: 10.1111/zoj12094

2757

2758 **Camp, C. L.** 1930. A study of the phytosaurs with description of new material from western North America.
2759 *Memoirs of the University of California*, **10**, 1-174.

2760

2761 **Case, E. C.** 1920. Preliminary description of a new suborder of phytosaurian reptiles with a description of a
2762 new species of *Phytosaurus*. *The Journal of Geology*, **28**, 524-535 DOI: 10.1086/622732

2763

2764 **Case, E. C.** 1922. *New reptiles and stegocephalians from the Upper Triassic of western Texas* (Vol. 321).
2765 Carnegie Institution of Washington, 126 pp

2766

2767 **Case, E. C., & White, T. E.** 1934. Two new specimens of phytosaurs from the Upper Triassic of western
2768 Texas. *Contributions from the Museum of Paleontology, University of Michigan*, **4**, 133-142.

2769

2770 **Chatterjee, S.** 1974. A Rhynchosaur from the Upper Triassic Maleri Formation of India. *Philosophical Transactions of the Royal Society of London Series B*, **267**, 209-261 DOI: 10.1098/rstb.1974.0001

2772

2773 **Chatterjee, S.** 1978. A primitive parasuchid (phytosaur) reptile from the Upper Triassic Maleri Formation of India. *Palaeontology*, **21**, 83-127.

2775

2776 **Colbert, E. H.** 1947. Studies of the phytosaurs *Machaerops* and *Rutiodon*. *Bulletin of the AMNH*, **88**, 53-96, 10 pls

2778

2779 **Cope, E. D.** 1881. *Belodon* in New Mexico. *American Naturalist*, 15, 922-923.

2780

2781 **Drevertmann, F.** 1918. Ein Parasuchier-Schädel aus dem schwäbischen Stubensandstein. *Bericht der Senckenbergischen Naturforschenden Gesellschaft in Frankfurt am Main*, **47**, 120-123.

2783

2784 **Dutuit, J. M.** 1977. *Paleorhinus magnoculus*, phytosaure du Trias supérieur de l'Atlas marocain. *Géologie Méditerranéenne*, **4**, 255-268.

2786

2787 **Emmons, E.** 1856. *Geological report of the midland counties of North Carolina*. Putnam. 352 pp., 14 pls DOI: 10.5962/bhl.title.34269

2789

2790 **Fraas, E.** 1896. *Die schwäbischen Trias-Saurier nach dem Material der Kgl. Naturalien-Sammlung in Stuttgart zusammengestellt*. Stuttgart (Schweizerbart). 18 pp.

2792

2793 **Gregory, J. T.** 1962. The genera of phytosaurs. *American Journal of Science*, **260**, 652-690 DOI:

2794 10.2475/ajs.260.9.652

2795

2796 **Gregory, J. T.** 1972. Vertebrate faunas of the Dockum Group, Triassic, eastern New Mexico and West

2797 Texas. *New Mexico Geological Society 23rd Fall Field Conference, Guidebook*, 120-123.

2798

2799 **Griffin, C. T., Stefanic, C. M., Parker, W. G., Hungerbühler, A., & Stocker, M. R.** 2017. Sacral anatomy

2800 of the phytosaur *Smilosuchus adamanensis*, with implications for pelvic girdle evolution among

2801 Archosauriformes. *Journal of Anatomy*, **231**, 886-905 DOI: 10.1111/joa.12681

2802

2803 **Heckert, A. B., Lucas, S. G., Hunt, A. P., & Harris, J. D.** 2001. A giant phytosaur (Reptilia: Archosauria)

2804 skull from the Redonda Formation (Upper Triassic: Apachean) of east-central New Mexico. *New Mexico*

2805 *Geological Society Guidebook*, **52**, 171-178.

2806

2807 **Heckert, A. B., & Lucas, S. G.** 2003. Stratigraphy and paleontology of the lower Chinle Group

2808 (Adamanian; latest Carnian) in the vicinity of St. Johns, Arizona. *New Mexico Geological Society*

2809 *Guidebook*, **54**, 281-288.

2810

2811 **Heller, F.** 1954. Ein Parasuchier-Schädelrest aus dem Oberen Burgsandstein von Coburg. *Geologische*

2812 *Blätter für Nordost-Bayern und angrenzende Gebiete*, 4, 1-14.

2813

2814 **Huene, F. von.** 1909. Vorläufige Mitteilung über einen neuen *Phytosaurus*-Schädel aus dem schwäbischen
2815 Keuper. *Centralblatt für Mineralogie, Geologie und Paläontologie*, **1909** 583-592.

2816

2817 **Huene, F. von.** 1911. Beiträge zur Kenntnis und Beurteilung der Parasuchier. *Geologische und*
2818 *Paläontologische Abhandlungen, Neue Folge*, **10**, 67-121.

2819

2820 **Huene, F. von.** 1922. Neue Beiträge zur Kenntnis der Parasuchier. *Jahrbuch der Preussischen Geologischen*
2821 *Landesanstalt*, **42**, 146-148.

2822

2823 **Hungerbühler, A.** 1998. *Cranial anatomy and diversity of the Norian phytosaurs of Southwestern Germany*.
2824 Unpublished PhD thesis, University of Bristol, 464 pp.

2825

2826 **Hungerbühler, A., & Hunt, A. P.** 2000. Two new phytosaur species (Archosauria, Crurotarsi) from the
2827 Upper Triassic of southwest Germany. *Neues Jahrbuch für Geologie und Paläontologie-Monatshefte*, **8**,
2828 467-484.

2829

2830 **Hungerbühler, A.** 2002. The Late Triassic phytosaur *Mystriosuchus westphali*, with a revision of the
2831 genus. *Palaeontology*, **45**, 377-418 DOI: 10.1111/1475-4983.00242

2832

2833 **Hungerbühler, A., Mueller, B., Chatterjee, S. & Cunningham, D. P.** 2013. Cranial anatomy of the Late
2834 Triassic phytosaur *Machaeroprotopus*, with the description of a new species from West Texas. *Earth and*
2835 *Environmental Science Transactions of the Royal Society of Edinburgh*, **103**, 269–312 DOI:
2836 10.1017/S1755691013000364

2837

2838 **Hunt, A. P.** 1994a. The phylogeny and biochronology of the Parasuchidae (Reptilia: Archosauria). *Journal*

2839 *of Vertebrate Paleontology*, **14**(3), 30A DOI: 10.1080/02724634.1994.10011592

2840

2841 **Hunt, A P.** 1994b. *Vertebrate paleontology and biostratigraphy of the Bull Canyon Formation (Chinle*

2842 *Group, Upper Triassic), east-central New Mexico with revisions of the families Metoposauridae*

2843 *(Amphibia: Temnospondyli) and Parasuchidae (Reptilia: Archosauria)*. Unpublished PhD thesis,

2844 University of New Mexico, 404 pp.

2845

2846 **Hunt, A. P., & Lucas, S. G.** 1989. New genotype designations for the phytosaurs *Mystriosuchus* and

2847 *Rutiodon* with a discussion of the taxonomic status of *Mystriosuchus*, *Clepsysaurus* and *Rutiodon*. Pp.

2848 340-348 in S. G. Lucas & A. P. Hunt (eds) *Dawn of the Age of Dinosaurs in the American Southwest*.

2849 New Mexico Museum of Natural History and Science, Albuquerque.

2850

2851 **Hunt, A. P., & Lucas, S. G.** 1993. A new phytosaur (Reptilia: Archosauria) genus. *New Mexico Museum of*

2852 *Natural History & Science Bulletin*, **3**, 193-196.

2853

2854 **Hunt, A. P., Lucas, S. G., & Bircheff, P.** 1993. Biochronological significance of the co-occurrence of the

2855 phytosaurs (Reptilia: Archosauria) *Angistorhinus* and *Rutiodon* in the Los Esteros Member of the Santa

2856 Rosa Formation, Santa Fe County, New Mexico, USA. *New Mexico Museum of Natural History &*

2857 *Science Bulletin*, **3**, 203-204.

2858

2859 **Hunt, A. P., Lucas, S. G., & Spielmann, J. A.** 2006. Sexual dimorphism in a large brachyrostral phytosaur
2860 (Archosauria: Crurotarsi) from the Late Triassic of western North America. *New Mexico Museum of*
2861 *Natural History and Science Bulletin*, **37**, 563-67.

2862

2863 **Irmis, R. B.** 2005. The vertebrate fauna of the Upper Triassic Chinle Formation in northern Arizona. *Mesa*
2864 *Southwest Museum Bulletin*, **9**, 63-88.

2865

2866 **Kammerer, C. F., Butler, R. J., Bandyopadhyay, S., & Stocker, M. R.** 2015. Relationships of the Indian
2867 phytosaur *Parasuchus hislopi* Lydekker, 1885. *Papers in Palaeontology*, **2**, 1-23 DOI: 10.1002/spp2.1022

2868

2869 **Kuhn, O.** 1936. Weitere Parasuchier und Labyrinthodonten aus dem Blasensandstein des mittleren Keuper
2870 von Ebrach. *Palaeontographica Abteilung A*, **83**, 61–98.

2871

2872 **Langston, W.** 1949. A new species of *Paleorhinus* from the Triassic of Texas. *American Journal of*
2873 *Science*, **247**, 324-341 DOI: 10.2475/ajs.247.5.324

2874

2875 **Lees, J. H.** 1907. The skull of *Paleorhinus*: a Wyoming phytosaur. *The Journal of Geology*, **15**, 121-151
2876 DOI: 10.1086/621382

2877

2878 **Li, C., Wu, X. C., Zhao, L. J., Sato, T., & Wang, L. T.** 2012. A new archosaur (Diapsida,
2879 Archosauriformes) from the marine Triassic of China. *Journal of Vertebrate Paleontology*, **32**, 1064-1081
2880 DOI: 10.1080/02724634.2012.694383

2881

2882 **Long, R. A., & Murry, P. A.** 1995. *Late Triassic (Carnian and Norian) Tetrapods from the Southwestern*
2883 *United States: Bulletin 4.* New Mexico Museum of Natural History and Science.

2884

2885 **Lucas, S. G., Heckert, A. B., Zeigler, K. E., & Hunt, A. P.** 2002. The type locality of *Belodon buceros*
2886 Cope, 1881, a phytosaur (Archosauria: Parasuchidae) from the Upper Triassic of north-central New
2887 Mexico. *New Mexico Museum of Natural History and Science Bulletin*, **21**, 189-192.

2888

2889 **Lydekker, R.** 1885. The Reptilia and Amphibia of the Maleri and Denwa groups. *Palaeontologia Indica*,
2890 *Series 1*, **1**, 1–38.

2891

2892 **Marsh, O. C.** 1896. A new belodont reptile (*Stegomus*) from the Connecticut River sandstone. *American*
2893 *Journal of Science*, **7**, 59-62.

2894

2895 **Mateus, O., Butler, R. J., Brusatte, S. L., Whiteside, J. H., & Steyer, J. S.** 2014. The first phytosaur
2896 (Diapsida, Archosauriformes) from the Late Triassic of the Iberian Peninsula. *Journal of Vertebrate*
2897 *Paleontology*, **34**, 970-975 DOI: 10.1080/02724634.2014.840310

2898

2899 **McCormack L, Parker WG.** 2017. A new occurrence of the phytosaur (Archosauriformes, Phytosauria)
2900 *Pravusuchus hortus* from the Monitor Butte Member (Upper Triassic; Chinle Formation) of Utah.
2901 *Journal of Vertebrate Paleontology Program and Abstracts*, 2017, 161 pp

2902

2903 **McGregor, J. H.** 1906. The Phytosauria, with especial reference to *Mystriosuchus* and *Rhytidodon*. *Memoirs*
2904 *of the American Museum of Natural History*, **9**, 27-101, 5 pls

2905

2906 **Mehl, M. G.** 1913. *Angistorhinus*, a new genus of Phytosauria from the Trias of Wyoming. *The Journal of*

2907 *Geology*, **21**, 186-191 DOI: 10.1086/622049

2908

2909 **Mehl, M. G.** 1922. A new phytosaur from the Trias of Arizona. *The Journal of Geology*, **30**, 144-157 DOI:

2910 10.1086/622860

2911

2912 **Mehl, M. G.** 1928. The Phytosauria of the Wyoming Triassic. *Journal of the Denison University*

2913 *Laboratories, Denison University*, **23**, 141–172.

2914

2915 **Meyer, H. von.** 1860. Briefliche Mittheilung an Prof. Bronn. *Neues Jahrbuch fur Mineralogie, Geognosie,*

2916 *Geologie und Petrefakten-Kunde*, 556-560.

2917

2918 **Meyer, H. von.** 1861. Reptilien aus dem Stubensandstein des oberen Keupers. *Palaeontographica*, **7**, 253-

2919 351, pls 28-47.

2920

2921 **Meyer, H. von.** 1863. Der Schädel des *Belodon* aus dem Stubensandstein des oberen Keupers.

2922 *Palaeontographica*, **10**, 227-246, pls 38-42.

2923

2924 **Meyer, H. von.** 1865. Reptilien aus dem Stubensandstein des oberen Keupers. *Palaeontographica*, **14**, 99-

2925 124, pls 23-29.

2926

2927 **Parker, W. G., & Irmis, R. B.** 2006. A new species of the Late Triassic phytosaur *Pseudopalatus*
2928 (Archosauria: Pseudosuchia) from Petrified Forest National Park, Arizona. *Museum of Northern Arizona*
2929 *Bulletin*, **62**, 126-143.

2930

2931 **Pinna, G.** 1987. I nuovi Lagerstaetten fossili del Triassico Italiano. *Le Scienze*, **224**, 62-70.

2932

2933 **Sereno, P. C.** 1991. Basal archosaurs: phylogenetic relationships and functional implications. *Journal of*
2934 *Vertebrate Paleontology*, **11**(S4), 1-53 DOI: 10.1080/02724634.1991.10011426

2935

2936 **Spielmann, J. A., & Lucas, S. G.** 2012. Tetrapod Fauna of the Upper Triassic Redonda Formation East-
2937 central New Mexico: The Characteristic Assemblage of the Apachean Land-vertebrate Faunachron. *New*
2938 *Mexico Museum of Natural History and Science Bulletin*, **55**, 1-119.

2939

2940 **Stocker, M. R.** 2010. A new taxon of phytosaur (Archosauria: Pseudosuchia) from the Late Triassic
2941 (Norian) Sonsela Member (Chinle Formation) in Arizona, and a critical reevaluation of *Leptosuchus* Case,
2942 1922. *Palaeontology*, **53**, 997-1022 DOI: 10.1111/j.1475-4983.2010.00983.x

2943

2944 **Stocker, M. R.** 2012. A new phytosaur (Archosauriformes, Phytosauria) from the Lot's Wife beds (Sonsela
2945 Member) within the Chinle Formation (Upper Triassic) of Petrified Forest National Park,
2946 Arizona. *Journal of Vertebrate Paleontology*, **32**, 573-586 DOI: 10.1080/02724634.2012.649815

2947

2948 **Stocker, M. R.** 2013. A new taxonomic arrangement for *Paleorhinus scurriensis*. *Earth and Environmental*
2949 *Science Transactions of the Royal Society of Edinburgh*, **103**, 1-13 DOI: 10.1017/S1755691013000340

2950

2951 **Stocker, M. R., & Butler, R. J.** 2013. Phytosauria. *Geological Society, London, Special Publications*, **379**,

2952 91-117 DOI: 10.1144/SP379.5

2953

2954 **Stocker, M. R., Zhao, L. J., Nesbitt, S. J., Wu, X. C., & Li, C.** 2017. A Short-Snouted, Middle Triassic

2955 Phytosaur and its Implications for the Morphological Evolution and Biogeography of

2956 Phytosauria. *Scientific reports*, **7**, 46028 DOI: 10.1038/srep46028

2957

2958 **Williston, S. W.** 1904. Notice of some new reptiles from the Upper Trias of Wyoming. *The Journal of*

2959 *Geology*, **12**, 688-697 DOI: 10.1086/621190

2960

2961 **Witmer, L. M.** 1997. The evolution of the antorbital cavity of archosaurs: a study in soft-tissue

2962 reconstruction in the fossil record with an analysis of the function of pneumaticity. *Journal of Vertebrate*

2963 *Paleontology*, **17**(S1), 1-76 DOI: 10.1080/02724634.1997.10011027

2964

2965 **Zeigler, K. E., Lucas, S. G., & Heckert, A. B.** 2002. A phytosaur skull from the upper Triassic Snyder

2966 Quarry (Petrified Forest Formation, Chinle Group). *New Mexico Museum of Natural History and*

2967 *Science Bulletin*~~*Upper Triassic Stratigraphy and Paleontology: Bulletin*~~, **21**, 171-178.

2968

2969 **Zeigler, K. E., Lucas, S. G., & Heckert, A. B.** 2003a. Variation in the Late Triassic Canjilon quarry (Upper

2970 Chinle Group, New Mexico) phytosaur skulls: a case for sexual dimorphism. *Paläontologische*

2971 *Zeitschrift*, **77**, 341 DOI: 10.1007/BF03006946

2972

2973 **Zeigler, K. E., Heckert, A. B., & Lucas, S. G.** 2003b. Phytosaur (Archosauria: Parasuchidae) cranial and
2974 mandibular material from the Upper Triassic Snyder quarry (Petrified Forest Formation, Chinle Group).
2975 *New Mexico Museum of Natural History and Science Bulletin*, **24**, 81-88.